JOURNAL OF ENGINEERING RESEARCH & SCIENCES

JENRS

www.jenrs.com
ISSN: 2831-4085

Volume 1 Issue 4
April 2022

EDITORIAL BOARD

Editor-in-Chief

Editorial Board Members

Editorial

In an era where the pursuit of knowledge transcends disciplinary boundaries, it is imperative to recognize the significance of research endeavours spanning a multitude of domains. From the intricate realms of acoustics to the complexities of cyber security, and from the challenges of e-learning during a pandemic to the nuances of human-computer interaction for older adults, the array of 18 research papers presented in this compilation underscores the breadth and depth of contemporary scholarship.

The first paper delves into the nuanced phenomenon of acoustic monochromatic radiation, shedding light on the resonant energy transfer from boundaries into sound waves with traveling distributions of phases. Through meticulous analysis, the authors unravel the intricate interplay between spatial frequencies, wave dimensions, and curvature of radiating boundaries, offering insights into resonant radiation phenomena [1].

Transitioning to the realm of cybersecurity, the second paper navigates the intricate landscape of public policy issues, cyber vulnerabilities, and automated defence capabilities. In an age marked by ubiquitous connectivity and digital dependence, understanding and mitigating cyber threats assume paramount importance. The paper furnishes a comprehensive overview, equipping decision-makers with the requisite knowledge to navigate the evolving cyber threat landscape [2].

Amidst the backdrop of the COVID-19 pandemic, the third paper elucidates innovative approaches to distance learning, leveraging internet technologies and online platforms to facilitate effective education delivery. By harnessing existing digital infrastructure and engineering tools, the paper exemplifies the resilience and adaptability of educational systems in times of crisis [3].

Venturing into the realm of structural engineering, the fourth paper presents a novel polynomial displacement function to evaluate the stability of rectangular thick plates. Grounded in the principles of 3-D elasticity theory, the paper offers an exact solution for stability analysis, addressing the limitations of conventional approaches and enhancing our understanding of plate behaviour [4].

In the domain of materials science and civil engineering, the fifth paper investigates the influence of aggregate nature on the fire performance of concrete exposed to high temperatures. Through meticulous experimentation and analysis, the authors discern the differential responses of concrete compositions, thereby informing the development of fire-resistant building materials [5].

Moving to the realm of agricultural science, the sixth paper introduces a hybrid evolutionary/fuzzy machine learning approach to predict plant growth and yield. By integrating genetic algorithms and fuzzy logic, the paper pioneers a robust forecasting model, facilitating informed decision-making in agricultural management [6].

Transitioning to the socio-political sphere, the seventh paper delves into the factors shaping political ideas and values, with a particular focus on the role of media, education, family, and youth participation. Through empirical analysis, the paper elucidates the dynamics of political socialization, offering insights into pathways for fostering positive political attitudes [7].

This paper comprehensively studies the detailed design procedure and analysis of flat belt conveyor components for light-duty applications. It includes calculations, finite element analysis (FEA), and stress analysis of pulleys, shafts, and conveyor belts, ensuring the safety and efficiency of conveyor systems [8].

The paper conducts a structural analysis, utilizing finite element simulation, of single-row deep groove ball bearings made from three different materials: Silicon Nitride, 440C Stainless Steel, and AISI 4140 Alloy Steel. It evaluates contact stress and total deformation to determine the materials' suitability for bearing applications [9].

This paper proposes an adaptive filtering technique using the Least Mean Square (LMS) Algorithm to identify the coefficients of Finite Impulse Response (FIR) filters. The methodology employs microcontrollers and adaptive filters to find the estimated weights of the transfer function, facilitating the design of complex resistive circuits [10].

The paper outlines a methodology for direct teacher-student interaction and evaluation in remote classrooms, particularly during the COVID-19 pandemic. It emphasizes active-participatory classes, collaborative activities, and feedback mechanisms using Moodle-based platforms for effective teaching and assessment [11].

This paper presents an algorithm for fire alarm systems designed to detect fire-colored areas in captured images. It describes the comparison process of captured pictures, fire detection, and system reset functionalities, offering a systematic approach to fire detection and monitoring using image processing techniques [12].

The paper explores the use of anaerobic digestion systems for managing rural and urban waste, focusing on the generation of biogas from various feedstocks. It discusses process kinetics, substrate degradation, biogas properties, and factors influencing biogas production, providing insights for efficient waste management practices [13].

This study conducts a literature review to identify critical factors in human-computer interaction for technology-enhanced health care systems catering to older adults. It emphasizes factors such as personal integrity, trust, technology acceptance, and accessibility, recommending user-centered design and adequate support for successful adoption [14].

The paper proposes procedures for selecting parameters of sine-wave filters to address increased voltage frequency output from frequency converters in power supply systems. It describes the structure of power supply systems and simulators, focusing on improving voltage quality and modulation index contributions [15].

This study investigates the adsorption of heavy metals, particularly Cadmium (Cd), from water samples using activated carbon derived from Date Tree Leaves (DTL). It evaluates the effectiveness of impregnating the activated carbon with Zinc Oxide catalyst for heavy metal removal, providing insights into sustainable water treatment solutions [16].

The paper analyzes multi-carrier pulse width modulation (MC-PWM) techniques for cascaded H-bridge multilevel inverters (CHB-MLI). It reviews various MC-PWM methods, conducts mathematical analysis, and performs simulation studies to evaluate harmonic reduction and input source balancing capabilities of different modulation techniques [17].

This study evaluates machine learning algorithms, specifically the Extreme Learning Machine (ELM) algorithm, for non-invasive estimation of blood pressure and waveform from Photoplethysmography (PPG) signals. It demonstrates high correlation and accuracy in estimating blood pressure values and waveform characteristics, paving the way for non-invasive blood pressure monitoring technologies [18].

In conclusion, the compilation of research papers presented in this editorial exemplifies the multifaceted nature of contemporary scholarship. By traversing disciplinary boundaries and embracing interdisciplinary collaboration, researchers continue to illuminate the complexities of our world and pave the way for transformative innovation and societal progress. As we

navigate the frontiers of knowledge, let us embrace the spirit of inquiry and collective endeavour, forging new pathways towards a brighter and more sustainable future.

References:

[1] V. Arabadzhi, “Resonant Radiation of Boundary with a Travelling Distribution of the Field,” *Journal of Engineering Research and Sciences*, vol. 1, no. 4, pp. 1–8, 2022, doi:10.55708/js0104001.

[2] R. Mazzolin, A. Madni, “An Overview of Cyber Security Considerations and Vulnerabilities in Critical Infrastructure Systems and Potential Automated Mitigation - A Review,” *Journal of Engineering Research and Sciences*, vol. 1, no. 4, pp. 09–21, 2022, doi:10.55708/js0104002.

[3] R. Hrischev, “Effective Approach Experience for Practical Training using Web-Based Platforms and Tools in the Context of the COVID-19 Pandemic,” *Journal of Engineering Research and Sciences*, vol. 1, no. 4, pp. 22–27, 2022, doi:10.55708/js0104003.

[4] F.C. Onyeka, C.D. Nwa-David, T.E. Okeke, “Study on Stability Analysis of Rectangular Plates Section Using a Three-Dimensional Plate Theory with Polynomial Function,” *Journal of Engineering Research and Sciences*, vol. 1, no. 4, pp. 28–37, 2022, doi:10.55708/js0104004.

[5] S. Hachemi, Z.E. Rahmouni, “A Review on the Effect of Varied Sand Types in Concrete at High Temperature,” *Journal of Engineering Research and Sciences*, vol. 1, no. 4, pp. 38–47, 2022, doi:10.55708/js0104005.

[6] C. Nikolopoulos, R. Koralik, “Evolutionary Learning of Fuzzy Rules and Application to Forecasting Environmental Impact on Plant Growth,” *Journal of Engineering Research and Sciences*, vol. 1, no. 4, pp. 48–53, 2022, doi:10.55708/js0104006.

[7] S. Salita, K. Maryam, “Factors Determining Political Socialization in Young People (A Case of Pakistani University Students),” *Journal of Engineering Research and Sciences*, vol. 1, no. 4, pp. 54–61, 2022, doi:10.55708/js0104007.

[8] Y. Patil, S.P.S. Gawade, V. Shinde, S. Jawade, “Design and Analysis of Flat Belt Conveyor for Segregation of Defective Products,” *Journal of Engineering Research and Sciences*, vol. 1, no. 4, pp. 62–67, 2022, doi:10.55708/js0104008.

[9] A. Galande, S. Pachpore, A. Pawar, “Modelling and Comparative Study for Deep Groove Ball Bearing Based on Structural Analysis using FE Simulation,” *Journal of Engineering Research and Sciences*, vol. 1, no. 4, pp. 68–73, 2022, doi:10.55708/js0104009.

[10] S.K.V. Rao, K. Kiran, N. Kumar, M. Mahadevaswamy, “System Identification of FIR Filters,” *Journal of Engineering Research and Sciences*, vol. 1, no. 4, pp. 74–80, 2022, doi:10.55708/js0104010.

[11] C.E.H. Briones, “Methodology for Learning Mathematics Based on Collaborative Work with the Support of ICT Tools and Virtual Environments of the UCN Campus,” *Journal of Engineering Research and Sciences*, vol. 1, no. 4, pp. 81–86, 2022, doi:10.55708/js0104011.

[12] M.Z. ur Rahman, S. Waseem, S. Riaz, Z. Riaz, A. Asif, A. Saddiqa, A. Asghar, “Image Processing and Data Storage for Fire Alarm,” *Journal of Engineering Research and Sciences*, vol. 1, no. 4, pp. 87–92, 2022, doi:10.55708/js0104012.

[13] A.M. Abubakar, K. Silas, M.M. Aji, “An Elaborate Breakdown of the Essentials of Biogas Production,” *Journal of Engineering Research and Sciences*, vol. 1, no. 4, pp. 93–118, 2022, doi:10.55708/js0104013.

[14] A. Ahmad, P. Mozelius, “Human-Computer Interaction for Older Adults - a Literature Review on Technology Acceptance of eHealth Systems,” *Journal of Engineering Research and Sciences*, vol. 1, no. 4, pp. 119–126, 2022, doi:10.55708/js0104014.

[15] P. Mikhail, “Determining the Parameters of the Sine-Wave Filter Factors Affecting Filtration Quality,” *Journal of Engineering Research and Sciences*, vol. 1, no. 4, pp. 127–136, 2022, doi:10.55708/js0104015.

[16] K. Silas, A.B. Ngulde, H.D. Mohammed, “Utilization of Date Tree Leaves Biomass for the Removal of Heavy Metals from Water,” *Journal of Engineering Research and Sciences*, vol. 1, no. 4, pp. 137–147, 2022, doi:10.55708/js0104016.

[17] J. Patel, V. Sood, “MC-SPWM and MC-THIPWM Methods for Symmetric and Asymmetric Design of CHB-MLI: A Study,” *Journal of Engineering Research and Sciences*, vol. 1, no. 4, pp. 148–160, 2022, doi:10.55708/js0104017.

[18] G. Tapia, R. Salas, M. Salinas, C. Saavedra, A. Veloz, A. Arriola, S. Chabert, A. Glaría, “An Extreme Learning Machine for Blood Pressure Waveform Estimation using the Photoplethysmography Signal,” *Journal of Engineering Research and Sciences*, vol. 1, no. 4, pp. 161–174, 2022, doi:10.55708/js0104018.

Editor-in-chief

Prof. Paul Andrew

JOURNAL OF ENGINEERING RESEARCH AND SCIENCES

Volume 1 Issue 4 April 2022

CONTENTS

JENRS

Received: 13 December 2021, Revised: 20 March 2022, Accepted: 27 March 2022, Online: 12 April 2022

DOI: https://dx.doi.org/10.55708/js0104001

Resonant Radiation of Boundary with a Travelling Distribution of the Field

Vladimir Arabadzhi *

Division of Geophysical Research, Institute of Applied Physics (RAS), Nizhny Novgorod, 603950, Russia

*Corresponding Author: Vladimir Arabadzhi, Ulianov st. 46, mobile phone +7 952 765 29 77, Email v.v.arabadzhi@appl.sci-nnov.ru

ABSTRACT: The problem of acoustic monochromatic radiation by boundary with a traveling distribution of phases of normal vibrational velocities is considered. It is shown that when the spatial frequency of the traveling phase of normal velocities approaches the wave number in the medium, the energy transfer from boundary into a "sliding" (with respect to the boundary) sound wave can resonantly increase to a value many times greater than the energy transfer from of the in-phase boundary, correspondingly, into the normal one (with respect to the boundary) sound wave at the same modules of amplitudes of vibrational velocities of boundary. In addition, the resonant energy transfer of the boundary into a "sliding" wave is the greater, the larger the wave dimensions of the radiating pattern on boundary. It is shown that when a similar traveling distribution of sound pressure (instead normal velocity) is specified at the boundary, there is no resonance. The influence of the curvature of the radiating boundary on the above phenomenon of resonant radiation was studied. It is shown that the resonant radiation of the boundary with given running phases of normal velocities generates a tangential (with respect to the boundary) constant in time radiation reaction force. It is shown that for the case of a linear chain of equidistant monopoles (or pulsing spheres separated from each other by medium) with a traveling phase (a traveling wave antenna) of their oscillatory velocities, the resonance does not appear.

KEYWORDS: Boundary, Pattern, radiation, Resonance, Phasor, Spatial frequency, Radiation pressure

1. Introduction

It is usually well-known that there is radiation (acoustical or electromagnetic monochromatic field in the far zone) at the spatial frequency $h_0 < k_0$ (k_0 -wave number in the medium) of sources, and at the spatial frequency $h_0 > k_0$ of sources radiation is absent or very small [1-7]. This is probably why the researchers did not consider this area in sufficient detail. Below, using several examples of very simple boundary value problems [8], it is shown that radiation power with an increase in the spatial frequency h_0 from $h_0 = 0$ to $h_0 > k_0$ (immediately before radiation falling to zero at $h_0 > k_0$) can reach infinity when approaching h_0 to k_0. This means the phenomenon of resonance, which is of particular interest to any physicist, especially since we are talking about such an important physical quantity as the surface density of the radiated power. On the other hand, it is known that the traveling amplitude distribution of radiating elements (separated from each other by the medium) in traveling wave antennas does not lead to resonant radiation [9]. In addition, many highly educated researchers, without delving into details (on the basis of the hastily applied relationship between pressure and velocity through the impedance of the medium), are inclined to declare that there is no fundamental difference between boundary radiation with a given pressure and boundary radiation with a given normal velocity. Thus the purpose of this work is to fill the above-mentioned small, but very common (as experience shows) gaps in understanding the process of wave radiation.

First, let's consider a sound field excited in a compressible nonviscous linear medium (in a half-space $z \geq 0$) by a traveling distribution (with a traveling phase [8])

$$U_0(\mathbf{r}, t) = U(h_0, \omega_0) \exp(i\omega_0 t - ih_0 x) \quad (1)$$

of normal vibrational velocities on the surface S (plane surface S, $z = 0$, $\mathbf{r} = (x, y, 0)$), where $U(\omega_0, h_0)$ is the complex amplitude of travelling wave on the time frequency ω_0 and spatial frequency h_0 of normal vibrational velocities (Fig. 1-a). Below we will consider the radiation of various patterns (as modifications of (1)) with a traveling phase.

2. Plane (acoustical field)

Particle velocity $\mathbf{v}(x, z, t)$ and sound pressure $p(x, z, t)$ are determined by potential ψ as

$$\mathbf{v}(\mathbf{r}, t) = -\operatorname{grad}(\psi), \quad p(\mathbf{r}, t) = \rho\psi_t', \tag{2}$$

where ρ is the mass density of medium at $z > 0$.

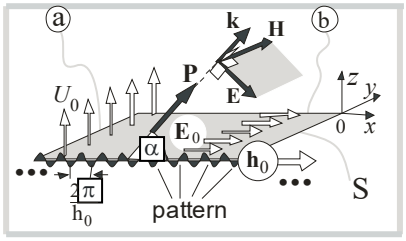

Figure 1. Radiation of the boundary: (a) acoustical radiation; (b) electromagnetic radiation.

Assuming the spatial two-dimensionality of the boundary value problem (i.e. $\partial / \partial y = 0$, $-\infty < y < +\infty$), let us substitute the solution in the equation

$$\psi''_{xx} + \psi''_{zz} = c^{-2}\psi''_{tt} \tag{3}$$

(c is the speed of sound in a compressible medium) for the acoustic wave potential $\psi(x, z, t)$ in the form

$$\psi(x, z, t) = X(x)Z(z)T(t) \tag{4}$$

with functions $X(x), Z(z), T(t)$ of separable variables x, z, t in the absence of waves incident on the boundary $z = 0$. In this case for wave potential $\psi(x, z, t)$ (in the absence of incident waves and satisfying the boundary condition (1) or $-\psi(x, z, t)_z' = U_0(x, t)$) we obtain the following expression

$$\psi(x, z, t) = \varphi(x, z, t) + \bar{\varphi}(x, z, t), \tag{5}$$

where

$$\varphi(x, z, t) = \frac{\exp\left(-iz\sqrt{k_0^2 - h_0^2}\right)}{\left(-i\sqrt{k_0^2 - h_0^2}\right)} \mathbf{I}[k_0 - |h_0|] e^{i\omega_0 t - ih_0 x} U(h_0, \omega_0), \tag{6}$$

$$\bar{\varphi}(x, z, t) = \frac{\exp\left(-z\sqrt{h_0^2 - k_0^2}\right)}{\left(-\sqrt{h_0^2 - k_0^2}\right)} \mathbf{I}[|h_0| - k_0] e^{i\omega_0 t - ih_0 x} U(h_0, \omega_0), \tag{7}$$

$\mathbf{I}[\xi]$ -Heaviside step function ($\mathbf{I}[\xi < 0] = 0$, $\mathbf{I}[\xi \geq 0] = 1$), (8)

thus $\psi = \varphi$ at $|h_0| < k_0$, $\psi = \bar{\varphi}$ at $|h_0| > k_0$, where $k_0 = \omega_0 / c$. Now we get the power flux density

$$W(h_0) = \operatorname{Re}[\rho(\psi_t')(\psi_z')^*]_{z=0} / 2 \tag{9}$$

$$\text{or} \quad W(h_0) = (\omega_0 \rho / 2)|U(h_0, \omega_0)|^2 \mathbf{I}[k_0 - |h_0|] / \sqrt{k_0^2 - h_0^2} \tag{10}$$

at the boundary $z = 0$. This is the work performed by a section of a strip of unit width (along the axis "x") and unit length (along the axis y) and averaged in time over a period $2\pi / \omega_0$). This is due to an abrupt change in the eigenvalue of the boundary value problem from purely real to purely imaginary when going from $|h_0| < k_0$ to $|h_0| > k_0$. For the reactive power flow, we obtain the expression

$$\bar{W}(h_0) = \operatorname{Im}[\rho(\psi_t')(\psi_z')^*]_{z=0} / 2 \tag{11}$$

$$\text{or} \quad \bar{W}(h_0) = \omega_0 \rho |U(h_0, k_0)|^2 \mathbf{I}[|h_0| - k_0] / \left(2\sqrt{h_0^2 - k_0^2}\right). \tag{12}$$

Normalizing to the value $W(0)$ (i.e. for $h_0 = 0$, or in a one-dimensional radiation problem), we obtain a simple expression that means the resonant dependence for relative active $W(h_0)$ and reactive $\bar{W}(h_0)$ power flux density (Fig. 2-a, 2-b)

$$\left[W(h_0) / W(0)\right]_1 = \mathbf{I}[k_0 - |h_0|] / \sqrt{1 - (h_0 / k_0)^2} \text{ (Fig. 2-a),}$$

$$\left[\bar{W}(h_0) / W(0)\right]_1 = \mathbf{I}[|h_0| - k_0] / \sqrt{(h_0 / k_0)^2 - 1} \text{ (Fig. 2-a),} \tag{13}$$

(14)

of the energy transfer of the boundary $z = 0$ (into the half-space $z \geq 0$). Lines **P** (Pointing vector) of power flow go out of the plane $z = 0$ at an angle of inclination

$$\alpha = \arccos(h_0 / k_0). \tag{15}$$

However, when the traveling pressure

$$\rho\psi_t'(x, t) \sim \exp(i\omega_0 t - ih_0 x) \tag{16}$$

is set at the boundary $z = 0$, there is no resonance in the following corresponding functions (instead (13), (14))

$$\left[W(h_0) / W(0)\right]_{\text{pl}} = \sqrt{1 - (h_0 / k_0)^2}\ \mathbf{I}[k_0 - |h_0|] \text{ (Fig. 2-c)} \tag{17}$$

$$\left[\overline{W}(h_0)/W(0)\right]_{p1} = \sqrt{(h_0/k_0)^2 - 1}\ \mathbf{I}\left[|h_0| - k_0\right] \quad \text{(Fig. 2-d)}, \tag{18}$$

(contrary to superficial judgment about the relationship between pressure and velocity through the impedance of the medium, see Figs. 2-c, 2-d).

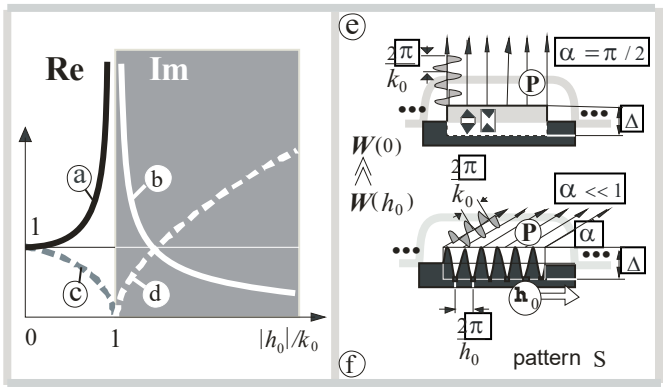

Figure 2. Resonant radiation of the infinite plane boundary S with: (a) normalized real power (13) for velocity pattern (1); (b) normalized imaginary power (14) for velocity pattern (1); (c) normalized real power (17) for given pressure pattern (16); (d) normalized imaginary power (18) for given pressure pattern (16), left white area corresponds to real part of power (radiation), right gray area means reactive imaginary power (no radiation); (e) radiation of normal wave by pattern with amplitude modulus Δ, phasor $h_0 = 0$, $\alpha = \pi/2$; (f) radiation of a "sliding" wave ($\alpha << 1$) with the same amplitude modulus Δ of the pattern, and with a phasor $h_0 \to k_0$.

Below, the value $\left[W(h_0)/W(0)\right]_n$ ($n = 1-5$, i.e. in various modifications) will also be called the transmission function (in terms of power) of a spatial low-frequency filter (due to boundary value problem, Fig. 1) of spatial frequencies h_0 or also the normalized (by $W(0)$) radiation resistance of a radiating pattern (pattern number $n = 1-5$) with spatial frequency h_0 along the vector called as phasor $\mathbf{h}_0$. Below the quantity $U_0(x,t)$ we also will call "pattern" with surface or boundary S.

The essence of the effect of resonant radiation: the wave generated by the pattern (1) at $\left|k_0 - |h_0|\right|/k_0 << 1$, takes much more energy for radiation (from the devices that support the pattern (1)) than the wave with $h_0 = 0$ (at the same fixed amplitude module $\Delta = |U(h_0,\omega_0)|$ of pattern (1), Fig. 2-e, 2-f). In turn, devices that support pattern (1) must have an infinite internal impedance $Z_U = \infty$ (or not depend on any wave pressure at $z > 0$) or an impedance $Z_U >> \rho c$ that is many times greater than the impedance ρc of the medium (at $z \ge 0$), for example: air ($z > 0$)—piezoceramic (thickness ℓ, $0 > z > -\ell$)—steel ($z < -\ell$).

Here is another explanation of the effect. When $\left|k_0 - |h_0|\right|/k_0 < 1$, the solution of equation (3) in the half-space $z > 0$ is a plane sound wave with a wave potential $\psi(x,z,t) = A\exp(i\omega t - ik_0 x\cos\alpha - ik_0 z\sin\alpha)$, where A is the magnitude. To fulfill condition (1) at the boundary $z = 0$, the amplitude A of the radiated wave must be increased at $|h_0| \to k_0$ (or $\alpha \to 0$) so that the projection $-[\psi_A(x,z,t)]'_z$ of particle velocities in the radiated wave ψ onto the axis "z" coincides with pattern (1), which magnitude has been given independently on α. But supporting a given pattern (1) at $\alpha \to 0$ requires more and more energy (energy of radiation).

3. Plane (electromagnetic waves).

The resonance characteristics (13), (14) described above are a property of the wave equation. Therefore, it is natural to assume the possibility of their appearance in the boundary value problem for an electromagnetic field. And indeed, for instance, the tangential electric field

$$\mathbf{E}_0 \sim \mathbf{h}_0 \exp[i\omega_0 t - ih_0 x] \tag{19}$$

($\mathbf{E}_0 \parallel (z=0)$, $\mathbf{h}_0 \parallel (z=0)$) on the plane S or $z = 0$ (see Fig. 1-b) determines the electromagnetic field in the entire half-space $z \ge 0$. When specifying a tangential electric field $\mathbf{E}_0$ on the plane $z = 0$ (we emphasize, not an electric current or a source on the right side of the boundary conditions, namely the field $\mathbf{E}_0$), we get the same resonance functions (13), (14) $\left[W(h_0)/W(0)\right]_1$ and $\left[\overline{W}(h_0)/W(0)\right]_1$.

4. Plane (acoustical radiation pressure). Let us return to the acoustic problem as in Section 2. The pattern $U_0(x,t)$ creates a nonzero complex amplitude of sine $\sin[\phi(x,t)]$ ($\phi(x,t)$ is the slope of the border $z = 0$ or a normal $\mathbf{n}(x,t)$, Fig. 3, $|\phi| << 1$ at $|\phi| << 1$) is equal to the following expression

$$(h_0/\omega_0)U(h_0,\omega_0)\exp(i\omega_0 t - ih_0 x). \tag{20}$$

Due to this, the local pressure force of the medium on the boundary $z = 0$ at the point x at t the moment has a tangential component

$$\mathbf{F}(x,t) = -(\mathbf{h}_0/|\mathbf{h}_0|)\,p(x,0,t)\sin(\phi(x,t)). \tag{21}$$

The average (for the time period $2\pi/\omega_0$ and for the spatial period $2\pi/h_0$) value of the force $\mathbf{F}$ (force per unit square of surface S, $z = 0$) is equal to

$$< \mathbf{F} >_{x,\,t} = -(\mathbf{h}_0 / |\mathbf{h}_0|)\,\mathrm{Re}[p(x,0,t) * \sin(\phi(x,t))]/2 \qquad (22)$$

$$\text{or} \quad < \mathbf{F} >_{x,\,t} = -(\mathbf{h}_0 / |\mathbf{h}_0|) c_{\mathrm{U}}^{-1} W(h_0)\ , \qquad (23)$$

where $c_{\mathrm{U}} = \omega_0 / h_0$ is the phase velocity of the pattern $U_0(x,t)$ (or the speed with which it would be necessary to translate the rigid profile

$$\eta(x) = -[U(h_0, \omega_0) / h_0 c_{\mathrm{U}}] \cos(h_0 x) \qquad (24)$$

along the axis "x" (i.e. $\eta(x) \to \eta(x - c_{\mathrm{U}} t)$, see (1)) in order to obtain the distribution $U_0(x,t)$ of normal velocities), $W(h_0)$ is the radiation power density of the boundary $z = 0$.

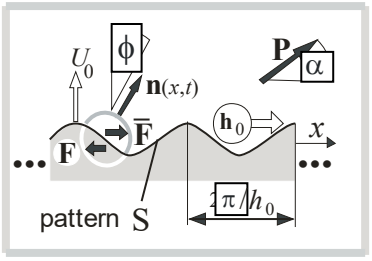

Figure 3. On the appearance of tangential acoustical radiation pressure on an infinite flat pattern.

Obviously: (a) $< \mathbf{F} >_{x,\,t} \neq 0$ is quadratic effect for $U_0(x,t)$; (b) $< \mathbf{F} >_{x,\,t} = 0$ at $W(h_0) = 0$ (i.e. at $|h_0| > k_0$). On the other hand, the pattern acts on the liquid with a force $\bar{\mathbf{F}} = -\mathbf{F}$ (or $< \bar{\mathbf{F}} >_{x,\,t} = - < \mathbf{F} >_{x,\,t}$) that can generate a flow in liquid. Thus, we have obtained the radiation reaction force for a perfectly linear compressible nonviscous medium (unlike [10]). Now consider the case when the pattern (1) of normal vibrational velocities (at the boundary $z = 0$)

$$U_0(x,t) = \sum_{h_{0\mathrm{n}}>0} u_{0\mathrm{n}} e^{i\omega_0 t - i h_{0\mathrm{n}} x} + \sum_{h_{0\mathrm{n}}<0} u_{0\mathrm{n}} e^{i\omega_0 t - i h_{0\mathrm{n}} x} \qquad (25)$$

represented by a set of sinusoids at spatial frequencies $\{h_{0\mathrm{n}}\}$ and with amplitudes $u_{0\mathrm{n}}$ ($\mathrm{n} = 1,2,3,\ldots$). Some of these sinusoids run to the left ($h_{0\mathrm{n}} < 0$), some of the sinusoids run to the right ($h_{0\mathrm{n}} > 0$). Accordingly, the projection $(< \mathbf{F} >_{x,t})_x$ of the tangential force $< \mathbf{F} >_{x,\,t}$ (per unit area of the plane $z = 0$) of the radiation reaction on the axis "x" is presented by term $(< \mathbf{F} >_{-})_x$ (caused by spatial harmonics running to the left, i.e. $h_{0\mathrm{n}} < 0$, $\mathrm{n} = 1,2,3,\ldots$) and term $-(< \mathbf{F} >_{+})_x$ (caused by spatial harmonics running to the right, i.e. $h_{0\mathrm{n}} > 0$, $\mathrm{n} = 1,2,3,\ldots$):

$$(< \mathbf{F} >_{x,t})_x = (< \mathbf{F}_{-} >_{x,t})_x - (< \mathbf{F}_{+} >_{x,t})_x\ , \qquad (26)$$

where, using (10) and (23), we can write

$$(< \mathbf{F}_{-} >_{x,t})_x = \sum_{h_{0\mathrm{n}}>0} |u_{0\mathrm{n}}|^2 c_{\mathrm{Un}}^{-1} \omega_0 \rho (k_0^2 - h_{0\mathrm{n}}^2)^{-1/2} \mathbf{I}(k_0 - |h_{0\mathrm{n}}|)\ , \qquad (27)$$

$$(< \mathbf{F}_{+} >_{x,t})_x = \sum_{h_{0\mathrm{n}}<0} |u_{0\mathrm{n}}|^2 c_{\mathrm{Un}}^{-1} \omega_0 \rho (k_0^2 - h_{0\mathrm{n}}^2)^{-1/2} \mathbf{I}(k_0 - |h_{0\mathrm{n}}|)\ , \qquad (28)$$

where $\mathbf{I}[\xi]$ -Heaviside step function (see (8)), $c_{\mathrm{Un}} = \omega_0 / |h_{0\mathrm{n}}|$. From (26)-(28) it is easy to see that the value (26) is the balance of the power of waves radiated to the right ($h_{0\mathrm{n}} > 0$) and the power of waves radiated to the left ($h_{0\mathrm{n}} < 0$).

5. Cylinder (azimuthal phasor)

Next, we will continue to consider examples of resonant radiation by various patterns. Let's consider patterns with a finite curvature of a bearing surface - an infinite cylindrical surface S of pattern with a cross-sectional radius R, on which a certain distribution $U_0(\mathbf{r},t)$ of normal vibrational velocities is given (Fig. 4-a).

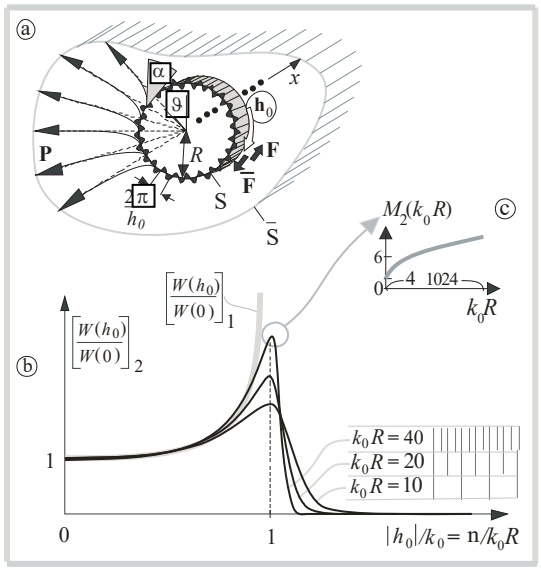

Figure 4. The phase runs along the azimuth ϑ of the cylinder S: (a) geometry of the boundary value problem; (b) normalized radiation resistance $[W(h_0)/W(0)]_2$ at different wave sizes k_0R of the cylinder cross-section, (the gray line shows the function $[W(h_0)/W(0)]_1$); (c) dependence of the peak value M_2 on k_0R.

Using the cylindrical wave equation (instead (3))

$$r^{-1}\left(r\psi_r'\right)_r' + r^{-2}\psi_{\vartheta\vartheta}'' = c^{-2}\psi_{tt}''\ , \qquad (29)$$

(where r, ϑ are the corresponding cylindrical coordinates of point $\mathbf{r}$) for pattern

$$-\left(\psi_r'\right)_{\kappa=K} = U_0(\mathbf{r},t) = \exp(i\omega_0 t - ih_0 R\vartheta) \qquad (30)$$

(the phase runs in the azimuthal direction ϑ, $0 \le \vartheta < 2\pi$, $-\infty < x < +\infty$, $\partial/\partial x = 0$) we obtain the normalized radiation resistance (Fig. 4-b)

$$\left[\frac{W(h_0)}{W(0)}\right]_2 = \frac{\mathrm{Re}\left[i\left(\mathrm{H}_\mathrm{n}^{(2)}(\xi)\right)/\left(\mathrm{H}_\mathrm{n}^{(2)}(\xi)\right)'_\xi\right]_{\xi=k_0R}}{\mathrm{Re}\left[i\left(\mathrm{H}_0^{(2)}(\xi)\right)/\left(\mathrm{H}_0^{(2)}(\xi)\right)'_\xi\right]_{\xi=k_0R}} \qquad (31)$$

of such a pattern, where, of course, only discrete points $h_0 = \mathrm{n}/R$ have a mathematical (and physical) meaning ($\mathrm{H}_\mathrm{n}^{(2)}(\xi)$ is the Hankel function of the second kind of the n–th order, $\mathrm{n} = 0,1,2,...$). Looking at the evolution of the graphs of the magnitude $\left[W(h_0)/W(0)\right]_2$ with increasing k_0R, one could assume that

$$\lim_{k_0R\to\infty}\left[W(h_0)/W(0)\right]_2 \overset{?}{=} \left[W(h_0)/W(0)\right]_1. \qquad (32)$$

However, the convergence of these values significantly slows down (this can be judged by the slowdown in the growth of the maximums (varying h_0)

$$M_2(k_0R) = \max_{h_0}\left[W(h_0)/W(0)\right]_2. \qquad (33)$$

Power flux lines $\mathbf{P}$ exit the cylinder surface at an sliding angle $\alpha = \arccos(h_0/k_0)$ of inclination (i.e. $\cos(\mathbf{h}_0\mathbf{P}) = h_0/k_0$, $0 \le \alpha \le \pi/2$, see Fig. 4-c) and become straight radial in the far zone at the distance $>> R^2 h_0$. In book [4], for example, the author could get the resonance dependence (Fig. 2-a) if he would normalized the ordinate by $W(0)$, and the abscissa by k_0 and considered the *discrete* azimuthal frequencies $h_0 = \mathrm{n}/R$ ($\mathrm{n} = 1,2,3,...$) as interpolation nodes on the continuous axis of spatial frequencies. Note that the integral flow of the Poynting vector $\mathbf{P}$ through an arbitrary closed cylindrical surface $\overline{\mathrm{S}}$ (which embraces S) is equal to the integral power flow on the surface S of the cylindrical radiating pattern (Fig. 4-a).

6. Cylinder (axial phasor)

Now for the cylindrical wave equation (instead (29))

$$r^{-1}\left(r\psi_r'\right)'_r + \psi''_{xx} = c^{-2}\psi''_{tt} \qquad (34)$$

we consider the pattern (boundary condition)

$$-\left(\psi_r'\right)_{\kappa=K} = U_0(\mathbf{r},t) = \exp(i\omega_0 t - ih_0 x), \qquad (35)$$

where the phase runs along the axis of the cylinder S ($-\infty < x < +\infty$, Fig. 5-a). So the normalized radiation resistance of such a pattern looks like

$$\left[\frac{W(h_0)}{W(0)}\right]_3 = \frac{\mathrm{Re}\left[i\left(\mathrm{H}_0^{(2)}(\xi)\right)/\left(\mathrm{H}_0^{(2)}(\xi)\right)'_\xi\right]_{\xi=k_0R\sqrt{1-(h_0/k_0)^2}}}{\mathrm{Re}\left[i\sqrt{1-(h_0/k_0)^2}\left(\mathrm{H}_0^{(2)}(\xi)\right)/\left(\mathrm{H}_0^{(2)}(\xi)\right)'_\xi\right]_{\xi=k_0R}} \qquad (36)$$

(Fig. 5-b). Note that here the argument ξ of the Hankel function $\mathrm{H}_0^{(2)}(\xi)$, when passing from $|h_0| < k_0$ to $|h_0| > k_0$, turns from purely real to purely imaginary. The quantity $\left[W(h_0)/W(0)\right]_3$ is closing to $\left[W(h_0)/W(0)\right]_1$ faster than $\left[W(h_0)/W(0)\right]_2$ (see the function

$$M_3(k_0R) = \max_{h_0}\left[W(h_0)/W(0)\right]_3, \qquad (37)$$

varying h_0, in Fig. 5-c). Power flux lines $\mathbf{P}$ exit the cylinder surface in a taper angle $\alpha = \arccos(h_0/k_0)$ (i.e. $\cos(\mathbf{h}_0\mathbf{P}) = h_0/k_0$, $0 \le \alpha \le \pi/2$).

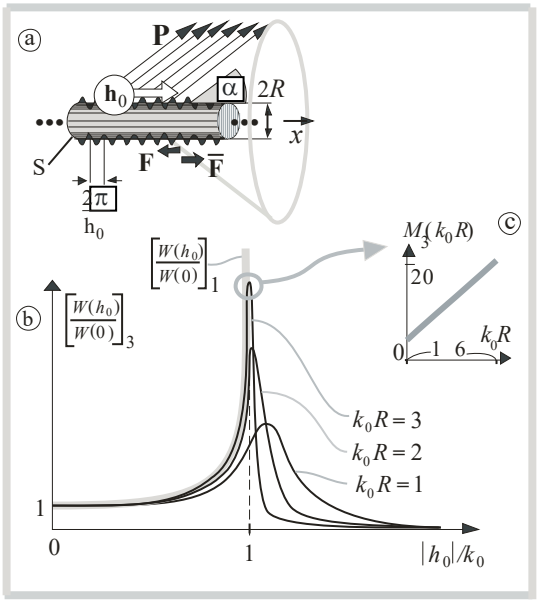

Figure 5. The phase runs along the axis "x" of cylinder S: (a) geometry of the boundary value problem; (b) normalized radiation resistance $\left[W(h_0)/W(0)\right]_3$ at different wave sizes k_0R of the cylinder cross-section, (the gray line shows the function $\left[W(h_0)/W(0)\right]_1$); (c) dependence of the peak value M_3 on k_0R.

7. Linear Chain of Acoustic Monopoles

Let us also consider the opposite example (with setting the speed, but without resonance) - a ruler (length $2L_0$) $2\mathrm{N}+1$ equidistantly (with a period $\ell = L_0/\mathrm{N}$, $k_0\ell << 1$, $\mathrm{N} = 1,2,3,...$) of distributed pulsating spheres

(acoustic monopoles) with radii $a << \ell$ (Fig. 6-a). Here, as in the previous sections, we set the normal vibrational velocity, but already on the surface of discrete pulsating spheres. The sinusoidal (with frequency ω_0) pulsations of the spheres are given the same amplitudes, and the phases of the pulsations are set linearly according to the law $\exp(-ih_0\ell\,\mathrm{n})$, where n is the sphere number ($-\mathrm{N} \le \mathrm{n} \le +\mathrm{N}$), $h_0 = |\mathbf{h}_0|$ is the phasor module $\mathbf{h}_0$. Thus this is a wellknown 3D travelling wave antenna [9]. Then, for the normalized radiation resistance of the pattern (chain of monopoles), we obtain the expression

$$\left[\frac{W(h_0)}{W(0)}\right]_4 = \frac{\int_0^{\pi}\sin(\vartheta)B^2(\mathrm{N},\ell,k_0,h_0,\vartheta)d\vartheta}{\int_0^{\pi}\sin(\vartheta)B^2(\mathrm{N},\ell,k_0,0,\vartheta)d\vartheta}, \qquad (38)$$

where

$$B(\mathrm{N},\ell,k_0,h_0,\vartheta) = \frac{\sin[(2\,\mathrm{N}+1)(k_0\cos(\vartheta)-h_0)\ell/2]}{\sin[(k_0\cos(\vartheta)-h_0)\ell/2]}. \qquad (39)$$

The function $[W(h_0)/W(0)]_4$ graph (Fig. 6-b) has no resonance, and

$$\lim_{L_0k_0\to\infty}\left[W(h_0)/W(0)\right]_4 = \mathbf{I}[k_0 - |h_0|]. \qquad (40)$$

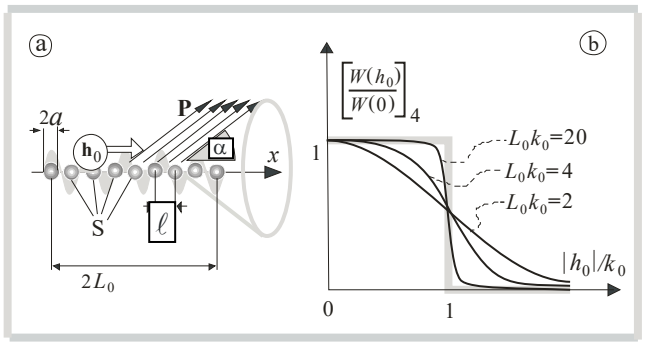

Figure 6. Linear chain of acoustic monopoles: (a) geometry of the boundary value problem; (b) normalized radiation resistance of the chain of monopoles at different wave sizes L_0k_0 at $k_0a << k_0\ell << 1$.

The difference between the boundary value problem and the previous ones lies in the absence of diffraction (small scattering on rigid fixed spheres) of the fields of pulsating spheres on each other due to their small wave sizes ($ka << 1$) and relatively large distances ($\ell >> a$) between their centers. Surface S becomes lumped into a set of $2\,\mathrm{N}+1$ small spheres (see Fig. 6-a). In other words, we summarize in the far zone the fields of the single pulsating spheres that each of them creates in a space free from other spheres. In the same way, there is no resonance when noninteracting spheres are placed on a ring (if we try to formulate the problem in Section 5 in a similar way). For ($ka << 1$) $\cap$ ($\ell >> a$) it is indifferent (for $[W(h_0)/W(0)]_4$) to make given velocity or pressure on the spheres. This is probably the reason for the absence of resonance. The maximum radiation power of the line of monopoles corresponds to the direction of the Poynting vector $\mathbf{P}$ in a cone with an inclination angle $\alpha = \arccos(h_0/k_0)$ (i.e. $\cos(\mathbf{h}_0\mathbf{P}) = h_0/k_0$, $0 \le \alpha \le \pi/2$). The radiation pressure is present as in above sections.

8. Spatially Localized Pattern on a Plane. For a rough estimate of the effect of amplification of acoustic radiation using a phasor $\mathbf{h}_0$ (at $|h_0| \to k_0$) at constant module of normal velocity amplitudes, we now consider (for the subsequent spectral representation) a pattern $U_0(\mathbf{r},t) = U_0(x,y,t)$ localized on the plane $z = 0$ ($-\infty < x, y < \infty$) in the following form:

$$U_0(x,y,t) = [\mathrm{sinc}(\pi x/L_0)\,\mathrm{sinc}(\pi y/L_0)]\exp(i\omega_0 t - ih_0 x), \qquad (41)$$

where $\mathrm{sinc}(\xi) = \sin(\xi)/\xi$, L_0 -space scale of localization. We need to estimate the ratio of the total power emitted by the pattern (41) at $h_0 = 0$ (Fig. 7–a) and the total power emitted by the pattern (41) at $h_0 \ne 0$ (Fig. 7–b). Below we will consider the boundary-value problem of radiation as a low-frequency filter of spatial frequencies with a transmission coefficient (13) (in terms of power (Fig. 7-c)

$$[W(h)/W(0)]_1 = \mathbf{I}[k_0 - h]/\sqrt{1-(h/k_0)^2}, \qquad (42)$$

where $\mathbf{I}[\xi]$ -Heaviside step function (see (8)),

$$h = \pm|\mathbf{h}| = \pm\sqrt{h_x^2 + h_y^2}, \qquad (43)$$

h_x, h_y are the components of the vector $\mathbf{h}$ ($\mathbf{h} \parallel (z=0)$) of the spatial frequency along the axes "x" and "y", respectively (Fig. 7-d). Let's write the spatial Fourier spectrum of pattern (41) as

$$\tilde{\tilde{U}}(h_x,h_y;h_0) = \int_{-\infty}^{\infty}\int_{-\infty}^{\infty}U_0(x,y,t)\exp[ih_x x + ih_y y]dxdy. \qquad (44)$$

Using the property

$$\int_{-\infty}^{+\infty}[\sin(\pi x/L_0)/(\pi x/L_0)]\exp(-ihx)dx = L_0\mathbf{I}[(\pi/L_0) - |h|] \qquad (45)$$

of the function $\sin(\xi)/\xi$, we obtain Fourier spectrum

$$\tilde{\tilde{U}}(h_x,h_y;h_0) = L_0^2\,\mathbf{I}[(\pi/L_0) - |h_x - h_0|]\,\mathbf{I}[(\pi/L_0) - |h_y|], \qquad (46)$$

and, accordingly, $[W(h_0)/W(0)]_5 = Q(h_0)/Q(0)$, where

$$Q(h_0) = \int_{-\infty}^{\infty}\int_{-\infty}^{\infty}\left[W(\sqrt{h_x^2+h_y^2})/W(0)\right]_1\left|\tilde{\tilde{U}}_0(h_x,h_y;h_0)\right|^2 dh_x dh_y. \qquad (47)$$

Fig. 7-e presents graphs of the magnitude $\left[W(h_0)/W(0)\right]_5$ for three wave sizes $2k_0L_0$ of the pattern (41) and the dependence of the maximum (at varying h_0) value (as peak)

$$M_5(2L_0k_0) = \underset{h_0}{\text{Max}}\left[W(h_0)/W(0)\right]_5 \qquad (48)$$

on wave size $2k_0L_0$ (or area of spatial localization) of the pattern (41). It is not hard to see that for $\left|k_0 - |h_0|\right|/k_0 \to 0$ (i.e. $|h_0|$ is closing to k_0) we obtain the value

$$\left[W(h_0 \approx k_0 - L_0^{-1})/W(0)\right]_5 \approx \sqrt{k_0L_0} >> 1. \qquad (49)$$

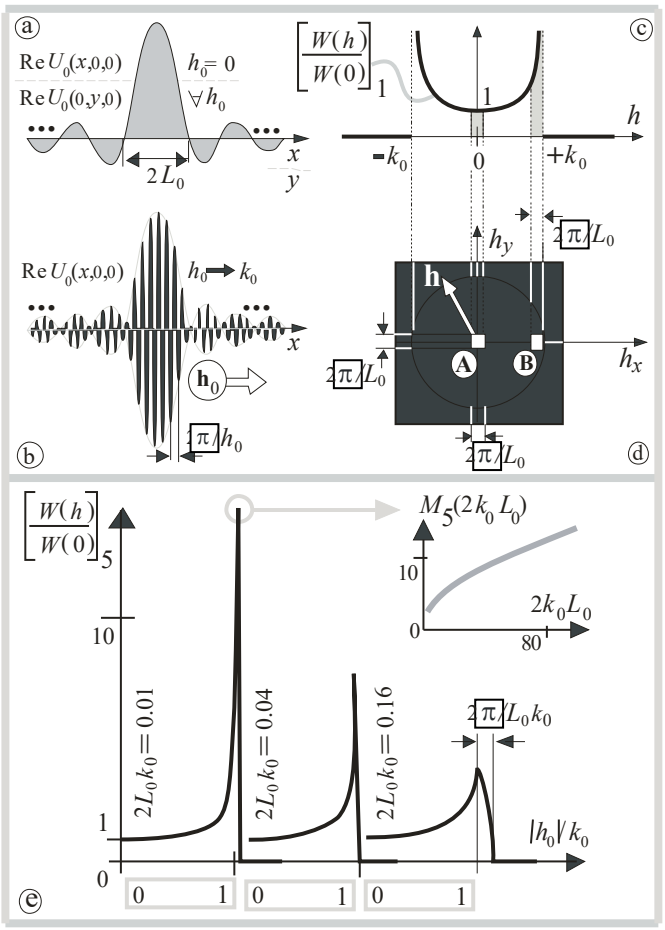

Figure 7. On the spatially localized pattern (41) on the infinite plane: (a) "x" $h_0 = 0$; (b) "x" $h_0 \to k_0$; (c) one dimensional section $\left[W(h)/W(0)\right]_1$ of low pass filter of boundary problem for pattern (41); (d) two dimensional (h_x, h_y, $h = \sqrt{h_x^2 + h_y^2}$) view on the low pass filter characteristics (black area means the no radiation) of boundary problem for pattern (41); (e) normalized radiation resistance $\left[W(h)/W(0)\right]_5$ of pattern (41) at different wave sizes $2k_0L_0$, and value M_5 of its peak as function of wave dimension $2L_0k_0$ of (41).

It can be seen from (49) that the larger the wave dimensions k_0L_0 of the pattern (41), the more effectively and resonantly the pattern with a running phase (at $\left|k_0 - |h|\right|/k_0 << 1$) radiates than the in-phase pattern (at $h = 0$) at a given fixed module $|U_0(0,0,0)|$ of pattern amplitude.

Note that for finite wave sizes of the radiating pattern (sections 5-8, in contrast to sections 2-4), the real part $W(h_0)$ of field power flux on the surface of the pattern and the imaginary part $\overline{W}(h_0)$ are nonzero at all spatial frequencies h_0.

9. Conclusion

In this work, the phenomenon of resonant sound emission by a boundary is analyzed analytically when a pattern is set on it in the form of a running sinusoidal spatial distribution of normal vibrational velocities at a certain temporal frequency (Section 1).

The initial problem is the resonant emission of sound by a spatially infinite harmonic distribution of normal velocities on an infinite plane (Section 2).

It is shown that setting a sinusoidal distribution of acoustic pressure on the plane does not generate resonant radiation (Section 2). In addition, it is shown that a linear chain of monopoles with a running phase of vibrational velocity amplitudes does not generate a radiation resonance (Section 7).

Further, the effect of the following factors on the magnitude of the resonant peak is estimated: surface curvature along the phasor (Section 5); surface curvature transversal to the phasor (Section 6); limitedness of the pattern in space (localization, Section 8).

A complete analogy of the phenomenon of resonant radiation in two problems is pointed out: (a) in the acoustic problem of Section 2; in the problem of electromagnetic radiation of a flat boundary, on which a traveling distribution of a tangential electric field with a polarization parallel to the phasor is specified (Section 3).

In practice, if we need to obtain the highest radiation power of a certain pattern with a limited dynamic range of actuators, then it would be most expedient to excite a sliding (with respect to the pattern) wave with a distribution of normal vibrational velocities with a traveling phase, and not excite a normal (with respect to the pattern) wave with an in-phase distribution normal vibrational velocities.

It has been shown that a resonantly radiating boundary with a traveling phase is capable of generating a time-constant tangential radiation reaction force and,

consequently, can be used, for example, in designing an acoustic pump or for an active control of hydrodynamic boundary layer (Section 4).

Conflict of Interest

The author declares no conflict of interest.

Acknowledgements

This work was supported by the Russian Ministry for Science and Higher Education, Project No. 0030-2021-0009.

References

[1] John William Strutt Rayleigh, *The Theory of Sound; Volume 2*, Franklin Classics, 978-0341849094, 2018.
[2] L.D. Landau, E.M. Lifshitz, *Course of theoretical physics (Fluid Mechanics)*, Vol. 6, Butterworth-Heinemann, 2 edition, Jan 15, 1987.
[3] L.M. Brekhovskih and O.A.Godin, *Acoustics of Layered Media*, Nauka, Moscow, 1989 (in Russian).
[4] Eugen Skudrzyk, *The Foundations of Acoustics (Basic Mathematics and Basic Acoustics)*, Springer, 1971.
[5] James Lighthill, *Waves in fluids*, Cambridge University Press, London, New York, Melbourne, 1978.
[6] Allan D. Pierce, *Acoustics. An Introduction to Its Physical Principles and Applications*, Third Edition, McGraw-Hill, Inc., 1980.
[7] John D. Jackson, *Classical electrodynamics*, New York: Wiley, 1999.
[8] V.V. Arabadzhi, *Solutions to Problems of Controlling Long Waves with the Help of Micro-Structure Tools*, Bentham Science Publishers, 2011.
[9] C.H. Walter, *Traveling Wave Antennas*, McGraw-Hill, 1965, Dover, 1970, reprinted by Peninsula Publishing, Los Altos, California, 1990.
[10] Robert T. Beyer, "Radiation pressure - the history of a mislabeled tensor," *Journal of Acoustical Society of America*, vol. 63, no. 4, pp. 1025-1030, 1978, doi:10.1121/1.381833.

Vladimir Arabadzhi. Education: Radiophysical faculty of Gorky State University, 1978, dissertation Ph.D – 1994. Research interests: (a) reducing of radiation and scattering of waves of various natures by physical bodies; (b) designing of devices that convert the vibrations of a boat on the surface of a liquid into unipolar pulses of a jet stream. Position: senior researcher in the Institute of Applied Physics (RAS).

JENRS

Received: 12 January 2022, Revised: 13 March 2022, Accepted: 31 March 2022, Online: 12 April 2022

DOI: https://dx.doi.org/10.55708/js0104002

An Overview of Cyber Security Considerations and Vulnerabilities in Critical Infrastructure Systems and Potential Automated Mitigation - A Review

Roberto Mazzolin [1,*], Asad Madni [2]

[1] RHEA Group, Ottawa, Canada
[2] Samueli School of Engineering, UCLA, Los Angeles, California, USA

*Corresponding Author: Roberto Mazzolin, Email: r.mazzolin@rheagroup.com

ABSTRACT: Executive leadership in government, military and industry are faced with many difficult challenges when trying to understand the complex interaction of public and government security policies, the vulnerabilities in the wide array of key technologies supporting critical infrastructure upon which society is vitally dependent, and the identification of key cyber security trends that will need to be considered in the future. This invited paper discusses public policy issues related to the threat environment and provides a comprehensive description of the various cyber vulnerabilities and risks arising from a broad range of technologies supporting critical infrastructure and highlights key requirements and design principles desired from next generation automated defence capabilities. This document provides a unique review of key aspects related to these separate but interrelated subject areas that will hopefully provide greater context, background and clarity for senior decision makers responsible for shaping development agendas for their organizations.

KEYWORDS: Critical Infrastructure, Mitigation, Leadership

1. Introduction

Senior executive leadership in the government, military and industry communities are faced with an increasing degree of complexity when confronting the contemporary cyber security threat to the critical infrastructure supporting our societies vital systems that support not only essential systems but also government legitimacy and societal stability. The discussion related to potential approaches is made even more complex when considering the current challenging threats against the broad range of technologies that comprise our critical infrastructure and their specific vulnerabilities. The nature of this environment is such that traditional approaches to securing this environment are no longer adequate and potential solutions will need to look toward innovative applications of emerging technologies.

This paper is divided into three sections. The first section highlights public policy issues related to the threat environment and the need for critical infrastructure cyber defense in systems supporting societal resiliency under the following headings: The impact of Cyber, The Threat Environment, Policy, Societal Stability, Critical Infrastructure and Defence and Security. The second section provides an overview of the cyber risk across a broad range of critical infrastructure technologies supporting automated systems under the following headings; Cloud Computing, SCADA, Vehicular Environment. Mobile Computing, Unmanned Aerial Vehicles, Aviation, Space and Artificial Intelligence. Finally, it highlights some key principles desired from next generation automated defensive capabilities. These are treated under the following areas; Mitigation and Automated Defence, Automated Cyber Defence, Automated Defence in Software Defined Radio and Cognitive Radio Networks.

This invited journal paper expands upon an initial paper "A Survey of Contemporary Cyber Security Vulnerabilities and Potential Approaches to Automated Defence" presented at the IEEE Syscon 2020 Conference in Montreal, Quebec, Canada [1]. This paper updates and expands upon the original paper in a number of areas. It

provides greater detail in the treatment of public policy considerations that apply to critical infrastructures in addition to identifying and explaining the potential impact of vulnerabilities inherent in key technologies that underpin these systems. This document adds new contributions in the area of Artificial Intelligence and further develops discussion related to Cloud Computing. It further expands the treatment of cyber security issues relating to SCADA and vehicular and mobile computing technologies. Finally, it further expands upon the initial treatment of techniques related to automated defence supporting mitigation approaches and the application of security in the areas of software defined and cognitive radio technologies that increasingly form the basis for next generation wireless networks. As such, the document serves to provide a unique treatment of a broad range of policy, technology, and future developmental considerations to support executive leadership synthesis of this wide-ranging subject matter.

2. Policy considerations

The impact of Cyber; a double-edged sword in an automated environment – The West's decisive technology superiority holds the potential for its demise. As technology increasingly permeates the functionality provided by critical infrastructure that supports society, our personal lives, economy, defence and security is critically dependent upon the security of internet and connected technologies.

Since the early days of the internet in the 90s, manual approaches to operating critical infrastructure have been rapidly superseded by the adoption of advanced technology in the interest of speed, efficiency and low cost. This focus on flexibility and openness have been at the expense of security.

Our society has arrived at an inflection point where the dependence on technology is ubiquitous, the average millenial has grown up in an online culture and technically expert senior leaders are rare. This paper is an invited paper that expands upon the original paper "A Survey of Contemporary Cyber Security Vulnerabilities and Potential Approaches to Automated Defence" presented at the IEEE Syscon 2020 Conference in Montreal, Quebec, Canada [1]. This paper will examine the nature and import of the cyber threat to the automated systems that power our societies and suggest a way forward in the interest of ensuring the integrity of these systems.

The Threat Environment – The threat presents itself daily in a variety of forms at the geopolitical and economic levels. The collective aggregation of the variety of the many diverse from thousands of cyber attacks across the broad range of systems supporting critical infrastructure could serve to cause grave impact to western innovation and commerce without reaching the threshold of spurring meaningful government engagement and response [2]. The increasing international investment in cyber security and the creation of military Cyber Commands highlights the awakening of many nations to this threat and notable announcements by international leaders have identified the cyber threat among the most serious economic and global security challenges.

Policy – National and institutional ability to address the difficult challenges that encompass the broad domain of cyberspace technology, operations and security are further complicated by the legal and policy development environment that lags rapid technology advancement. Governments are developing an increasing appreciation of the fragility of the national infrastructure and the potential destructive effects of a cyber attack whose effect would be analogous to that of a conventional military attack, but difficult to attribute and more subdued and difficult to identify over an extended period of time. A former Chairman of the House Intelligence Committee, Mike Rogers, indicated that 95% of private networks are vulnerable and had already been penetrated, and introduced the Cyber Intelligence Sharing and Protection Act (CISPA) in November 2011. Further, cyber security expertise is in critically short supply, with the cited global shortage forecasted in 2020 according to the 2019 $(ISC)^2$ Cybersecurity Workforce Study, being 4.07 million cyber security professionals to adequately defend organizations. While efforts to recruit and develop qualified personnel continue, federal policy focused on ensuring privacy, the corporate culture of focusing on the bottom line and the defence and security communities' kinetic warfighting culture may resist supporting these programs.

Societal Stability – Modern democratic societies are confronted with significant challenges in efforts to confront systematic cyber conflict whose intent is institutional destabilization of a targetted state. To that end, information security activities such as assessments are required to develop coordinated, pre-event frameworks that ensure institutional stability, public trust, and limit challenges to the state. Such assessments can take the form of Model Based Simulation and Emulation and supporting exercises that replicate bespoke environments and enable the development of detailed tactics, techniques and procedures or "playbooks" to counter threats. Theories based on Dwight Waldo's theoretical work on nation state stability dependencies depending on factors of legitimacy, Authority, Institutional Knowledge, Bureaucratic Control, and Confidence establish the criteria upon which societies may be destabilized and crippled by a coordinated cyber campaign to reduce institutional entropy [3]. Emerging societal cyberwarfare theories advocate the development of defence strategies in anticipation of massive state actor initiated automated attacks to mitigate risk for societal

system compromise. An important aspect relates to the informational aspect of cyber security, which if manipulated effectively, impacts the confidence and trust that a population has in its government and societal systems. Recent news coverage of impacts on electoral integrity serve as important examples of the scope of potential impact.

Critical Infrastructure - When considering national security, one must recognize the intrinsic relationship between traditional concepts of physical security and economic security. To that end, given societal dependence on the Internet of Things (IOT), and activities related to Health and Insurance, Banking, Financial and Personal Privacy interests, attacks against infrastructure supporting such areas would result in the potential for devastating cyber security events that could threaten our way of life. Critical infrastructure includes technology-based systems and services that provide critical functionality to ensure the security, economic prosperity, and social well-being of the public. Examples of such systems include transportation, communications, water, energy, finance, health, agriculture and government services among others. This potential threat to these areas is further accentuated by the many complex logical, physical and geographic interdependencies and collections of interacting components. As computer systems become more integrated, the distinction between security and safety decreases.

Defence and Security – Militaries serve as extensions of national power and cyber now represents a central element of the contemporary military art. Armed forces have evolved the nature of their operations as we see the establishment of Cyber and Space Commands in most countries. Cyber security is a central consideration in modern military operations given the dependency of command and control, weapon systems, precision timing, intelligence, surveillance and reconnaissance and supporting space systems on networking and automated processing technology. To this end, as the commercial environment has led the development of technology over the past 30 years, this has driven the impetus for enhanced military/industry cooperation. This aligns to the significantly increased emphasis placed on cyber and data protection in the military environment, and cybersecurity research has increased dramatically since 2011. Significant effort has been devoted to the investigation of offensive capabilities that are convergent with the evolving threat to address military mission specific requirements. One example of such an incident is the example of possible Asian military hackers that had attacked two US satellites at least 4 times between 2007 and 2008. Russian cyber attacks, such as those launched against Georgia and the Ukrainian power grid in conjunction with physical proxy operations illustrate the new nature of hybrid operations that are conducted just below the threshold that would normally trigger political or military response on the part of the international community. This potential threat applies to broader national critical infrastructure upon which many military installations and associated communities depend.

When considering the national industry base as a critical element supporting national economic security, such threats, particularly associated with the theft of data from defence contractors and associated subcontractors warn that the West's technical leadership and strategic military advantage are at risk with the ensuing compromise of related national security interests. In this instance, advanced persistent threats (APTs) involving sophisticated infiltration techniques that are beyond the ability of most government agencies and businesses to counter are particularly relevant. Such techniques can be countered through a combination of defence in depth and detection capabilities along with the development of response and recovery plans and security and awareness training.

3. Critical infrastructure technologies

Cloud Computing – Security has been a critical consideration in decisions surrounding the movement of critical institutional data to off site premises. To that end, cloud technology and associated security measures have evolved and new approaches are being used to ensure that data is secured. Recent reports from market research predict that the cloud security market will expand at an annual growth rate of approximately 49% around the globe, thereby highlighting the importance of this area. This growth is driven by increased collaboration between cloud service providers and security solution vendors, along with the perceived reduced ownership costs. Here cloud-based security solutions effectively reduce operational costs to an organization as the maintenance, operation and infrastructure costs and associated risk are handled by a third party. Challenges to this model exist as many new vendors are entering the open source security software market. The clear emphasis within this community is placed on web-based safeguards.

Key emerging trends include greater reliance on a hybrid cloud where data is kept local but applications are provided by multi-provider public cloud infrastructures. There is greater emphasis on protection of data at rest, notwithstanding the traditional focus of securing data in transit. This is achieved through the use of encryption and data centric security in light of the increasingly malicious environment and advanced persistent threats that target this environment. Additional restrictions arise from the imposition of data residency and sovereignty laws as a result of nation state surveillance and related privacy considerations and regulations. To address this, tokenization techniques which substitute critical information with fewer sensitive substitutes are used to counter unauthorized access and data surveillance.

Malware threats and hactivism, given their capability to launch large scale denial of service attacks and wipe out data are driving greater emphasis on server security. The increasing use of an increasing variety of devices such as smartphones, internet connected printers, smart televisions, DVD players, and peripheral devices, mandates the employment of increasingly comprehensive security strategies to protect their services. Multi-Factor authentication is driven by the weakness of traditional username and password approaches. Such techniques involve the increasing use of single use codes that are transmitted to separate users' devices and accounts to protect very sensitive information, and is increasingly being used in financial and healthcare industries. Finally, breach insurance has become an increasing trend. As the reality of "not a matter of if, but when" compromises will occur, enterprises are taking a more pragmatic approach to cloud security. This is forcing enterprises to consider adoption of cloud insurance along with the application of security measures to combat risks.

Supervisory Control and Data Acquisition (SCADA) – Smart city initiatives which depend on highly interconnected traffic control, building automation, electrical grids, communications, water, HVAC, video/security, systems are subject to security threats to architectures in light of the many vulnerabilities. The significant security concerns relate to principal vulnerabilities related to control system environments that are present in a number of areas. As communication systems increasingly link smart grids and associated systems, the corresponding increase in access points translates into greater surface exposure and complexity. Further, given that smart grid systems increasingly use similar commercial service providers and computing technologies, a greater proportion of the infrastructure will be exposed to similar vulnerabilities. Additional risk is incurred as increased automation further generates, gathers and processes data in new ways as smart grid technologies embrace and automate new functions.

There is a requirement to reconsider SCADA threat models to represent a broader security context and develop more unified frameworks that coalesce security and safety risk. Intelligent automated tools and techniques specific to SCADA systems are being developed to enable more progressive methods of risk management so as to require minimal human intervention to control processes and provide defence in depth.

The perception that SCADA systems are difficult to attack is contrary to reality as many tools openly exist on the Internet, such as the Shodan computer internet search engine that provides a search engine for network devices such as routers, servers and load balancers and provides detailed information on potential targets including authentication techniques that in many instances are not updated. SCADA architectures typically support a variety of components that sense process variables and operate equipment connected to programmable logic and process automation controllers, remote terminal units, intelligent electronic devices. These local processors often communicate over various ranges to host computers using a variety of legacy wireline connections such as leased dial up lines, ADSL, cable and fibre in addition to wireless communications such as private radio, cellular, spread spectrum, WLAN or satellite networks. These connect to host computers that serve as a central point for monitoring and control of overall system processes and databases and display statistical control information and reports.

SCADA architectures primarily TCP/IP, UDP and other IP based protocols as well as proprietary industry protocols like Modbus TCP and Modbus over TCP or UDP. Architectural decisions are often driven by practical considerations related to existing and available communications infrastructure, particularly at remote sites, signalling protocols, installation budgets and the ability to meet future needs. Such systems typically comprise hundreds of thousands of input/output channels at speeds of up to 1Mb/s. Hardware and software used in SCADA systems has evolved over the decades with a greater dependence on personal computers and TCP/IP which in turn have become of increased concern due to terrorist threats. Internet and mobile connectivity architectures have evolved, and as such, security concerns have led to the introduction of new features such as encryption and dedicated access controls. Although systems historically were isolated from the Internet, notwithstanding the limited connectivity, these systems are still vulnerable to both external and internal threats through the exploitation of vulnerabilities within operating systems, data storage software as well as custom and vendor software, databases and applications. Commercial standardization is creating pressure to use open market COTS technologies that rely upon complex software applications involving time criticality, embedded systems, distributed, intelligent, fault tolerant, distributed and heterogeneous systems. Notwithstanding the greater awareness of terrorist related risks and hostile state based attacks, such threats are often misunderstood or underestimated. Further architectural challenges relate to an increased reliance on web technologies such as ActiveX, Java and OPC to support internal communications between client and server modules.

Web based applications are increasingly targetted by automated cyber attacks as web development has emerged as a key software development platform and secure web-based software development remains immature. Consequently, Web application vulnerabilities are still exploited by highly sophisticated Web worms. Further, the common software environment upon which all SCADA systems are developed present similar vulnerabilities which may be more easily and widely

exploited. Although UNIX based systems have served as the historical standard, they have now been displaced by Linux and Windows based operating systems which contain a greater range of vulnerabilities that may be more readily exploited over time. A further cultural challenge compounding such vulnerabilities relates to the expectation on the part of plant operators that software should run for extended periods of time without oversight, monitoring, modification or patching even though SCADA vendors annually release enhanced versions based on new technologies and to compete for market opportunities. The vulnerabilities associated with Linux and Windows based operating systems centre around the larger number of lines of code. Typically cited studies of software reliability estimates that Linux kernels have more than 15000 bugs for 2.5 million lines of code, whereas Windows has a proportionally larger number of bugs commensurate with its increased size. As operating system bugs pose higher risk than those in application programs, a serious concern arises given the high concentration of Windows in computers supporting SCADA environments. In this case, the principal vectors for exploitation are software design, operations and human interfaces.

A cultural element exists related to challenges in software intensive control system design given that development requires both Control Engineers and Software Programmers, who have different perspectives and working practices, and frequently lack the overarching picture for the overall responsibility associated with ensuring enterprise level security. The unique nature of the vulnerabilities that exist in the SCADA environment that may not be modeled or understood by these practitioners creates further challenges. As there are comparatively few global SCADA system providers, the commonality of technology between the various SCADA systems, the often inter-related corporate systems that they support, and the Internet, represent a principal cause of further significant risk.

Risk management and vulnerability of SCADA systems is a relatively new area of development as the practice as the CERT and NIST began publishing SCADA vulnerabilities in 2005. Companies have been reticent to divulge vulnerabilities and compromises of their systems and few standards exist to provide guidance. Key issues that require attention include critical path protection, safety policies and procedures, knowledge management, system development skills in both control system engineering and software development for distributed control systems. Further effort is required in the areas of enhanced security feature development for sensor networks, micro-kernal architecture operating systems and increased software security features.

Additional system design concerns relate to adherence to accepted standards during the requirements and development phases of the system lifecycle and integration of new technologies. Further security architecture and associated policy recommendations include the implementation of more rigorous security for corporate and enterprise network connections to the internet, a complementary security zone architecture to isolate critical networks, and the addition of multiple screened subnets or demilitarized zones with no transit traffic. Further, architectural solutions should permit no connections between security zones that are not firewall protected and that inventories of remote access paths entering the architecture be taken to ensure that no connections bypass a firewall infrastructure. Finally, any remote access should be through a VPN connection with strong access controls. Additional policy measures include greater innovative risk management approaches using adaptive, proactive discovery solutions that focus on identifying and mitigating both natural and man-made disruptions through various vectors such as human error, sabotage and terrorism.

Vehicular Environment – Many cyber defence concerns in the vehicular environment across the spectrum of manually operated to fully automated controlled vehicles. The complexity arises from the many electronic control units (ECUs), typically numbering from 30-100, more than 100 actuators, 4000 signals, and typically between 70-100 sensors that are interfaced to both wired and wireless external interfaces for sensors receiving input from accelerometers, cameras, radars, sonars, temperature and rain sensors to control the vital vehicle functions such as navigation, steering and braking. When combined, over 25 Gbytes of data is produced per hour. Consequently, key safety features are vitally reliant upon the ability of these ECUs to communicate with one another. Attacks against such systems may be launched via wireless means by accessing the vehicle telematics system that is responsible for managing an impressive amount of information and typically contain more than 100 million lines of code. Uconnect, an entertainment system, is one example of such a protocol that interfaces to the internet for both GPS navigation and entertainment.

Generally, vehicle based cyberattacks occur in three phases; first by gaining access to the vehicles' ECU, followed by injection of malware into the ECU, and finally activation of the code. Generally, such an attack is complex and expensive as the nature of egress must be gained via direct and indirect physical connections as well as short and long range wireless connections in order to gain full control over a vehicles automated functions. Potential avenues to mitigation involves the analysis of the Controller Area Network (CAN) packet traffic over extended time periods to detect anomalous traffic and disconnect the associated automated functionality. The CAN is the preferred bus for in-vehicle communications

to exchange data as it is reliable in noisy electromagnetic environments. This is accomplished by collecting data streams to detect offending code and associated IP addresses. Additionally, WiFi and Bluetooth signal blockers may be used to protect against untrusted wireless connections near the vehicle. Commercial 3G/4G telematics and IEEE 802.11p protocols are used to provide general connectivity and inter vehicle communications as major software developers seek to gain a strong hold on the vehicle market space. This exposes vehicles to the wide array of Internet of Everything (IoT) threats most commonly experienced on more traditional networks. Vehicles currently rely on multiple of ECUs with processing power in the order of 100MB to manage a variety of processes and peripherals connected via Bluetooth and proprietary manufacturer systems like the GM OnStar system. The simple, low level CAN bus supports data transfer at speeds ranging from 125kbp/s - 1MB/s. The CANbus standard is also used in the aerospace and industrial automation sectors.

The inherent weakness with this protocol is that it does not implement any security features such as sender identification and authentication, thereby facilitating spoofing. Therefore all security functionality must be provided by higher level applications. CAN bus hacking can be achieved by simple chipsets to bypass encryption within the vehicle prior to reading and writing data from a vehicles ECU memory. It can then be wirelessly triggered to launch a programmed attack. Given that all vehicular systems are connected to the CAN Bus, automated wireless access typically involves targeting power door locks, MP3 via iPod, infecting USBs and discs either directly or remotely through interconnected devices and OBD-II diagnostic ports. The dedicated OBD-II port is the most common avenue of access and dedicated Windows diagnostic scan tools are readily available that are designed to both gather information and program ECUs, which can serve as a ready access for malevolent actors. Short range devices include WiFi, Bluetooth, WiFi, wireless key fobs, keyless entry, tire pressure monitoring and RFID systems. Depending on the frequency band used, these may be effectively targeted by placing a wireless transmitter within 5-300 metres from the vehicle. For example, as vehicles increasingly employ Bluetooth to enable hands free calling, a compromised smartphone can be used as an access point into the vehicles telematics environment and enable access to critical vehicle ECUs.

A significant development is the increasing adoption of the SAR J2534 Passthru standard. This is a Windows based Data Definition Language application programming interface that can communicate over both wireless and ethernet with the CAN bus and facilitate injection of malicious binary code via a shell injection interface to control a vehicles' programming. Consequently, a PassThru device compromise via WiFi or Ethernet connectivity may be used to affect multiple vehicles via subsequent connections to activate viruses on specific dates or when a specific event or vehicle condition is met. Of further note, electric cars may also be subject to compromise through connectivity via charging infrastructure.

The abundance of programs developed by third parties for the mobile device market has created a demand for vehicle manufacturers to rapidly offer infotainment capabilities which can download software. Longer range broadcast receivers that provide access to GPS, Digital Radio, Satellite Radio, Radio Data Systems and Traffic Message Channel signals are now integrated into increasingly complex vehicle telematic systems. GM OnStar, Ford Sync, Lexus Enform, Toyota Safety Connect, Mercedes Mbrace, and BMW Assist all connect via data and 3/4/5G cellular voice and SMS data networks to internet based location and navigation, crash reporting, diagnostics, mechanical fault alerts, anti theft remote tracking and disablement, hands free data access convenience and safety. Again, connectivity to vehicle telematics enables CAN bus access and the opportunity to exploit the vulnerabilities of these well understood commercial protocols. Although vehicle hacking presents significant challenges, the interactive nature of traditional computer exploits would be more difficult to effect given the nature of vehicular infrastructure. Therefore, the most likely scenarios for such attacks would be related to serious crimes such as erasing information from vehicular event data recorders and theft, and targeted attacks against very high value targets, kidnapping and assassination.

Mobile Computing – The Google's Android, Apple's iOS and RIM Blackberry have accounted for the vast majority of the mobile device market within the US. This has driven access to portals, productivity tools and back end transactional and reporting systems to provide convenience, functionality and efficiency for the commercial workforce. This presents significant data security issues as users, when choosing a smartphone, generally do not consider the mobile platform that their company supports. Although Blackberry had afforded greater security, iPhone and Android devices have been targeted by increasing malware as criminals saw greater egress to these environments. Relatively few users appear sensitive to the threats as the installation of security applications onto smartphones is comparatively low, thereby placing the onus on companies to protect their networks.

Two major areas that impact mobile security involve application markets and file synching and transfer services. Given the demand for easily downloadable applications and the current immature state of security development in this market, industry will need to more closely examine the application review process or create increasingly proprietary application stores to counter

irresponsible downloading of applications. Here the significant volume of data breaches result from data that is constantly moving between host storage sites which is either lost or intercepted in transit. Mitigation approaches include the use of encrypted virtual private networks through centrally managed platforms to ensure that the mobile device environment maintains a security posture commensurate with that of enterprise desktops and servers. This environment however, can still be infected through the importation of infected applications. Key enterprise policy governance regarding all connected devices should focus on greater centralized mobile device management, strong access governance through password and two factor` authentication. An additional step should involve implementation of mobile application software to support the protection of endpoints and enable network administrators to handle increasingly sophisticated threats.

Unmanned Aerial Vehicles (UAVs) – The rapid increase in use of UAVs and drones supporting first responder, military and commercial civilian environments has generated an increased emhphasis on security. A notable event demonstrating both the vulnerability of previously believed sophisticated and secure systems as well as national capacity and intent involved the 2011 Iranian cyber attack that led to the capture of a US military UAV in northeastern Iran. Key vulnerabilities impacting UAVs arise from the use of autopilot components taken from larger aviation applications. These include GPS, magnetometers, inertial measurement units (IMUs), actuators, manual controls and associated payload technologies such as video, radio relay and telemetry links. Magnetometers and IMUs which receive onboard platform sensor input, can cause crashes if given wrong information. Actuators are managed by information from main processing boards that also derive data from sensors and pre-programmed hardware and firmware commands are subject to denial of service from malicious data injection attacks. Wireless spoofing attacks have been well demonstrated and traditional approaches to ensure signal integrity against sophisticated attacks are inadequate. Spoofing of GPS, video feeds and Automatic Dependent Surveillance-Broadcast (ADS-B) devices can also lead to complete loss of platform control. The pervasive IEEE 802.xx and WIFI protocols in the 925 MHz, 2.4 and 5 GHz frequency bands provide a ready environment for hacking.

There are a number of readily available applications such as SkyGrabber, which can receive commercial satellite feeds, SkyJack, which enables the control of multiple drone, and Snoopy, which is a capability that enables distributed WIFI, RFID. 802.11 tracking and profiling. All these can be employed to monitor and perform unauthorized control over UAV functions in the absence of radio frequency link encryption. Given the obvious challenges associated with the employment of encryption, particularly in sensitive government and military environments, potential approaches to mitigation could involve the use of software to identify abnormalities and counter data injection attacks against UAV system components and correlate with other on-board sensors to recognize and rationalize incongruities.

Ground stations are subject to vulnerabilities associated with smart device applications that are used to operate and control UAVs. The wide range of malware that impact traditional networks can also be used to penetrate and exploit UAV systems. For example, key logger software has been detected onboard UAVs as well as in associated ground station infrastructures despite efforts to segregate such mission specific networks from the internet. In this instance, effective mitigation measures should include the strong management of smart devices and associated software applications to ensure the secure download and use of applications. Additional threats to ground station capabilities involve hardware based attacks against USBs that facilitate surveillance, traffic flooding and cause battery exhaustion. The reliance on Android based mobile device operating systems that provide a familiar PC based environment facilitates common software based attacks such as botnets, trojans, key loggers, rootkits and worms. Such embedded malware can be used to gather sensitive information and gain control of the infrastructure and disrupt operations. The implementation of encryption, authentication, firewalls and development measures such as fuzz testing to identify and counter security vulnerabilities, particularly malware in foreign sourced hardware and software is effective, however, there is no guarantee that testing can detect all malware, particularly bespoke code targeting specific capabilities.

Aviation – Commercial airline incidents in recent years have generated awareness regarding the potential for penetration of aircraft and the compromise of pilot control over vital on-board systems. Aircraft infrastructure is comprised of a complex array of separate systems supporting specific functions that are mediated by an over-arching software component that can be compromised through corrupted traffic in the various sub-components. Topical theories highlight potential vulnerabilities to wireless radio signals transmitted by small devices or platform based attacks against in-flight entertainment systems. There is a challenge in dealing with radio frequency based vulnerabilities given the requirement for various transponders, cockpit radios and Aircraft Communications Addressing and Reporting System (ACARS) to exchange status information with air traffic control.

As it regards the aircraft data bus, access to critical platform and data networks supporting aircraft control can be achieved gained via connections between passenger service computer network using USB ports and Ethernet. Android based hacks against the Flight Management System (FMS) have been demonstrated by

monitoring the systems communications and injecting bespoke code to modify navigations parameters and ADS-B and ACARS systems. A further vulnerability relates to the emergency intervention system that enables a ground based remote operator to land an aircraft using the autopilot.

NextGen navigation systems employ GPS data instead of traditional radar to track aircraft movement. Currently, the positioning information exchanged between aircraft and ground control systems are unencrypted and communication is established without mutual authentication. One potential attack scenario against the navigation system involves the injection multiple spoofed aircraft position inputs to overwhelm air traffic control and corrupt the position, location, direction and velocity data of other aircraft provided to pilots. Further navigation based attacks can be launched through the use of radio frequency jamming against radar by injecting false returns or noise and repeater based techniques to disrupt radar receivers that are designed to receive highly concentrated energy transmissions. Such jamming and flooding "denial of service" techniques against ground based radars can result in the loss of critical messages which could drive the emergency adoption of less accurate and inefficient surveillance and control mechanisms. This would cause compromise of surveillance and collision avoidance systems with disastrous consequences in dense traffic environments near major urban centres. In light of such vulnerabilities, the development of aircraft and navigation system software and hardware integrity standards for the aviation industry represent imperative elements of air worthiness standards to counter an increasing cyber threat.

Space – Virtually all earth-based critical infrastructure have some dependency on space based capabilities. The 2014 hacking of a US NOAA weather satellite forced the associated Satellite Data Information System offline, preventing the dissemination of forecasting data to international weather agencies for 48 hours. Cyber threats against space assets involve tracking and monitoring satellite transmissions along with electronic attacks against satellites and related services at ground segments, associated communication links. Ground segments that provide telemetry, communications, tracking and command of space nodes and launch mission functions can easily attacked, either electronically or physically, and result in disruption, degradation and destruction of the space capability.

Electronic attack involves jamming uplink and downlink signals to jam or spoof information through the satellite. Uplink jamming can disrupt command and payload links and imparts a broad based effect as all recipients of the satellite's transmission are affected. Downlink jamming, is primarily oriented at preventing selected users from receiving a satellites broadcasts and navigation signals and is achieved by transmitting radio frequency transmissions with enough power to overcome the satellites downlink signal. Smart jamming differs from traditional broadband or traditional techniques as it simulates or spoofs the targeted satellite signal to furnish targeted users with erroneous data. This technique has a more local effect, typically limited to tens or hundreds of kilometers depending on downlink signal strength, as it requires the jammer to operate from line of sight, however, it is potentially more effective as lower power jamming transmitters may be employed. As satellite telemetry contains information related to system mission, health and status, a successful downlink attack will disrupt essential information flow and potentially have more immediate effect. Spoofing involves a variety of techniques to capture, alter and retransmit transmissions to mislead intended recipients. Other threats against satellite systems include kinetic, directed energy (laser, particle beam and radio frequency weapons) and nuclear effects.

Artificial Intelligence – As an enabling technology, Artificial intelligence (AI) technology is of particular relevance as it will comprise a foundational element of any automated cyber defence system. It has evolved from its origins in the 1950s to modern machine learning, expert systems and neural networks that seek to replicate the functioning of the human brain. AI now exceeds the performance of the human brain in many activities once considered too complex for any automated system to master. The application of AI is currently making its greatest impact in the areas of threat detection and the shaping and execution of cyber defence work flows. Traditional approaches to threat detection were based on software code that involved pattern matching programs that would search for signatures or specific patterns that would provide potential indicators of compromise. The application of AI now goes beyond the detection of individual signatures to detection of malicious behaviour such as phishing, ransomeware and compromising applications on mobile devices and networks. This is complementary to the earlier signature based detection approaches, however, in order to "teach" AI systems, there is a reliance on the development of large databases of threat artifacts that have been accumulated over time. Although focused signatures may be developed and deployed quickly, AI "learning" requires considerably more time.

Consequently, in the near term, AI is largely being deployed in more narrowly defined cyber defence applications supporting signature detection. However, future AI development will need to focus to a greater extent toward complementing the human operator in synthesizing the wider range of actions occurring on a network. This analytical and decision support functionality will enable more sophisticated situational awareness and the ability to posture more sophisticated approaches to defence, for example the detection and understanding of heuristic behaviour on a network as opposed to responding to individual instantiations of threats. Further, given the increasing complexity of

malicious code, there is a role for AI to assist defence analysts and operators to not only detect such code, but also understand its capabilities so as to enable more adequate response.

Although predictions of the pace of AI development have been mixed, current trends suggest the potential for human-level cognition or even artificial superintelligence could be a realisable in the nearer term, with some predictions of an AI explosion by 2045 [4], greatly enhancing the capacity of the human brain. When considering the potential offensive and defensive actions that may be realized on networks supporting critical infrastructure, it is clear that such technology could afford decisive strategic advantage in political, economic and military environments. As such, this creates the impetus behind focused efforts on the part of leading nations in the development of AI supporting cyber security.

A corollary to this when considering the application of AI to sensitive critical infrastructure based applications given their ley impacts on society, is the challenge of ensuring the processes supporting complex AI systems is understandable to humans. This involves ensuring that input data, algorithms and associated results are clear and readily interpretable. The acceptance of AI systems will be fundamentally dependent on enhanced transparency, most notably in mission-critical applications impacting life and death.

4. Future automated defence capabilities

Mitigation and Automated Defence – There are a variety of approaches to resolving the myriad of challenges cited above arising from rapid technology advancements, however the nature of various systems operating in disparate environments prevents a single uniform approach to addressing the plethora of potential attack vectors. Current antivirus systems represent only a partial solution and fail to maintain pace with the rapidly evolving malicious software environment. A wide range of malicious software variants are readily available on the dark web for less than tens of thousands of dollars, and in many instances they easily bypass commercially produced antivirus protection products. The isolation of networks also do not ensure security as the level of sophistication associated with weaponized software by state based entities to penetrate networks can readily exploit the inevitable security lapses that exist in organizations. One classic example is the Stuxnet virus that exploited USB devices to gain access to critical SCADA infrastructure that had been thought to be on a physically isolated network and impervious to penetration.

Automated Cyber Defence – Traditional approaches to institutional cyber security have involved providing perimeter security at border entry points and static policy enforcement. The increasing openness of enterprise network environments in light of Covid driven remote work requirements has introduced greater risk given the broadened aperture and more fragile network posture. Once having penetrated the established network perimeter, an intruder will have greater freedom to move about within the network. To maintain pace with this threat, concepts surrounding the protection of networks must evolve to one where adaptive responses play a principal role and multiple defensive layers must be established that permeate the entire network environment so as to avoid reliance on a single defensive boundary.

Current research and development efforts are aggressively pursuing adaptive security methods by developing new measures that are broader and deeper in scope, and employ increasingly intelligent and effective artificial intelligence driven defence techniques in addition to pressing security perimeters inward. One example of such an approach is the shift from firewalls on network perimeters to managed firewalls that are distributed on individual hosts within the network and embedding application specific filtering throughout the application stack.

Potential methodologies in this vein involve the implementation of managed execution environments that provide automated responses to incidents to prevent the protected applications and environments from future attacks of the same or analogous incursions. As incursions and associated effects are detected, the intended response is provided through the application of the specific networks' input/output mediation policy so that the network may then restored to pre incursion state. Such a response in turn supports the development of further policy adaptation via the application of decision tree classifiers, which may be reinforced by fuzzy experiments to develop a more precise model of the specific incursion. The associated responses can then be implemented as secondary policy patches. Such a protocol enables the blocking of future events that are similar in content, signature or character. Such approaches can provide quasi real-time responses to incursions that contain detectable system conditions. These depend upon software engineering of self improving software systems that integrate a number of complementary technologies such as decision tree classifier generation, deep execution introspection and targeted fuzz testing under the auspices of a managed execution environment. Further development is needed to optimize the balance between speed and precision in protocol adaptation and associated generalized signature combinations that are tailored to specific applications and timing dependencies.

The implementation of successful automated adaptive cyber defence strategies must be effective in mitigating threats and be enforceable under specific network states and capabilities. Successful active cyber defence requires synchronized, real time capabilities to discover, analyze and defend against threats and vulnerabilities. The scope of these measures must be capable of spanning a highly diverse range of network monitoring and management activities to detect attacks and safely mitigate them. To do so, multiple network configurations are required. For

example the migration of key services from one server to another which involves a high degree of complexity. Consequently, the key properties of any successful active cyber defence strategy are consistency, enforceability and effectiveness. Consistency ensures that the sequence of configurations avoid mutual contradiction. Enforceability relates to the ability of the network to reconfigure active cyber defence strategies without incurring violations arising from misconfigurations or resource limitations, and effectiveness means that the desired effect is delivered, either through target disruption or neutralization [5].

As cyber attacks against enterprise and critical infrastructure increase in frequency and impact, there is a heightened appreciation for the merit of a persistent presence on networks. Consequently, active cyber defence to provide automated, adaptive, steerable responses is developing in importance. There are a number of approaches such as network layer solutions that use multiple behavioural models to invoke different routing of traffic through a core network. To achieve this, several conditions must be in place. First, the detection of behaviour that is inconsistent with a users past serves as a proxy for compromised systems or credentials, but renders high false positive rates. Secondly, the automatic redirection of future traffic from a potentially compromised system must provide a graded response that balances the cost of false positives against the risk of allowing the potentially malicious behaviour to continue. These conditions enable the development of a framework to link real-time situational awareness technologies to automated steerable responses that can provide decision support to human operators.

Traditional network defence in depth techniques afford attackers an asymmetric advantage as they permit free movement and propogation about the network once access is gained through the exploitation of credentials and access permissions of valid users. These techniques also fail to identify indirectly observable behaviours such as purpose, time on target and sequences of specific actions such as access attempts. Consequently, many current defences prove inadequate as they typically employ signature-based attributes as opposed to distinguishing between normal and abnormal behaviour such as goals, capability and sequence of action. Further, enterprise organizations often fail to apply appropriate isolation given the technical difficulty, related inefficiencies and impact on productivity. One approach involves adaptive partial quarantines to impede or isolate attackers that may appear to be behaving normally, without impacting the activities of valid users and defenders. Such strategies involve automatic, behaviour triggered, adaptive quarantines to quickly and selectively change access to defender resources without interfering with the normal work of valid users and hosts. This addresses the problem of isolating malicious users and systems without negatively impacting the mission critical work of valid users. Such a capability leverages two well developed areas of research, namely behaviour analysis and containment [6].

A further area of activity involves the use of cognitive informatics to counter distributed denial of service attacks against critical infrastructure and domestic defences. Such attacks are simple to initiate as malware is readily available and easy to implant by multiple malevolent users. One ongoing trend is the use of mobile phone botnets to launch attacks and it is expected that major State based actors have the capacity to perform DDOS attacks against other nations' critical infrastructure. The automated defence of such systems may be facilitated through cognitive learning. This is an emerging area of research related to Cognitive Radio Networks. Potential cognitive based design guidelines and algorithms focus on all OSI network, transport and application layers. Information technology artifacts may then be created, evaluated, improved and redesigned until new knowledge is acquired. In such an approach, Cognitive engines require large amounts of information to drive engine development. The development of such environments rely on focused areas of work such as the separation of authenticated and unauthenticated services, the placement of proxies between clients and servers, and micro segmentation of clients during distributed denial of service attacks.

Automated Defence in Software Defined Radio and Cognitive Radio Networks – Clearly, Software Defined Radio (SDR) and Cognitive Radio Networks introduce entirely new classes of security threats [7]. Such classes comprise sniffing, spoofing, jamming, side channel, replay, reinjection and flooding attacks. Sniffing involves monitoring traffic on a communication channel, either encrypted or unencrypted, to obtain confidential information which could include the identities of the sender and receiver in addition to traffic control parameters that could enable a deeper understanding of the network infrastructure.

Spoofing involves the transmission of signals, whose parameters could be seen as valid and representing an authorized user. The intent is to send erroneous information, inject malicious code or gain control of the communication channel. Jamming is ostensibly a denial of service attack that degrades or disrupts valid communications from occurring on a channel and effectively blocks accurate reception of messages by authorized users. Side channel attacks involve collecting and analyzing information related to physical parameters such as electromagnetic radiation from integrated circuits as they are processing. This non-invasive technique is used to breach confidentiality and is typically used to carry out RFID attacks against credit cards in wallets. Replay involves copying a legitimate message and retransmitting it, thereby causing confusion an corruption of legitimate traffic. It can also be used in support of broader flooding attacks that impact the availability and

integrity of a communications channel. Reinjection is similar to a replay attack; however, the message is modified before retransmission in order to compromise the channel integrity and confidentiality. Finally, flooding involves sending such a large volume of messages such that the receiving terminal is overwhelmed and cannot process all of them, thereby compromising the availability and integrity of the communication channel.

SDR allows devices to adapt quickly and function optimally in changing network environments as various attacks are discovered. Further, the Internet of Things imposes the additional challenge of an explosion of sensors which lack the appropriate protections for confidentiality, integrity and availability. The resolution of such a challenge is dependent upon a multi-layered approach. Potential techniques involve the identification of source IP addresses and the use of big data to increase scalability to enable deeper analysis of counter distributed denial of service correlation metrics and analyze which organizations have been attacked using the same IP addresses. Other approaches involve coordinated concealment and proxy solutions to defend Web services. A weakness with this approach is that workflow is sent to a proxy where the service IP address must still be protected against the malevolent client.

When deploying SDR in mobile network environments, a supporting configuration model supporting users and services must be developed that continuously and dynamically adapts its configuration in order to immediately detect malicious sources. Here, a number of significant challenges exist for open and random access environments. The instance of unlicensed secondary users accessing channels when not being used by licenced primary users may be addressed via a-priori authentication. IP tracking based on packet marking and recognition technology to detect attacking packets are main approaches against distributed denial of service attacks and facilitate tracking. Further methods involve implementation of jamming resistant control channels.

Another counter distributed denial of service approach in cognitive radio networks involves furnishing the cognitive engine with information that can identify specific authenticated clients that are potential threats. These can be repeatedly broken down into much smaller groups until one client remains and enable the cognitive engine to rapidly and precisely identify a specific malicious client and remove them from a trusted list and protect servers supporting authenticated clients [8]. Currently large enterprise networks composed of continuously changing networked devices are routinely subject to targeted cyber attacks. Typically, a high volume of information related to attacks reside in various locations and remain unexamined until after attackers have achieved their objectives. Future cyber information management platforms will need to simplify cyber event data that is stored in the many recesses of distributed networks within hours and minutes as opposed to the months currently taken. Most current approaches to automated and operator assisted cyber defence are inadequate in defending against targeted cyber attacks because they focus on a limited number of aggregated one-dimensional characteristics across a number of devices and they are not able to cover all the network devices and observables resident on those devices. They further lack the ability to express and identify the deeper semantic required to identify targeted attacks among the vast multitude of low-level network activity. Progressive solutions will need to address these issues by being able to automatically detect network devices and develop metadata indices of information related to network activity and decompose and federate semantic queries to devices instead of extracting and aggregating information in central stores [9]. These integrated results will then need to be presented in the form of an established ontology.

Such solutions would facilitate information management and eliminate inefficient manual processes by enabling access to all network related data sources via federated query interfaces that leverage new web ontology, semantic query and cyber defence languages and return query results in an integrated, semantically meaningful and immediately useful manner. The intent is for intricate activity patterns to be identified within the network regardless of the type of device, operating system and location of logs. Cyber defenders would then be able to focus on the forensic analysis of data without being burdened by the encumbrance of managing and executing the activities required to laboriously collect data and process it.

From an overall system security perspective, the system must have the ability to function in a contested network environment. In so doing, there are a number of major features that it must possess. All sources of data in the environment must be accessible through well defined languages and interfaces. Additionally, there is a requirement for minimal network loading through scalable distributed architectures to deal with large, complex networks. Further, data must be retained at the network edge through federated access to observables. Finally, coverage over both legacy and new devices and associated intelligent information extraction needs to be provided.

Current commercial offerings focus on high volume commodity technologies marketed to commercial and government organizations that face attacks from broad set targets. Consequently, these capabilities are inadequate in identifying the necessary cyber observables to successfully counter targeted attacks [10].

5. Conclusion

The contemporary threat permeates itself across a variety of technology areas supporting societal critical infrastructure; each with their own particular characteristics in light of the nature of technology

implementation in these environments. Given the pervasiveness of contemporary information technology in support of critical societal infrastructure supporting the broader national economic and security interests, a significantly increased role exists for cyber and data protection. Of particular note are advanced persistent threats that take advantage of sophisticated infiltration techniques that most government agencies and businesses cannot counter collectively. However, if addressed individually, these techniques can be countered. This leads to consideration of specific vulnerabilities that require specialized knowledge of such bespoke systems, are difficult to foresee and predict and require near real time detection and response based on the aggregation of complex observables. The sophisticated nature of current state, terrorist and criminal threats require enterprises to better understand their systems and implement more automated processes to ensure resiliency and support the limited human cyber security professionals charged to oversee protection of these systems.

Traditional risk management approaches to assessing and implementing security on large enterprise networks supporting critical infrastructure have been based on passive and reactive techniques given that such environments had historically been based on more clearly defined and understood technologies. The increasing diversity and complexity of modern networks supporting critical infrastructure have rendered such approaches inadequate to provide the sole means of assessing and guiding the development and management of their protection. To that end, automated approaches to threat assessment and defence are increasingly needed. However, in order to posture such automated approaches within an enterprise environment, an appreciation of the nature of various considerations related to the broader strategic context of security along with a detailed understanding of vulnerable technologies.

References

[1] R. Mazzolin, A. Madni, "A Survey of Contemporary Cyber Security Vulnerabilities and Potential Approaches to Automated Defence", *IEEE SYSCON 2020 Conference, 2020*, Montreal, Quebec, Canada

[2] Salvador Llopis Sanchez, Robert Mazzolin, Ioannis Kechaoglou, Douglas Wiemer, Wim Mees, Jean Muylaert. "Chapter 108-1 Cybersecurity Space Operation Center: Countering Cyber Threats in the Space Domain", *Springer Science and Business Media LLC, 2019*.

[3] J. Kallberg, B. Thuraisingham, E. Lakomaa, "Societal CyberwarTheory Applied: The Disruptive Power of State Actor Aggression for Public Sector Information Security", *2013 European Intelligence and Security Informatics Conference, 2013.*

[4] Seth D. Baum, Ben Goertzel, and Ted G. Goertzel, 2011. "How long until human-level AI? Results from an expert assessment." *Technological Forecasting & Social Change, vol. 78, no.1 (January)*, pages 185-195, 2011.

[5] B. Benyo, D. Musliner, "Automated Self-Adaptation for Cyber Defense Pushing Adaptive Perimeter Protection Inward", *2013 IEEE 7th International Conference on Self-Adaptation and Self-Organizing Systems Workshops*, 9-13 Sept. 2013.

[6] M. Alsaleh, E. Al-Shaer, "Towards Automated Verification of Active Cyber Defense Strategies on Software Defined Networks", *SafeConfig'16*, Oct 24, 2016.

[7] Christopher S. Oehmen, Thomas E. Carroll, Patrick C. Paulson, Daniel M. Best et al. "Behavior-dependent Routing", Proceedings of the 2015 Workshop on Automated Decision Making for Active Cyber Defense, *SafeConfig '15, 2015*.

[8] G.. Baldini, et al. "Security Aspects in Software Defined Radio and Cognitive Radio Networks: A Survey and a Way Ahead", *IEEE Communications Surveys and Tutorials*, Vol 14, no 2, pp 355-379, 2012.

[9] T.Booth, K. Andersson, "Critical Infratructure Network DDOS Defense via Cognitive Learning", *14th IEEE Annual Consumer Communications and Networking Conference (CCNC)*, Las Vegas, Nevada, USA, 2017.

[10] M. Atigehetchi, J. Griffith, I. Emmons, D. Mankins, R. Guidorizzi, "Federated Access to Cyber Observables for Detection of Targetted Attacks", *MILCOM 2014*, October 2014.

Brigadier General (Retired) ROBERTO MAZZOLIN is the Chief Technology Strategist at the RHEA Group, a multinational company providing bespoke engineering solutions, systems development and security services for space, military, government and other critical infrastructure. During his military career, he served in a variety of key command and staff roles at all ranks. Notable appointments during his military service include responsibility for all Canadian Armed Forces and Department of National Defence strategic network, signals intelligence, electronic warfare and cyber operations, strategic cyber policy development, and responsibility for the engineering and program management of the Canadian Army command, control, communications, computers and intelligence, surveillance and reconnaissance system. He also served at United States Cyber Command as the Vice Director for Strategic Policy, Plans, Force Development and Training. He is a Senior Fellow at the Centre for International Governance Innovation and has written numerous publications and spoken extensively in a wide array of international engineering, commercial and industry fora. General Mazzolin holds a Bachelor of Electrical Engineering from the Royal Military College of Canada, a Master of Science with specialization in electronics and guided weapon systems from Cranfield University, U.K., a Master of Arts in Security and Defence Management and Policy from the Royal Military College of Canada, and a Ph.D. in Engineering Management from California Coast University, USA. He is a licensed Professional Engineer and a Senior Member of the Institute of Electrical and Electronics Engineers. He is an officer of the Canadian Order of Military Merit, and his many awards include the US Legion of Merit, the US Meritorious Service Medal, the Canadian Chief of Defence Staff Commendation and the Italian Army Chief of General Staff's Encomio Solenne ("Solemn Commendation"), in recognition of professionalism and courage for combat actions in Somalia.

DR. ASAD M. MADNI served as President, COO & CTO of BEI Technologies Inc. from 1992 until 2006. Prior to BEI he was with Systron Donner Corporation for 18 years in senior technical & executive positions, eventually as Chairman, President & CEO. He is currently, an Independent Consultant, Distinguished Adjunct Professor and Distinguished Scientist at UCLA ECE Department, Faculty Fellow at the UCLA Institute of Transportation Studies and Connected Autonomous Electrical Vehicle Consortium, and Executive Managing Director & CTO of Crocker Capital.

Dr. Madni received an A.A.S. from RCA Institutes Inc., B.S. & M.S. from University of California Los Angeles (UCLA), Ph.D. from

California Coast University and S.E. (Program for Senior Executives) from MIT Sloan School of Management. He is credited with over 200 refereed publications, 69 issued or pending patents, and is the recipient of numerous national and international honors and awards and has been elected a fellow or an eminent member by some of the world's most prestigious scientific and technical academies and societies. He has been awarded 6 honorary doctorate degrees and 6 honorary professorships. In 2019, IEEE HKN named its top award *"The Asad M Madni Outstanding Technical Achievement and Excellence Award"* to recognize and honor his nearly 50 years of technical and philanthropic accomplishments, and visionary leadership.

JENRS

Received: 28 January 2022, Revised: 08 March 2022, Accepted: 28 March 2022, Online: 12 April 2022

DOI: https://dx.doi.org/10.55708/js0104003

Effective Approach Experience for Practical Training using Web-Based Platforms and Tools in the Context of the COVID-19 Pandemic

Radoslav Hrischev*

Control Systems Department, Technical University–Sofia, Branch Plovdiv, Plovdiv, Bulgaria

*Corresponding Author: Radoslav Hrischev, Email: hrischev@tu-plovdiv.bg

ABSTRACT: This article is a result of the need to quickly and efficiently organize distance learning for students during the pandemic caused by COVID-19. Some e-learning opportunities provided by internet technologies, web-based platforms, online engineering tools are presented. Examples of training students in business information systems based on learning platforms and demo systems are presented, as well as the use of engineering tools for the design of production equipment on the websites of specialized companies. The common in these examples is the possibility of effective training without long preparation and additional expenses for the development of specialized learning platforms and simulators. The practical results of this non-standard approach to e-learning during a pandemic are also discussed.

KEYWORDS: e-learning, information systems, ERP systems, web-based design tools

1. Introduction

Coronavirus COVID-19 change our lives in all its aspects, including education. The accelerating e-learning in recent years from an opportunity for remote learning has become the just possible opportunity for effective learning in pandemic time [1]. This also applies to education at technical universities [2]. Carrying out the various technical specialties without access to auditoriums and work in laboratories, and on the other hand the observance of the topics and activities set in the curricula was a serious challenge. The only solution was to use cloud platforms for distance learning and access to specialized software simulators. But the development or implementation of specialized tools - Moodle, Office 365 from Microsoft, GSuite from Google, requires time and additional resources. It also takes time to train students and teachers. On the other hand, not every university has ability to install private cloud and simulation systems due to the budget restrictions, limitation of licensing rights and hardware and software requirements.

At the same time, everyone has access to the Internet with satisfactory quality via smartphone or computer. Therefore, there is an excellent opportunity to learn using shared resources on social networks, free web-based platforms, demonstration systems available via the Internet. The Internet provides a wide range of opportunities for interactive information exchange, online training, webinars, cloud collaboration technologies [3]. Many companies also provide free access demo systems, shared educational resources, and web-based design tools. Thus arose the idea of using such free platforms and web-based tools in the process of training students and professionals in various disciplines at universities during a pandemic.

This article aims to illustrate practical examples and results of the use of the Internet in the process of education students in the disciplines of Information systems in industry and Design of manufacturing apparatus.

2. E-learning of Information systems using shared resources in Internet and collaboration with vendors and implementers

The modern information systems are at the heart of human progress in recent years. This is especially true for the business and industry. Therefore, the education of students in the disciplines of Information systems is

extremely important. The focus of computer science education is usually on the development of information systems (programming, architecture, databases, communication).

But businesses need not so much the development of new systems as the skills to implement, customize, administer, and effectively use existing, proven systems. The implementation of business management information systems by specialized software developers not only optimizes the processes in the organization, but above conveys the experience of leaders in the industry. Such are integrated management systems or ERP systems. They cover all (or almost all) information flows in the company and based on a sustainable information and communication infrastructure, are the perfect tool for complete business process management in real time. Enterprise Resource Planning (ERP) software has evolved over the years to include functionalities that cover all business operations. There are a wide variety of systems for small and large organizations, many of which offer integrated capabilities. However, identifying the ERP software that is most appropriate for a particular organization can be a difficult process, often involving many investigations and simulations. Students need to receive basic knowledge, and why not, practical skills to work with such information systems. Training engineers in various specialties to work with ERP systems is an important task for universities. But how to introduce students to the various integrated systems? The best way is to use shared learning resources and work with real systems. Therefore, most of the leading developers of ERP systems provide specialized training platforms.

2.1. OpenSAP training platform

In the process of training students in information systems in industry specialty is especially useful to use specialized platforms of the leader software company - SAP CE [4]. SAP is one of the world's leading producers of software for the management of business processes, developing solutions that facilitate effective data processing and information flow across organizations. This is the most widely used ERP system in the world and therefore its knowledge gives a competitive advantage to engineers who have experience working with this system.

OpenSAP [5] is an Enterprise platform for massive open online courses (MOOCs) - Figure 1. OpenSAP is provided by SAP and hosted at the Hasso Plattner Institute in Potsdam, Germany. Every student can enroll for free in courses, which are provided free of charge. While the MOOC concept is already quite popular in academia, SAP is one of the first companies to build a platform for training and adopt it for business-related training purposes. Compared to most of e-learning formats, OpenSAP courses return to tried and trusted classroom concepts and transfer them to an online medium. It a typical learning process - courses have a defined duration; the courses are based on lectures (pdf and video). Students need to submit homework on a weekly basis and adhere to deadlines. The homework is graded and gives points required to the final achievement. The students have opportunity to discuss the course content in an online forum.

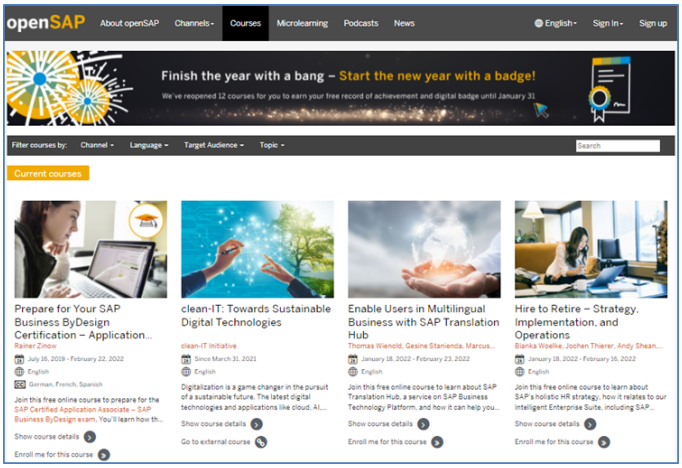

Figure 1: OpenSAP learning platform

In pandemic time when students are more time at home it's a very useful opportunity to receive additional knowledge. Timely acquaintance of students with this type of opportunity for free training in business management systems leads to higher engagement and motivation of students.

The experience of the last three years in our university shows that 15-20% of students manage to complete the course they have chosen and receive an international certificate. This certificate is a significant advantage in the job search of young engineers.

2.2. SAP University Alliances Learning platform

Universities training students in ERP systems and SAP can join the SAP University Alliances community [6]. The SAP University Alliance Learning Center -Figure 2, provides courses and simulators for organizing exercises in the curriculum. The developed simulators for training to work in the SAP modules give students not only the opportunity to be familiar with the working interfaces and functionalities, but also to acquire practical skills for performing most working operations.

All operations in a selected module are presented, performed by students and their work is evaluated. The simulators allow for students to acquire practical skills for working with a real system, and professors to assess the acquired skills. In Figure 3 is present one of simulators - Sales & Distribution (SD) module of SAP version R/3,

provided from SAP University Alliances learning platform.

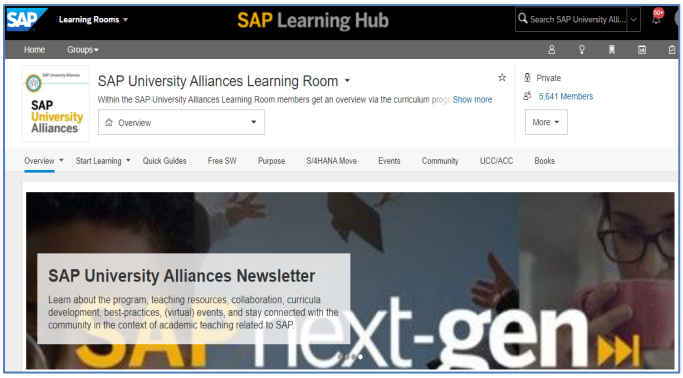

Figure 2: SAP University Alliances learning hub

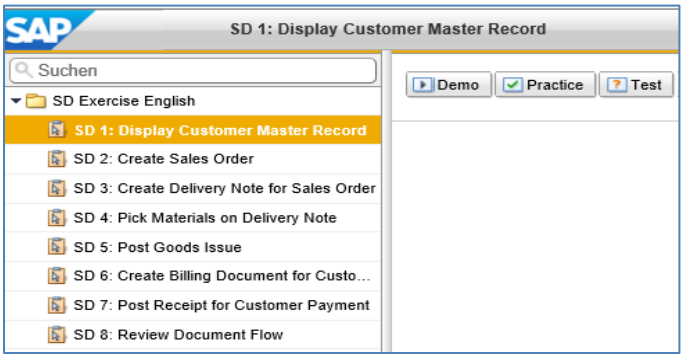

Figure 3: Simulator of Sales & Distribution module

Using these simulators becomes an exciting experience for students, because it is no different from working with a real ERP system, while at the same time together with the accumulation of knowledge allows students to improve their practical skills. On the other hand, it allows the professor to introduce a competitive element in the exercise process. The result of this type of training is better engagement and motivation of students.

2.3. Use of free and demo cloud-based integrated information systems for remote learning

Many developers of business management software companies provide demos of the systems SAP HANA, Oracle Enterprise Resource Planning, Unit4's Business World ERP, Microsoft Dynamics 365, Cetec ERP. However, they cannot be used for training because they usually require hosting, installation and additional configuration. There are also open-source ERP solutions out there. The training of students is not always appropriate to be conducted in English, because most of the specialties are taught in Bulgarian. Therefore, after careful investigation we decide to use demonstration version of ERP system, hosted from Bulgarian software company developer of ERP systems – bg ERP [7]. The main screen is shown in Figure 4.

The developer of bgERP, Bulgarian software company Experta ltd. hosted for our student fully functional copy for training purposes, accessible remotely from everywhere by phone, tablet, computer. This solution allowed the professors development of exercises for remotely trained in administration of the system, distribution of access and permissions for users. Roles and functionalities are defined to demonstrate the interaction of the different modules of the system tasks by functionalities and modules. For example, we set following users: CEO, Worker, Stock, Salesman, HR and Administrator. Role-playing games are preferable form of education and all students enthusiastically engage in the exercises.

Figure 4: Bulgarian Open-Source system bgERP

To the presented using of shared platforms, we added the lectures by SAP implementers. Specialists from the biggest implementer of SAP in Bulgaria Scalefocus Ltd. prepare lectures for students on practical aspects of the implementation process.

The result of the applied teaching methods are the excellent results of the students trained in the discipline of Information systems in industry. Additionally, the certification of 5-7% of students is great opportunity for the new engineers.

3. E-learning using web-based tools for the design of electric drives of industrial apparatus

The electric drives of the manufacturing mechanisms are a basic and important element of the production apparatus. That is why the biggest manufacturers of electric drives are developing specialized tools for designing electric drives for various manufacturing devices. Of course, they are oriented to the basis of their own production - electric motors, gearboxes, frequency inverters and other equipment.

SEW-EURODRIVE, ABB, Mitsubishi Electric, SERVOTAK as a world leader in drive technology and pioneers in drive-based automation, provide online drive selection tools for various production mechanisms. The use of these tools makes it possible step by step to design electric drives of the main types of drives as elements of automation systems - conveyors of different types, transport mechanisms, different types of lifting mechanisms, pumping equipment, various servo drives and more. others. The companies provide access to web-based tools after simple registration without any restrictions.

These free tools are an excellent opportunity for e-learning of students in disciplines related to the design of electric drives of industrial apparatus, developing exercises without need of specialized simulators. Which are the used design tools in our practice?

3.1. Web-based tools for the design of electric drives of industrial apparatus

SEW-EURODRIVE USA provides access to a specialized PT Pilot web-based tool [8] for online design of drives of various production mechanisms - conveyors, lifting and transport mechanisms.

PT Pilot - Figure 5, is compatible with all major browsers for PC and MacOS. No installation or purchase required. PT Pilot is an advanced online selection tool that provides all the following functions: calculator and formulas for drive applications, includes thermal and mechanical evaluations of the operation of mechanisms, 2D or 3D electronic CAD files, prepares an offer with a net price, and allows online ordering the selected equipment and spare parts using implemented from companies ERP systems, SAP from example.

This possibility is a demonstration of connection between the two disciplines presented in this article - Information systems in industry and automated design and ordering of production apparatus and spare parts.

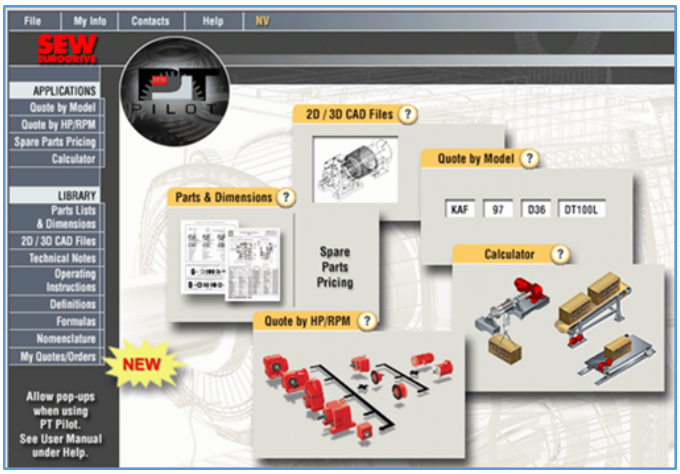

Figure 5: Main screen of PT Pilot, provided from SEW EURODRIVE USA

Specialized tool Calculator, part of PT Pilot, Fiure.6, provides the opportunity for preparation of exercises for training in the design of following manufacturing apparatuses as part of technological lines – belt conveyor, roller conveyor, travel drive, crane hoist, lift, palletizer, travel drive. In practice, this is a tool for automated design of machines and electric drives according to pre-set parameters of the technological process.

ABB is a leading global engineering company, one of the engines of industry transformation to achieve a more productive and sustainable future. By adding its own design software developments to its portfolio of production mechanisms, robotics and automation, ABB provides its customers with a finished product that expands the boundaries of technology, increases the efficiency of production. Part of the software tools provided free of charge online by ABB is the specialized tool DriveSize Web [9]. It contains current versions of the catalog of engines and drives of ABB.

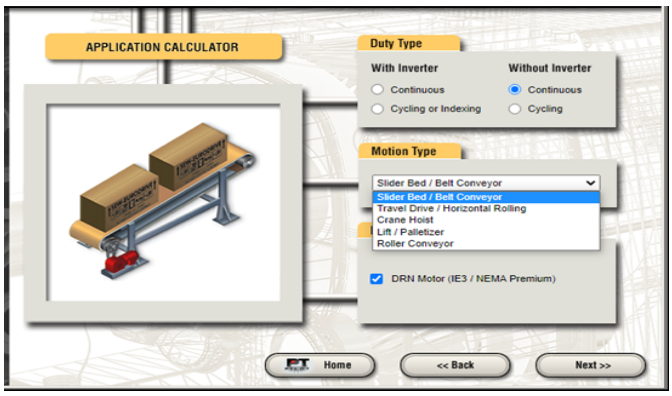

Figure 6: Calculator module of PT Pilot

DriveSize, Figure 7, assists engineers in selecting optimal drives for variable speed production machines from ABB drives. DriveSize consists of a user interface, a computing part and product databases.

Figure 7: Main screen of DriveSize Web – design toll of ABB

This tool is very convenient for conducting remote training of students in the design of positioning mechanisms, pumps and fans apparatus.

SERVOTAK's engineering solutions focus on users who need precise actuators with superior quality and performance. The company's goal is exceptional reliability, robustness and an innovative approach to problem solving. The Servotak website [10] consists of the web-based Engineering Calculator tool – Figure 8. This tool allows online design of various production devices - conveyors, turntables, elevators, vehicles.

The Engendering Calculator assists specialists in sizing different parts of the production mechanisms. Mathematical algorithms for calculating the parameters of

the mechanisms and their electric drive are provided, as well as detailed interactive methods for calculations. Therefore, this application can be used as an engineering guide for future engineers.

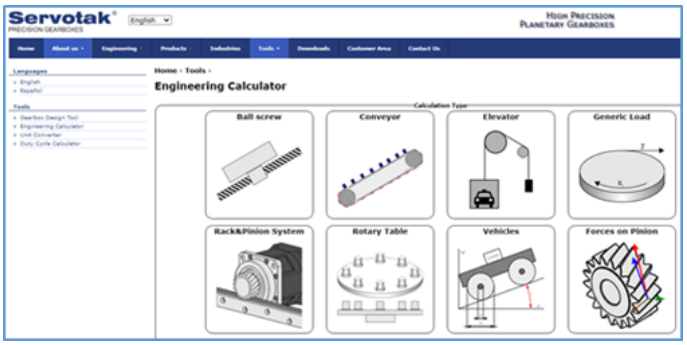

Figure 8: Engendering Calculator of SERVOTAK.

3.2. Web-based tools as part of e-learning in pandemic time

In the conditions of the pandemic, there was a need for rapid implementation of distance e-learning. In these conditions, the university proved E-Learning platform /usually Moodle/ as an excellent solution for sharing lectures, materials and conducting tests and exams. But what to do with laboratory exercises? Teaching students to design manufacturing apparatus and their electric drives without access to laboratories was a major challenge for faculty during the pandemic. Therefore, interactive online laboratory exercises have been developed based on the web-based tools presented on the SEW-EURODRIVE, ABB and SERVOTAK websites. Laboratory exercises were developed for the design of production mechanisms and drives for various production devices: transport trolleys, belt conveyor, roller conveyor, lifting mechanisms, palletizer, rotary table, elevator, pumps and fans. The laboratory exercises were conducted with students in the disciplines Automated Manufacturing Apparatus and Design of Electric Drive Systems. Each student in each exercise was given an individual task online, which they had to solve with the help of interactive tools on the company's websites.

From the first exercise, there was great interest from side of the students. Most of them with passion and enthusiasm begin to study these tools on their own, to develop examples and send the results, designed as extracurricular activities.

The results from using these online tools are already in detail presented [11]. There are two positive trends in the use of these approaches:

- Student engagement increases. After the transition to distance e-learning and the presentation of new laboratory exercises, respectively, attendance increased by more than 30%.
- Higher success is achieved. Due to the increased interest and commitment of students, student grades increased by 17%. Assessment also takes place in an online environment with tests in Moodle or Google Form.
- In parallel with the learning process, students get acquainted with the official websites of industry leaders and their proposed training platforms and tools for designing devices in the field of control systems.
- Students learn to use web-based tools for interactive design. This allows them to compare different design methods. They discover the advantages and characteristics of design tools provided by different equipment manufacturers.

Without absolutes the role of e-learning better for students, the ability to use the Internet to attend classes, the use of real tools for the design of production apparatus and electric drives provided by companies, world leaders in the field of automated production, causes interest and commitment among students.

4. Conclusions

In the COVID-19 time, the Internet has become a natural environment for communication and sharing. But the Internet is not only an opportunity for social contacts, it is also one of the preferred ways to share knowledge in the form of available resources for learning and research in public and private networks. E-learning platforms and free specialized engineering tools of technology giants in various fields are an excellent opportunity to train students in various scientific and applied fields [3], [12]. The proposed examples of training in the disciplines of Information Systems in industry and Design of manufacturing apparatus and the results of this approach illustrate the benefits of using these tools in a pandemic for educational purposes. In this article presents only some examples in two disciplines, but this approach is also applicable in other areas of education, because platforms, shared materials and specialized tools for other engineering disciplines can be easily found.

References

[1] Robert Power, "E-Learning Essentials 2020", Power Learning Solutions, 2020: ISBN: 978-1-9993825-2-0.
[2] Nicole Buzzetto-Hollywood, Advanced Principles of Effective e-Learning, Informing Science Press, USA, 2007
[3] M.Q. Huynh, U.N. Umesh, J.S. Valacich, "E-Learning as an emerging entrepreneurial enterprise in universities and firms", Communications of the AIS, 2003, 12, 48-66.
[4] SAP SE official site https://www.sap.com.
[5] OpenSAP training platform https://open.sap.com.
[6] SAP University Alliances Learning platform https://community.sap.com/topics/university-alliances.

[7] bgERP official site https://bgerp.com.
[8] SEW EURODRIVE official site http://www.seweurodrive.com/s_ptpilot/.
[9] ABB official site https://new.abb.com/drives/software-tools/drivesize.
[10] SERVOTAK official site https://www.servotak.eu/tools.
[11] R. Hrischev, N. Shakev, "Using of interactive web-based electric drive design tools in e-learning in pandemic time", *IEEE, 2020 International Conference Automatics and Informatics (ICAI)*, pp. , DOI 10.1109/ICAI50593.2020.9311383.
[12] C. Odoyo, Samuel O. Olala, "Covid-19 Pandemic as a Catalyst to E-Learning Acceptance in 2020", International Journal for e-Learning Security (IJeLS), Volume 9, Issue 1, 2020, pp.610-615, DOI: 10.20533/ijels.2046.4568.2020.0076

Radoslav Hrischev has completed his PhD in Control Systems from the Moscow University of Civil Engineering and Architecture, Russia in 1992.

He works as a developer and implementer of Information systems in various fields. For more than 20 years he has worked as an IT manager for international companies and is responsible for the implementation of ERP systems. His research interests are information systems in industry, information security and control systems.

JENRS

Received: 09 February 2022, Revised: 22 March 2022, Accepted: 28 March 2022, Online: 12 April 2022

DOI: https://dx.doi.org/10.55708/js0104004

Study on Stability Analysis of Rectangular Plates Section Using a Three-Dimensional Plate Theory with Polynomial Function

Festus Chukwudi Onyeka [1, 2], Chidobere David Nwa-David [2], Thompson Edozie Okeke [3,*]

[1] Department of Civil Engineering, Edo State University Uzairue, Edo State, 312102, Nigeria.
[2] Department of Civil Engineering, Michael Okpara University of Agriculture, Umudike, Abia State, 440109, Nigeria.
[3] Department of Civil Engineering, University of Nigeria, Nsukka, Enugu State, 410101, Nigeria.

* Corresponding author: Okeke, Thompson Edozie, edozie.okeke@unn.edu.ng
Corresponding author ORCID: https://orcid.org/0000-0002-2668-9753

ABSTRACT: In this paper, a polynomial displacement function is developed to evaluate the stability of rectangular thick plate that is freely supported at the third edge and other three edges simply supported (SSFS). Employing three-dimensional (3-D) constitutive relations which consist of entire stress components, the functional for total potential energy was obtained. The governing equations plate was obtained through the variation of the 3-D theory of elasticity to get the slope and deflection relations. The solution of equilibrium equations gives an exact polynomial deflection and rotation function which was gotten after replacement of the variables of total potential energy while the solution of the governing equation gave the expression for the deflection coefficient of the plate. The direct variation method through deflection coefficient was applied to get the formula for calculation of the critical buckling load. Furthermore, the model followed strictly from the first principle of 3-D theory of elasticity without state of stress assumption through the thickness axis of the plate, so that it is able to eliminate the stress under-estimation problem from the approximation and 2-D refined plate theory approach, when the thickness becomes thicker. The result of the present study using the established 3-D model yields an exact solution which shows that it can be used with confidence in the stability analysis of any type of plate boundary condition.

KEYWORDS: SSFS rectangular plate, Energy variation method, 3-D plate theory, Exact polynomial deflection function, Stability analysis of thick plate.

1. Introduction

Plates are three-dimensional structural elements whose parallel plane surface dimensions are large compared with the thickness [1]. In recent times, thick plates have many applications in engineering structures such as offshore platform structures, ship hulls and decks, aircraft wings, building floor, roof, slabs, and spacecraft panels. Hence the research interest in thick plates has greatly increased.

To describe the plate problem in a state of three-dimensional stress, three dimensional theory of elasticity is mostly required [2]. However, plates behavior largely depends on their span-to-depth ratio. Hence, plates are classified as thin, thick or moderately thick plates [3]. According to [4], rectangular plates with $50 \leq a/t \leq 100$ are classified as thin plate, $20 \leq a/t \leq 50$ as moderately thick and $a/t \leq 20$ as thick plate.

Thick plate analysis involves research areas such as plate vibration, bending and buckling [5]. Under the influence of in-plane compressive loads, the plate material gradually becomes unstable at the critical value of the loads. This phenomenon is called buckling [6, 7]. Based on the stress - strain relationship, plate buckling problem is classified as elastic and inelastic (plastic) buckling. When the critical buckling load is smaller than the elastic limit of the plate material, it is considered as the elastic buckling problem otherwise the problem is called inelastic buckling [8]. It is therefore necessary to

determine the critical buckling loads of a plate to ensure a safe design. Although the research on plate buckling is still progressive, more attention is drawn to developing and implementing varying methods for solving them depending on the properties of the plate. Generally, the methods employed in solving the buckling problems of plates can be grouped into three namely: classical methods, numerical methods, and the energy methods [9].

The classical methods also called the equilibrium (Euler) methods are analytical methods that seek to obtain closed form solutions for solving the governing partial differential equilibrium equations of the plate buckling problem within the plate domain, subject to the boundary conditions of loading and the restraints of the plate edges [10]. They include the Fourier series method, Navier's double trigonometric series method, the separation of variables method, and the methods of integral transformation. When applied to plates with fixed edges, free edges and mixed support conditions, mathematical and analytical difficulties are encountered. To obtain approximate solutions to the plate problem, numerical methods are used. These methods include the weighted residual methods, finite difference methods, finite element methods, and finite strip methods [11]. To overcome the rigorous routine inherent in classical and numerical methods, variational method can be applied. The energy methods such as Ritz variational method, Kantorovich variational method, Rayleigh-Ritz method, and Galerkin method; with respect to the displacement function minimizes the total potential energy functional to derive the characteristic buckling equation from which the buckling loads are obtained.

Series of theories has been developed and applied to analyze the buckling behavior of plates. One of these theories is the classical plate theory (CPT) [12], which is mostly employed in the analysis of thin plates, underestimates deflections, and over-estimates buckling loads and natural frequencies in thick plates. Reissner and Mindlin proposed the shear deformation plate theories to overcome the limitations of CPT [12, 13]. These theories are also called the Refined Plate Theories (RPT) which consists of first-order shear deformation theory (FSDT) [14] and higher-order shear deformation theories (HSDT) [15, 16, 17].

FSDT cannot produce accurate results because of the inclusion of a shear correction factor which alters some geometric parameters in the analysis. Reddy's and Ritz's theory in HSDT considers the satisfaction of the transverse shear-free surface conditions assuming a parabolic distribution of transverse shear strains throughout the thickness [18, 19, 20]. In this theory, there is no need for shear correction factor. Although these refined plate theories addressed the gap in CPT and are suitable for thick plate analysis, they are inadequate for a three-dimensional plate analysis. A 3-D theory is required for precise analysis of a three-dimensional plate; hence this study is essential.

2. Literature review

The authors in [21] derived the governing plasticity equations using Stowell's and Bleich's principles, also formulated the shape function by applying Taylor's series truncated at the fifth term. The authors in [22] studied rectangular that is clamped at all edges under biaxial compression using Galerkin's method. Accurate buckling load coefficients were obtained for the same boundary condition using polynomial shape function that was based on Tailor-Mclaurin series. The outcome of their study revealed that the buckling coefficients reduce consistently when the increment in aspect ratios is recorded from 1 to 2, thus, cannot be accurate in predicting the buckling load of thick plate rather thin plate only. They did not consider thick plate assumptions rather limited their study to CPT. More so, both studies failed to cover the plate that is freely supported at the third edge and other three edges simply supported (SSFS) condition and the authors did not consider the use of polynomial functions.

Authors in [23], employed refined trigonometric shear deformation plate theory to analyze the buckling behavior of a simply supported plate under both biaxial and uniaxial compression using the virtual work principle. The result obtained from the study showed excellent agreement when compared with other refined theories. The exponential shear deformation theory presented by [24] accurately predicted the critical buckling loads of the isotropic thick plates. The use of shear correction factors was unnecessary as the theory took account of transverse shear effects. The authors in [23, 24] did not consider the plate as a typical 3-D plate and could not employ the exact polynomial shear deformation functions in their analysis thereby making their work inexact. The polynomial shape functions were used by the authors in [25, 26] analyzed the buckling behavior of the same thick rectangular plate that is simply supported under uniaxial compressive loading. To derive the governing equations of the plate, the authors applied polynomial shape theory. The equation for formulating the non-dimensional critical buckling load parameters of the plates was obtained by solving the direct governing equation with satisfied plate boundary conditions. The authors in [25] and [26] considered a 3-D theory in their study and applied energy methods in the formulation of governing equation of the plate, but the authors in [25] used an assumed shape function which is not a close-form solution. Both authors failed to take into account the plate with the SSFS edge condition.

To analyze the buckling behavior of clamping plate, the authors in [27] adopted work principle approach. The

buckling coefficients of the plate were obtained and a numerical model was developed using the polynomial displacement function. The authors did not take a thick plate into consideration as their assumption is limited to the classical plate theory which is not reliable for thick plate analysis. Their study did not apply trigonometric functions and SSFS plate was not considered. In [28] and [29], the authors applied both trigonometric and polynomial displacement function to determine the critical buckling load of clamped thick rectangular plate using the analytical three-dimensional plate theory that is formulated and derived from the variational energy method, but could not apply it to a rectangular plate structure that is freely supported at the third edge and other three edges simply supported (SSFS).

In the study carried out by [30], the authors applied third order energy functional to analyze the stability of CCSS and CCCS plates within the plate domain and using the combination of the product of the stress and strain at every point in the plate. The authors formulated the third order strain energy equation by incorporating the direct variation method into the third order total potential energy functional which was obtained through the addition of strain energy to the external load. The study did not consider the current shape function and boundary condition or study the plate as a typical 3-D structure which should involve all the six stress element for the thick plate analysis. The authors in [29] applied the variational energy approach to obtain the critical buckling load of a 3-D CSSS thick rectangular plate using a new displacement theory. From the compatibility equation obtained from first principle, the displacement functions were derived and applied in analyzing the plates and this yielded exact solutions. In contrast to refined plate theories, their theory analyzed all the stress elements of the plate, but SSFS thick plate was not taken into account.

The authors in [31] actually studied the static analysis of a three edge simply supported, one support free (SSFS) rectangular thick plate and author in [32] studies thick plate with one edge clamped and other three edges simply supported (CSSS) using RPT. Both authors [31, 32] obtained expressions for the analysis of critical imposed load of the plate at specified limit state or elastic yield stress. They neither determine the critical buckling load that may occur due to compressive load on the plate nor applied an exact 3-D plate theory for reliable results.

The physical properties of SSFS plate material is that, the three edges are supported by a beam and the other remaining edge are free of support, depicting the relevance of the present study. This is because the boundary condition depends on the type of beam/column support in the plate, thus when SSFS initial condition occurs in the a plate material, analyzing it as any other type of plate as mentioned in the literature will not account for stresses induced. This is because, stresses are induced due to the applied load (in-plane load) in this case, and hence, non-negligible error results. Also, the thick plate assumption made in this work made it clear that the deformation line after bending is no longer normal to the mid-plane of the plate thereby considering the effect of shear deformation which may arise if the thickness of the plate are enhanced.

It can be noted in the literature that other shape functions like an exponential, trigonometric and hyperbolic were used, which are not flexible enough to handle all types of plate boundary conditions such as SSFS. This work filled the gap as they applied the variation energy method with a polynomial displacement function to a three-dimensional stability rectangular plate under uniaxial compressive load. Furthermore, compared with previous studies, the distinguishing feature of this current study with other works is that previous studies used an assumed the deflection function while the present study is tends to obtain an exact polynomial deflection function from the equilibrium equation developed. Apart from the work in [26, 28, 29], no work can be seen that adopted the 3-D plate theory to evaluate the stability of rectangular thick plate. The work in [26, 28, 29] did not study the plate that is freely supported at the third edge and other three edges simply supported (SSFS); so this research work is needed.

This study is focusing on the stability analysis of SSFS rectangular plates section subjected to a uniaxial compressive load using a three-dimensional plate theory with polynomial displacement function. In this work, the aspect ratio effect of the critical buckling load of the plate was evaluated to show its capacity of the derived model to analyze different categories of plate, by presenting a novel formula for determining the critical buckling load of a thick rectangular plate.

3. Methodology

In this work, and displacement in x, y and z axis; u, v and w respectively are applied and presented in Equation (1), (2) and (3) (see [1]):

$$u = F(z)\theta_x \quad (1)$$

$$v = F(z)\theta_y \quad (2)$$

where; F is deformation profile, θ_x slope in x-axis and θ_y is slope in y-axis of the plate.

It can be seen in figure 1, that the six strains and stress elements required for the analysis were determined in line with the work of authors in [2].

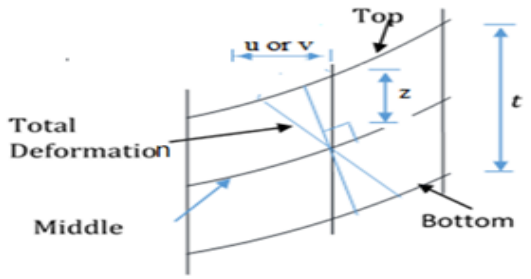

Figure 1: displacement of x-z (or y-z)

3.1. Formulation of Total Potential Energy

The energy [∏] equation were obtained in line with the authors in [7] and presented as:

$$\Pi = \frac{D^* ab}{2a^2}\int_0^1\int_0^1\left[(1-\mu)\left(\frac{\partial\theta_x}{\partial R}\right)^2 + \frac{1}{\beta}\frac{\partial\theta_x}{\partial R}.\frac{\partial\theta_y}{\partial Q} + \frac{(1-\mu)}{\beta^2}\left(\frac{\partial\theta_y}{\partial Q}\right)^2 + \frac{(1-2\mu)}{2\beta^2}\left(\frac{\partial\theta_x}{\partial Q}\right)^2 + \frac{(1-2\mu)}{2}\left(\frac{\partial\theta_y}{\partial R}\right)^2 + \frac{6(1-2\mu)}{t^2}\left(a^2{\theta_x}^2 + a^2{\theta_y}^2 + \left(\frac{\partial w}{\partial R}\right)^2 + \frac{1}{\beta^2}\left(\frac{\partial w}{\partial Q}\right)^2 + 2a.\theta_x\frac{\partial w}{\partial R} + \frac{2a.\theta_y}{\beta}\frac{\partial w}{\partial Q}\right) + \frac{(1-\mu)a^2}{t^4}\left(\frac{\partial w}{\partial S}\right)^2 - \frac{N_x}{D^*}.\left(\frac{\partial w}{\partial R}\right)^2\right] dR\,dQ \quad (3)$$

Where; N_x is the uniform applied uniaxial compression load of the plate.

3.2. Compatibility Equations

By differentiation of total potential energy with respect to θ_x and θ_y and establish the relation between the rotation and deflection [8] gives:

$$\frac{\partial\Pi}{\partial\theta_x} = \frac{D^* ab}{2a^2}\int_0^1\int_0^1\left[(1-\mu)\frac{\partial^2\theta_x}{\partial R^2} + \frac{1}{2\beta}.\frac{\partial^2\theta_y}{\partial R\partial Q} + \frac{(1-2\mu)}{2\beta^2}\frac{\partial^2\theta_x}{\partial Q^2} + \frac{6(1-2\mu)}{t^2}\left(a^2\theta_x + a.\frac{\partial w}{\partial R}\right)\right] dR\,dQ = 0 \quad (4)$$

$$\frac{\partial\Pi}{\partial\theta_y} = \frac{D^* ab}{2a^2}\int_0^1\int_0^1\left[\frac{1}{2\beta}.\frac{\partial^2\theta_x}{\partial R\partial Q} + \frac{(1-\mu)}{\beta^2}\frac{\partial^2\theta_y}{\partial Q^2} + \frac{(1-2\mu)}{2}\frac{\partial^2\theta_y}{\partial R^2} + \frac{6(1-2\mu)}{t^2}\left(a^2\theta_y + \frac{a.}{\beta}\frac{\partial w}{\partial Q}\right)\right] dR\,dQ = 0 \quad (5)$$

Given that [2];

$$\theta_x = \gamma_{xz} - \frac{1}{a}.\frac{\partial w}{\partial R} = \frac{c}{a}\frac{\partial w}{\partial R} \quad (6)$$

$$\theta_y = \gamma_{yz} - \frac{1}{a\beta}.\frac{\partial w}{\partial Q} = \frac{c}{a\beta}.\frac{\partial w}{\partial Q} \quad (7)$$

where c is a quantity whose expression or value shall be obtained later.

Hence, for zero integrands, the true solution was gotten by simplifying and factorizing the outcome of the compatibility equation to give the algebraic solution in Equation (8) which is the relation of known and unknown variable to get the constant quantity c.

$$\frac{6(1-2\mu)(1+c)}{t^2} = -\frac{c(1-\mu)}{a^2}\left(\frac{\partial^2 w}{\partial R^2} + \frac{1}{\beta^2}\frac{\partial^2 w}{\partial Q^2}\right) \quad (8)$$

3.3. Governing Equations

The governing differential equation was obtained after the total potential energy was minimized with respect to deflection (w) and its solution yields the exact polynomial deflection function:

$$\frac{\partial\Pi}{\partial w} = \frac{D^*}{2a^2}\int_0^1\int_0^1\left[\frac{12(1-2\mu)}{t^2}\left(\frac{\partial^2 w}{\partial R^2} + \frac{1}{\beta^2}.\frac{\partial^2 w}{\partial Q^2} + a.\frac{\partial\theta_x}{\partial R} + \frac{a}{\beta}\frac{\partial\theta_y}{\partial Q}\right) + 2\frac{(1-\mu)a^2}{t^4}.\frac{\partial^2 w}{\partial S^2} - 2\frac{N_x}{D^*}.\frac{\partial^2 w}{\partial R^2}\right] dR\,dQ = 0 \quad (9)$$

By factorizing and simplifying the outcome, gives:

$$\left(\frac{\partial^4 w_1}{\partial R^4} + \frac{2}{\beta^2}.\frac{\partial^4 w_1}{\partial R^2\partial Q^2} + \frac{1}{\beta^4}.\frac{\partial^4 w_1}{\partial Q^4} - \frac{N_{x1}a^4}{gD^*}.\frac{\partial^2 w_1}{\partial R^2}\right) w_S + \frac{w_1}{g}\left(\frac{(1-\mu)a^4}{t^4}.\frac{\partial^2 w_S}{\partial S^2}\right) = 0 \quad (10)$$

One of the possibilities of Equation (10) to be true is for the terms in each of the two brackets sum to zero. That is:

$$\frac{\partial^4 w_1}{\partial R^4} + \frac{2}{\beta^2}.\frac{\partial^4 w_1}{\partial R^2\partial Q^2} + \frac{1}{\beta^4}.\frac{\partial^4 w_1}{\partial Q^4} - \frac{N_{x1}a^4}{gD^*}.\frac{\partial^2 w_1}{\partial R^2} = 0 \quad (11)$$

$$\frac{(1-\mu)a^4}{t^4}.\frac{\partial^2 w_S}{\partial S^2} = 0 \quad (12)$$

The solution of Equation (11) to get an exact deflection and slope of the plate.

$$w = \Delta_0\,[1\ \ R\ \ R^2 R^3 R^4]\begin{bmatrix}a_0\\a_1\\a_2\\a_3\\a_4\end{bmatrix}.[1\ \ Q\ \ Q^2 Q^3 Q^4]\begin{bmatrix}b_0\\b_1\\b_2\\b_3\\b_4\end{bmatrix} \quad (13)$$

Similarly:

$$\theta_x = \frac{c}{a}.\Delta_0.[1\ \ 2R\ \ 3R^2\ \ 4R^3]\begin{bmatrix}a_1\\a_2\\a_3\\a_4\end{bmatrix}.[1\ \ Q\ \ Q^2 Q^3 Q^4]\begin{bmatrix}b_0\\b_1\\b_2\\b_3\\b_4\end{bmatrix} = \frac{A_{2R}}{a}.\frac{\partial h}{\partial R} \quad (14)$$

And;

$$\theta_y = \frac{c}{a\beta}.\Delta_0.[1\ \ R\ \ R^2 R^3 R^4]\begin{bmatrix}a_0\\a_1\\a_2\\a_3\\a_4\end{bmatrix}.[1\ \ 2Q\ \ 3Q^2\ \ 4Q^3]\begin{bmatrix}b_1\\b_2\\b_3\\b_4\end{bmatrix} = \frac{A_{2Q}}{a\beta}.\frac{\partial h}{\partial Q} \quad (15)$$

where:

$$A_{2R} = c.\Delta_0.\frac{\partial h}{\partial R}.A_Q \quad (16)$$

$$A_{2Q} = c.\Delta_0 \frac{\partial h}{\partial Q}.A_R \quad (17)$$

The constants; c, Δ_0, A_R and A_Q, thus, putting Equations (13), (14) and (15) into (3), simplifying gives (see [8]):

$$\prod = \frac{D^* ab}{2a^4}\left[(1-\mu){A_{2R}}^2 k_{RR} + \frac{1}{\beta^2}\left[A_{2R}.A_{2Q} + \frac{(1-2\mu){A_{2R}}^2}{2} + \frac{(1-2\mu){A_{2Q}}^2}{2}\right]k_{RQ} + \frac{(1-\mu){A_{2Q}}^2}{\beta^4}k_{QQ} + 6(1-2\mu)\left(\frac{a}{t}\right)^2\left([{A_{2R}}^2 + {A_1}^2 + 2A_1A_{2R}].k_R + \frac{1}{\beta^2}.[{A_{2Q}}^2 + {A_1}^2 + 2A_1A_{2Q}].k_Q\right) - \frac{N_x a^2 {A_1}^2}{D^*}.k_R\right] \quad (18)$$

where:

$$k_{RR} = \int_0^1\int_0^1\left(\frac{\partial^2 h}{\partial R^2}\right)^2 dRdQ;\ k_R = \int_0^1\int_0^1\left(\frac{\partial h}{\partial R}\right)^2 dRdQ \quad (19a)$$

$$k_{QQ} = \int_0^1\int_0^1\left(\frac{\partial^2 h}{\partial Q^2}\right)^2 dRdQ;\ k_Q = \int_0^1\int_0^1\left(\frac{\partial h}{\partial Q}\right)^2 dRdQ \quad (19b)$$

$$k_{RQ} = \int_0^1\int_0^1\left(\frac{\partial^2 h}{\partial R\partial Q}\right)^2 dRdQ \quad (19c)$$

Minimizing Equation (18) with respect to A_{2R} gives:

$$(1-\mu)A_{2R}k_{RR} + \frac{1}{2\beta^2}[A_{2Q} + A_{2R}(1-2\mu)]k_{RQ} + 6(1-2\mu)\left(\frac{a}{t}\right)^2[A_{2R} + A_1].k_R = 0 \quad (20)$$

Minimizing Equation (18) with respect to A_{2Q} gives:

$$\frac{(1-\mu)A_{2Q}}{\beta^4}k_{QQ} + \frac{1}{2\beta^2}[A_{2R} + A_{2Q}(1-2\mu)]k_{RQ} + \frac{6}{\beta^2}(1-2\mu)\left(\frac{a}{t}\right)^2([A_{2Q} + A_1].k_Q) = 0 \quad (21)$$

Rewriting Equations (20) and (21) gives:

$$\left[(1-\mu)k_{RR} + \frac{1}{2\beta^2}(1-2\mu)k_{RQ} + 6(1-2\mu)\left(\frac{a}{t}\right)^2 k_R\right]A_{2R} + \left[\frac{1}{2\beta^2}k_{RQ}\right]A_{2Q} = \left[-6(1-2\mu)\left(\frac{a}{t}\right)^2 k_R\right]A_1 \quad (22)$$

$$\left[\frac{1}{2\beta^2}k_{RQ}\right]A_{2R} + \left[\frac{(1-\mu)}{\beta^4}k_{QQ} + \frac{1}{2\beta^2}(1-2\mu)k_{RQ} + \frac{6}{\beta^2}(1-2\mu)\left(\frac{a}{t}\right)^2 k_Q\right]A_{2Q} = \left[-\frac{6}{\beta^2}(1-2\mu)\left(\frac{a}{t}\right)^2 k_Q\right]A_1 \quad (23)$$

Solving Equations (22) and (23) simultaneously gives:

$$A_{2R} = G_2A_1 \quad (24)$$

$$A_{2Q} = G_3A_1 \quad (25)$$

Let:

$$G_2 = \frac{(c_{12}c_{23} - c_{13}c_{22})}{(c_{12}c_{12} - c_{11}c_{22})} \quad (26)$$

$$G_3 = \frac{(c_{12}c_{13} - c_{11}c_{23})}{(c_{12}c_{12} - c_{11}c_{22})} \quad (27)$$

$$c_{11} = (1-\mu)k_{RR} + \frac{1}{2\beta^2}(1-2\mu)k_{RQ} + 6(1-2\mu)\left(\frac{a}{t}\right)^2 k_R \quad (28)$$

$$c_{22} = \frac{(1-\mu)}{\beta^4}k_{QQ} + \frac{1}{2\beta^2}(1-2\mu)k_{RQ} + \frac{6}{\beta^2}(1-2\mu)\left(\frac{a}{t}\right)^2 k_Q \quad (29)$$

$$c_{12} = c_{21} = \frac{1}{2\beta^2}k_{RQ};\ c_{13} = -6(1-2\mu)\left(\frac{a}{t}\right)^2 k_R;\ c_{23} = c_{32} = -\frac{6}{\beta^2}(1-2\mu)\left(\frac{a}{t}\right)^2 k_Q \quad (30)$$

Minimizing Equation (18) with respect to A_1 and simplifying the outcome gives:

$$6(1-2\mu)\left(\frac{a}{t}\right)^2\left([1+G_2].k_R + \frac{1}{\beta^2}.[1+G_3].k_Q\right) - \frac{N_x a^2}{D^*}.k_R = 0 \quad (31)$$

Rearranging Equation (31) and simplify the outcome to gives:

$$\frac{N_x a^2}{D^*} = 6(1-2\mu)\left(\frac{a}{t}\right)^2\left([1+G_2] + \frac{1}{\beta^2}.[1+G_3].\frac{k_Q}{k_R}\right) \quad (32)$$

3.4. Numerical Analysis

A numerical analysis is performed on the rectangular thick plate that is freely supported at the third edge and other three edges simply supported (SSFS) under compressive load as presented in the Figure 2.

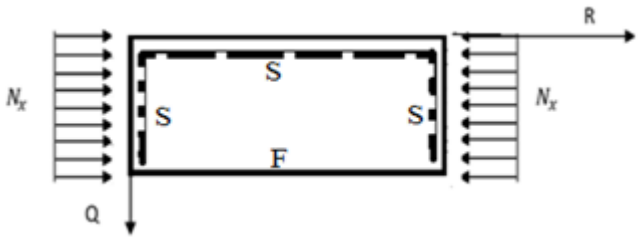

Figure 2: A Section of SSFS Rectangular Thick Plate under Uniaxial Compressive Load

The boundary conditions of the plate in figure 3 are as follows:

$$\text{At } R = Q = 0; \text{deflection } (w) = 0 \quad (33)$$

$$\text{At } R = Q = 0, \text{bending moment}\left(\frac{d^2w}{dR^2} \text{ and } \frac{d^2w}{dQ^2}\right) = 0 \quad (34)$$

$$\text{At } R = Q = 1;\ \text{deflection } (w) = 0; \left(\frac{d^2w}{dQ^2}\right) = 0 \quad (35)$$

$$\text{At } R = Q = 1; \left(ie.\frac{d^2w}{dR^2}\right) = 0;\ \text{shear force}\left(\frac{d^3w}{dQ^3}\right) = 0 \quad (36)$$

$$\text{At, } Q = 1; \text{slope} = \frac{2}{3b_5}\left(ie.\frac{dw}{dQ} = \frac{2}{3b_5}\right) \quad (37)$$

Substituting Equations (33-37) into established equation and solving gives the following constants:

$$a_0 = 0;\ a_1 = \frac{F_{a4}}{24};\ a_2 = 0;\ a_3 = \frac{-F_{a4}}{2} \quad (38)$$

$$b_0 = 0;\ b_1 = -\frac{7}{3}b_5;\ b_2 = 0;\ b_3 = \frac{b_5}{6};\ F_{b4} = -\frac{2b_5}{3} \quad (39)$$

Substituting the constants of Equation (38) and (39) into established equations gives;

$$w = \left(F_{a4}\frac{R}{24} - F_{a4}\frac{R^3}{12} + F_{a4}\frac{R^4}{24}\right).\left(b_5\frac{Q}{52} - b_5\frac{Q^3}{36} + b_5\frac{2Q^4}{72} - b_5\frac{Q^5}{120}\right) \quad (40)$$

Simplifying Equation (40) which satisfying the boundary conditions of Equation (33-37) gave;

$$w = \frac{F_{a4}}{24}.\frac{b_5}{360}(R - 2R^3 + R^4)(7Q - 10Q^3 + 10Q^4 - 3Q^5) \quad (41)$$

Recall from that;

$w = A_1.h$

Let the amplitude,

$$A_1 = \frac{F_{a4} \times b_5}{8640} \quad (42)$$

And;

$$h = (R - 2R^3 + R^4) \times \left(\frac{7Q}{3} - \frac{10}{3}Q^3 + \frac{10}{3}Q^4 - Q^5\right) \quad (43)$$

Thus, the polynomial deflection functions after satisfying the boundary conditions is:

$$w = A_1(R - 2R^3 + R^4).\left(\frac{7Q}{3} - \frac{10}{3}Q^3 + \frac{10}{3}Q^4 - Q^5\right) \quad (44)$$

Using the polynomial displacement function, the solution of stiffness coefficients for deflection of rectangular thick plate analysis subjected to the SSFS boundary condition was obtained and presented in Table 1.

Let; the polynomial stiffness coefficient values of SSFS plate $k_{RR} = 4.0258$; $k_{RQ} = 1.0331$; $k_{QQ} = 0.1875$; $k_R = 0.4074$; $k_Q = 0.10466$

Where; the Poisson's ratio of the plate be 0.3.

4. Results and Discussions

In this section, a numerical solution of the problem of a thick rectangular plate that is freely supported at the third edge and other three edges simply supported (SSFS) presented in Figure 2, is obtained using the Equation presented in the previous section. The non-dimensional value of the critical buckling load for an isotropic SSFS rectangular plate under uniaxial compression is presented in the Figures 1 through 11, different aspect ratio respectively. The numerical and graphical comparison was made to show the disparities between the present study and the literature under review to show the effect of aspect ratio on the buckling load in a 3-D stability analysis of rectangular plate at varying thickness. The span to thickness ratio considered is ranged between 4 through 1500, which is obviously seen to span from the thick plate, moderately thick plate and thin plate (see [4]). On the other hand, the length and breadth ratio (aspect ratio) in consideration in this study includes; 1.0, 1.5, 2.0, 2.5, 3.0, 3.5, 4.0, 4.5 and 5.0. Meanwhile, in this study, more attention is to be given to the effect of aspect ratio on the buckling load for thicker plate. This is because, the effect of shear deformation was considered in the analysis, and that made it possible to predict accurately the buckling load of any type of plate ranging from thin through thick plate.

The present work obtained non-dimensional result of buckling load of the plate by expressing the displacement function of the plate in the form of polynomial to analyze the effect of aspect ratio of the critical buckling load of the plate. Figure 3 in Figure 11 contains the graphical representation of the result of the non-dimensional critical buckling load SSFS rectangular thick plate using the established exact polynomial displacement function. The value of the critical buckling load N_{xcr} decreases as the aspect ratio of the plate increases, as shown in Figure 3 to Figure 11, the value of critical buckling load decreases. This means that the failure in a plate structure is bound to occur as the in-plane load on the plate increases and gets to the critical buckling.

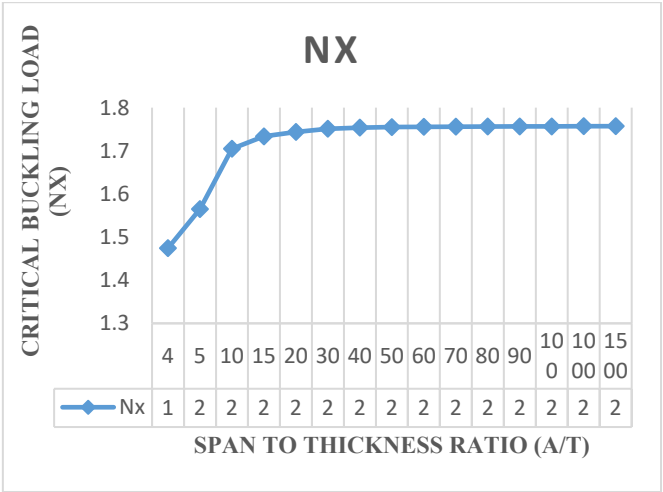

Figure 3: Graph of Critical buckling load (N_{xcr}) versus span-thickness ratio of a rectangular plate at aspect ratio of 1.0

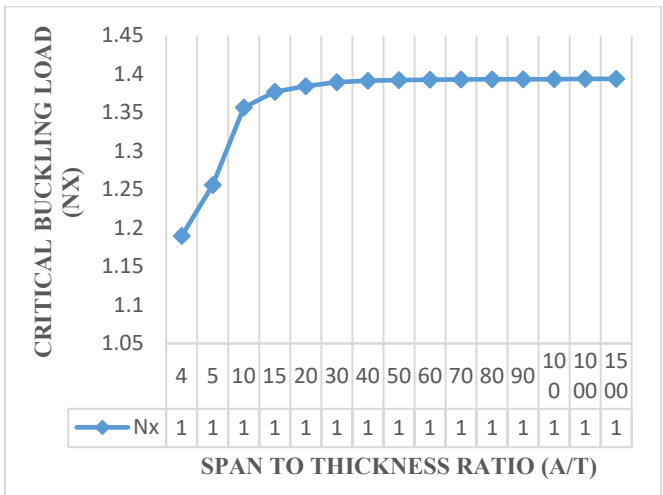

Figure 4: Graph of Critical buckling load (N_{xcr}) versus span-thickness ratio of a rectangular plate at aspect ratio of 1.5

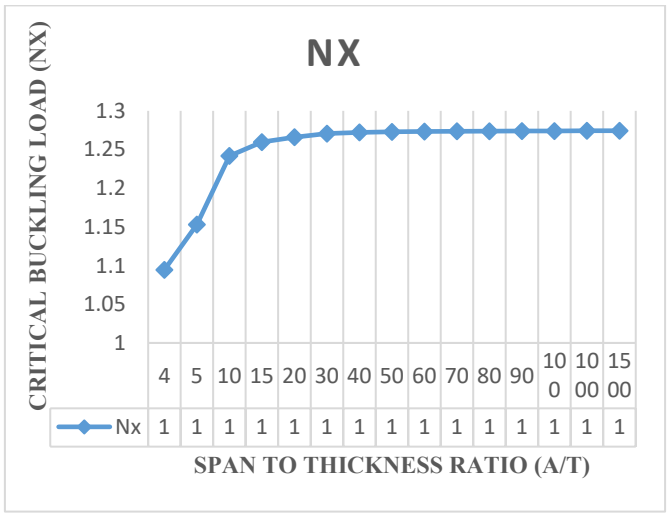

Figure 5: Graph of Critical buckling load (N_{xcr}) versus span-thickness ratio of a rectangular plate at aspect ratio of 2.0

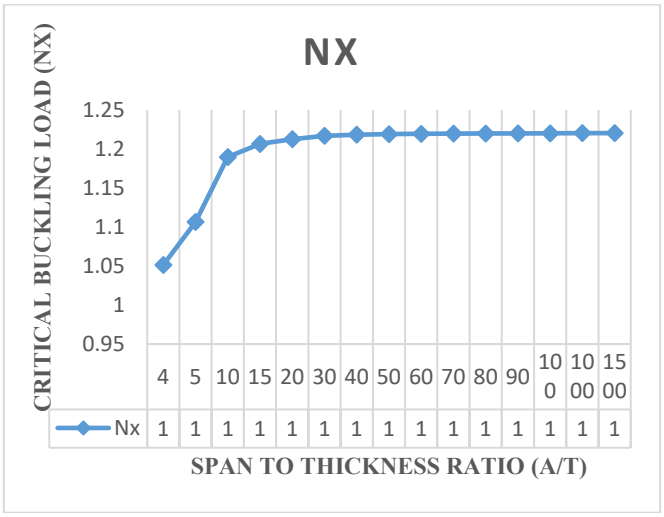

Figure 6: Graph of Critical buckling load (N_{xcr}) versus span-thickness ratio of a rectangular plate at aspect ratio of 2.5

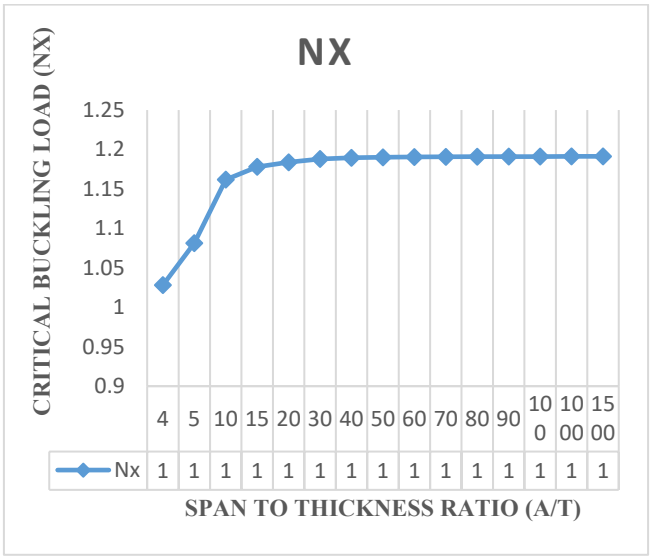

Figure 7: Graph of Critical buckling load (N_{xcr}) versus span-thickness ratio of a rectangular plate at aspect ratio of 3.0

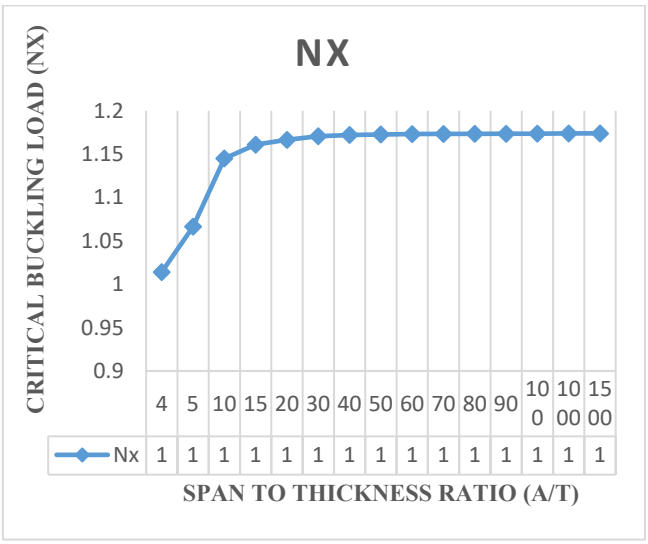

Figure 8: Graph of Critical buckling load (N_{xcr}) versus aspect ratio of a rectangular plate at length-width ratio of 3.5

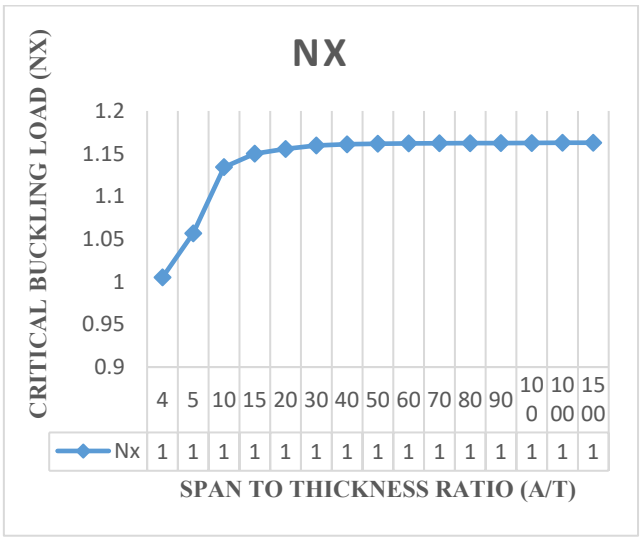

Figure 9: Graph of Critical buckling load (N_{xcr}) versus span-thickness ratio of a rectangular plate at aspect ratio of 4.0

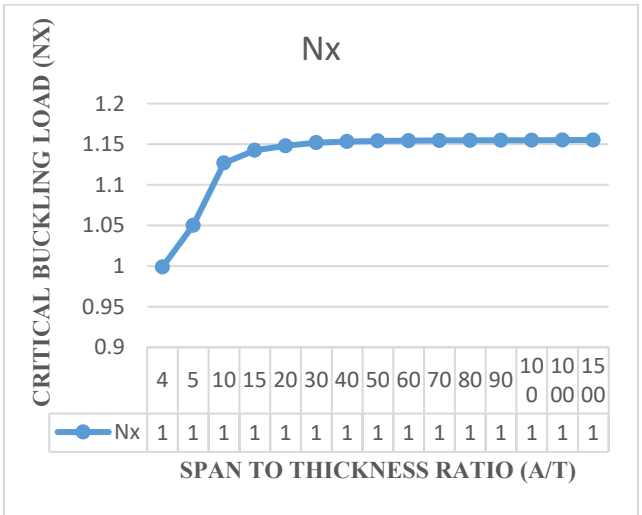

Figure 10: Graph of Critical buckling load (N_{xcr}) versus span-thickness ratio of a rectangular plate at aspect ratio of 4.5

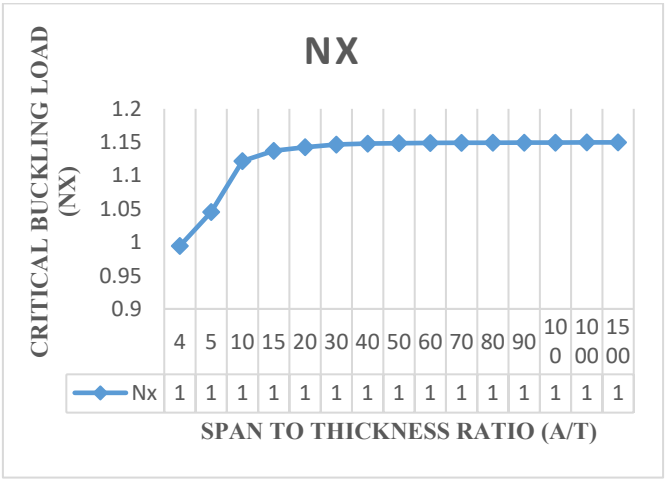

Figure 11: Graph of Critical buckling load (N_{xcr}) versus span-thickness ratio of a rectangular plate at aspect ratio of 5.0

The results obtained in the Figures reveals that the values of critical buckling load increase as the span-thickness ratio increases. This reveals that as the span or the depth of the plate is altered, it affects the performance in terms of the serviceability of the plate. Thus, caution must be taken when selecting the depth and other dimensions along the x and y co-ordinate of the plate to ensure safety and accuracy of the analysis.

The present theory predicts the buckling load of 1.29, 1.50, 1.52, 1.53, 1.54, 1.54, 1.54, 1.54, 1.54, 1.54, 1.54, 1.54, 1.54 and 1.54 for a square plate in the span to thickness ratio of 4, 10, 15, 20, 30, 40, 50, 60, 70, 80, 90, 100, 1000 and 1500. Looking closely at the result of buckling load for the present study at the span to thickness ratio of 30 and beyond, it is seen that the value of critical buckling load of the plate maintained a constant value of 1.54 for square plate, 1.22 for aspect ratio of 1.5, 1.11 for aspect ratio of 2.0, 1.07 for aspect ratio of 2.5, 1.04 for aspect ratio of 3.0, 1.03 for aspect ratio of 3.5, 1.02 for aspect ratio of 4.0, 1.01 for aspect ratio of 4.5, 1.01 for aspect ratio of 5.0. This shows that the result of the critical buckling load of thin and moderately thick plate using the 3-D theory is the same for the stability analysis of rectangular plate under the SSFS boundary condition. The Figures 3 to 12 proofs that the value of critical load for thin plate and thick plate (see [29]) which described the thin and moderately thick plate as the one whose span to thickness ratio is equal or less than 30.

It can be deduced that the present model using a derived shape function is safer and more credible to use as it considered the six stress elements to yield the exact solution for the analysis of thick plate that is freely supported at the third edge and other three edges simply supported (SSFS). Hence, the result of the present analysis, which contains all the stress element and ensured that the variation of the stresses through the thickness of the plate which induced buckling are uniformly distributed, showed that the present method can be used with confidence for stability analysis of plate.

5. Conclusion

The buckling of an isotropic thick plate that is freely supported at the third edge and other three edges simply supported (SSFS), was investigated. The 3-D theory using energy methods with polynomial shape function was employed. The solution obtained showed a good agreement with results from previous works. It is observed that the classical plate theories give reliable results for thin plates, refined plate theories the 2-D refined plate theory (RPT) is only an approximate relation for buckling analysis of thick plate and when applied to the thick plate will under-predicts buckling loads as they neglect the transverse normal stresses along the thickness axis of the plate while 3-D theory with exact shape functions developed in this study yield exact solution for the buckling analysis of thick plates.

6. Recommendation

The polynomial displacement function developed in this study produces an exact solution as they emanated from a complete three-dimensional theory which is more reliable solution in the stability analysis of plates and, can be recommended for analysis of any type of rectangular plate subjected to such loading and boundary condition.

7. Contribution to Knowledge

The major contribution to knowledge in this study is the novel formula for calculating the critical buckling load of the plate which was derived from the principle of elasticity and satisfied SSFS boundary condition when solved with polynomial shape function.

The exact deflection and slope model which was established from the 3-D stability analysis derived from equilibrium equation using static elastic theory to get exact polynomial displacement functions of the plate.

References

[1]. F. C. Onyeka, B. O. Mama, T. E. Okeke, "Elastic Bending Analysis Exact Solution of Plate using Alternative I Refined Plate Theory," *Nigerian Journal of Technology (NIJOTECH)*, vol. 40, no. 6, pp. 1018 – 1029, 2021. doi: http://dx.doi.org/10.4314/njt.v40i6.4

[2]. F. C. Onyeka, B. O. Mama, "Analytical Study of Bending Characteristics of an Elastic Rectangular Plate using Direct Variational Energy Approach with Trigonometric Function," *Emerging Science Journal*, vol. 5, no. 6, pp. 916–926, 2021. **doi:** 10.28991/esj-2021-01320

[3]. K. Chandrashekhara, *Theory of Plates*, University Press (India) Limited, 2000.

[4]. F. C. Onyeka, F. O. Okafor, H. N. Onah, "Application of Exact Solution Approach in the Analysis of Thick Rectangular Plate," *International Journal of Applied Engineering Research*, vol. 14, no. 8, pp. 2043-2057, 2019.

[5]. F. C. Onyeka, E. T. Okeke, "Analytical Solution of Thick Rectangular Plate with Clamped and Free Support Boundary Condition using Polynomial Shear Deformation Theory," *Advances in Science, Technology and Engineering Systems Journal*, vol. 6, no. 1, pp. 1427-1439, 2021, doi:10.25046/aj0601162..

[6]. A. Hassan, N. Kurgan, "Modeling and Buckling Analysis of Rectangular Plates in ANSYS," *International Journal of Engineering*

& Applied Sciences (IJEAS), vol. 11, no. 1, pp. 310-329, 2019. doi: http://dx.doi.org/10.24107/ijeas.531011.

[7]. F. C. Onyeka. B. O. Mama, C. D. Nwa-David, "Analytical Modelling of a Three-Dimensional (3D) Rectangular Plate Using the Exact Solution Approach," *IOSR Journal of Mechanical and Civil Engineering (IOSR-JMCE)*, vol. 19, no. 1 Ser. I, pp. 76-88, 2022. doi: 10.9790/1684-1901017688.

[8]. F. C. Onyeka, F. O. Okafor, H. N. Onah, "Buckling Solution of a Three-Dimensional Clamped Rectangular Thick Plate Using Direct Variational Method," *IOSR Journal of Mechanical and Civil Engineering (IOSR-JMCE)*, vol. 18, no. 3, pp. 10-22, 2021, doi: 10.9790/1684-803031022.

[9]. S. P. Timoshenko, J. M. Gere, W. Prager, *Theory of Elastic Stability*, Second Edition. In Journal of Applied Mechanics (2nd ed.), vol. 29, no. 1, McGraw-Hill Books Company, 1962. doi:10.1115/1.3636481.

[10]. F. C. Onyeka, D. Osegbowa, E. E. Arinze, "Application of a New Refined Shear Deformation Theory for the Analysis of Thick Rectangular Plates," *Nigerian Research Journal of Engineering and Environmental Sciences*, vol. 5, no. 2, 901-917, 2020.

[11]. C. C. Ike, "Kantorovich-Euler Lagrange-Galerkin's Method for Bending Analysis of Thin Plates," *Nigerian Journal of Technology (NIJOTECH)*, vol. 36, no. 2, pp. 351-360, 2017.

[12]. J. N. Reddy, *Classical Theory of Plates*, In Theory and Analysis of Elastic Plates and Shells, CRC Press, 2006. doi: 10.1201/9780849384165-7.

[13]. F. C. Onyeka, O. M. Ibearugbulem, "Load Analysis and Bending Solutions of Rectangular Thick Plate," *International Journal of Emerging Technologies*, vol. 11, no. 3, pp. 1030-1110, 2020.

[14]. R. D. Mindlin, "Influence of Rotatory Inertia and Shear on Flexural Motions of Isotropic, Elastic Plates," *J. Appl. Mech. Trans. ASME*, vol. 18, no. 1, pp. 31-38, 1951.

[15]. F. C. Onyeka, E. T. Okeke, J. Wasiu, "Strain–Displacement Expressions And Their Effect On The Deflection And Strength Of Plate," *Advances in Science, Technology and Engineering Systems*, vol. 5, no. 5, pp. 401-413, 2020, doi:10.25046/AJ050551.

[16]. A. S. Sayyad, Y. M. Ghugal, "Bending and Free Vibration Analysis Of Thick Isotropic Plates By Using Exponential Shear Deformation Theory," *Journal of Applied and Computational Mechanics*, vol. 6, pp. 65-82, 2012.

[17]. F. C. Onyeka, B. O. Mama, C. D. Nwa-David. "Application of Variation Method in Three Dimensional Stability Analysis of Rectangular Plate Using Various Exact Shape Functions." *Nigerian Journal of Technology*, vol. 41, no. 1, pp. 8-20, 2022. doi: http://*dx.doi.org/10.4314/njt.v41i1.2*

[18]. J. N. Reddy, N. Phan, "Stability and Vibration of Isotropic, Orthotropic and Laminated Plates According to a Higher-Order Shear Deformation Theory," *Journal of sound and vibration*, vol. 98, no. 2, pp. 157-170, 1985.

[19]. F. C. Onyeka, O. T. Edozie, "Application of Higher Order Shear Deformation Theory in the Analysis of thick Rectangular Plate," *International Journal on Emerging Technologies*, vol. 11, no. 5, pp. 62-67, 2020.

[20]. F. C. Onyeka, T. E. Okeke, "New Refined Shear Deformation Theory Effect On Non-Linear Analysis of A Thick Plate Using Energy Method." *Arid Zone Journal of Engineering, Technology and Environment*, vol. 17, no. 2, 121-140, 2021.

[21]. D. O. Onwuka, U. G. Eziefula, O. M. Ibearugbulem, "Inelastic Buckling of Rectangular Panel with a Simply Supported Edge and Three Clamped Edges," *International Journal of Applied Science and Engineering*, vol. 14, no. 1, pp. 39-48, 2016.

[22]. S. E Iwuoha, "Biaxial Buckling Coefficients of Thin Rectangular Isotropic Plates, Having One Edge Simply Supported and The Other Edges Clamped," *International Journal of Scientific & Engineering Research*, vol. 9, no. 7, pp. 1918-1925, 2018.

[23]. S. M. Gunjal, R. B. Hajare, A. S. Sayyad, M. D. Ghodle, "Buckling Analysis of Thick Plates Using Refined Trigonometric Shear Deformation Theory," *Journal of Materials and Engineering Structures*, vol. 2, pp. 159-167, 2015.

[24]. A. S. Sayyad, Y. M. Ghugal, "Buckling Analysis of Thick Isotropic Plates by Using Exponential Shear Deformation Theory," *Applied and Computational Mechanics*, vol. 6, pp. 185-196, 2012.

[25]. J. C. Ezeh, I. C. Onyechere, O. M. Ibearugbulem, U. C. Anya, L. Anyaogu, "Buckling Analysis of Thick Rectangular Flat SSSS Plates using Polynomial Displacement Functions," *International Journal of Scientific & Engineering Research*, vol. 9, no. 9, pp. 387-392, 2018.

[26]. F. C. Onyeka, B.O. Mama, T. E. Okeke, "Exact Three-Dimensional Stability Analysis of Plate Using A Direct Variational Energy Method," *Civil Engineering Journal*, vol. 8, no. 1, pp. 60–80, 2022. DOI: http://dx.doi.org/10.28991/CEJ-2022-08-01-05.

[27]. V. T. Ibeabuchi, O. M. Ibearugbulem, C. Ezeah, O. O. Ugwu, "Elastic Buckling Analysis of Uniaxially Compressed CCCC Stiffened Isotropic Plates," *Int. J. of Applied Mechanics and Engineering*, vol. 25, no. 4, pp. 84-95, 2020. doi: 10.2478/ijame-2020-0051.

[28]. F. C. Onyeka, F. O. Okafor, H. N. Onah, "Buckling Solution of a Three-Dimensional Clamped Rectangular Thick Plate Using Direct Variational Method," *IOSR Journal of Mechanical and Civil Engineering (IOSR-JMCE)*, vol. 18, no. 3 Ser. III, pp. 10-22, 2021. doi: 10.9790/1684-1803031022.

[29]. F. C. Onyeka, F. O. Okafor, H. N. Onah, "Application of a New Trigonometric Theory in the Buckling Analysis of Three-Dimensional Thick Plate," *International Journal of Emerging Technologies*, vol. 12, no. 1, pp. 228-240, 2021.

[30]. S. Uzoukwu, O. M. Ibearugbulem, C. E. Okere, J. I. Arimanwa, "Stability Analysis of Rectangular CCSS and CCCS Isotropic Plates using 3rd Order Energy Functional," *Global Scientific Journals*, vol. 9, no. 1, pp. 637-649, 2021.

[31]. F. C. Onyeka, C. D. Nwa-David, E. E. Arinze, "Structural Imposed Load Analysis of Isotropic Rectangular Plate Carrying a Uniformly Distributed Load Using Refined Shear Plate Theory," *FUOYE Journal of Engineering and Technology (FUOYEJET)*, vol. 6, no. 4, pp. 414-419, 2021. doi: http://dx.doi.org/10.46792/fuoyejet.v6i4.719.

[32]. F. C. Onyeka, "Critical Lateral Load Analysis of Rectangular Plate Considering Shear Deformation Effect," *Global Journal of Civil Engineering*, vol. 1, pp. 16-27, 2020. doi:10.37516/global.j.civ.eng.2020.0121.

Engr. Dr. F. C. Onyeka has done his bachelor's degree (B.Eng) in Civil Engineering from Anambra State University, Uli, Nigeria in 2006. He has done his master's degree (M.Eng) and doctorate degree (Ph.D) in Structural Engineering from University of Nigeria Nsukka in 2010 and 2018 respectively. His research area includes; Structural Engineering Mechanics, Plates and Shell theory and Theory of Elasticity, Variation Calculus and Stability of structures.

He is a University lecturer and a renowned researcher in the area of Structural Engineering Mechanics. He has about 54 publications which includes journals and conferences both locally and internationally with awards in some research breakthrough.

He is a member of professional bodies which includes; corporate member of Nigeria Society of Engineers (NSE) and member Nigeria Institute of Civil Engineers (NICE), a registered engineer in Council for regulation of Engineering in Nigeria (COREN).

Engr. Okeke, Edozie Thompson obtained bachelor's degree (B.Eng) in civil engineering from Enugu state University of Science and Technology in 2006. He got master's degree (M.Eng) in structural engineering at University of Nigeria Nsukka, in 2014. He currently undergoing Ph.D program at the University of Nigeria Nsukka. He is a University lecturer and a renowned researcher in the area of Structural Engineering Mechanics with about 12 publication which includes journals and conferences both locally and internationally. He is a member of professional bodies which includes; corporate member of Nigeria Society of Engineers (NSE) and member Nigeria Institute of Civil Engineers (NICE), a registered engineer in Council for regulation of Engineering in Nigeria (COREN).

Engr. Nwa-David, Chidobere David obtained B. Eng (First class honors' in Civil Engineering) from Michael Okpara University of Agriculture, Umudike, M. Eng (Structural Engineering) from Department of Civil Engineering, Federal University of Technology, Owerri. He is a University lecturer and a renowned researcher and his area research interests cut across all areas of civil engineering with specialized focus on structural engineering particularly in dynamics of structures, elasticity theory of plates, structural mechanics, concrete materials, variational calculus, sustainable structural systems, sustainable construction materials and studies with soft computing techniques. He is a Registered Engineer, Council for the Regulation of Engineering in Nigerian (COREN). He has participated in conferences where he presented papers. He has several scholarly articles published in local and international journals.

JENRS

Received: 23 February 2022, Revised: 03 April 2022, Accepted: 04 April 2022, Online: 12 April 2022

DOI: https://dx.doi.org/10.55708/js0104005

A Review on the Effect of Varied Sand Types in Concrete at High Temperature

Samya Hachemi [*,1], **Zine Elabidine Rahmouni** [2]

[1] LARGHYDE Laboratory, Civil engineering department, University of Biskra, 07000, Algeria
[2] Civil engineering department, University of Msila, 28000, Algeria
*Corresponding author: Samya HACHEMI, Biskra, 07000, Algeria, s.hachemi@univ-biskra.dz

ABSTRACT: In fact, aggregates in concrete generally occupied a considerable proportion of volume (60%-75%); sand constitutes about 30% to 50% of aggregates volume. It is well known that the nature of aggregates plays an important role on quality and properties of concrete. This suggests that the behavior of concrete exposed to high temperature is strongly linked to the nature and mineralogy of aggregates (coarse and fine aggregates). Furthermore, the description of the effect of high temperature on the components of concrete is intended to improve understanding of how concrete responds when it is exposed to elevated temperature. The fire performance of concrete depends on the thermal, physical and mechanical properties of its components. Sand can be classified into two groups according to its mineralogical nature: Siliceous and Calcareous, these two types of sand undergo different reactions when they are exposed to high temperature. Few studies have been published and showed that the nature of sand affects the concrete behavior at high temperature. This paper summaries the states-of-the-art studies on the mechanical and physical behavior of concrete made with different types of sand after being exposed to elevated temperature. It is revealed that the fire-response of concrete made with calcareous sand is different from that of concrete made with siliceous sand.

KEYWORDS: Aggregates, Behavior, Concrete, High temperature, Sand

1. Introduction

Hardened concrete is a heterogeneous multi-phases material consisting of a mixture of aggregates, occupying 60 to 75% of concrete volume and hydrated cement paste which represents 25 to 40% of concrete volume. Each component plays a well-defined role, that of filling attenuator of volume variations (recessed and rising in temperature and source of mechanical strength for aggregates) and that of binder and gives the concrete material its properties of rigidity and resistance for cement paste [1].

For a good concrete mix, fine aggregates need to be clean, hard, strong, and free of absorbed chemicals and other fine materials that could cause the deterioration of concrete. Unfortunately, majority of the natural sand used (rolled sand: sand of river, dune sand, and sand of sea) is selected for the price and the availability [2, 3]. Properties of sand affect the durability and performance of mortar, as fine aggregates is an essential component of concrete.

In [4], the author showed that manufactured sand is a best alternative for natural sand in terms of strength and durability and the concrete mix with 60% replacement has given good durable properties. Tebbal [5] studied the effect of using crushed sand (CS) as partial replacement of dune sand (DS) in various percentages (0, 1/3, 2/3, and 100%) on the physic-mechanical properties of HPC made with binary natural fine aggregates (DS and CS) at aggressive environment. Different types of high performance concrete (HPC) are made of using materials and products manufactured in Algeria: Portland Artificial CPJ CEMII 42.5 cement, superplasticizer (SP), two fractions of gravel (3/8 mm) and (8/15 mm) mm and two fillers (silica fume and granulated slag) with two types of sand CS (0/5 mm) and DS (0/5 mm). The experimental study shows that the parameters of workability of HPC are improved when the CS is partially replaced by the DS (<2/3). However, for high content of DS (>1/3), additional quantities of water is needed to meet the workability properties. The mechanical strengths decrease by adding

the DS to CS, but they reach acceptable values with CS in moderate dosages. The HPC performances are significantly better than the control concrete made up with the same aggregates. The specification tests of durability show that the water absorbing coefficients by capillarity increase after adding DS to the CS [5].

In the recent years, there were often fires in tunnels and buildings which cause very serious consequences in terms of human and economic losses. When concrete is subjected to high temperature, the material is the seat of numerous degradation processes. Among them, the aggregate-paste incompatibility may have a direct influence on the material stability [6].

The behavior of concrete structures exposed to high temperature depends on many simultaneously interacting factors ranging from composition of materials to the characteristics of fire and stress conditions.

Aggregates play an important role in concrete because they constitute the skeleton through which the efforts are transmitted. Under the effect of temperature, the aggregates decompose and undergo significant chemical and mineralogical transformations that modify the micro-structural characteristics of the material. Generally, the majority of aggregates used for making concrete are stable up to 500°C [7].

Recent studies have reported and showed that the nature of aggregates affects concrete behavior at high temperature [8–10]. Sand can be classified into two groups: Siliceous and Calcareous. These two natures of fine aggregates undergo different reactions when they are exposed to high temperature. Up to 300°C, commonly used aggregate materials are thermally stable. The quartz of siliceous sand can cause cracking at the paste-aggregates interface at about 575°C, due to the crystal transformation of quartz α to quartz β which is associated with a volume expansion of the order of 1%–5.7% [11, 12]. A similar distress can begin above 700°C in the case of carbonate sand, where calcium carbonate ($CaCO_3$) starts to decompose into free lime (CaO) and carbon dioxide (CO_2).

In [13], the author was interested to the effect of high temperature on color and residual compressive strength of concrete. This study identified the relationship between temperature change and a change in color and a decrease in compressive strength in a heat exposed concrete structure. For this study, concrete specimens were manufactured and heated to variable temperatures (100°C, 200°C, 300°C, 400°C, 500°C, 600°C, 700°C, and 800°C). Whereupon, the color change and the residual compressive strength were measured for analysis. The result of the study shows that color change and residual compressive strength in concrete structure temperature have a consistent relationship; therefore, it may be possible to know how much compressive strength of concrete exposed to high temperature reduces by measuring color changes and estimating heating temperature [13].

The purpose of this paper is to identify the relationship between the sand type of concrete and their behavior at high temperatures. Six types of concrete are made of using materials and products manufactured in Algeria: Portland Artificial CPJ CEMII 42.5 cement, superplasticizer (SP), two fractions of gravel 15 mm and 25 mm and two types of sand: Siliceous Sand (SS) and Calcareous Sand (CS).

2. Test Programs

2.1. Materials

The experimental investigation of some mechanical and physical properties is carried out on concrete with two different types of sand: CS and SS. The specific densities of these two types of sand measured in the laboratory according to standard NF P 18-554 [14] are 2600 kg/m^3 and 2200 kg/m^3, respectively. The maximum size for the two types of sand was 5 mm; the particle size distribution is shown in figure 1. SS and CS physical properties are summarized in table 1.

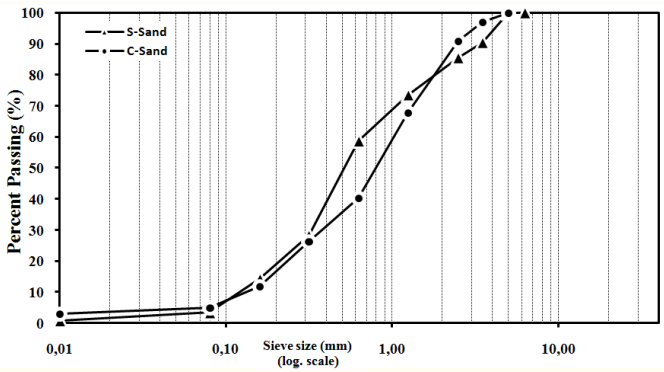

Figure 1. Particle size distributions of sand used [15].

Table 1. Physical properties of SS and CS [15].

Properties	S-Sand	C-Sand
Apparent density (g/cm^3)	1.70	1.64
Absolute density (g/cm^3)	2.60	2.20
Sand equivalent (%)	85.0	54.0
Finesse modulus	2.65	2.63
Water content (%)	0.35	0.20
Water absorption (%)	1.03	3.92

All mixtures are made with Portland cement (CPJ CEM II/A 42.5) and coarse calcareous aggregates with a maximum size of 25 mm (specific density is about 2630 kg/m3). The mixture proportions of the different concretes are presented in Table 2. The water used for the different concrete mixtures comes from the laboratory tap.

There were six series, concrete with fine aggregate as SS and concrete with fine aggregate as CS and each series comprised of many cubic specimens. Cubic specimens (100×100×100 mm^3) were made and cured under water at

room temperature until test time, then, they were removed from water and dried for 2 next days in room temperature (for minimizing the risk of spalling of concrete).

Table 2. Mix proportion of concrete (kg/m³) [15].

Mix	w/c	C	w	SS	CS	Aggregate 25 mm	Aggregate 15 mm	SP (%)
SS-C1	0.60	329	199	715	-	646	390	-
SS-C2	0.42	475	199	715	-	646	390	-
SS-C3	0.27	610	168	715	-	646	390	1.50
CS-C1	0.60	329	199	-	715	646	390	-
CS-C2	0.42	475	199	-	715	646	390	-
CS-C3	0.27	610	168	-	715	646	390	1.50

Specimens were placed in an electrical furnace and heated at a constant rate of 3°C/min [16]; they were allowed to cool naturally to room temperature inside the electrical furnace in order to prevent thermal shock. Physical and mechanical tests were performed on unheated and heated samples in order to compare the initial and residual properties.

2.2. Physical properties

The specimens were weighted in different states using an electronic digital balance for determining the mass loss M_{loss}, water porosity P and density D according to the standard NF EN 12390-7 [17]. The dimensions of width, length and height of concrete specimens were measured, before and after heating to get the variation of specimen's volume Vv. These properties were determined according to the following Equations:

$$M_{loss} = \frac{M_{initial} - M_{heated}}{M_{initial}} \quad (1)$$

$$P = \frac{M_{sat} - M_{heated}}{M_{sat} - M_{sat+imm}} \quad (2)$$

$$D = \frac{M_{heated}}{M_{sat} - M_{sat+imm}} \quad (3)$$

$$Vv = Vt / V_{20} \quad (4)$$

where:

$M_{initial}$ is the initial mass (before heating);

M_{heated} is the heated mass (after heating) weighed in the air;

M_{sat} is the saturated mass measured in the air;

$M_{sat+imm}$ is the saturated mass measured in the water;

V_{20} is the volume of specimen before heating;

V_t is the volume of specimen after heating.

2.3. Mechanical properties

For compressive strength, uniaxial compression tests were performed on cubic specimens using a hydraulic press according to the standard NF EN 12390-3 [18]. Relative values of compressive strength were expressed as a ratio between strength after heating and strength of unheated material.

The ultrasonic pulse velocity UPV value was determined for quick checking the quality of concrete specimens before and after heating. UPV test were performed in accordance with the standard AFNOR P 18-418 [19]. If the path length is known, then the UPV can be calculated from the path length divided by the transit time.

3. Effects of high temperature on SS and CS (according to the literature)

This part presents an analysis of the physical properties and macroscopic observations of two types of sand after their exposure to heating-cooling cycles. The results obtained provide more knowledge of the changes induced on sand by temperature.

Figure 2 presents the results of a differential thermal analysis (DTA) that allows determining, by endothermic and exothermic peaks, the temperatures at which instability can occurs in aggregates. According to research of Felicetti [7], the majority of aggregates used for the manufacture of concrete are stable up to 500°C.

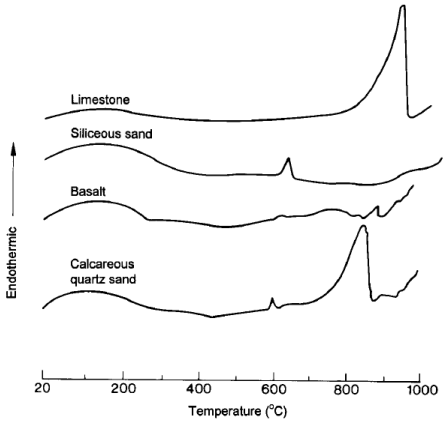

Figure 2. ATD curves of four types of aggregates (10°C/min) [20].

SS contains approximately 20% of bound water. Between 120°C and 600°C, this water is able to partially release by reducing the resistance of this material. In fact, the quartz present in the siliceous aggregates is a building of tetrahedral (a silicon atom surrounded by four oxygen atoms) which undergoes a slight rotation of the bonds to form a crystalline structure of hexagonal symmetry starting from a temperature of 575°C. This variation in the chemical structure of quartz (transformation of α-quartz into β-quartz) is accompanied by a dilatation in the order of 1 to 5.7% [7, 20–22]. Both of these phenomena can cause damage to the concrete structure.

3.1. Macroscopic observations of the effects of temperature on sand

The two types of sand are intact after the heat treatment of the samples to 150°C, no macroscopic degradation was observed. From this temperature, changes on some grain

were observed compared to the initial state (20°C). The descriptions of these changes as well as the photographs of the samples before and after the heat treatment are given in figures 3 and 4.

3.1.1. Siliceous Sand SS

The grains of SS remain intact up to 400°C. From this temperature, a variation in the color of SS grains has been observed. Slight and gradual reddening occurs throughout the increase in heating temperature (600°C and 900°C). This red coloration is explained by the dehydration of goethite (iron hydroxide FeO(OH)) which transforms into ferric oxide (Fe_2O_3) from 300°C [23]. Photographs of SS samples before and after heat treatment are summarized in Figure 3.

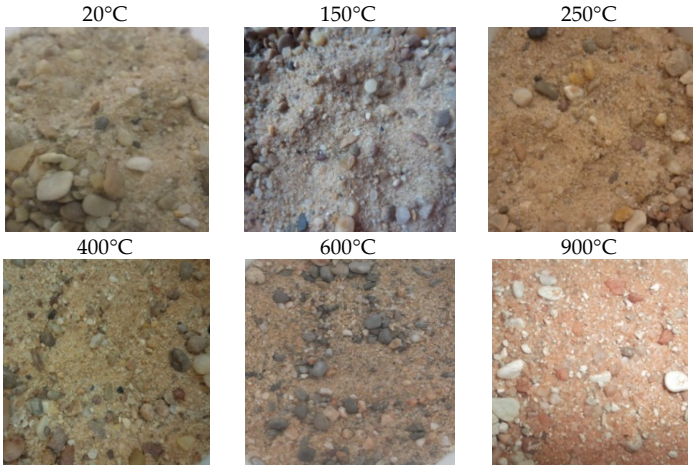

Figure 3. Photographs of SS before and after exposure to different temperatures [24].

3.1.2. Calcareous Sand CS

According to the figure 4, it is clearly noticed that the color of calcareous sand grains remains unchanged until 600°C.

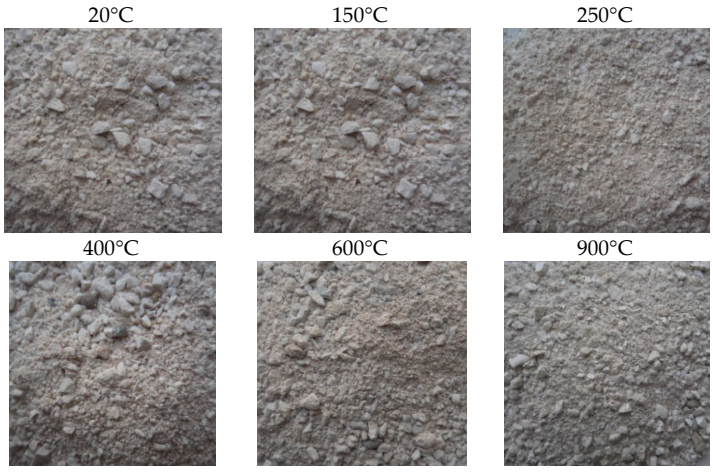

Figure 4. Photographs of CS before and after exposure to different temperatures [24].

After the heating of 900°C, the majority of the CS grains becoming gray. The formation of the white layer on the surfaces of CS is the consequence of the decarbonation of the limestones, the calcite ($CaCO_3$) transforming itself into lime (CaO) following the departure of CO_2 [25–28]. After cooling, the CaO reacts with the moisture of the air and transforms into portlandite $Ca(OH)_2$ [29].

After heating cycles of 600 to 900°C, the increase of the thickness of decarbonated layer with increasing temperature has been observed.

3.2. Mass loss of sand as a function of temperature

The mass losses of CS and SS are grouped in Figure 5. The mass losses of CS and SS were determined by weighing the samples before and after each heating-cooling cycle.

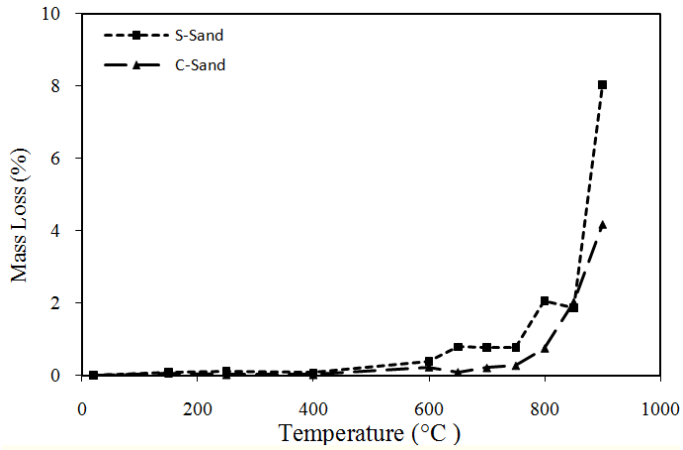

Figure 5. Mass loss of CS and SS [24].

Mass loss values are negligible (less than 0.2%) for temperature cycles of 150°C, 250°C and 400°C. Beyond 600°C, the mass loss of sands increases.

CS samples lose less mass than samples of SS. This difference in mass loss can be attributed to the departure of water trapped in the micro -porosity of SS. The mass loss of CS samples is approximately steady at up to 800°C (less than 1%). After heating to 900°C, the mass loss of CS is twice as low as that of SS.

Calcareous aggregates exhibit stable thermal behavior up to a temperature of 650°C [20]. Beyond this temperature, $CaCO_3$ decomposes (decarbonation) giving carbon dioxide (CO_2) and calcium monoxide (CaO). During the cooling process, the free lime (CaO) can react with moisture to give Portlandite $Ca(OH)_2$ with a 40% volume increase [21]. This reaction leads to increased cracking and damage to the concrete structure, which may explain the decrease in residual mechanical resistance for limestone aggregates heated above 700°C. These results confirm the research of Tsymbrovska [30] and Tebbal [31].

4. Effects of high temperature on concretes prepared with different type of sand

Many literatures of effects of high temperature on concretes concluded that when aggregates are subjected to a rise of temperature, they can present thermal instabilities

(mineralogical modifications and thermal expansion) which strongly influence the behavior of concrete tempered with these aggregates during a rise of the temperature. It is therefore important to know the behavior of aggregates at high temperatures to facilitate the understanding concrete behavior at high temperature.

4.1. Residual compressive strength

The compressive strength at 28 days is the main characteristic used to distinguish between different types of concrete. It allows understanding the process of degradation of concretes subjected to high temperature. The residual compressive strengths of concrete prepared with siliceous sand (SS-C1, SS-C2 and SS-C3) are compared to the residual compressive strengths of concrete prepared with calcareous sand (CS-C1, CS-C2 and CS-C3).

Figure 6 shows the evolution of the residual and relative compressive strength as a function of the heating temperature.

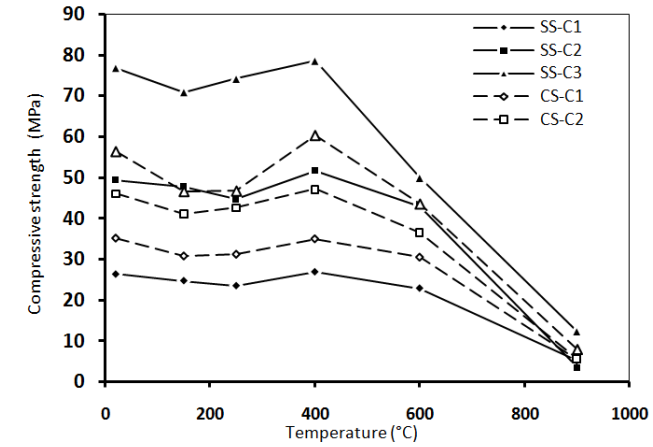

Figure 6. Evolution of compressive strength (a) and relative compressive strength (b) with temperature [15].

The evolution of the compressive strength of different concretes with temperature has three distinct phases. From 20 to 250°C, concretes show a slight decrease in compressive strength. This first phase can be explained by the thermal expansion of water. This dilation weakens the bonds between the leaves of the HSCs and discards them. Hager [32] explained this phase by the dehydration of ettringite takes place, followed by the decomposition of gypsum between 150°C and 170°C. Between 200°C and 250°C, slight variations in flux to the continuous dehydration of C-S-H, a so-called "water plug" develops in concrete pores [33].

Around 400°C, the compressive strength increases. This phase is attributed to the departure of water which allows a re-increase of attraction forces and the approximation of CSH leaves. This gain in resistance has been observed by many researchers [15, 24, 25, 31].

Above 400°C, the compressive strength decreases more rapidly. In this range, cement paste contracts, whereas aggregates expand. Therefore, the transition zone and bonding between aggregates and paste are weakened [34].

For concrete contained calcareous sand (CS-C1 with w/c=0,6), an improvement of about 30% in the residual compressive strength compared to SS-C1 is noted in the temperature range of 20°C to 600°C. The nature of the phase changes will depend upon the mineralogical composition of cement, its C/S ratio (mols of lime per mol of silica; CaO/SiO_2), the amount of fine particles (quartz) and the temperature and pressure levels that have been reached [35].

The influence of the presence of calcareous sand in concrete brought to high temperature depends on the ratio w/c. This sand improves the residual compressive strength of concretes C1 with ratio of w/c = 0.6 and decreases those of concretes C2 and C3 whose w/c ratio are 0.42 and 0.27, respectively. The improvement in the compression behavior of CS-C1 concrete seems to be related to the absorption coefficient of the CS sand used. This sand has a higher absorption coefficient than SS, which leads to a decrease in the amount of mixing water and consequently an improvement in compressive strength. This result is similar to research of Tebbal [5].

From Figure 5, it can be seen that SS-C3 concrete made from SS has better room temperature resistance than CS-C3. After heating up to 400°C, figure 5 shows a better evolution of residual compressive strength of SS-C3 concrete and a less evolution for concrete CS-C3. This can be explained by the higher density and low absorption of SS that leads to a stronger concrete [25].

At room temperature (20°C), the presence of CS modified slight the compressive strength of CS-C3 concrete. This concrete has a compressive strength lower about 27% than that of SS-C3 concrete with SS. The use of CS for the preparation of high performance concrete does not improve the compressive strength of concrete.

Between 150°C and 250°C, the decrease in residual compressive strength was greater after heating. The decreases of compressive strength at these temperatures were 34% and 37%, respectively. In other hand, the specimens of CS-C3 at the same temperatures show greater damage by cracking compared to SS-C1 concretes.

The photos in Figure 7 show the surface conditions of CS-C3 concrete after heating to 150°C and 250°C. The cracks have been visible to the naked eye and the opening of these cracks is greater than SS-C3 concrete treated at the same temperatures.

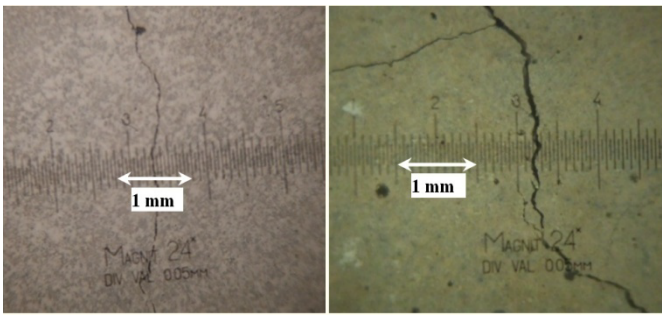

Figure 7. Optical microscopy of the CS-C1 specimen after heating to 150°C and 250°C [24].

These results join the observations made by other researchers like Rahmouni [36] which indicates that concrete containing CS present the higher loss of compressive strength (figure 8).

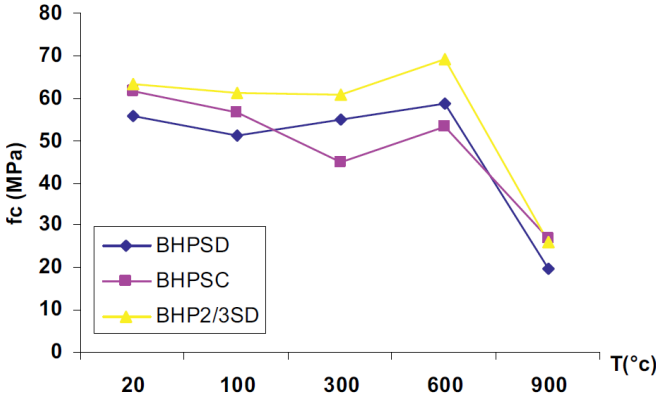

Figure 8. Residual compressive strength with temperature [36].

Note : BHPSD: HPC with 100 % of SD. BHPSC: with 100 % of CS . BHP2/3SD: with 2/3 of SD.

Furthermore, Rahmouni [36] pointed out that the loss of compressive strength of high performance concrete contained SS remains moderate up to 600°C and accelerates beyond this temperature. The best compression behavior of concrete with SS can be explained by an improvement of adhesion resistance of interface aggregate/paste. The low w/c ratio indeed leads to a decrease in the porosity of the transition zone.

It was reported also in reference [36] that between 600°C and 900°C, the loss of compressive strength of high performance concrete prepared with silico-calcareous sand is due to spalling and bursting of flint.

4.2. UPV

Measurement of UPV is one of the various non-destructive test methods used to obtain the maximum information on the quality of concretes subjected to a rise in temperature.

Figure 9 shows the evolution of UPV of concretes tested after exposed to high temperature. The measurements were repeated three times for each specimen who gave 9 measurements for each point shown in the figure. The UPV of concretes made with SS or CS sand is very affected by the rise in temperature. The decrease of UPV values means an increase of concrete degree damage [37]. However, the UPV values of concretes contained CS are better than those of concretes containing SS.

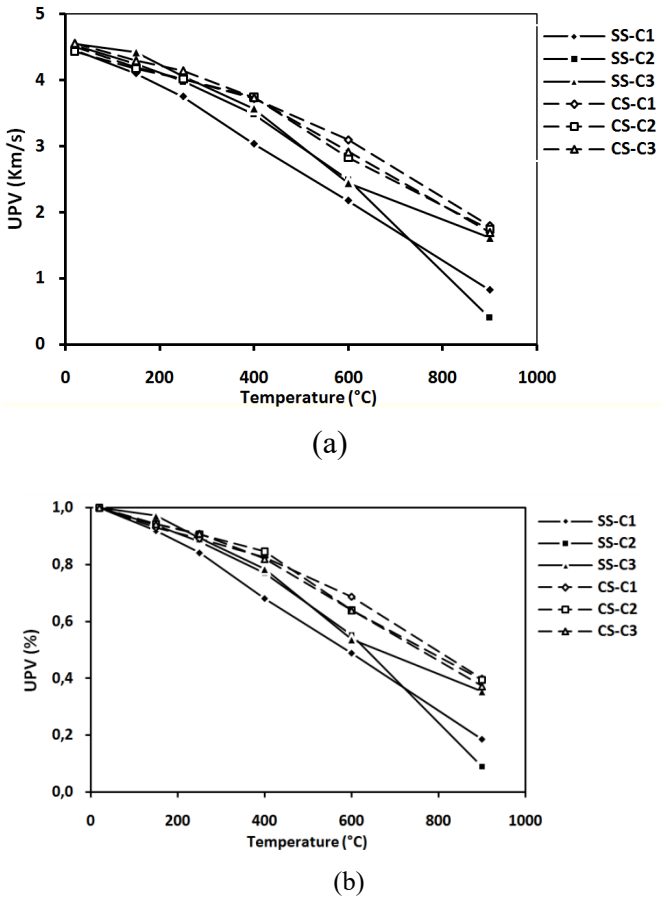

Figure 9. (a) Evolution of UPV with temperature; (b) Evolution of relative UPV with temperature [15].

4.3. Mass loss

Figure 10.a illustrates the evolution of mass loss of concretes contained SS and CS as a function of the heating temperature [15]. The second figure (10.b) shows the effect of high temperature on the evolution of the mass loss of three concretes, these concretes mixes were prepared with different fine aggregates (sand): CS, SS or silico-calcareous sand reported by Rahmouni [36].

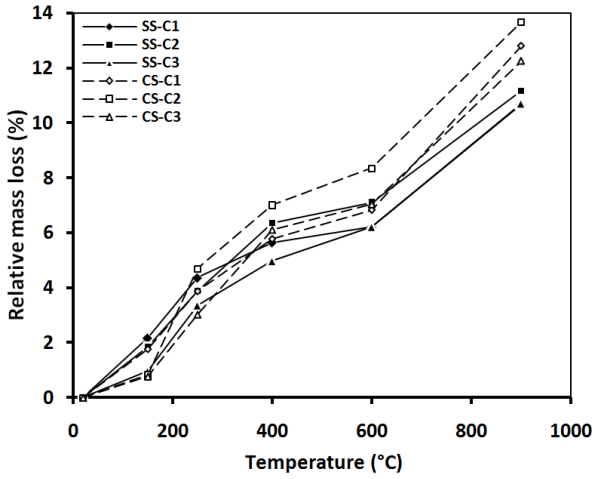

(a)

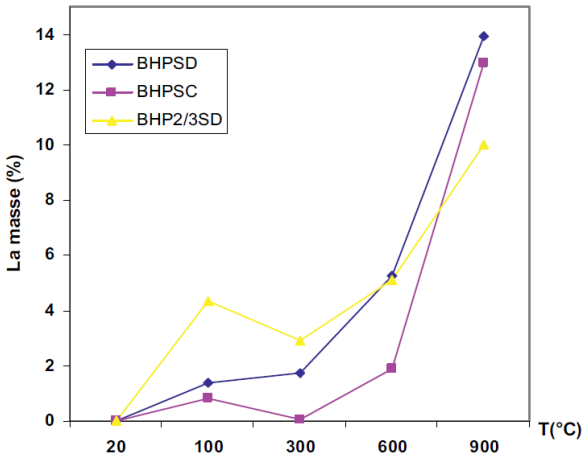

(b)

Figure 10. Evolution of mass loss of concrete as a function of temperature, (a)-[15], (b)-[36].

Above 250°C, the evolution of mass loss as a function of temperature is related to the type of sand used [15, 36]. Concretes containing SS have the lowest mass loss compared to concretes containing CS. The greatest mass loss of concretes containing CS can be explained by the departure of CO_2 from calcium carbonates which cause an increase in mass loss from 600°C [38].

4.4. Porosity

Figure 11 shows the evolution of water porosity of concretes containing CS compared to that of concretes containing SS.

The porosity of concrete is strongly modified with temperature.

Above 400°C, the concrete prepared with CS has a little higher porosity than concrete containing SS. This is due to the decarbonation of calcite ($CaCO_3$) which is transformed into lime (CaO) following the departure of CO_2. The rehydration of CaO by the presence of water is accompanied by significant swelling. This increase in volume is responsible for the additional cracking and decohesion of aggregates with the cement past. Similar behaviors had already been observed experimentally by Xing [38].

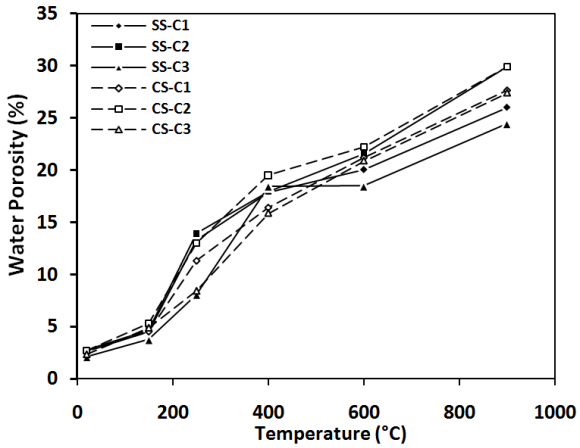

(a)

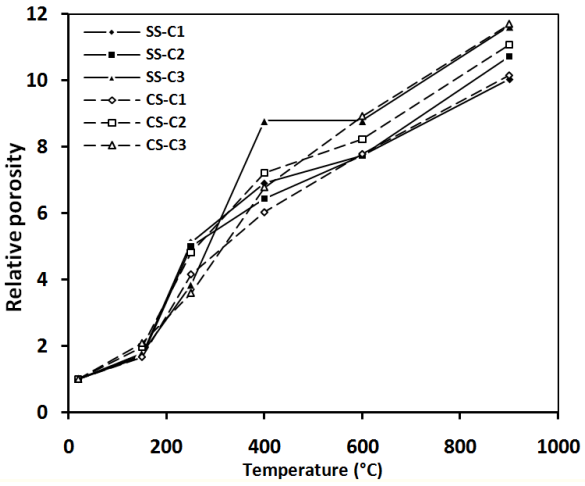

(b)

Figure 11. (a) Evolution of water porosity with temperature; (b) Evolution of relative water porosity with temperature [15].

4.5. Density

Figure 12 shows the evolution of density obtained on all the concretes studied as a function of the heat treatment.

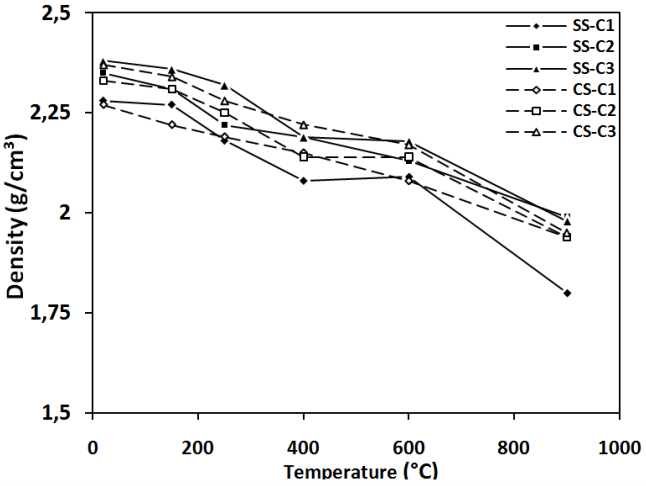

(a)

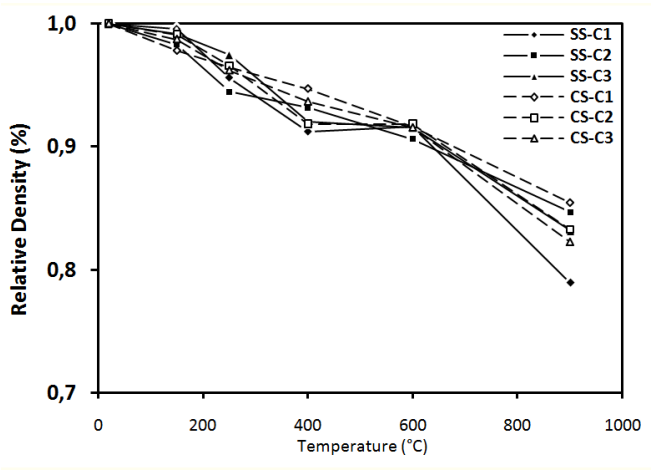

(b)

Figure 12. (a) Evolution of density of different concretes as a function of temperature; (b) Evolution of relative density with temperature [15].

It is clear that the decrease of concretes containing SS is similar to that of concretes containing CS, about 8% at 600°C and between 16% and 17% at 900°C.

4.6. Volume

The analysis of the different volume variation curves presented in Figure 13 shows that the variation in concrete volume is influenced by the nature of sand.

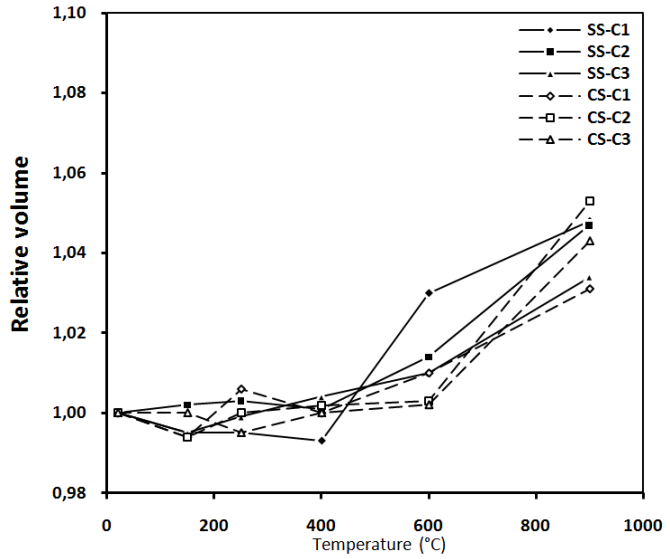

Figure 13. Variation of concretes volume at different temperatures [15].

In the temperature range of 20 to 250°C, all concretes show a decrease in volumes, which results in the removal of water contains in the cement paste. At the beginning of the heating cycle, the cement paste expands and then shrinks; hence the shrinkage phase begins at a lower temperature (125°C) [39].

In the range of 400 to 900°C, the concretes containing SS have higher volume variations than concretes containing CS. This variation is related to the nature of the SS, which undergoes a volume increase of about 1% during the quartz change at 575°C, which contributes to the significant cracking of concrete [39].

4.7. Cracks

The evolution of cracks for different concretes after their cooling was followed by Hachemi [15]. The opening of cracks was determined using an optical microscope (Table 3).

Table 3. Widths of macro-cracks of different concretes after heating to 400°C, 600°C and 900°C [15].

Mixtures	Width of cracks (mm)					
	400°C		600°C		900°C	
	min	max	min	max	min	max
SS-C1	< 0,05	0,08	< 0,05	0,25	< 0,05	0,70
SS-C2	< 0,05	0,05	< 0,05	0,10	< 0,05	0,50
SS-C3	< 0,05	0,05	< 0,05	0,08	< 0,05	0,35
CS-C1	< 0,05	0,05	< 0,05	0,10	< 0,05	0,60
CS-C2	< 0,05	0,05	< 0,05	0,10	< 0,05	0,50
CS-C3	< 0,05	0,05	< 0,05	0,10	< 0,05	-

Figure 14 shows different cracks occurred in cement paste using the optical microscope.

Before 400°C, no cracks have been see with the naked eye on the specimens, but cracks of small aperture were observed (less than 0.05 mm). This damage can be caused by the high thermal expansion of water within the pores, which can induce high tensile stresses in the solid skeleton and possible cracks [40]. Then, concrete cracking develops progressively with increasing temperature.

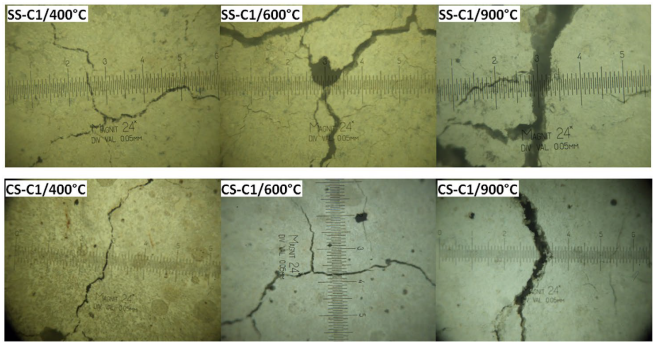

Figure 14. Crack patterns observed in SS-C1 and CS-C1 specimens after heating to 400°C, 600°C and 900°C [24].

Concretes specimens heated to 400°C are characterized by the presence of open cracks. The crack opening varies from 0.04 to 0.08 mm depending on the type of concrete and sand used. Beyond this temperature, the amount and the opening of cracks become larger and visible to the naked eye. These cracks are located on the specimen's surface and extend into the cement paste towards the inside of specimens. Concrete cracking, which manifests from the temperature of 400°C, is mainly due to the difference in the directions of the thermal deformation of cement paste (shrinkage) and aggregates (expansion) [39]. The opposite evolution of cement paste and aggregates generates deformative incompatibilities at the cement-

aggregate interface, which generate tensile stresses in cement paste and compressive stresses in aggregates. This opposite behavior of aggregates-cement paste could therefore causes microcracks in the material [41].

After heating to 600°C, numerous network-connected cracks were observed; these cracks appear in the cement paste. The opening of these cracks was about 0.05 to 0.25 mm for concrete made with CS. Concrete specimens containing SS have the lowest crack openings.

After heating cycle of 900°C, the opening and the depth of the cracks become larger. Greater cracking is observed with an opening up to 0.70 mm. These crack openings could indeed be accompanied by loss of material which would affect the total mass loss of the specimens treated at this temperature.

Concrete specimens containing SS have the lowest crack openings. It is also observed that the opening of the cracks was smaller for concretes with lower w/c ratio.

5. Conclusion

The use of two different nature of sand in the manufacturing of concrete leads to a different behavior when exposed to high temperature.

For temperature higher than 600°C, concretes made with CS present greater mass loss than concretes made with SS, which can be explained by the decomposition of calcite $CaCO_3$ and the departure of CO_2. The carbonates of CS lead to an additional damage of concrete (higher porosity) when compared to concretes containing SS in the range temperature of 600 to 900°C.

The difference in the high temperature behavior of SS and CS leads to different thermal behavior of concrete. Concretes containing SS show an increase of volume higher than that of concrete containing CS after a heating to 600°C. This can be explained by the increase of SS volume due to transformation of quartz α to quartz β which occurs at 573°C. However, density of concretes does not depend on the nature of sand. The evolution of density of concretes made with SS was very close to that of concretes made with CS.

The evolution of residual compressive strength of concretes depends on the mineralogical nature of sand and the w/c ratio from 20° to 600°C. For a high w/c, CS-concretes have the best residual compressive strength while with a lower w/c; SS-concretes behave the best. For the UPV tests, concretes contained SS present the lowest values of UPV than that of concretes contained CS. In addition, CS-Concretes show less cracking than the SS-concretes.

Conflict of Interest

The authors declare no conflict of interest.

References

[1] C. De Sa, "Etude hydro-mécanique et thermo-mécanique du béton - Influence des gradients et des incompatibilités de déformation," (Ph. D Thesis, Ecole Normale Supérieure de CACHAN, 2007).

[2] M. Bederina, Z. Makhloufi, A. Bounoua, T. Bouziani, M. Quéneudec, "Effect of partial and total replacement of siliceous river sand with limestone crushed sand on the durability of mortars exposed to chemical solutions," *Construction and Building Materials*, vol. 47, pp. 146-158, 2013, doiI: 10.1016/j.conbuildmat.2013.05.037.

[3] T. Celik, K. Marar, "Effects of crushed stone dust on some properties of concrete," *Cement and Concrete Research*, vol. 26, pp. 1121-1130, 1996, doi: 10.1016/0008-8846(96)00078-6.

[4] M. Yajurved Reddy, D. V. Swetha, S. K. Dhani, "Study on properties of concrete with manufactured sand as replacement to natural sand," *International Journal of Civil Engineering and Technology*, vol. 6, pp. 29-42, 2015,

[5] N. Tebbal, Z. Rahmouni, "Influence of local sand on the physic-mechanical comportment and durability of high performance concrete," *Advances in Civil Engineering*, vol. 8, pp. 1-10, 2016, doi: 10.1155/2016/3897064.

[6] T.T.H. Le, H. Boussa, F. Meftah, "Effect of aggregates morphology on the THM behaviour of concrete at high temperatures," *In: Proceedings of Fracture Mechanics of Concrete and Concrete Structures - High Performance, Fiber Reinforced Concrete, Special Loadings and Structural Applications (FraMCoS-7)*, pp. 1758-1765, 2010.

[7] R. Felicetti, P.G. Gambarova, "Expertise and assessment of materials and structures after fire," *Int : fib bulletin 46: fire design of concrete structures-structural behaviour and assessment. International Federation for Structural Concrete (fib) 1rst ed*, pp. 63-114, 2008, doi : doi.org/10.35789/fib.BULL.0046.

[8] I. Hager, T. Tracz, J. Śliwiński, K. Krzemień, "The influence of aggregate type on the physical and mechanical properties of high-performance concrete subjected to high temperature," *Fire and Materials*, vol.40, no. 5, pp. 668-682, 2015, doi:10.1002/fam.2318.

[9] J-C. Mindeguia, P. Pimienta, H. Carré, C. La Borderie, "On the influence of aggregate nature on concrete behavior at high temperature," *European Journal of Environmental and Civil Engineering*, vol. 16, pp. 236-253, 2012, doi:10.1080/19648189.2012.667682.

[10] Z. Xing, R. Hébert, A-L. Beaucour, B. Ledésert, A. Noumowé, "Influence of chemical and mineralogical composition of concrete aggregates on their behaviour at elevated temperature," *Materials and Structures RILEM*, vol. 47, pp. 1921-1940, 2014, doi: 10.1617/s11527-013-0161-y

[11] Z. P. Bazant, M. F. Kaplan, *Concrete at High temperatures, Material properties and mathematical models*, Concrete Design & Construction Series, 426 p. Longman Group Limited, 1996.

[12] G.A. Khoury, Y. Anderberg, K. Both, J. Fellinger, N.P. Hoj, C. Majorana, "Fire design of concrete structures-materials, structures and modeling," *State of art report, FIB Bulletin*, N° 38, 2007, doi: 10.35789/fib.BULL.0038.

[13] J. Lee, K. Choi, K. Hong, "The effect of high temperature on color and residual compressive strength of concrete," *In: Proceedings of Fracture Mechanics of Concrete and Concrete Structures - High Performance, Fiber Reinforced Concrete, Special Loadings and Structural Applications (FraMCoS-7)*, pp. 1772-1775, 2010.

[14] AFNOR French standardization P 18-554, *Aggregates – Measurement of densities, porosity, absorption coefficient and water content of fine gravel and pebbles*, French Association for Standardization (AFNOR), Tour Europe cedex 7 92049, Paris, 1990.

[15] S. Hachemi, A. Ounis, "The influence of sand nature on the residual physical and mechanical properties of concrete after exposure to elevated temperature," *European Journal of Environmental and Civil Engineering*, vol. 23, pp. 1003-1018, 2019, doi: 10.1080/19648189.2017.1327893.

[16] ISO/TR 15655, *Fire resistance – Tests for thermo-physical and mechanical properties of structural materials at elevated temperatures for*

fire engineering design, Technical report, Geneva, 2003.
[17] European Standard NF EN 12390-7, *Test for hardened concrete Part 7: Density of concrete,* ISSN 0335-3931, The French Association of Standardization (AFNOR), 11 avenue Francis de Pressensé 93571 Saint-Denis La Plaine Cedex, 2001.
[18] European Standard NF EN 12390-3, *Test for hardened concrete Part 3: Compressive strength of test specimens*, ISSN 0335-3931, The French Association of Standardization (AFNOR), 11 avenue Francis de Pressensé France 93571 Saint-Denis La Plaine Cedex, 2003.
[19] French Association for Standardization AFNOR P 18-418, *Concrete – Sonic auscultation - measurement of the sonicwave transmission time in concrete*, Tour Europe cedex 7 92080, Paris defense, 1989.
[20] B. A. Scherefler, D. Gawin, G. A. Khoury, C. E.Majorana, "Physical, Mathematical & numerical modeling," *Course on Effect of Heat on Concrete. International Centre for Mechanical Sciences (CISM)*, 2003.
[21] C. Alonso, C. Andrade, M. Castellote, G. A. Khoury, "Microstructure – Solid Phases," *Course on Effect of Heat on Concrete. International Centre for Mechanical Sciences (CISM)*, 2003.
[22] V. Wetzig, "Destruction mechanisms in concrete material in case of fire, and protection systems," *In: 4th Int. Conf. on Safety in Road & Rail Tunnels (SIRRT)*, pp. 281-290, 2001.
[23] J. P. Ingham, "Application of petrographic examination techniques to the assessment of fire-damaged concrete and masonry structures," *Materials Characterization,* vol. 60, pp. 700-709, 2009, doi: 10.1016/j.matchar.2008.11.003.
[24] S. Hachemi, "Etude du comportement du béton soumis à haute température : Influence du type de béton et de la nature des constituants," (Ph. D Thesis, Université de Biskra, 2015).
[25] S. Hachemi, A. Ounis, "L'influence de la nature du sable sur les propriétés physiques et mécaniques du béton soumis à haute température," *Courrier du Savoir*, Université de Biskra, Algérie, vol. 24, pp. 151-162, 2017.
[26] Z. Xing, A-L. Beaucour, R. Hebert, A. Noumowe, B. Ledesert, "Influence of the nature of aggregates on the behaviour of concrete subjected to elevated temperature," *Cement and Concrete Research,* vol. 41, pp. 392-402,2011, doi:10.1016/j.cemconres.2011.01.005.
[27] R. Niry, A-L. Beaucour, R. Hebert, A. Noumowe, B. Ledesert, R. Bodet, "Thermal stability of different siliceous and calcareous aggregates subjected to high temperature," *MATEC Web of Conferences*,vol. 6, pp. 1-9, 2013, doi:10.1051/matecconf/20130607001.
[28] Z. Xing, R. Hébert, A-L. Beaucour, B. Ledésert, A.Noumowe, "Influence of chemical and mineralogical composition of concrete aggregates on their behaviour at elevated temperature," *Materials and Structures RILEM,*vol. 47, pp. 1921-1940, 2013, doi : 10.1617/s11527-013-0161-y.
[29] M. Khattab, S. Hachemi, M.F. Al Ajlouni, "Evaluating the physical and mechanical properties of concrete prepared with recycled refractory brick aggregates after elevated temperatures' exposure, " *Construction and Building Materials*, 311, 2021, https://doi.org/10.1016/j.conbuildmat.2021.125351
[30] Tsymbrovska, "Effect of heating–cooling cycles on transient creep strain of high performance," *high strength and ordinary concrete under service and accidental conditions materials and structures,*vol. 48, pp. 1561-1579, 1998, doi : 10.1617/s11527-014-0254-2.
[31] N. Tebbal, Z. RAHMOUNI, M. Maza, "Combined effect of silica fume and additive on the behavior of high performance concretes subjected to high temperatures," *mining science,* vol. 24, pp. 129-145, 2017, doi : 10.5277/msc172408.
[32] I. Hager, "Behaviour of cement concrete at high temperature," *Bulletin of the Polish Academy of Sciences: Technical Sciences,* vol. 61, pp. 145-154, 2013, doi:10.2478/bpasts-2013-0013.
[33] S. Rao, K. Rahul, A. Pradesh, "Studies on bacterial concrete exposed to elevated temperatures and thermal cycles," *Studies,* vol. 3, pp. 126-135, 2013.
[34] M. Belouadah, Z. Rahmouni, N. Tebbal, "Effects of glass powder on the characteristics of concrete subjected to high temperatures," *Advances in Concrete Construction*, vol. 6, pp. 311:322, 2018, doi: 10.12989/acc.2018.6.3.311
[35] G. Verbeck, L.E. Copeland, "Some physical and chemical aspects of high pressure steam curing," *In: Menzel Symposium on High Pressure Steam Curing (ACI SP-32),* pp. 1–131, 1972, doi:10.14359/6597.
[36] Z. Rahmouni, N. Tebbal, H. Haroun Abdellah, "Influence de la nature des granulats sur le comportement rhéologique du béton à hautes températures, " *MATEC Web of Conferences*, vol. 01, pp. 04-11, 2014, doi: 10.1051/matecconf/20141101010.
[37] M. Khattab, S. Hachemi, H. Benzetta, "Assessment of quality of recycled brick concrete using Ultrasonic pulse velocity, " *ASPS Conference Proceedings, First International Conference on Energy, Thermofluids and Materials Engineering, ICETME 2021.*
[38] Z. Xing, "Influence de la nature minéralogique des granulats sur leur comportement et celui du béton à haute température," (Ph. D Thesis, Université de Cergy-Pontoise, 2011).
[39] G. I. Hager, "Comportement à haute température des bétons à haute performance – Evolution des principales propriétés mécaniques," (Ph. D Thesis, Ecole Nationale des Ponts et Chaussées et l'Ecole Polytechnique de Cracovie, 2004).
[40] J-C. Mindeguia, "Contribution expérimentale a la compréhension des risques d'instabilité thermique des bétons," (Ph. D Thesis, Université de Pau et des Pays de l'Adour, 2009).
[41] P. Pliya, "Contribution des fibres polypropylène et métalliques à l'amélioration du comportement du béton soumis à une température élevée," (Ph. D Thesis, Université de Cergy-Pontoise, 2010).

Samya Hachemi has done her bachelor's degree in 2000. She has done her engineering's degree from University of Biskra in 2006. She has completed her PhD degree in 2015 from the university Mohamed Khider Biskra.

JENRS

Received: 21 February 2022, Revised: 26 March 2022, Accepted: 27 March 2022, Online: 12 April 2022

DOI: https://dx.doi.org/10.55708/js0104006

Evolutionary Learning of Fuzzy Rules and Application to Forecasting Environmental Impact on Plant Growth

Chris Nikolopoulos [*,1], **Ryan Koralik** [2]

[1] Department of Computer Science, Bradley University, Peoria, IL 61625, USA

[2] Data Science Manager, Nielsen, Schaumburg, IL 60173, USA

[*] Corresponding author: Chris Nikolopoulos, chris@bradley.edu

ABSTRACT: Prediction of plant growth and yield is one of the essential tasks that enables growers of food and agricultural products to effectively manage their crops. In this paper, a hybrid evolutionary/fuzzy machine learning approach is introduced where a genetic algorithm is deployed to learn the optimum membership functions of relevant fuzzy sets and a knowledge base of fuzzy rules. This hybrid approach is then used to build a model which determines how ozone and carbon dioxide levels in the atmosphere affect plant growth by predicting the basal width growth of a plant. The hybrid forecasting model was tested on a data set collected from soybean fields and proved to be an extremely accurate and robust fuzzy predictor. It was able to predict the basal width growth of the plant with an average of 0.19% relative absolute value error.

KEYWORDS: Fuzzy logic, Genetic algorithms, Machine learning, Forecasting in Agriculture

1. Introduction

Prediction of plant growth and yield is one of the essential tasks that enables growers of food and agricultural products to effectively manage their crops to meet demand and minimize cost, by knowing the supply amount that will be needed to meet demand, resources needed to produce that amount, the effect of various environmental factors to their crop, etc. Recent studies have examined the effects of ozone and carbon dioxide in the atmosphere to plant growth and yield [1], [2].

Traditionally, predictive models of plant growth and yield were based on statistical methods like regression analysis, etc. [3] - [5]. More recently, after the advent and increased popularity of Artificial Intelligence (AI) and Machine Learning (ML), more and more forecasting techniques using algorithms from these areas are being applied to the problem of forecasting plant growth and yield. For example, decision trees or deep learning approaches [6]-[9].

In this paper, we introduce a hybrid fuzzy/evolutionary machine learning algorithm for learning a fuzzy knowledge base from a data set of soybean plant instances. The genetic algorithm optimizes the fuzzy sets membership functions which define each fuzzy set so that the resulting forecasting model is the most accurate and robust fuzzy predictor.

This hybrid evolutionary/fuzzy algorithm is then used to learn a knowledge base of fuzzy rules to determine how ozone and carbon dioxide levels in the atmosphere affect soybean plant growth, which of course, in turn affects the yield.

The growth parameter that was targeted for prediction was the plant's basal width. A comparative study was also contacted, comparing the fuzzy logic approach with a hybrid, fuzzy logic with genetic optimization, approach in order to evaluate the performance achieved by the different methods. It is found that the hybrid machine learning algorithm outperforms the fuzzy logic approach used alone.

2. Fuzzy Logic and Genetic Algorithms

The aim of this research was to build a fuzzy logic forecasting system to determine how ozone and carbon dioxide affects plant growth. The system is a hybrid forecasting system, based on a fuzzy logic inference engine and a genetic algorithm optimization (GA) module. The GA module is used to find the optimum membership functions to be used for defining the fuzzy sets (fuzzy variables) used in the knowledge base. The

knowledge base itself is comprised by a set of fuzzy inference rules.

In Boolean and predicate logic, statements can either be true (1) or false (0). Fuzzy Logic generalizes traditional logic by allowing statements to be true, partially true, somewhat true, etc. Fuzzy systems and fuzzy controllers have been extensively applied in industry and business with great success over the past several years. Sample lists of actual applications are in Aerospace, Automotive, Business, Chemical Industry, Defense, Electronics, Financial, Industrial, Manufacturing, Marine, Medical, Mining and Metal Processing, Robotics, and Securities. Other fields that have used Fuzzy Logic Systems have include agriculture, ecology, environmental sciences, geology, fisheries, and oceanography. These Fuzzy Logic Systems help decrease costs in research as well as improving accuracy of the assessments by automating processes not amenable to automation by traditional Boolean or predicate logic based intelligent systems [10] - [12].

Advantages of Fuzzy Logic over the logic programming or other approaches were exhibited in the current project as well. These include,

• Linguistic, not numerical, variables are used, making it similar to the human logic, therefore a fuzzy logic system may have better explanation facilities.

• Simplicity allows the solution of previously unsolved problems because they do away with complex analytical equations used to model traditional control systems

• Rapid prototyping is possible because a system designer doesn't have to know everything about the system before starting work.

• They're cheaper to make than conventional systems because they're easier to design.

• They have increased robustness.

A fuzzy knowledge base is comprised by fuzzy sets (variables/attributes) and fuzzy rules. Fuzzy rules also operate using a series of if-then statements, for example, "If the room gets hotter, then spin the fan blades faster". A fuzzy set is defined by its membership function. There are many alternate ways, proposed in the literature, for setting up a fuzzy forecasting system [3], [10]. Our system specifications are described in the following paragraphs.

There are many alternate definitions for the set operations of complement, union, intersection, and implication for fuzzy sets [1]. The membership functions, that we used in this project, to define the fuzzy logical operators are:

$\mu A \cap B(x) = \min (\mu A(x), \mu B(x))$.

$\mu AUB(x) = \max (\mu A(x), \mu B(x))$.

$\mu A \Rightarrow B(x) = \mu \neg AVB(x) = \max (1- \mu A(x), \mu B(x))$.

$\mu not (A) (x) = 1- \mu A(x)$.

Fuzzy control, which uses fuzzy rules, is the most important application in fuzzy theory. Three steps are taken to create a fuzzy controlled machine:

1) Fuzzification (Using membership functions to convert crisp inputs to fuzzy facts)

2) Rule evaluation (Application of fuzzy rules, the fuzzy inference engine)

3) Defuzzification (converting the fuzzy output back into crisp or actual output)

Fuzzification:

- Input values are translated into linguistic concepts, which are represented by fuzzy sets.
- In other words, membership functions are applied to the measurements and the degree of truth in each premise is determined.

Rule Evaluation:

- Define the fuzzy rules.
- The fuzzy rules are merely a series of if-then statements.
- Plot the membership functions.
- A Fuzzy implication is of the form

IF (X1 is A1 and … Xn) is An THEN Y is B,

where Ai's, and B are fuzzy sets.

Consider this rule and assume that the fact X is A' holds for some fuzzy set, A', different than A. There are many alternate ways proposed in the literature to define the firing of a fuzzy rule in the inference engine. In this project, we used the following implication formula. We calculate the membership function of fuzzy inference B' as:

$\mu B'(Y) = \max x1 \ldots xn [\min (\mu A1'(X1) \ldots \mu An'(Xn), \mu iA1 \ldots An \Rightarrow B(X1....Xn, Y))]$.

Defuzzification:

- Converts the derived fuzzy membership function of B' to a crisp number (output). We used the weighted averages method for doing so.
- Physical systems need discrete values and hence Defuzzification is important.

The other major component of our system is based on the evolutionary approach of solving optimization problems, using Genetic Algorithms (GA).

GA is an Optimization technique mimicking Darwin's theory of Evolution [10]. The basic GA process that we followed for solving our problem is as follows:

- Encode candidate solutions as "DNA" strings (sequence of symbols, the "individuals").
- Pick a population size p, and construct an initial random population of p individuals.
- Define a fitness function: Population→real numbers R, that assigns a number to an individual measuring its "goodness" as a solution. The bigger the fitness, the better the individual is as a solution.
- Define appropriate implementations of the genetic operators, reproduction (survival of the fittest), crossover and mutation.
- Define the mutation rate m%.
- Repeat the genetic operators, until convergence criterion is met:

- Reproduction (survival of the fittest)
- Crossover
- Mutation.

The GA optimization technique has proven itself to be one of the best available such methods and has been applied in almost every area and enterprise from engineering, to medicine, to business and financial applications. One big advantage of GA is that it is a minimum knowledge algorithm, i.e. it does not require extensive and deep knowledge of the problem domain for getting a solution. Many mathematical optimization problems that we do not know how to solve are thus ideally attacked using this approach. The fundamental theorem of Genetic Algorithms proves that convergence to an optimum can be achieved as close as desired as the number of iterations of the GA approaches infinity. In practice of course, given the finite number of iterations that we perform, depending on the problem, we may not always be able to reach within a desired x% of the optimum in real time..

3. Data Set and Research Goal

The goal of this research is to build a fuzzy logic forecasting system to determine how ozone and carbon dioxide affects plant growth. The training/testing data set was provided by the Biology Department at Bradley University and was measured and collected over a period of time at soybean fields around Central Illinois.

The data shows the growth level in basal diameter of soybean plants as a time series and at different carbon dioxide and ozone levels. Four different experimental groups were involved: low carbon dioxide and low ozone levels, high carbon dioxide and low ozone levels, low carbon dioxide and high ozone levels, high carbon dioxide and high ozone levels. The low level of carbon dioxide is 370ppm, which is the current level in the atmosphere and the high level is 550ppm, which is the level expected in the year 2050. The low levels of ozone change daily as they are based on the levels in the atmosphere that day and the high ozone levels are 20% greater than the atmospheric levels of the day. There were four rings per group that each contained 25 plants, so that 100 trials were performed for each of the experimental groups. Each of the plants' basal width, as a measure of growth, was measured twice a month for twelve months.

The data set was preprocessed by taking the basal widths for each ring and then finding an average for all of the widths. Then each of the four corresponding rings was averaged with each other to find an average for each group for the day. This was done for every seven days, and then the growth was found by taking the later date and subtracting it from the earlier date. The two basal width increases were found and then averaged to come up with the actual basal width increase for each group.

4. Building the Fuzzy Forecasting Model

We created membership functions of the input variables ozone and carbon dioxide levels and the output variables basal diameter from the provided training data set using statistical measures such as the mean and the range of the data. Other statistical measures such as the first and third quartile, based on each of the experimental group's data, were experimented with but did not result in a significant improvement of the system.

A fuzzy rule base was then created and implemented using the JFS Fuzzy Logic Programming Environment to fuzzify the input and defuzzify the output. Analysis of the system results has been conducted by comparing the outputs of the program to the testing data set given from the experiment. The error between the output from the fuzzy forecasting system and the actual output from the training data set was computed.

The domains used for the input fuzzy variables were as follows. The domain for the experimental set for the O3 level was in the range 0-20, the domain used for the fuzzy set O3 level was 0-30 to allow for graceful degradation of the fuzzy set. The domain for the experimental set for the CO2 level was in the range 370-550, the domain used for the fuzzy set CO2 level was 300-700 to allow for graceful degradation of the fuzzy set.

The membership functions of the fuzzy sets, which will result in the least system error, were derived by experimentation.

The membership functions used were triangles that were centered at 325 and 565 ppm for low CO2 and high CO2 levels respectively, 0% and 21% increase for low and high O3 levels respectively, and 45, 71, and 92 hundredths of a millimeter increase for low, average, and high increase in basal diameter respectively.

A sample of the fuzzy rule knowledge base created is the following:

If CO2 level is low and O3 increase is low then basal width is low.

If CO2 level is low and O3 increase is high then basal width is low.

If CO2 level is high and O3 increase is low then basal width is average.

If CO2 level is high and O3 increase is high then basal width is high..

5. System Optimization Using Genetic Algorithms

We next experimented with using the genetic algorithm optimization approach to find an optimum set of membership functions for defining the fuzzy sets involved. And improve the accuracy of the system by minimizing the average absolute value error on the testing set. A membership function was encoded as an individual in the genetic population as described below. The reproduction, crossover, and mutation operators which were used to evolve the population of the encoded membership functions are defined as below.

Algorithm 1: GA(Fitness, Fitness_threshold, p, r, m)

//Fitness=the fitness function which measures the "strength" (goodness) of an individual.
//Fitness_threshold=termination criterion, max fitness to achieve or max number of iterations
//p=population size
//r=fraction of population to be replaced by crossover
//m=mutation rate (how often to mutate)
//k=max number of iterations
{ create a new generation of individuals, P_i, by:

a. Selection/reproduction:

Probabilistically select p members of P to add to P_i. The probability of selecting individual h is P(h)= Fitness(h)/(Σ_j Fitness(hj)

b. Crossover:

Probabilistically select r*p/2 pairs of P individuals, according to P(h). For each pair <h1, h2>, produce 2 off-springs using the crossover operator defined below. Add off-springs to P_i.

c. Mutate:

Choose m% of members of P_i, with uniform probability. For each, apply the mutation operator defined below on a randomly selected bit.

d. Update: new population P= P_i, i=i++;

e. For each individual h in P, evaluate its fitness, fitness(h) }

-Return the population individual H with the highest fitness in the final generation (or among all generations).

End of algorithm

After experimentation, the initial population size, p, for the most successful run was selected to be 8 individuals.

Each triangular membership function was encoded as a string of 16 digits as follows.

The first 3 digits were the center for the triangle membership function of the fuzzy set CO2 low. The next 3 digits were the center for the triangle membership function of the fuzzy set CO2 high. The next 2 digits were the center for the triangle membership function of the fuzzy set O3 low. The next 2 digits were the center for the triangle membership function of the fuzzy set O3 high. The next 2 digits were the center for the triangle membership function of the fuzzy set basal diameter increase low. The next 2 digits were the center for the triangle membership function of the fuzzy set basal diameter increase average. The final 2 digits were the center for the triangle membership function of the fuzzy set basal diameter increase high.

The fitness function of an individual was 1/error where error is the average absolute value error calculated by:

Σi=1n |actual i-predicted i|/n.

A 2-point crossover was used, where 2 digits were picked by random and the parents were crisscrossed. Mutation was done at 1 or 2 points of the assigned numbers to the triangular distribution.

The best individual, the one that resulted in the smallest error, was found early in generation 4 among the max 100 iterations, with fitness of .128341. Using those membership functions result in a system percent error of .077918. For the process of how the generations evolved, see graph in figure 1.

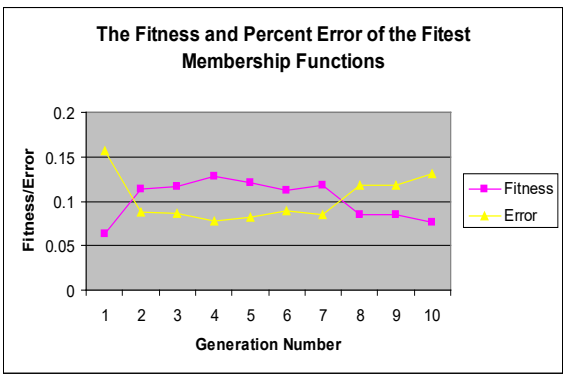

Figure 1: Fitness vs percent error during training

6. Synopsis of Results

Even though the fuzzy predictor model was satisfactory in accuracy by itself, the GA algorithm was

able to learn the most appropriate membership functions from the data itself, automating the process and eliminating the need of the human knowledge engineer to figure out such memberships. The GA process was able to calibrate the membership functions to a degree that improved the system performance as shown below.

The following, table 1 and figure 2, give the average output from the real training data as compared to the fuzzy model output:

Table 1: Actual vs. Model Predicted value of Basal Width increase at different Levels of CO2 and O3

	Actual	FL System	Error% FL	FL+GA Hybrid	Error % FL+GA Hybrid
LL	49.5	49.875	0.757	49.641	0.282
LH	55	54.594	0.738	55.124	0.218
HL	69	69.375	0.543	68.920	0.115
HH	88	88.242	0.275	88.142	0.159
Average error			0.578		0.193

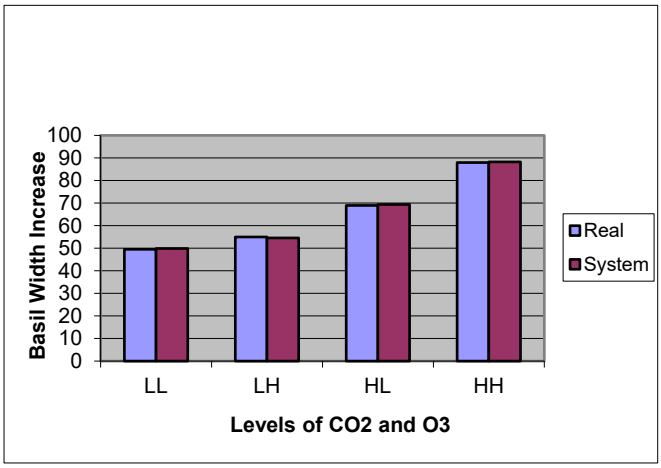

Figure 2: Actual vs. Model Predicted value of Basal Width increase at different Levels of CO2 and O3

The average error in thousandths of a millimeter is calculated as follows:

$$\text{Average error} = (1/n) \sum_{i=1}^{n} |\text{actual}_i - \text{predicted}_i|,$$

where n=4 in this case, corresponding to {LL, LH, HL, HH}.

The average computed error was about 5.7 thousandths of a millimeter for the Fuzzy logic system and 1.9 thousandths for the FL+GA system, for an overall forecasting improvement of over 33% when the GA was used to learn the membership functions.

Graph 3, given below, shows the basal width increase of the plants at many different levels of CO2 and O3:

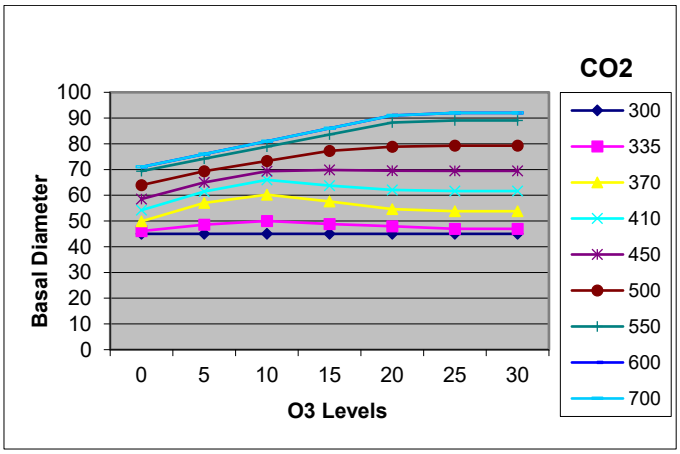

Figure 3: O3 and CO2 levels vs basal width growth

We observe that for low CO2, the amount of O3 has no effect on the diameter since the amount of O3 does not improve the growth of the diameter. For high levels of CO2, increased O3 levels will increase diameter up to a certain level of O3, after which continual increase of O3 might actually hurt the plant. That critical point of O3 level that gives the maximum growth tends to be higher as the level of CO2 is higher.

For any given levels of CO2 and O3, the present system can predict the basal diameter of the plant within the error of 1.9 thousandths of a millimeter.

7. Conclusions

In this paper, a hybrid fuzzy/evolutionary machine learning approach was introduced for learning a fuzzy knowledge base from a data set. This approach was then used to learn a knowledge base of fuzzy rules to determine how ozone and carbon dioxide levels in the atmosphere affect plant growth, specifically basal width, which of course, in turn affects the yield.

The results of a comparative study, comparing the fuzzy logic approach with the hybrid, fuzzy logic plus genetic optimization approach, showed that the performance achieved by the hybrid approach was superior and far more accurate in forecasting the growth parameter, by a factor of more than 30%. Given the levels of CO2 and O3, the hybrid forecasting system can predict the basal diameter of the plant after growth within an error of 1.9 thousandths of a millimeter.

Conflict of Interest

The authors declare no conflict of interest.

References

[1] Khan, S., Nazneen, S., Ali, N., 2021. Effects of ozone phytotoxicity in reducing the yield and nutritional quality of chilli, (Capsicum annuum L.) Environmental Science and Pollution Research, vol. 28, pages8889–8897

[2] Shao, Z., Zhao, Y., Zhang, Y., Wang, Y., Yang, L., 2021. Effect of

ozone stress on yield characteristics of indica-japoic hybrid rice Yongyou 538 in two consecutive growing seasons, Environmental and Experimental Botany, vol. 186, 104447

[3] Becker-Reshef, I., Vermote, A., Lindeman, M., Justice, C., 2010. A generalized regression-based model for forecasting winter wheat yields in Kansas and Ukraine using MODIS data. Remote Sens. Environ. 114, 1312-1323..

[4] Drummond, S. T., Sudduth, K. A., Joshi, A., Birrell, S. J., and Kitchen, N. R., 2003. Statistical and neural methods for site specific yield prediction. Trans. ASAE 46, 5.

[5] obell, D.B, Burke, M., 2010. On the use of statistical models to predict crop yield responses to climate change. Agric. Forest. Meteor. 150, 1443–1452.

[6] Archontoulis, S., Licht, M., Dietzel, R., 2015. In-Season Forecasting of Plant Growth, Soil Water-Nitrogen, and Grain Yield. Iowa State University Farm Progress Reports: Volume 2015, Issue 1

[7] Daniel, J., Andrés, P., Héctor, S., Miguel, B. & Marco, T. 2008, "A survey of artificial neural network-based modeling in agroecology" in Soft Computing applications in industry Springer, , pp. 247-269.

[8] Kamilaris, A. & Prenafeta-Boldú, F.X. 2018, "Deep learning in agriculture: A survey", Computers and Electronics in Agriculture, vol. 147, pp. 70-90.

[9] Liakos, K., Busato, P., Moshou, D., Pearson, S. and Bochtis, D., 2018. Machine learning in agriculture: A review. Sensors, 18(8), p.2674.

[10] Cornelius T., Leondes, K., 1998. Fuzzy Logic and Expert Systems Applications. Academic Press, (1998).

[11] Theile, M., 2009. Exact Solutions to the Traveling Salesperson Problem by a Population-Based Evolutionary Algorithm. Evolutionary Computation in Combinatorial Optimization

[12] Nikolopoulos, C., 1997. Expert Systems. CRC Press/MarcelDekker, New York, USA.

CHRIS NIKOLOPOULOS has received his bachelor's degree from National Kapodistrian University of Athens, Greece in 1976. He has done his master's degree from Colorado State Univeristy in 1978 and Michigan State University in 1986. He has completed his PhD degree in Mathematics from Colorado State University in 1981.

He is a Senior Fulbright Scholar with over ninety refereed journal and proceedings publications, eights patents and numerous research grants from government and industrial entities in the areas of Artificial Intelligence, Machine Learning and Data Science.

RYAN KORALIK has done his bachelor's degree from Bradley University in 2006. He then earned his master's degree in Statistics from Colorado State University in 2008.

He has extensive industrial experience in statistical and data science applications and currently he is a Data Science Manager with Nielsen, USA.

JENRS

Received: 21 February 2022, Revised: 26 March 2022, Accepted: 27 March 2022, Online: 12 April 2022

DOI: https://dx.doi.org/10.55708/js0104007

Factors Determining Political Socialization in Young People (A Case of Pakistani University Students)

Salita *, **Khoula Maryam**

Department of Economics, Pakistan Institute of development Economics, Islamabad, 45320, Pakistan

* Corresponding Author: Salita; Rawalpindi, Pakistan; +92-335-5389516; salitashuaib@gmail.com

ABSTRACT: This paper aims at determining the factors responsible for shaping as well as building political ideas and values. By conducting a survey in a Public University in Pakistan and filling of questionnaires by the respondents, results were obtained. Estimation results showed that Media and education emerged as the domineering factors significantly contributing in the political socialization process. Both variables were positive and significant at 1% level of significance. While, family and youth participation had a lesser contribution. As these variables were though positive but statistically significant at 10% level of significance. Thereby, in accordance with the results it has been suggested that influence of media and education be enhanced in a control environment to induce positive political attitudes.

KEYWORDS: Political Socialization, Media, Education

1. Introduction

Emergence of newly established states soon after the turmoil experienced in WWII, imparted a dire need for political stability as well as a framework for proper functioning of the economy. The process was lengthy and challenging for it required a framework which would not only help in running and functioning of the economy but also in lessening the trauma experienced by the masses and thus shaping their ideas for a better society. This steered the course of literature towards a deeper studying and understanding of politics by theorists and policy makers. Many profound literary works were carried out as well as transformed into policies and later implemented.

However, on another side of a coin, developing countries even today are struggling towards attaining political stability. Therefore, it's of prime importance to consider factors that shape our political ideas and norms and later model our society.

The term was coined by [1] and was defined as the process of development of political values that were influenced by personal experiences and social agents. Predominantly, the stimuli that sprouts such behavior include family, educational institutes, peers and media (inclusive of print, electronic and social) as explained by [2] Moreover, the understanding of the subject is crucial not only for development of a viable political culture but also to allow for individuals to learn and have personal growth as well as to socialize in a political set-up [3].

In recent years, the concept and idea has picked up steam. A research analysis by [4] highlighted the importance of political socialization (PS) in determining political inclinations of youth, understanding of prevalent norm in a society, the political learning, and the socialization process. Therefore, it is needed that an extensive study be conducted for thorough understanding of the subject matter.

Though literature on different aspects of PS remain adequate, however, in context of Pakistan it is almost negligible. Therefore, the current study will a bridge the gap and contribute towards the body of existing literature. Moreover, factors responsible for formulation of political values and ideas will be identified. This will be accomplished by employing and making use of first-hand information gathered through questionnaires. Not only this, but domineering factor will also be identified which by appropriate measures can be enhanced for desired results in terms of PS in the country.

2. Literature Review

The scientific theories about political socialization have two distinct positions [5]. One of this suggest that aim of political socialization is to strengthen the existing system while the other extreme believed that aim of political socialization is to aware people that they are being manipulated by current political system. The aim of other theoretical perspective is to assist people in developing self-political identity in prospect of political socialization.

The components essential for theory of political development are Illustrated by [6]. A theory shall consider the unique nature of political assignation and could not only depend upon extension of cognitive, social and emotional development. It was argued that democracy is vital as it promotes effective citizens' participation. Youth at the age of 18 attain right to vote and became cognitively and emotionally intact. But the presence of all these factor did not guarantee the active participation of the youth. Inclusion of youth as a co-participant is need to be ensured. If politics become part of youth's life and are given opportunity to participate then democracy would be sustained in future as well [6].

In study of [7] political socialization is defined and the views of different theorist upon political socialization are highlighted. Political socialization is considered as a process by which the political dogmas and ideas are formulated in a society. In a society there are several means for promoting the political socialization the most important agents for political socialization are family, peers and media. Sociological theories deliberated political socialization as long run process which is considered to be crucial for a society.

Similarly, the classical theorists regarded political socialization critical as it is seen as a way to promote democracy and could enhance participation rate of civil society. The modern theorist saw mass media as a driving force behind political socialization. Whereas the societal, culture and institutional approach to political socialization stressed on government institutions, family and school as mean for disseminating the political values in a society [7].

In addition to the theoretical literature, a number of previous researchers have conducted empirical studies to establish the components that influence political socialization. The following is a summary of these studies:

Diversity in group of people exists on the basis of education, gender and age thus it is most commonly observed that participation level of group political socialization differ from each other [8] analyzed the political socialization among youths, targeted sample included 16-18 years' students. Different variables were employed for examining their role in determining political socialization among youths. Variables included in the model were age, gender, discussion with parents and peers, activate participation in voluntary work, education level and media's role. Results indicated that parents, peers and voluntary work participation appeared to have a highly significant impact on political socialization among youth. Variable for media was significant indicating media also influence political socialization. By taking into account gender differences it was found that political socialization among young girls was more compared to boys.

The relationship between news use and political socialization among youths is studied by [9]. In order to measure news delivery different variables like TV news, newspaper and radio broadcast were used. For capturing new media blogs and text messaging were employed. For gauging political socialization two indices were utilized namely government appraisal and political trust. Targeted sample included people aged 18 to 35 years and sample size in study was 321. Regression analysis was used to analyze the impact of news consumption on political socialization. It was concluded that if news is related to the foreign country then it would have limited impact on political socialization in domestic country. News consumption variables appeared to be unrelated with political socialization because individuals were likely to expose more to foreign news compared with domestic news. Interpersonal communications among a group or in a community were found to be significant in determining political socialization.

In the past study of [10] the association between education and political socialization is examined. Sample size contained 525 adolescences from Kenya. Three factors of political socialization (political information, political interest and support for political system) were taken in education category with no level of education was added in order to judge how educated people behave differently in socializing politically. Regression analysis was carried out for empirical analysis. It was found that more educated adolescences usually have the more information about the political system similarly adolescence with the higher level of education were more likely to take interest in political activities and supported for political system. It was concluded that education was the most effective mode for political socialization in Kenya therefore [10] suggested that government should focused more on education policies in order to improve political socialization.

Political discussion with friends and family is seen as a vital factor in framing the political attitude of an individual, thus it is also considered to be a factor of political socialization. Analysis conducted by [11] explored the political socialization among youth by gauging the political discussion of youth within family and friends. Sampling technique used was random sampling as well as structure interviews were conducted for data collection. After empirical analysis it was found that parents with more level of education encouraged their children to engage in political discussion. Consequently, low level of political discussion was observed in family where father had distant political views. Media was found to have mediating affect in parental political discussion.

Study conducted by [8] aimed at analyzing the impact of age, gender, discussion with parents and peers, activate participation in voluntary work, education level and

media's role on political socialization similarly [10], [9], [11] also focused on role of media and education in determining Political Socialization. The study will fill the literature gap, as there is no study to the best of my knowledge, which examines the political socialization in young people in context of Pakistan.

3. Methodology and Data

3.1 Methodology

To accomplish the desired outcome and obtain data of the required variables questionnaire was developed. It was amalgam of both, qualitative and quantitative type thereby including closed and open-ended questions. The questions used were of open ended, multiple choice and dichotomous type. Moreover, the information obtained was codded and interpreted using the IBM SPSS Software. This provided the statistical analysis that was required for the current study, which contributes in understanding data and analyzing trends as well as validate assumptions and make accurate conclusions and thus forecasts.

Study was conducted to determine the general political opinion in context of Pakistan. The targeted sample was Public University Students and was chosen due to time and resources constraint.

3.2 Variables

The variables chosen for the current analysis are Age, Gender, Educational level, Family, Mass Media, Education and Youth Participation. These have been taken into consideration, in harmony with the studies by [12]-[15]. The involvement of public and private employees can also influence political socialization, but this variable was neglected because the study's focus sample was university students who were not employees of any organization.

3.3 Estimation Technique

Following econometric model has been considered for empirical analysis of the nexus considering the studies by [10] and [9].

$$Political\ Socialization_i = \beta_o + \beta_1 Gender_i + \beta_2 Age_i + \beta_3 Education_i + \beta_4 Media_i + \beta_5 Family_i + \beta_6 Youth\ Participation_i + \mu_i \quad (1)$$

where, i= cross sections and μ= error term

4. Results and Discussions

4.1 Graphical Statistics

The graphical results obtained by employing the SPSS software have been obtained and explained in the succeeding paragraphs.

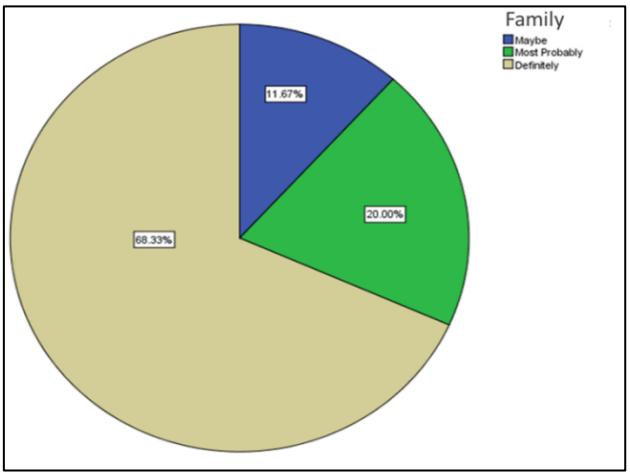

Figure 1: Displaying responses of the variable Family

To check the impact of Family Environment on PS, questions related to this factor were asked. Here 68.33% and 20% respondents thought that friendly home environment definitely and most probably contributed in PS respectively. While the remaining 11.6% were did not consider it as a possible factor, as presented in figure 1.

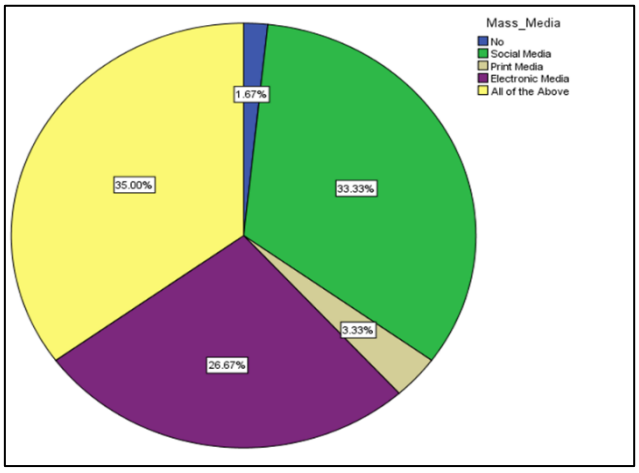

Figure 2: Displaying responses of the variable Mass Media

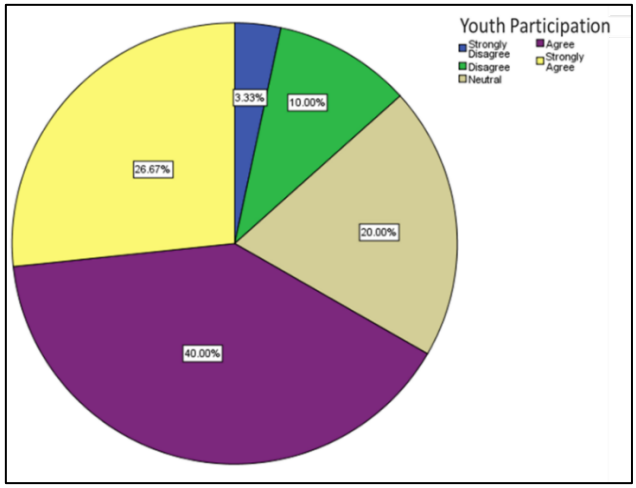

Figure 3: Displaying responses of the variable Youth Participation

As displayed in Figure 2, on response upon Mass Media 33.33% respondents consider social media as an important factor in determining PS. 26.6% think that electronic media is an important element. 3.33% gave

importance to print media and 35% respondents consider all of the above factors playing significant role in determining PS. While only 1.67% respondents thought that there was no role of media in PS.

Response on Youth Participation in PS was also different among respondents. Here 26.67% respondents were strongly agreeing and 40% agreed that Youth Participation is major factor in building PS. 3.33% strongly disagreed and 10% disagreed from the role of youth in PS. While 20% remained indifferent towards the role of young people in PS, as shown in Figure 3.

The last important variable was Education, the chosen respondents were of education of 14 years, 16 years, 18 years and above. Here the respondents with 16 years of education were 51.67%, 18 years and above were 45% and only 3.33% were of 14 years' education. Here 51.67% respondents with 16 years' education, 45% respondents with 18 years and above education and 3.33% respondents with 14 years' education considered that education plays important role in PS, as depicted in Figure 4.

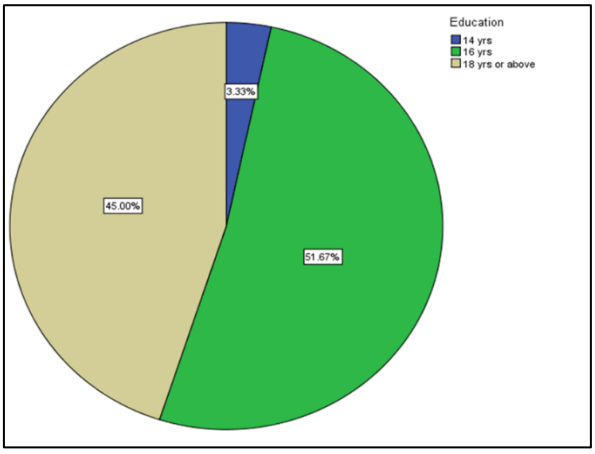

Figure 4: Displaying responses of the variable education

4.2 Empirical Estimates of Political Socialization

The results obtain after running regression are displayed in the Table 4.1.

Table 1: Estimates of Political Socialization

Panel A: Estimation Results: Dependent Variable Political Socialization	
Regressors	***Model***
Gender	0.017
	(0.033)
Age	0.034
	(0.038)
Family	0.024*
	(0.012)
Media	0.114***
	(0.019)
Youth Participation	0.03*
	(0.015)
Education	0.396***
	(0.076)
Panel B: Diagnostic Tests	
Observations	60
P-value	0.000
Adjusted R-Squared	0.484

Note: *, **, *** denotes significance at 10%, 5% and 1%, respectively while Standard Errors are in the parenthesis.

This study has provided a considerable theoretical realization as well as imperative and informative material for all participating factors in this PS. The demographic factors like age and gender were taken along with other factors like family environment, media, youth participation and education. The results indicate significance of family environment, media, youth participation and education in construction of PS, while the age and gender remained insignificant. A survey was conducted through proper questionnaires on sample of 80 respondents.

Gender appeared positive but statistically insignificant suggests that might not have much contribution in formation of political ideas. The results were in line with [12] who finds that female and male respondents report similarly levels of interest in paying attention to politics and government, regardless of what family type they live in. However, males report somewhat higher interest in politics and government than females. Civic engagement among young men and young women, while similar, is not equal.

Age was statistically insignificant but depicted the desired sign shows that that one-year increase in age will increase PS by 1.7 percent. It does not affect the process of PS.

Family environment is the primary agency in forming PS. In our results Family appear to be positive and statistically significant at 10% indicates that a friendly home environment increases building of PS to 2.4 percent. A study done by [16] got the same results that family is the most important agent determining the extent and direction of political learning. He suggests four important functions performed by family that include direct teaching of PS, developing child`s personality and perception toward PS, self-identification (political self) and placing its members within a network of social and economic relationships. Family plays important roles in instilling in youth basic, positive, general beliefs, attitudes, and opinions and cognitive understanding of the political system.

The emergence of internet and digital communication technologies has great contribution largely in the revolution of youth oriented media. Social networking media has changed the concept of old media. Now our societies are using Facebook, Twitter and blogs as a source of information.in our results Media was positively influences PS and it is statistically significant at 1% shows that 1 percent increase in use of media conveys 1.14

percent increase in PS. Study of [13] also found that the social networking sites have great impact on voters because influence of one network member is highly dependent on the members of other. Furthermore, it is evident that social networking media play vital role during the presidential campaign as each of the social media site provide platform to obtain political information to its user. It also aids in development of political ethics and values.

Youth Participation was positively related with political socialization and statistically significant at 10% level of significance illustrate that 1 percent increase in Young Participants brings 0.3 percent increase in Political Socialization. The results are similar with [14] who argues that, in recent decades, the ways that citizens choose to interact with politics have changed significantly. These changes, she claims, are evident in the types of participation, agencies (the organizations through which citizens participate) and the targets (who or what the participant aims to influence) of political participation. [16] also finds that a strong majority of youth believe that they can make a difference by participating in politics and that they have the knowledge and skills necessary to participate in politics. At the same time, a majority of youth also believe that the leaders in government care very little about people like them. A significant percentage of youth believe that they have the skills and knowledge to participate in politics. These findings are also supported by the study of [17], which reports that a vast majority of the youth (61.8 percent) have trust in democracy and peaceful change as they believe that their vote can be a promoter for change.

Education is positively related with political socialization and was statistically significant at 1% demonstrate that 1 percent increase in Education carries 3.96 percent increase in Political Socialization. These results are supported by the study conducted by [15] who concluded that according to the standard socioeconomic model of participation socioeconomic status is strongly related to political participation. People with more education and higher incomes tend to participate more because they are more conscious of the impact of politics on their lives and aware of the legitimate ways to influence government actions.

5. Conclusion

To sum up, the factors like Family, Media, Youth Participation and Education were the main agents of, while Age and Gender had no significant role in formation of Political Socialization. Though some studies suggest that male appears to be more active in political socialization but in our study it comes insignificant. Family is the most important factor as it is the primary source in building political and social ideas. Education is important because it shapes our ideas and beliefs and teach us patriotism. Media is considered to be a weapon in the modern world that can be used according to the conditions. Every kind of media is in use for promoting political campaigns, slogans, and slowly and gradually changing the minds of people and people follow such campaigns actively. Last but not the least the young people involvement in politics brings a lot of changes. Awareness among people increases and they are not blindly following any leader. The young people thinks and question and that causes a big change in the political movements of the current world.

Some major conclusions can be drawn from the results obtained after estimation. From graphical representation it has come to surface that majority of the respondents, regard family as an important variable in shaping of political views. In particular, it has been highlighted that a friendly home environment contributes more towards formation of favorable political values than a conservative or restricted one. Social media too emerged as a significant variable that helps reform political ideas and social media has been given a higher weightage in this respect than any other form.

A sizeable portion of the sample placed youth participation in political activates as viable channel for PS and are further of the opinion that this influences government policies. In addition, the level of education of an individual appeared to have substantial impact on an individual's political views, as projected by the survey.

While from the estimation results, media and education emerged as the most important conduits in Political Socialization process. Both variables were significant at 1% level of significance and appeared positive. This was in concordance with the studies by [13] and [15] , respectively. Family and youth participation too appeared to have important role in PS but comparatively less than of media and education. Both variables were positive and statistically significant at 10% level of significance.

5.1 Policy Recommendations

In line with the findings from the conducted study some recommendations have been made. However, it is important to consider that results were based on a sample that was restricted to just one institute in the city. Therefore, all projections are in accordance with that. Though it should be noted that results even from such small sample can be generalized to understand the general view point. The recommendations are as follows:

- Promotion and up gradation of the existing education system by means of increased governmental expenditures as well as contributions of professors in the respective fields. This will allow for better

understanding of the surrounding and awareness of youth towards political state in the country.
- Emphasis on the media sector, because the media shapes the perceptions of young, and positive messages from the media can inspire constructive public action.
- Insurance of political, social, and economic stability.
- Provision of conducive environment for enrichment of political ethics and ideas.

5.2 Limitations and Guidelines for Future Endeavors

Due to time and resource constraint the selected sample was confined to just one public university. Therefore, for future reference it is recommended that the sample size be enlarged so as to make reliable predictions and thereby deduce plausible conclusions. Additionally, other possible variables such as religion, locality, income and ethnicity have been excluded following the principle of Parsimony. However, inclusion of these variables can add some strength, volume as well as a deeper understanding of the subject.

References

[1] H. Hyman, "Political Socialization", *Glencoe, III: Free Press*, pp.120-210, 1959.

[2] E. Ljungberg, "Political Socialization," *Politica,* vol. 45, no 2, pp. 133-147, 2003.

[3] V. Sapiro, "Not Your Parents Political Socialization: Introduction for a New Generation," *Annual Review of Political Science,* vol. 7, pp. 1-23, 2004, doi: 10.1146/annurev.polisci.7.012003.104840.

[4] F. I. Greenstein, "A Note on the Ambiguity of "Political Socialization: Definitions, Criticisms, and Strategies of Inquiry," *The Journal of Politics,* vol. 32, no 4, pp. 969-978, 1970, doi: /10.2307/2128390.

[5] H. Dekker, "Political Socialization and Research", In Book: Politics and European Younger Generation: Political Socialization in Easter, 1991.

[6] H. &. Y. J. McIntosh, Toward a Political Theory of political socialization of Youth. Handbook of Research on Civic Engagement in Youth, pp. 23-41., 2010.

[7] J. A. &. H. R. L. Bill, Comparative politics: The Quest for Theory. Merrill Publishing Company, pp. 120-199., 1973.

[8] E. Quintelier, "Political Socialization among Young People. Evidence from a two-year panel study," in *In PIDOP conference.*, 2011, doi :10.1177/0192512111412632.

[9] D. J. Martin, "News Use and political socialization among Young Jordanians," *The International Communication Gazette,* vol. 73, no 8, pp. 706-731. , 2011, doi:10.1177/1748048511420094.

[10] J. Keller, "Education, Ethnicity and political socialization in Kenya," *Comparative Political Studies,* pp. 442-468. , 1980, doi:10.1177/001041408001200405.

[11] K. &. Y. C. Levinsen, "Political Discussion with Family and Friends: Exploring the Impact of Political Distance," *The Sociological Review,* vol. 6, no 3, pp. 72-91. , 2015, doi:10.1111/1467-954x.12263.

[12] G. D. &. W. D. E. Wekkin, "A Causal Analysis of the Political Socialization of High School Seniors in Arkansas," *Midsouth Political Science Review,* vol. 9, p. 119, 2008.

[13] S. Richey, "The Autoregressive Influence of Social Network Political Knowledge on Voting Behavior," Cambridge University Press U.K, pp. 527-542., 2008, doi: 10.1017/s0007123408000264.

[14] P. Norris, " Young People and Political Activism: From the Politics of Loyalties to the Politics of Choice? Young People and Democratic Institutions: from Disillusionment to Participation.," In *Council of Europe Symposium.*, Strasbourg,pp. 10-25, 2003.

[15] S. Kim, "Voluntary Associations, Social Inequality, And Participatory Democracy from A Comparative Perspective," *University of Chicago Press,* pp. 223-235., 2008, doi: 10.1108/s1479-352020140000011016.

[16] Cohen, "The Attitudes and Behavior of Young Black Americans," *University of Chicago, Center for the Study of Race, Politics, and Culture,* pp. 601-615, 2007.

[17] Centre for Civic Education of Pakistan, "Civic Health of Pakistani Youth: Study of Voice, Volunteering and Voting Among Young People," in *Centre for Civic Education of Pakistan*, Islamabad, pp. 30-45, 2009.

Appendix

Questionnaire

INFLUENCE OF SOCIOECONOMIC FACTORS ON POLICTICAL SOCIALIZATION IN PAKISTAN

The purpose of this questionnaire is to gather information on people's attitudes, motivation, and opinions towards political socialization in Pakistan and to gauge the general interest of the public in politics.

The questionnaire is divided into 2 different sections. In Section 1, you are requested to give some personal, demographic information. While in Section 2, you are presented with multiple choice questions in relation to political socialization. All responses of questionnaire will be kept confidential. We would be very grateful for your contribution.

SECTION I: DEMOGRAPHIC INFORMATION

1. Please provide the following information.

Gender:

a. Male
b. Female

Age:

a. 15-20
b. 20-25
c. 25-30
d. 30-35

Religion:

a. Muslim
b. Christian
c. Others

Home Town:

a. Punjab
b. Khyber Pakhtunkhwa
c. Sindh
d. Balochistan
e. Gilgit Baltistan
f. Other

Monthly Family Income:

a. Below 50,000
b. Above 50,000

Education Level:

a. 14 years
b. 16 years
c. 18 years and above

Political Affiliation: (Are you a member of any political or religious party?

a. Yes
b. No

SECTION II

2. Political socialization is the process through which political culture, ideas and orientations are transmitted in a society, so which agent promotes political socialization in your view?

a. Family, peers, society
b. Media
c. Education
d. Existing laws

2. A friendly home environment encourages discussion and building of positive ideas.

a. Definitely
b. Most probably
c. Maybe
d. Not at all

3. A conservative family environment hampers thinking and political views.

a. Definitely
b. Most probably
c. Maybe
d. Not at all

4. When do the basic political attitudes and values form in an individual?

a. Childhood
b. Teenage years
c. Adulthood

5. Do you think that the mass media in Pakistan is playing an important role in formation of political views of individual? If yes, which form of media is most effective?

a. Yes
- Social Media (Facebook, Twitter, Instagram, Whatsapp etc.)
- Print Media (Newspapers, Magazines etc.)
- Electronic Media (News Channels)

b. No

6. Which of the following is true about schools and political activism?

a. Higher level of education correlates to higher level of political activism.
b. Higher level of education correlates to lower level of political activism.
c. There is no correlation between education and political activism.

7. Which of the following is true about the connection between religion and politics?

a. A religious person is more interested in politics.
b. A religious person is less interested in politics.
c. A less religious person is more interested in politics.
d. A less religious person is less interested in politics.

8. Politically active people are generally

a. Urbanites
b. Villagers
c. Working/ Business class (irrespective of geographic location)

9. Which of the following Pakistani ethnicities are least likely to have a party affiliation?

a. Balochs
b. Punjabis
c. Pathans
d. Sindhis
e. Others

10. Which of the following factors play an important role in forming an individual's political views? (Can select more than one option)

- ☐ Economic Conditions
- ☐ Family Association
- ☐ Educational Background
- ☐ Religion
- ☐ Ethnicity
- ☐ Age

- Mass Media

11. People should listen to several sides of a political issue before making a decision. Do you agree with this statement?

a. Strongly Agree
b. Agree
c. Neutral
d. Disagree
e. Strongly Disagree

12. Youth involvement in political activism influences government policies?

a. Strongly Agree
b. Agree
c. Neutral
d. Disagree
e. Strongly Disagree

13. Do you think educated and illiterate people, both, act irrationally when it comes to political discussions?

a. Definitely
b. Most probably
c. Maybe
d. Not at all

14. Should political fields be introduced into the educational system to develop and influence the mind-set of the youth?

a. Definitely
b. Most probably
c. Maybe
d. Not at all

15. In your opinion how much importance should be given to Political Socialization?

a. More importance
b. Less importance
c. Is already adequate

16. In concordance with the previous question, what do you think should be the mode for enactment of positive political socialization in our society?

JENRS

Received: 29 January 2022, Revised: 07 March 2022, Accepted: 20 March 2022, Online: 12 April 2022

DOI: https://dx.doi.org/10.55708/js0104008

Design and Analysis of Flat Belt Conveyor for Segregation of Defective Products

Yash Patil *, Shivraj Patil, Suhas Gawade, Vaishnav Shinde, Samidha Jawade

Department of Mechanical Engineering, MIT World Peace University, Pune, 411029, India

*Corresponding Author: Yash V. Patil, Jalgaon, (+91) 7030680486, 3101yashpatil@gmail.com

ABSTRACT: Belt conveyor system is mostly used in industries for transportation of raw materials and finished products. This paper includes study of detailed design procedure and analysis of flat belt conveyor components for light duty applications. Belt conveyors used for segregation of defective products up to 2 kg maximum load whose conveyor capacity is 2 TPH and speed of the conveyor will be 3.5 m/min. Our paper includes study of design calculation of conveyor and FEA analysis of pulley, shaft and conveyor belt. 3D model is created using solid work software. FEA is done on ANSYS and Inventor software with appropriate loading condition, considering calculated tension. Stress analysis of shaft, pulley and belt is done to find highest stressed area of belt conveyor. By following the design procedure for flat belt conveyor system, all geometrical parameters obtained are within limits and design of conveyor is safe. In FEA, contact status and contact pressure between belt and pulleys are properly sticky and in contact. Max stress acting on belt is 58.85 MPa and deformation will occur at 87.88 MPa. Stress on shaft comes out to be 13.17 MPa.

KEYWORDS: Conveyor Belt, Design and FEA Analysis, Flat Belt, Segregation of Defective Product.

1. Introduction

Belt conveyor is commonly used equipment in industries for continues transportation of materials [1]. Belt conveyors are categorized in two industrial categories. First category for material handlings like for carrying boxes in the factories and bulky materials handling like used for transportation of industrial or of agriculture materials, like grains, coals, and ores, generally in outdoor location. Belt conveyors are more reliable, provide high stability and more conveyor capacity, have less maintenance [2].

Conveyor belt systems are classified according to their operational mechanisms such are rollers, chains, screw, spiral, vibrating, and pneumatics [3]. Selection of conveyor systems are based on functioning requirement, sizes, shapes or weights of materials, travelling distances, speed requirement, atmospheric conditions and economical.

Conveyor belt consist of two or more pulleys, with continuous loop of materials, around which conveyor belt rotate. One or both the pulleys are powered, to provide motion to belt and carryout the material on the belt from one to another end. The powered pulleys are called drive pulleys while unpowered pulleys are called idlers. Rollers are used in between both pulleys to support belt and to improve efficiency and maintain speed and minimize belt sag. [4]

Belts are made up from one or many layers of materials may be from rubbers. Belt used for materials handling has 2 layers. Inner layer of materials provides linearly strengths or shapes known as carcass and above layers known as cover. A carcass is mostly of cottons or the plastics web or meshes. Covers are of different rubbers and plastics compound specified by use of belt [4].

Cover may be made up from more exotic material for unusual application like silicones for heating or gum rubber when tractions are essential. [4] Conveyor technologies are also useful for conveyor transportation like movable sidewalks and lifts, also in manufacturing assembly line.

This paper studies about design and analysis of a flat belt conveyor system for separation of defective products from conveyor line in industries where products are manufactured in bulk. During inspection of final products lot of man power is required and is more time consuming. Sometimes due to human error damaged products are added in selected lot, which directly affects reputational and economical losses of firms. Therefore, to avoid this

problem, we have designed and analyzed a conveyor system which automatically segregates defective products, using pneumatic actuators and sensors, according to their geometrical parameters and minimizes inspection time and cost associated during process with no human touch required using python interfacing. 3D model is designed as per analytical values obtained using solid works software. FEA analysis is also made of pulley, shaft and conveyor belt.

2. Problem Statement:

Metal materials like steels, aluminum, copper plate or strip, are mostly used in automobile's manufacturing, bridges construction, aerospace fields or other pillar industries. But during actual industrial production processes, processing tools gets damaged due to harsh industrial environment, which leads to certain quality problems to metal material product. Few product surfaces show defects in large-area or the periodic characteristic not only impact on subsequent production but also threatens the quality of terminal product, which causes economical or reputational losses to manufacturing industries. [5] So we have designed conveyor mechanism on the detection of defective product and segregation with the help of sensors, pneumatic actuators and python program interfacing.

3. Material and Methods

The defective product sorting machine consists of flat belt conveyor mechanism. Pneumatic cylinder and proximity sensors are used for detection and sorting of defective product. Flange mounted motor with gear box is connected at head pulley shaft. Complete sorting unit is operated using python interfacing.

Material to be sorted can be fed with the help of hopper or manually. Both the head and tail end pulleys are kept of same diameter and same as shaft. Rubber belt carries out the material till the sensor senses the products, and if the product is sensed to be defective product then DAC pneumatic actuator operates and product get sorted from queue. Conveyor system is designed, for maximum load up to 2 kg.

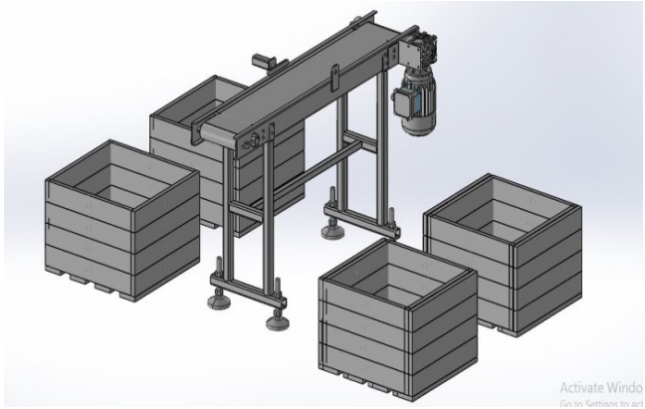

Figure 1. Isometric view sorting mechanism

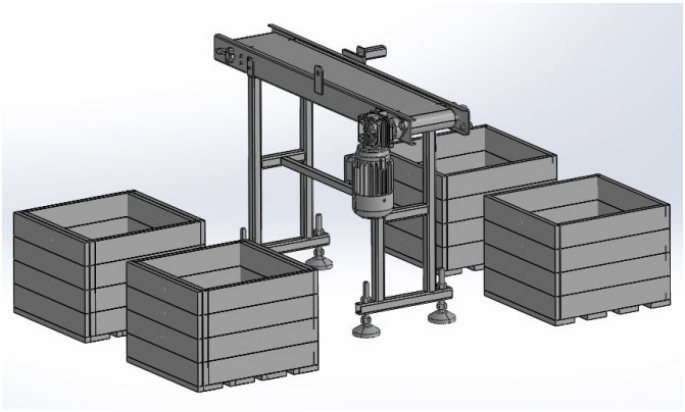

Figure 2. Front view of sorting mechanism

4. Design of Conveyor:

Design flat belt conveyor system for sorting of defective products having conveyor capacity of 2 tones/hr. and maximum weight to be carried is up to 2kg. Center distance between both pulleys is 1000mm and height of conveyor is 518 mm. Other specifications:

a. Material density: 1.5 tones/m³
b. Inclination angle: 0°
c. Angle of repose: 45°
d. Lump size: 120mm
e. Conveyor speed: 3.5 m/min

4.1. Belt Speed and Width Calculations:

Determine the width of conveyor speed using the relation,

B= 2*Amax+ 200 ...for solid material

B= Amax+ 200 ...for fine material

Where, Amax denotes lump size

For solid material, the belt width comes out to be 440mm.Selecting the standard belt width of 400 mm from PSG design data book [6].

Now, check for the belt speed,

$$B = 1.11\left[\left\{\frac{Q}{\rho * C * V}\right\}^{\frac{1}{2}} + 0.05\right] \quad (1)$$

where, B = Belt Width

Q = Conveyor Capacity = 2 tones/m³

ρ = Density of Material =1.5 tones/m³

C = Surface Factor for Type of Idler

C = 240 (For flat belt)

V= Belt Speed (m/sec)

So, the value of belt speed is 0.0576 m/sec i.e. around 3.5m/min which is less than 1.5 m/sec, the allowable speed for 400 mm width belt. Therefore the belt width of

400 mm is acceptable. The obtained values are compared with design data given in PSG design data book.[6]

4.2. Resistances of belt at top and bottom run

Resistance of belt at top run [$\mathcal{W}o$]:

$$\mathcal{W}o = C * f * L[(Gg + Gb)\cos\delta + Gro] \pm H(Gg + Gb) \quad (2)$$

Where, C= secondary resistance factor

C= 9 (for conveyor length ≤ 3 m)

f = 0.02 (for standard conveyors)

L= length=1000m

Gg=weight of conveyed material per meter length, kgf/m= 9.65 kg/m

Gb =weight of belt per meter length kgf/m = 5 kgf/m

δ = inclination angle = 0°

H= height of conveyor = 518.16 mm

$$\therefore \mathcal{W}o = 10.227 \text{ kgf}$$

Resistance of Belt at Bottom Run [Wu]:

$$\mathcal{W}u = C * f * L[Gb * \cos\delta] \pm H * Gb \quad (3)$$

$$\therefore \text{Wu} = 3.4908 \text{ kgf}$$

Power (P) can be determined as;

Power = Resistance of Belt at Top Run + Resistance of Belt at Bottom Run

$$P = \mathcal{W}o + \mathcal{W}u \quad (4)$$

$$P = 13.7178 \text{ kgf}$$

4.3. Belt Tension Calculations

Effective force on belt is given by;

$$P = T1 - T2 \quad (5)$$

Also,

$$\frac{T1}{T2} = e^{\mu\theta} \quad (6)$$

Where, μ = coefficient of friction between belt and pulley

μ = 0.3

θ = angle of lap

Considering angle of lap over load pulley as 200° > 165° to avoid slip of belt during running conditions

$$\frac{T1}{T2} = e^{0.3*200*\frac{\pi}{180}}$$

$$\therefore \text{T1} = 2.8496 \text{ T2}$$

$$\therefore \text{T2} = 7.416*10^3 \text{N} \quad (7)$$

Putting in equation 5,

$$T1 = 2.8496 * 7.416 * 10^3$$

$$\therefore \text{T1} = 21.132 *10^3 \text{ N}$$

Maximum belt tension on carrying side is 21.132*10³ N and minimum slack side tension is 7.416*10³ N.

4.4. Selection of Driving Unit

$$\text{Power, P} = \frac{\text{Force} \times \text{Velocity}}{\text{Transmission}} \quad (8)$$

$$\therefore \text{P} = \frac{(T1-T2)*V}{\eta f}$$

Where, ηf = transmission efficiency

ηf = considering efficiency as 95%

$$\text{P} = \frac{13.716*10^3 \times 0.0576}{0.95}$$

$$\therefore \text{P} = 831.6227 \text{ W}$$

$$\therefore \text{P} = 0.8316 \text{ KW}$$

Therefore, from PSG design data book a Flange Mounted Motor of 1.1 kW ratings and 1000RPM is selected. [6] The motor will be connected to the gear box to reduce and maintain the rpm of driving pulley shaft.

4.5. Conveyor Pulley

As the conveyor is flat belt conveyor system both the pulleys are of same diameter having same length and material as well. [6]

For the belt width selected of 400 mm, from PSG design data book selected the standard diameter of conveyor pulley drum, D, to be 110mm and have standard face width of 450 mm and edge clearance of about 25 mm is considered on both ends of pulley.[7]

4.6. Belt length and thickness

Center distance between pulleys is 1000mm checking for the minimum center distance required for conveyor using the relation,

$$C > 2 (d1+d2) \quad (9)$$

$$C > 2(100+100)$$

$$C > 400 \text{ mm}$$

Therefore center distance greater than 400 mm will be accepted as per requirement. Therefore taking center distance between pulleys as 1000 mm as given.

For open belt drive system length of shaft can be determined as;

$$L = \frac{\pi}{2}\left[(Dl + Ds) + 2C + \frac{1}{4C}(Dl - Ds)^2\right] \quad (10)$$

where, C is center distance

Dl = diameter of large pulley and

Ds = diameter of small pulley

$$\therefore \text{L} = 2314.1595 \text{ mm}$$

But taking into considerations, initial tension, the belt length should be shortened by 1%

L = 2291.018 ≅ 2290 mm

For rubber belt coefficient of frictions is taken as $\mu = 0.4$

Design power(Pdes)=service factor*required power (11)

Design power (Pdes) = 0.997 KW

Design stress for rubber belt material can be taken as 1.5 MPa & Density of rubber belt is 1140kg/m³.

Design stress in belt can be calculated as,

$$\sigma' = \sigma max * Cspd * Cw \quad (12)$$

$$Pdes = bt(\sigma' - \rho v^2)\left(1 - \frac{1}{e^{\mu\alpha}}\right) * v \quad (13)$$

where α= angle of lap=200°

α= 3.49 rad

bt =11509.80 mm²

So, selecting standard Rubber Belt as;

Length of belt =2290 mm

Width of belt = 450 mm

Thickness of belt = 3 mm

4.7. Pulley Shaft Calculations:

Length of shaft considering the belt width of 400 mm and clearance of 50 mm and width of bearings on both ends of shaft, [8]

$$L = B + 100 + 50 \quad (14)$$

L = 550 mm

Max bending force on pulley,

$$Mmax = \frac{W}{2} X \frac{l}{2} = 3.925 \times 10^6 \text{ N*mm} \quad (15)$$

Twisting moment on shaft,

$$Mt = \frac{P X 60}{2\pi N} \quad (16)$$

To find N, Velocity of belt (V),

$$V = \frac{\pi D N}{60} \quad (17)$$

N = 11 RPM

$$Mt = \frac{p \times 60}{2 \pi N}$$

Mt = 721.921 x 10^3 N*mm

Equivalent torque on shaft;

$$Meq = \sqrt{Mmax^2 + Mb^2} \quad (18)$$

$$= \sqrt{(3.925 \times 10^6)^2 + (721.92 \times 10^3)^2}$$

Meq = 3.990 X 10^6 N-mm

Selecting the carbon steel material of grade C45 from PSG design data book having properties,

$\sigma y = 360$ N/mm²

FOS = 4

(τ) = 45 N/mm²

Considering torsional failure of shaft;

$$Mteq = \frac{\pi}{16} * \tau * ds^3 \quad (19)$$

ds = 50 mm

Selecting standard shaft of 50 mm diameter and 550 mm length of C45 grade material for both pulleys from PSG design data book.

4.8. Selection of Bearing:

Bearings are machine elements which supports other moving machines elements. [8] Bearings permit the relative motion between the contact surfaces of the members, while carrying the load. [9] Deep Groove Ball Bearings are selected for both the pulley shafts having

d = Internal diameter = 50 mm

D = Outer diameter = 80 mm and

w = width of bearing = 16 mm

5. FEA for Conveyor Belt, Pulley and Shaft:

Analytical design executed successfully using ANSYS workbench and inventor softwares. By applying accurate force and constraint are simulated in ANSYS and inventor to achieve precise result. FEA is performed to find maximum and minimum von mises stress on belt pulleys and shaft, contact status and maximum contact pressure between belt and pulley and stress on shaft at bearing end.

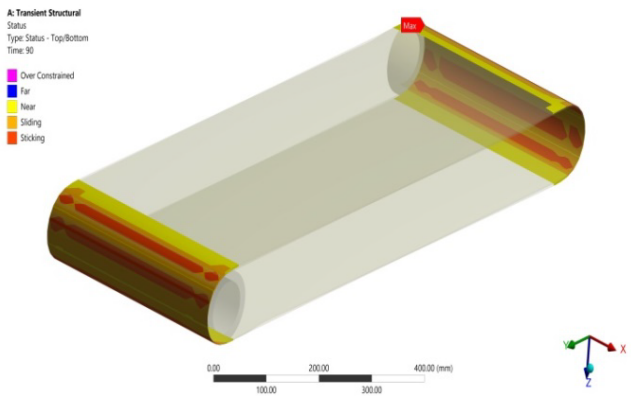

Figure 3. Contact Status between Belt and Pulley

For FEA all the standard material's properties are considered. Dead weights for both pulleys are considered. Resultant tensions are obtained and applied as uniform radial pressures on a pulley surfaces in area of angle of wrap, and over belt width as well. Torque obtained for driven pulley is applied on drive end of shaft. Initial 3D simulation model of pulley system is designed using solidworks and catia softwares.

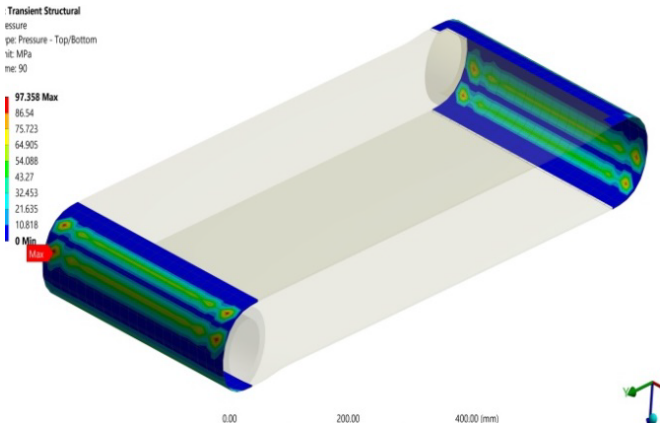

Figure 4. Contact Pressure

The contact status between belt and pulley shows the belt is properly in contact and sticked with pulley and the maximum contact pressure between belt and pulley is 97.35 MPa.

The tensions acting on the belt calculated by analytical methods on carrying side and slack side are $21.132*10^3$ N and $7.416*10^3$ N. The maximum stresses on belt are analyzed using ansys software.

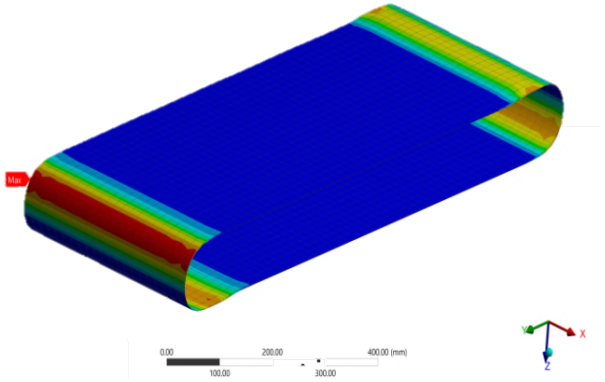

Figure 5. Stresses in Belt

Maximum von mises stresses in shaft is 58.85 MPa. Deformation of belt at worst conditions, occurs at 87.88 MPa

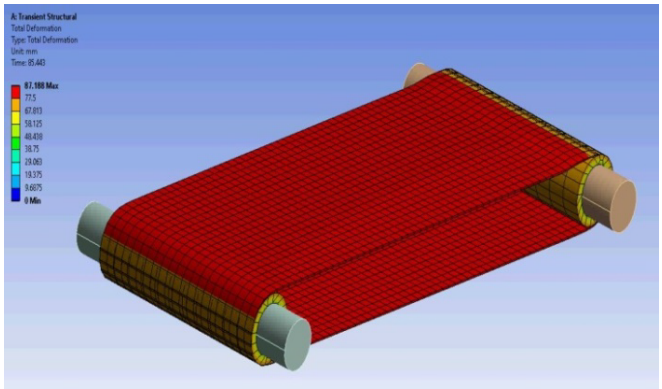

Figure 6. Deformation of belt at worst condition at 87.88MPa

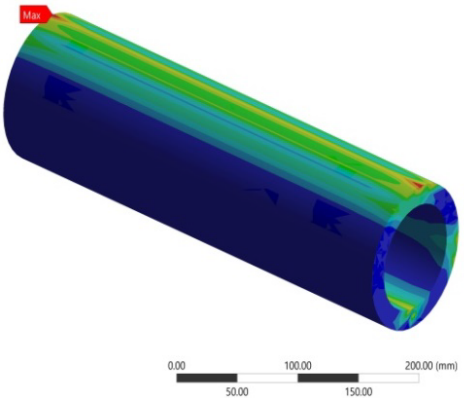

Figure 7. Maximum Stress on Pulley is 11.39 MPa

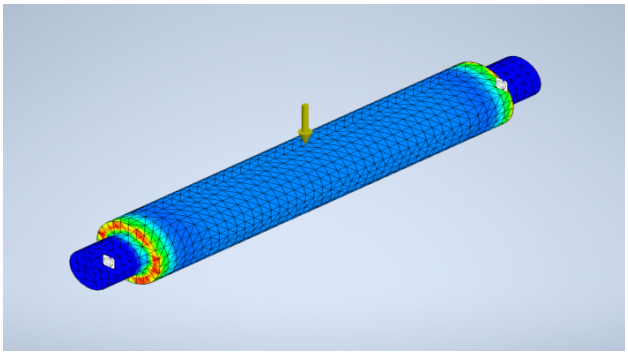

Figure 8.Von Mises Stress on Shaft 13.17 MPa

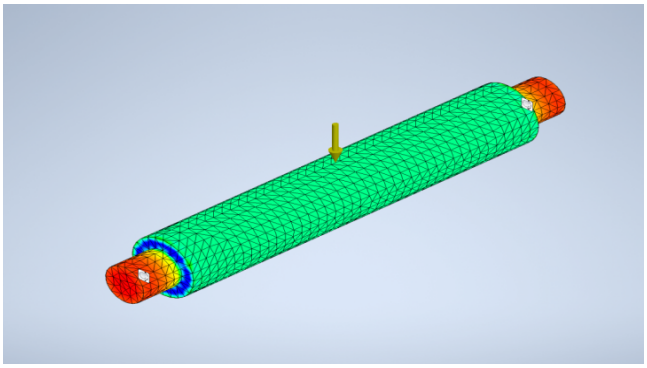

Figure 9. Max Stress on Shaft at Bearing Ends 0.08 MPa

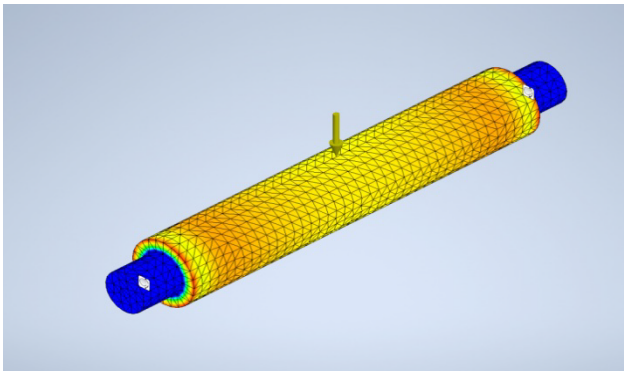

Figure 10. Max Stress on Shaft Due to Pulley and Belt

Maximum stresses on shaft due to pulley are 12.47 MPa. The analysis is done for belt, pulley and shaft for carrying side is within range and hence design is safe. Similarly, the analysis is done for tail side arrangement.

6. Conclusion

This paper is based on theoretical calculations, designing and FEA of flat belt conveyor systems for sorting

of defective products. The main purpose to design the system is to minimize inspection time of product on conveyor line and to minimize the manpower required for inspection and sorting. The system is operated through python interfacing and the design is easily understandable.

Through our design the defective products are inspected and get sorted, if found defective, without any human touch. Components of the conveyor system are analyzed using Ansys and inventor software. The results achieved are within acceptable range and design is safe. Hence, the conveyor system is designed successfully.

7. Future Scope

Our defective product sorting system inspects and segregates defective products without any human touch. But it has limitations to segregate products in multiple sections. In future using latest technology and resources the design and components can be modified as per requirements to main minimize inspection time and manpower. Also, this kind of systems can also be designed for various types of raw materials for heavy duty applications.

Acknowledgement

Our guide Prof. Mrs. Samidha Jawade, Assistant Professor, Department of School Of Mechanical Engineering-MIT World Peace University, Pune. She has encouraged and motivated us throughout this project, and helped in every step of project development.

8. Conflicts of Interest

The authors declare no conflict of interest.

9. References

[1] P. K. V. Konakalla Naga Sri Ananth, Vaitla Rakesh, "Design and Selecting the Proper Conveyor-Belt," *International Journal of Advanced Engineering Technology E*, vol. IV, no. II, pp. 43–49, 2013.

[2] L. Zhao, Y. Lin, "Typical failure analysis and processing of belt conveyor," *Procedia Engineering*, vol. 26, pp. 942–946, 2011, doi:https://doi.org/10.1016/j.proeng.2011.11.2260.

[3] M. R. Sayali Todkar, "Design of Belt Conveyor System," *International Journal of Science, Engineering and Technology Research*, vol. 7, no. 7, pp. 458–462, 2018.

[4] Z. B. R. gunasegaran Madasamy, "Automated Mechanical SOrting Device for Mixed Household Wastes," *LAP Lambert Academic Publishing*, no. February 2013, pp. 50, 2013.

[5] P. Elamurugan et al., "Automatic material segregation using PLC," *International Journal of Engineering and Technology(UAE)*, vol. 7, no. 2, pp. 376–380, 2018, doi:https://doi.org/10.14419/ijet.v7i2.24.12088.

[6] PSG college of engineering, *307Design_Data_Data_Book_Of_Engineers_By_PSG* (Coimbatore, India: Kalaikathir Achchagam).

[7] K. S.J. Ojolo, J.I. Orisaleye, Adelaja, A.O., "Design and Development of Waste Sorting Machine," *Journal of Emerging Trends in Engineering and Applied Sciences (JETEAS)*, vol. 2, no. 4, pp. 576–580, 2011.

[8] Bhandari V. B., *Design of Machine Elements - V. B. Bhandari - Google Books* (1994).

[9] P. K. Shanjenbam Brojendro Singh, Abu Salah Muslaha Uddin Laskar, Biltu Roy, Aminul Hoque Choudhury, Zahidul Islam, Jakir Hussain Mollah, Shadeed Masood Ul Hoque, Mohsin Ali, "Design of Municipal Dry Waste Segregating Machine Using Conveyor," *International Journal of Innovative Research in Science, Engineering and Technology (An ISO*, vol. 5, no. 5, pp. 7156–7162, 2016.

Yash V. Patil has done his diploma in Mechanical Engineering from Sou. Venutai Chavan Polytechnic, Pune in 2018. He has done his bachelor's degree in mechanical engineering from MIT World Peace University, Pune in 2021.

Shivraj B. Patil has done his diploma in Mechanical Engineering from Padmabhooshan Vasantraodada Patil Institute of Technology, Sangli in 2018. He has done his bachelor's degree in Mechanical Engineering from MIT World Peace University, Pune in 2021.

Suhas R. Gawade has done his diploma in Mechanical Engineering from New Polytechnic, Kolhapur in 2018. He has done his bachelor's degree in Mechanical Engineering from MIT World Peace University, Pune in 2021.

Vaishnav V. Shinde has done his diploma in Mechanical Engineering from Institute Of Civil And Rural Engineering, Kolhapur in 2018. He has done his bachelor's degree in Mechanical Engineering from MIT World Peace University, Pune in 2021.

JENRS

Received: 24 January 2022, Revised: 01 March 2022, Accepted: 01 April 2022, Online: 12 April 2022

DOI: https://dx.doi.org/10.55708/js0104009

Modelling and Comparative Study for Deep Groove Ball Bearing Based on Structural Analysis using FE Simulation

Avinash Galande*, Swanand Pachpore , Ashish Pawar

School of Mechanical Engineering, Dr. Vishwanath Karad MIT- World Peace University, Pune, Maharashtra, India
*Corresponding author: Avinash Ashok Galande, Pune, 9370092704, avinashgalande96@gmail.com

ABSTRACT: A deep groove ball bearing is a rotary element designed for supporting a radial as well as axial load, low friction, and widely used due to little noise and vibration which supports high rotational speeds. In this article, the author carried out a structural analysis (using FE Simulation) of a single row deep groove ball bearing for estimating contact stress and total deformation for three grades of materials viz. Silicon Nitride (Si3N4), 440C Stainless Steel, and AISI 4140 Alloy Steel. Under the scope of the study, modeling is done using Autodesk Platform and analyzed using ANSYS as an FEA tool. The natural boundary conditions were applied to estimate the fatigue life of bearings under standard operating conditions. The obtained results indicate Silicon nitride material was found to be more significant amongst all materials taken for considerations.

KEYWORDS: Deep groove ball bearing, Silicon nitride, Equivalent stress, Equivalent strain

1. Introduction

Most of the industries uses single row deep groove ball bearing most common type of rolling bearings. For the movement of machine elements concerning each other different types of bearings are used flawlessly for supporting skyscrapers and allowing them for movement at the time of earthquakes, bearings can make excellent watches happily tick away. If there is nothing like bearings, all would have ground to rest, including many of those whose joints are containing sliding bearings, The DGB usage is the most widely in industry and the market share of DGB bearings is about 80 % of total industrial rolling element bearings. For better load carrying capacity double row deep groove ball bearings are more suitable for bearing arrangements [1]. While designing the bearings and selecting its applications load capacity is the important thing. Also, it has high authority on fatigue life prediction of bearings. Ball bearings are the most commonly used machine elements. Having the same physical parameters double row deep groove bearings are wider than single row bearings, also they consist of higher loading capacity [2]. There are two types of bearings, contact bearings, and non-contact bearings. From which Contact-type bearings consist of contact between elements, it consists of sliding, flexural and rolling bearings. Mechanical contact shows stiffness in the direction which is normal to the direction of motion and it can be very high, but their life can be limited by wear and fatigue. In case of machine design, the designer decide to use bearings then it is very much mandatory thing for them to calculate strength (contact), the lifetime of bearing, and radial and axial rigidity of rolling bearings. But still, it is very difficult thing to calculate the contact strength, radial rigidity, and total lifetime of the rolling bearings precisely in theory [3]. A thrust load of about 70 % can be supported using a DGB bearing of its radial load. In Past, a lot of researchers have analyzed effectiveness for bearing defect detection using statistical parameters for different conditions [4]. To find out the location of stress concentrations also to determine the minimum and maximum of shear stress in rolling ball bearings finite element analysis is used [5]. Condition monitoring of bearings has a very big role in the maintenance of any rotating machines such as bearings for detecting the fault earlier [6]. The bearing failure causes economical loss. Various analysis protocols are well articulated for industrial components for structural loading [7].

2. Design consideration in deep groove ball bearing

In ball bearings, it consists of inner, outer races and a set of balls. All races have a ring with a groove for placing the balls as shown in Fig. The shape of the groove is made such that the ball fits loosely in the groove. The race has dents for pressing each ball on it, the contact between ball and race contains finite pressure and they show finite

contact between them. Each ball and race contacts have opposite forces and sliding motions [8].

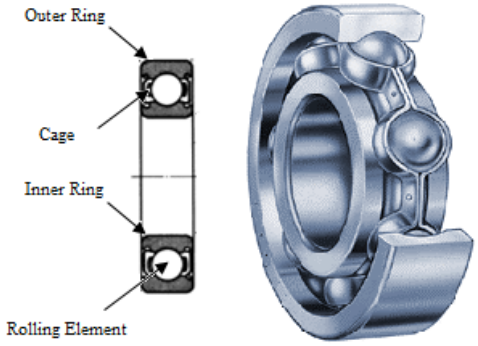

Figure. 1. Deep groove ball bearing [9]

As per Hertz's theory, the contact between two bodies having curved surfaces under force W is considered. Rolling elements and races have line contact or theoretical point contact between them. But the elliptical shape is formed due to elastic deformation in the contact area between two curved bodies of point contact. In machine elements and setups, it includes vibrations and sudden shocks. Also, there can be high contact stresses. The over-temperature of bearing can alter the state of lubrication and form premature failure of bearing or machinery element due to increment in heat further. These deep groove ball bearings can withstand both radial and axial loads in a particular direction, are quite easy to mount, and maintenance requirement is also less than other types of bearings. If there is a need for higher load capacity mandatory, hence double row bearing can be a better alternative for single row DGB bearing.

The usage of deep groove ball bearings is wider in industry and they acquire around 80 % of the industrial market share. To provide preload that induces stiffness of bearing it is crucial to provide a suitable amount of interference [10].

The objectives and scope of the study are to design the SKF 6302 Ball Bearing and study the structural stress analysis for high performance. their consequence on fatigue life of bearing. After analysis, a comparison is made between silicon nitride, stainless steel alloy (AISI 440c), and 4140 Alloy steel bearings following structural and contact stresses.

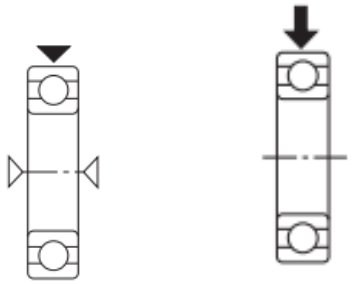

Figure. 2. Loading in Deep groove ball bearing (Axial and Radial with Axial combined) [8]

3. Modelling and simulation

3.1. Materials used for analysis

The developed model was analyzed for three different materials namely Silicon Nitride, AISI 4140 Alloy Steel, and 440C Stainless Steel; and materials properties used for those materials are stated in Table 1.

Table 1. Material properties

Parameter	Materials		
	Silicon Nitride	AISI 4140 Alloy Steel	440C Stainless Steel
Density (Kg/m^3)	3395	7861	7799
Young's modulus (Pa)	3e12	4.15e8	1.9e11
Poisson's ratio	0.23	0.3	0.285
Bulk modulus (Pa)	2.27e12	3.45e8	1.66e11
Shear modulus (Pa)	1.171e12	1.596e8	8.39e10

Table 2. Dimensions of bearing

d	15 mm
D	42 mm
B	13 mm
d_1	23.7 mm
D_2	36.23 mm
$r_{1.2}$	min. 1 mm

3.2. Analytical Calculations

For analytical approach Hertz theory of contact stress is considered. Hertz theory include mathematical analysis of the affiliation between, the overall contact area size, the stresses distributed in two bodies having some curvature, the profile of the geometry. This study includes elliptical contact surface between the applied load, inner race and balls [11].

I. Steps to Determine the Contact Stresses –

Step 1: Consideration of applied load on DGB bearing.

Step 2: Determine the design P_d load at which the ball bearing will be subjected. The static shaft analysis determines the axial (Fa) and radial (Fr) forces. Defining of the equivalent load p-value is done using Equation

$$P = XF_r + YF_a \quad (1)$$

As in this study only axial force acting on the bearing is considered, equation (1) can be termed as,

$$P = 0 + YF_a$$

Determination of the design load value using axial force P with V as a rotation factor

$$P_d = V \quad (2)$$

The value of V =1.2 if outer ring is rotating and V = 1 if inner ring is rotating.

II. Steps to Determine the Contact Area of the Ball Bearing

Step 3: Now find the total curvature of contact area, in current study analysis of curvature is done between inner race and ball bearing. Total curvature of ball bearing in the directions x and y is termed as

$$\frac{1}{R} = \frac{1}{R_X} + \frac{1}{R_Y} \quad (3)$$

$$\frac{1}{R_x} = \frac{1}{r_{aX}} + \frac{1}{r_{bx}} \quad (4)$$

$$\frac{1}{R_y} = \frac{1}{r_{ay}} + \frac{1}{r_{bY}} \quad (5)$$

Here, r_{ax} is ball radius in x direction and r_{ay} is ball radius in y direction. So $r_{ax} = r_{ay}$. Also r_{bx} and r_{by} are radius of curvature from ball bearing centre to exterior ring and radius of curvature of external ring respectively. The overall analysis in this study is performed on the whole DGB bearing.

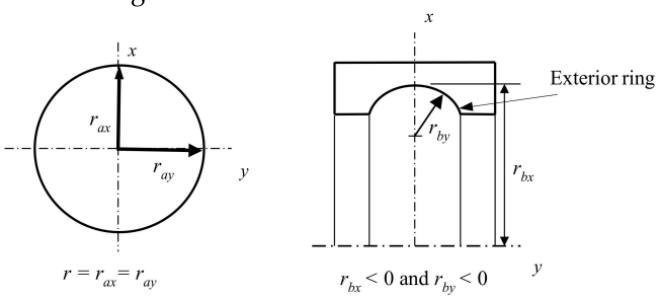

Figure.3. Race of ring and ball ratio [11]

Step 4: The radius of ring R_r, the curvature's index (a_r), elliptical parameter (k_e) can be determined from catalogues as this bearing is standard SKF bearing.

Step 5: Now effective elasticity module (E') is determined as:

$$E' = \frac{2}{\frac{1-v_a^2}{Ea} + \frac{1-v_b^2}{Eb}} \quad (6)$$

In this, v_a and v_b are the Poisson coefficient of the ball and inner/outer ring respectively. Also, E_a and E_b are the elasticity module of ball and rings.

Step 6: Calculate a and b for ellipse dimensions, as the contact area between the ball and ring is of ellipse form. Values of a and b are for determined as a and b are half of the (Dy) and (Dx) ellipse diameters written as:

$$D_y = 2\left(\frac{(6K_e^2\varepsilon P_d R)^{\frac{1}{3}}}{(\pi E')^{\frac{1}{3}}}\right) \quad (7)$$

$$D_x = 2\left(\frac{(6\varepsilon P_d R)^{\frac{1}{3}}}{(\pi k_e E')^{\frac{1}{3}}}\right) \quad (8)$$

These equations are used for determining the values of a and b.

III. Determination of the equivalent Principal Stress Values

Step 6. Now the maximum contact stress P_{max} is determined using the equation as:

$$P_{max} = \frac{6PD}{\pi D_x D_y} \quad (9)$$

The equation for Von-Mises Stress is

$$\sigma_{VM} = \sqrt{\sigma_1^2 + \sigma_2^2} + \sigma_3^2 - \sigma_1\sigma_2 - \sigma_2\sigma_3 - \sigma_3\sigma_1 + 3(\tau_1^2 - \tau_2^2 - \tau_3^2) \quad (10)$$

In this, the stress acting on the bodies (inner and outer ring, ball), is given by $\sigma_{1,2,3}$ and $\tau_{1,2,3}$.

IV. The equation for maximum deformation (δ) is as:

$$\delta = \Im\left[\left(\frac{9}{2\varepsilon R}\right)\left(\frac{F}{\pi k\gamma}^2\right)\right]^{1/3} \quad (11)$$

V. Equivalent strain (ξ) is calculated using below equation[12]:

$$\xi = \frac{\sigma\gamma}{2} \quad (12)$$

3.3. CAD Modelling of bearing

The Deep Groove Ball bearings are modeled using Autodesk Fusion 360 and analyzed using the ANSYS workbench simulation tool used for Finite Element Analysis, static structural model setup was used for

analysis. The standard SKF deep groove ball bearing model was considered under scope of study.

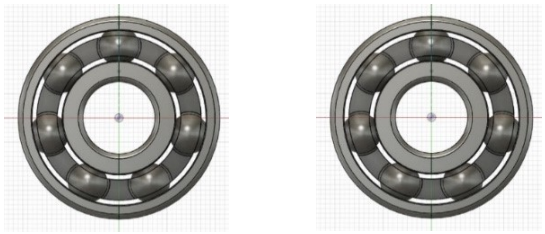

Figure. 4. CAD model

3.4. Boundary conditions

The natural boundary conditions are applied as per the images attached below with tetrahedron meshing and locations of axial load are highlighted with red color [13].

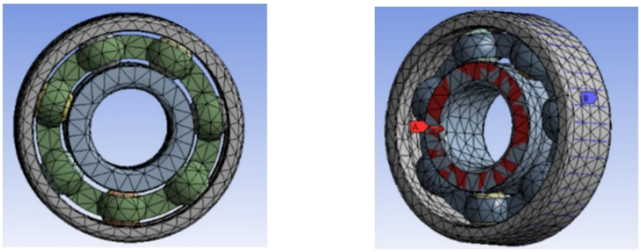

Figure. 5. Model with meshing and natural boundary conditions

3.5. Results and discussion

The resulted analytical and simulated values with the given loading conditions the output such as total deformation, Equivalent Elastic Strain, and Equivalent Stress was compared for all selected materials, and results are tabulated below. After comparing the theoretical and numerical results, the difference is varying in the range of about 5% to 7% which is in better agreement.

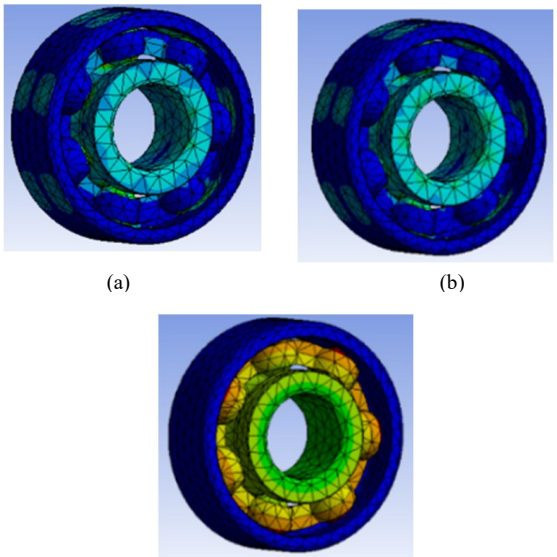

(a) (b)

(c)

Figure. 6 Results for Alloy steel 4140 , a) Equivalent strain, b) Equivalent stress c) Total deformation

New material silicon nitride is used for evaluation in different types of bearings and loading conditions for comparing and choosing the better material among the results of analysis of different materials. In this study DGB bearing is modelled using fusion 360 tools and then simulated for structural stress analysis using ansys tools. Analytical calculations are performed based on Hertz theory. By correlating these theoretical and numerical results the best material among the three different used materials is decided. The FE simulation and analytical approach is noble, provides the finest results and it is less expensive[14]. In terms of axial load the results using proposed methodology for this study also suggests that silicon nitride is best suitable material under standard loading conditions. Also when other researchers worked on the different types of bearing under suitable loading conditions, the results indicated silicon nitride as a better bearing material choice if only axial load is concerned.

3.5.1. Silicon Nitride

Table 3. Silicon Nitride

Name	Total deformation	Equ. Elastic Strain	Equi. Stress
Min	0	1.5251e-006 m/m	1.9041e+005 Pa
Max	3.1116e-005 m	5.6229e-004 m/m	1.4892e+008 Pa

3.5.2. Alloy steel 4140

Table 4. Alloy steel 4140

Name	Total deformation	Equ. Elastic Strain	Equi. Stress
Min	0	2.0414e-006 m/m	1.5232e+005 Pa
Max	7.2709e-005 m	7.8877e-004 m/m	1.5719e+008 Pa

3.5.3. Stainless Steel 440c

Table 5. Stainless Steel 440c

Name	Total deformation	Equ. Elastic Strain	Equi. Stress
Min	0	2.1834e-006 m/m	1.5617e+005 Pa
Max	7.757e-005 m	8.4235e-004 m/m	1.5766e+008 Pa

4. Conclusions

From the investigation carried out to investigate structural properties of deep groove ball bearing, following conclusions can be drawn while taking account the limitations of this study:

Table 6. Analytical and simulated results of DGB bearing using three different materials

Sr. No.			Total Deformation	Equ. Elastic Strain	Equi. Stress
1	Silicon Nitride	Analytical	3.3016e-005 m	5.9113e-004	149.97 MPa
		Simulated	3.1116e-005 m	5.6229e-004	148.92 MPa
2	Alloy steel 4140	Analytical	6.9012e-005 m	7.5677e-004	154.46 MPa
		Simulated	7.2709e-005 m	7.8877e-004	157.19 MPa
3	Stainless steel 440C	Analytical	7.4431e-005 m	8.1675e-004	153.19 MPa
		Simulated	7.757e-005 m	8.4235e-004	157.66 MPa

Silicon Nitride Material was found to be more significant as compared to specified loading conditions. From the analysis completed in this study we can by observing the structural analysis outcomes under the same loading conditions of three materials it is found that the bearings when uses silicon nitride material shows less maximum equivalent stress among the all used materials. Also we can see from the results table that the total deformation is also fewer while using silicon nitride as a bearing material compared to other traditional materials

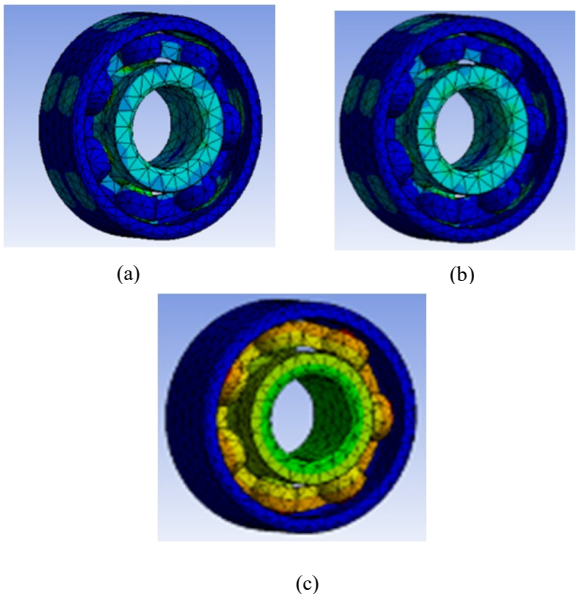

Figure. 7 Results for Stainless Steel 440c , a) Equivalent strain, b) Equivalent stress c) Total deformation

Silicon Nitride Material was found to be more significant as compared to others in specified loading conditions. From the analysis completed in this study we can conclude that the stress and deformation values w.r.t. axial load while using silicon nitride material are found to be within acceptable range compared to other materials. This acceptable ranges are from the standards set by many bearing manufacturing companies. As compared to other traditional metal bearings, bearings of silicon nitride are harder than metal, there is a reduction in contact with the bearing track, which appeared in higher corrosion resistance, 80 % less friction, and higher operating temperature. It also consists of low density about 40 % of steel, so it naturally decreases the centrifugal force and it can operate in high temperature environments.

Future scope – In near future work as various materials are being continuously developed and modified. So as per bearing industry standards and need, various materials can be used for further study under the scope of finding the better materials for use in bearing in specific loading and operating conditions.

Conflict of Interest

The authors declare no conflict of interest.

References

[1] K. Venkata Saikiran Raju, G. Thammi Raju, and N. Harsha, "Modeling and structural stress analysis of thrust bearings," in *Materials Today: Proceedings*, Vol. 18, pp. 2163–2171, 2019, DOI: 10.1016/j.matpr.2019.06.711

[2] V. Tijare, S. Nagaraj, J. Sastry, and M. Mulinti, "Load capacity estimation of elliptical contact rolling bearings," *Materials Today: Proceedings*, Vol. 24, pp. 1686–1695, 2020, DOI: 10.1016/j.matpr.2020.04.491

[3] S. Li, "A mathematical model and numeric method for contact analysis of rolling bearings," *Mechanism, and Machine Theory*, Vol. 119, pp. 61–73, Jan. 2018, DOI: 10.1016/j.mechmachtheory.2017.08.020

[4] P. H. Jain and S. P. Bhosle, "Study of effects of radial load on vibration of bearing using time-Domain statistical parameters," in *IOP Conference Series: Materials Science and Engineering*, Vol. 1070, No. 1, p. 012130, Feb. 2021, DOI: 10.1088/1757-899x/1070/1/012130

[5] Z. Yongqi, T. Qingchang, Z. Kuo, and L. Jiangang, "Analysis of stress and strain of the rolling bearing by FEA method," in *Physics Procedia*, Vol. 24, pp. 19–24, 2012, DOI: 10.1016/j.phpro.2012.02.004

[6] D. S. Shah and V. N. Patel, "A dynamic model for vibration studies of dry and lubricated deep groove ball bearings considering local defects on races," *Measurement*, Vol. 137, pp. 535–555, Apr. 2019, DOI: 10.1016/j.measurement.2019.01.097

[7] S. S. Pachpore, M. K. Botre, A. S. Patil, and P. V. Jadhav, "Development and validation of transportation methodology by predicting dynamic behavior of container for safe transportation," in *Techno-Societal 2018*, pp. 943–953, 2020, DOI: 10.1007/978-3-030-16848-3_86

[8] C. H. Simmons, D. E. Maguire, and N. Phelps, "Bearings and applied technology," *Man. Eng. Draw.*, pp. 519–545, 2020, doi: 10.1016/b978-0-12-818482-0.00035-9.

[9] M. Yakout, "Life Prediction of Rolling Element Bearings using Vibration Modal Analysis", Thesis, Alexandria University In partial fulfillment of the requirement, 2019.

[10] X. Zhou, H. Zhang, X. Hao, X. Liao, and Q. Han, "Investigation on thermal behavior and temperature distribution of bearing inner and outer rings," *Tribology International*, Vol. 130, pp. 289–298, Feb. 2019, DOI: 10.1016/j.triboint.2018.09.031

[11] Baldomero Villa-Covarrubias, Manuel R. Piña-Monarrez, Jesús M. Barraza-Contreras, Manuel Baro-Tijerina, Stress-Based Weibull Method to Select a Ball Bearing and Determine Its Actual Reliability, Appl. Sci. 2020, 10, 8100; doi:10.3390/app10228100

[12] Dominik Bedacht, Christian Buennagel, Shafiul Monir, Ikeya Uria, Yuriy Vagapov, Numerical Investigation and Static Structural Analysis of Deep Groove Ball Bearings using ANSYS FEA, 2020 27th International Workshop on Electric Drives: MPEI Department of Electric Drives 90th Anniversary (IWED), Moscow, Russia. Jan 27 – 30, 2020. DOI: 10.1109/IWED48848.2020.9069562

[13] S. Tripathy, R. Panicker, S Shrey, R. Naik, SS. Pachpore, "Voice Controlled Upper Body Exoskeleton: A Development For Industrial Application," *International Journal of Scientific & Technology Research*, vol. 9, no. 06, pp. 1032–1037, 2020. DOI: 10.48550/arXiv.2009.08033

[14] Nandurdikar, AKASH S., ANURAJ R. Naik, S. S. Pachpore, PADMANABH A. Manurkar, and VIVEK S. Nalawade. "Design of shock absorber test rig using mechanical exciter to determine transmissibility and natural frequency." *Int. J. Res. Publ. Eng. Technol* 3, no. 3,108-111, 2017, DOI: 10.5281/zenodo.1463647

AVINASH GALANDE has done his bachelor's degree in mechanical engineering from Marathwada mitra mandal's college of engineering, Maharashtra. Currently pursuing master's degree in CAD/CAM/CAE from MITWPU, Pune, Maharashtra. His current research area includes FEA and Biomedical Healthcare Technology.

Prof. SWANAND PACHPORE, Pursuing Ph.D. (Mechanical Engineering) at MIT World peace university, Pune, India. Now he works as Assistant Professor at MITWPU. His current research interests include Knowledge Based Engineering, Biomedical Healthcare Technology (Dental Application)

Prof. ASHISH PAWAR, (M.Tech. (Mechanical Engineering(CAD/CAM)). He works as Assistant Professor at MIT World peace university. His current research interests include Recognition and Data Generation Using CAD Tools, Feature Extraction.

JENRS

Received: 28 February 2022, Revised: 23 March 2022, Accepted: 28 March 2022, Online: 12 April 2022

DOI: https://dx.doi.org/10.55708/js0104010

System Identification of FIR Filters

Sudheesh Kannur Vasudeva Rao*, Kiran, Naveen Kumar, Mahadevaswamy

Department of ECE, Vidyavardhaka College of Engineering, Mysuru, Karnataka, India-570002

*Corresponding Author: Sudheesh K V, Vidyavardhaka, 9945765761 Email: sudheesh.kv@vvce.ac.in
Corresponding Author ORCID Author 1: 0000-0001-6392-1737, ORCID Author 2: 0000-0001-5275-5067, ORCID Author 3: 0000-0001-6922-8095
ORCID Author 4: 0000-0003-4891-1236

ABSTRACT: Identification of Finite Impulse Response (FIR) filters refer to finding out the coefficients also known as the weights of its transfer function. Adaptive filtering using Least Mean Square (LMS) Algorithm is used to find the estimated weights of the transfer function, using ATMEGA16 processor. This method can be used to find the coefficients of complex resistive circuits. This is done by constantly comparing the FIR system with Adaptive filter until the difference signal is zero, both the systems are fed with same input signals.

KEYWORDS: System Identification, Finite Impulse Response Filter, Adaptive Filter, Least Mean Square Algorithm, NLMS Algorithm, RLS Algorithm.

1. Introduction

System Identification is the process of determining the attributes of the system by repetitive experimentation. Here, the system to be examined is a Finite Impulse Response (FIR) filter. If the Impulse response of a system is having finite number of coefficients such a system is called finite impulse response filter. A network consisting of only resistive components can be considered as a FIR filter having only one coefficient in its impulse response. The idea is to provide a linear model to the unknown system using adaptive filter that represents the best possible representation to the system to be identified, i.e., find the approximate weights of response (h[k]) of that particular system to impulse input[1-3]. Figure 1 shows block diagram of simple identification of system using LMS.

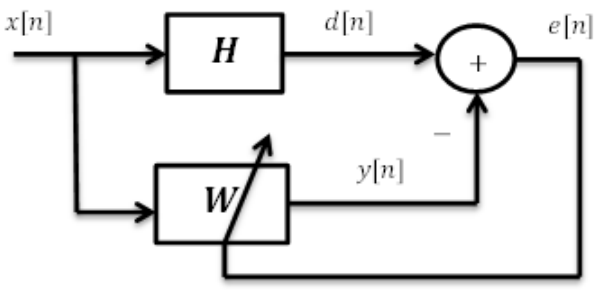

Figure 1: Generalized Block diagram of LMS algorithm used for System Identification

d[n]: Output of the system H for input signal x[n]

y[n]: Output of the Adaptive filter

e[n]: error function

2. Related Work

In [1], the author presented an identification of a system using stochastic gradient algorithm, which is known as least mean square algorithm. These filters are implemented using Digital Signal Processing (DSP), for increasing performance these are implemented using ASICs or FPGA. The main logic here is taking gradient descent for estimating a time varying signal. This will find min value and by way of taking increasing steps in negative direction of gradient. It is done in order to reduce error signal value.

Basically, using these two equations the unknown system is identified using LMS algorithm.

$$e(n) = d(n) - y(n) \quad (1)$$

$$c(n+1) = c(n) + \mu\, e(n).x(n) \quad (2)$$

where μ is the main parameter which decides the efficiency of the adaptive output signal. We should make sure to keep it to desired value so that it will converge properly. The main reason for using LMS algorithm is that it is comparatively very simple to implement in both hardware as well software as it is computationally simple and efficiently uses memory.

In [2], author proposed comparative analysis of three commonly used adaptive filtering algorithms in System identification is they are Least Mean Square (LMS), Recursive Least Square (RLS) and normalized least mean square (NLMS) algorithms. LMS is computationally simple than the other two, NLMS is its normalized form and RLS is a complex but efficient algorithm.

The LMS adaptive filter updating equations are similar to the above paper, in NLMS the major challenge in finding the appropriate value of the step size is overcome by normalizing the input and its updating equation is as shown,

$$c(n+1) = c(n) + \left(\frac{\mu}{||x(n)||^2}\right).e(n).x(n) \quad (3)$$

The RLS is a recursive algorithm which has good convergence but computationally complex moreover, it requires predefined conditions and information to update the estimation.

In [3], the author has presented the LMS algorithm which is improved by an approach called LMS-GA. The genetic searching methodology is integrated with LMS algorithm to speed the process and reduce time in this algorithm. This algorithm also preserves the simplicity of LMS algorithm, has fewer computation and has fast convergence rate. The LMS-GA algorithm out performs the basic LMS algorithm.

In [4], the author has presented a method to overcome the problem of decrease in performance when signal to interference ratio (SIR) is low this overcomes by the use of varing step size in Least mean square method. It provides a different non linear relationship between step factor and error of adaptive system. The relationship is written as represented in eq. (4). This algorithm is not sensitive to interference and has better performance when compared to the commonly used LMS algorithm when the SNR is less.

$$\mu(n) = \beta\left(\frac{1}{1+\exp(-\alpha|e(n)|)-0.5}\right) \quad (4)$$

In [5], the author has proposed an adaptive filtering method when the system is scattered. This method applies l1 relaxation, to enhance LMS type adaptive filters performances two new algorithms are introduced, they are the zero-attracting least mean square (ZA-LMS) and the reweighted zero-attracting least mean square (RZA-LMS). By combining a l1 norm penalty in the coefficients into the quadratic Least mean square cost function ZA-LMS can be obtained. To better the filtering ability further RZA-LMS is designed utilizing a re-weighted ZA, numerically RZA-LMS's performance is better than ZA-LMS. Both algorithms are compared in performance with the typical LMS algorithm which results in improved ZA-LMS and RA-LMS in comparison to the typical LMS both in steady-state performance and transient performance when the system is scattered, it also shows the reduced MSE from ZA-LMS algorithm.

In [6], the author has presented LMS algorithm with variable step size along with a functional relationship between the difference signal and step-size which is nonlinear in nature. A hop parameter (αn) is used in this algorithm to remove the disturbances of independent noise by varying the step-size. This algorithm also presents a similar method that is based on the Sigmoid function (SVSLMS) whose size of step is high although the difference signal is approximately to zero. The system formula of SVSLMS algorithm is represented in eq. (5).

$$\mu(n) = \beta\left(\frac{1}{1+exp(\alpha|e(n)|)} * 0.5\right) \quad (5)$$

The simulation results run on a Computer confirms that the method is better compared to the previous algorithms in performance, the convergence properties are better at the beginning of adaptation while establishing very less eventual miss-adjustment.

In [7], the author has proposed two new versatile adaptive calculation methods, in particular Prominent subspace least mean square (PS-LMS) and PS-LMS+. This helps for quicker estimation of unknown models, which are scattered in transfer domain. PS-LMS calculations are valuable for quick recognizable proof of varying unknown systems and furthermore enhances the union speed of standard Least mean square calculation if the system to be found is scattered and has long impulse response. To decrease the error PS-LMS+ adaptive method was introduced as shown in Figure 2. Performances of PS-LMS and PS-LMS+ algorithms are compared with typical algorithms such as LMS, RLS, PN-LMS, μ-law PN-LMS adaptive methods by conducting experiments. The outcome furnishes a quicker speed of convergence with compromise of marginally higher computational intricacy compared to typical LMS algorithm.

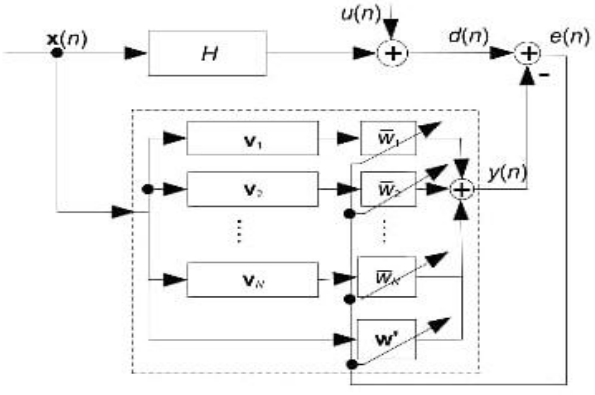

Figure 2: Realization of PS-LMS+ utilizing equal PS-LMS and LMS adaptive algorithm

In [8], the author has explained NLMS (normalized least mean square) algorithm whose behaviour is same as that of Least mean square-SAS algorithm. In NLMS algorithm the gradient estimation error is used, which will be present in normal adaptive process, this acts as perturbing noise. NLMS algorithm is easy and simple, which increases the computational speed in comparison to LMS algorithm which has comparatively small step size. In LMS-SAS Edmonson uses estimated gradient vector for finding perturbing noise. Author has shown that NLMS is better when compared to LMS-SAS algorithm. And

efficiency is greater compare to GLMS algorithm because it does not require any cooling schedule.

In [9], the author has compared different methods to find the unknown system and other distinct PI controllers are developed to identify response of system. To identify the existence of different model parameters several system identification models are utilized and accuracy of the model is most vital step to design efficiently. The states of the linear system can be estimated using the Kalman filter (KF), it comprises of two major steps first prediction step and then correction steps. Non-linearity in the state space model can be seen as a result of extension and Extended Kalman Filter (EKF) is used for this identification, which is shown in Figure 3. Parameters of the system and its internal states can be estimated efficiently using extended Kalman filter.

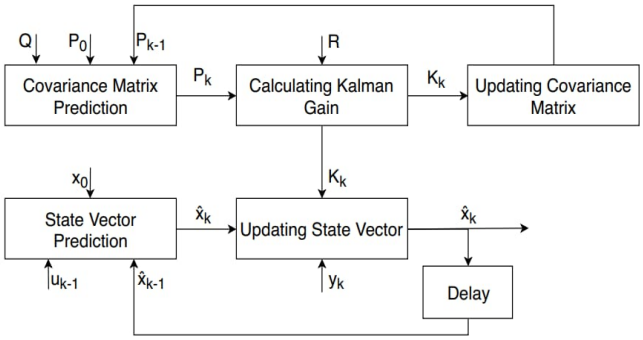

Figure 3: Typical EKF algorithm block diagram

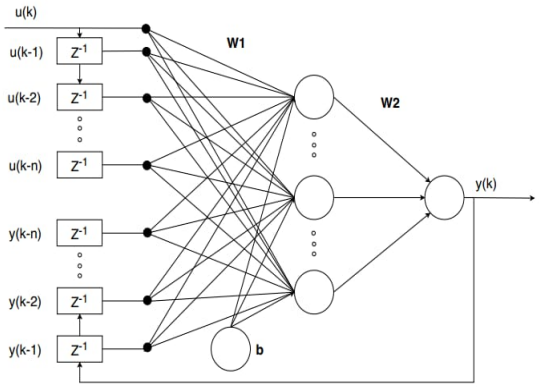

Figure 4: NARX neural network's typical block diagram

Nonlinear Autoregressive Exogenous Model (NARX) is a multi-layer recurrent perceptron neural system network, which can be utilized as a black-box identifying technique. Both parallel and series-parallel architecture can be seen in NARX. The simple block diagram is shown in Figure 4. The major benefit of this estimation method is that, it is not necessary to have information about the system to be found and it is effective for both linear and nonlinear systems. A high convergence rate can be obtained in all the other methods other than the LMS. The MSE comparison between LMS and NARX gives mid accuracy in comparison to RLS and EKF. Highest precision can be realized using EKF but this result in increase in cost and complexity.

In [10], the author has proposed a simple way of using adaptive IIR filter in system identification. The improved genetic search approach of Least Mean Square (LMS) algorithm that is Least Mean Square-Genetic Algorithm (LMS-GA) helps in searching the multi-model error surface of the IIR filter. This helps in avoiding local minima and in finding the optimal weight vector. Genetic Algorithm (GA) is an optimization approach used in applications of vast, nonlinear and potentially discrete systems. In GA, a population of strings called chromosomes which represent the candidate solutions to an optimization problem is evolved to a better population. GA as the maximization of fitness function is given by,

$$F(t) = \frac{1}{1+f(t)} \quad (6)$$

here the cost function to be minimized is represented as f(t). The cost function f(t) is taken as the Mean Square Error (MSE) in adaptive filtering which is given by

$$f(t) = \varepsilon_{j^2} = \frac{1}{t_e}\sum_{i=1}^{t_e}[d(n) - y_j(n)]^2 \quad (7)$$

here t_e represents the size of window along which errors are accumulated and y_j (n) is the estimated output for the jth set of estimated parameters. Graph of MSE versus Iterations is shown in below Figure 5.

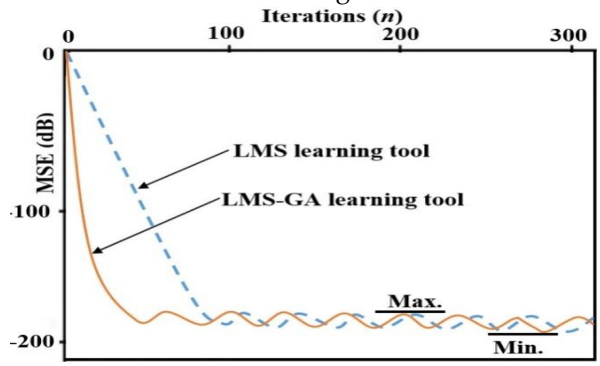

Figure 5: The LMS-GA convergence performance for adaptive IIR filter.

To understand parameters of the digital filters (FIR and IIR) and to minimize error signal the adaptive algorithms LMS and LMS-GA are adopted. The characteristics and the simplicity of the standard LMS learning algorithm can be preserved with comparatively fewer computations and fast convergence rate using LMS-GA algorithm [11-15].

3. Methodology

The methodology of the system is demonstrated in Figure 6. The unknown FIR system to be recognized and the adaptive system both are fed with the same input signal. For the input a White noise generator is used which generates white noise signal.

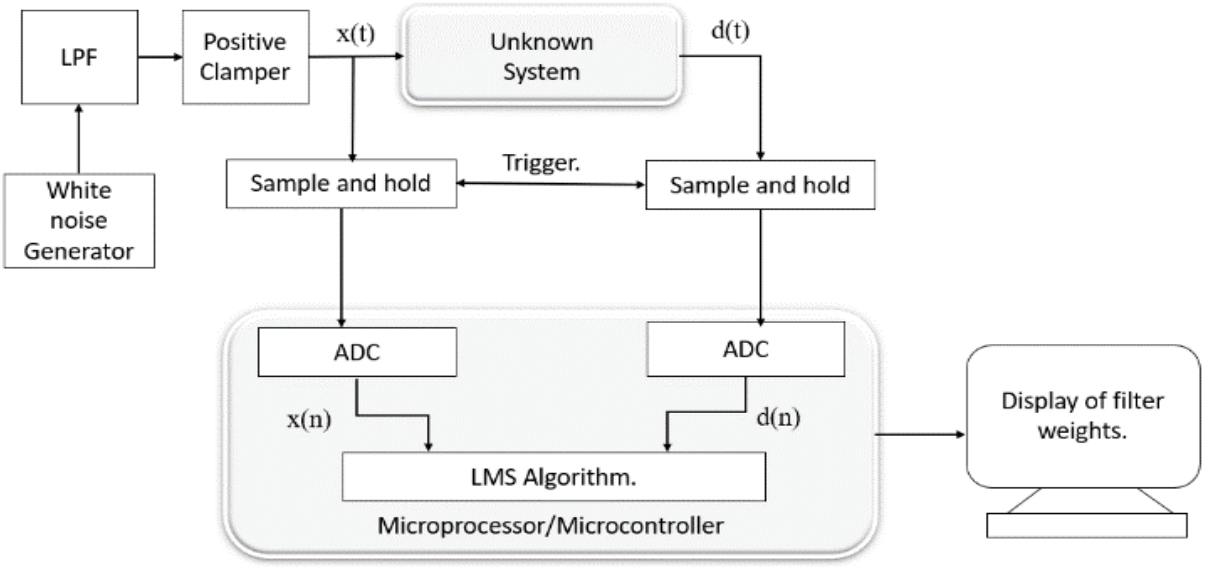

Figure 6: Block Diagram representation of system identification.

This is passed to a low pass filter to attenuate higher frequencies as the speed of the sampling in the ATMEGA16 is limited. Then, this signal clamped using a clamper circuit to eliminate negative components in the signal. Since the applied signal is Analog and the adaptive filter used is a digital filter, the input signal that is fed to the adaptive filter and the output from the unknown FIR filter must be passed through a Sample and hold circuit. Both the sampling processes should be triggered simultaneously. The output from both the FIR system and the adaptive filter is compared to obtain the difference signal. This difference signal is basis for further calculations. This error signal is used update the adaptive filter coefficients. This process continues until the difference between the signals is negligible. The entire process of the LMS algorithm is implemented in the ATMEGA16 processor. Then the output coefficients i.e., the impulse response coefficients of the FIR filter are displayed on the screen using Putty.

3.1 ATMEGA16 Interconnection

Microcontroller is the most important component of this system. Here, we have used ATMEGA16 as our microcontroller and its interconnections and pins used for this system are shown in Figure 7.

3.2 Work contribution and Working of LMS Algorithm

As discussed earlier the adaptive filtering algorithm adopted is LMS. The working of LMS code in the ATMEGA16 is as shown in the flowchart Figure 8. The steps involved are:

- Read the values, one from the input given to the unknown system into the ADC channel0 further stores it into x[i] and another from output of the unknown system into the ADC channel1 and store it in the variable d.

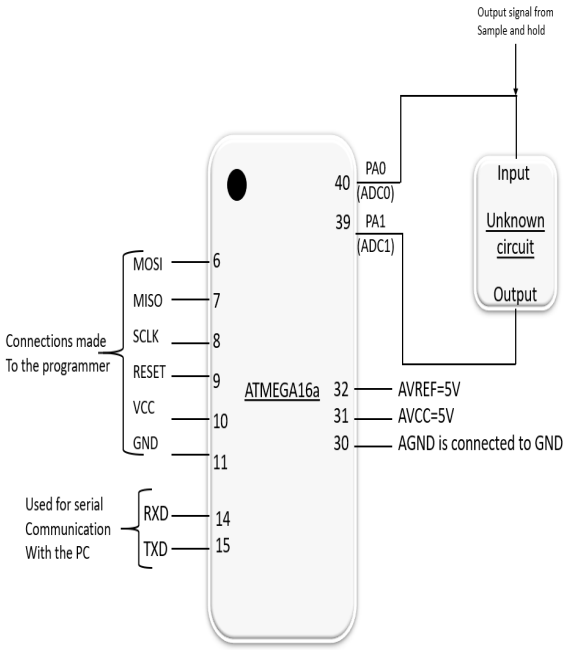

Figure 7: Interconnection of ATMEGA16a

- Assume A[i]=x[i], where a[i] as the input to adaptive filter.
- find the adaptive filter output 'y' using formula in (8)

$$y = y + (A[i] * W[i]) \quad (8)$$

- Calculate error using (9) and update the coefficients of the filter using (10).

$$e[n] = d[n] - y[n] \quad (9)$$

$$W[n+1] = W[k] + (\mu * x[n] * e[n]) \quad (10)$$

- Check if error is less than 0.001, if yes display the coefficients of the unknown undefined system

and stops the method else repeat the similar process until the condition is satisfied.

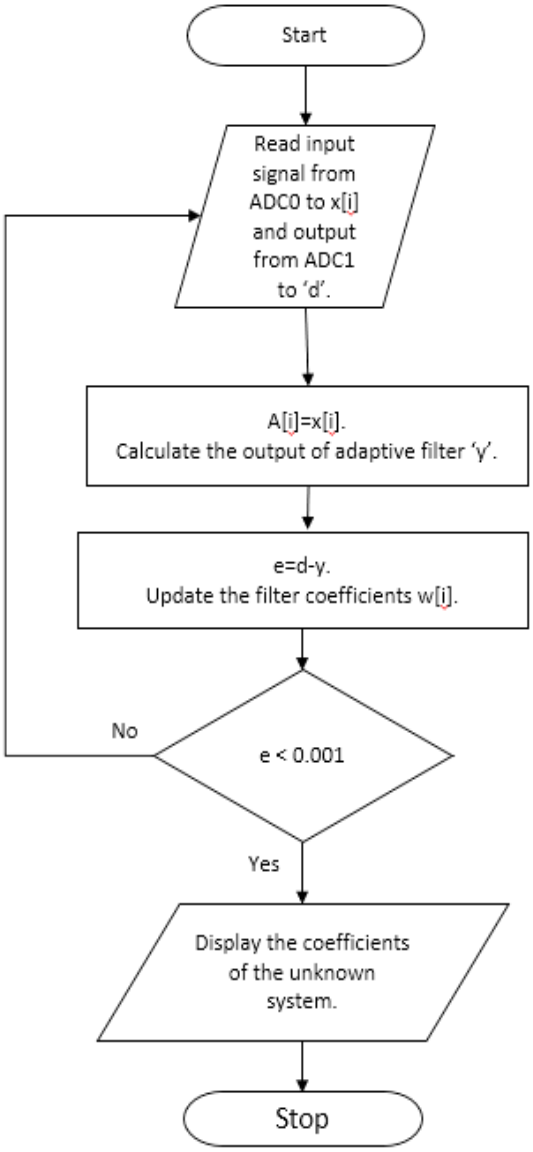

Figure 8: Flowchart of LMS Algorithm

4. Results

The FIR circuit is tested with resistive circuit. The output obtained was reduced to half. This half value will be the filter coefficient (weights). Below shows the Figure 9 of simple FIR resistive circuit with same resistor value.

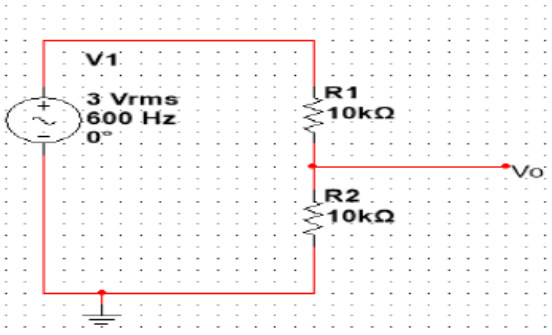

Figure 9: Series Resistive Circuit with same resistor value

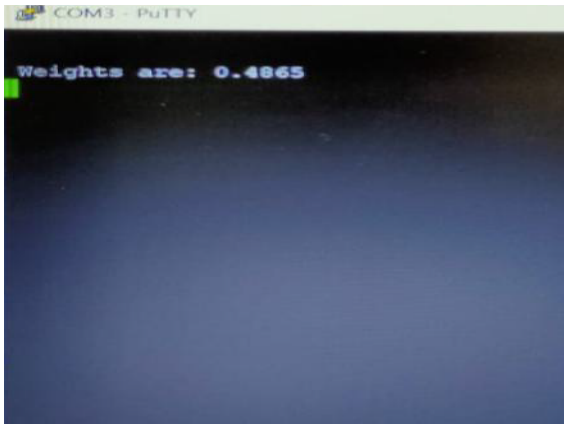

Figure 10: Result of Series same Resistive Circuit

Using puTTy the output was read from TTL converter. The weighted value is approximately equal to 0.5 is as shown in Figure 10.

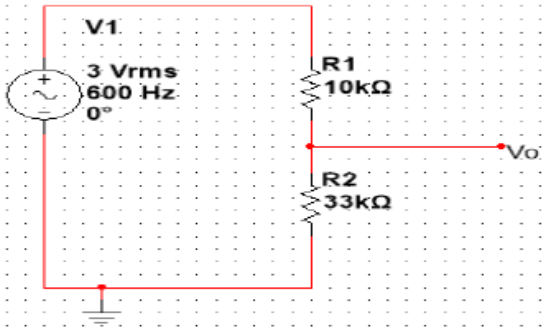

Figure 11: Series Resistive Circuit with different resistor value

Figure 12: Result of Series Different Resistive Circuit

To understand parameters of the digital filters (FIR and IIR) and to minimize error signal the adaptive algorithms LMS and LMS-GA are adopted. The characteristics and the simplicity of the standard LMS learning algorithm can be preserved with comparatively fewer computations and fast convergence rate using LMS-GA algorithm. The model is also determined for different FIR circuit and verified for accurate results. Figure 11 shows the two resistive circuit having different value. LMS adaptive filtering algorithm is implemented but it is not most accurate. In order to overcome this, different adaptive techniques of filtering can be realized. NLMS algorithm in which the input is normalized, LMS-GA which uses a genetic search approach, LMS with varying step size and other such algorithms have been developed. The obtained

results were approximately equal to 0.76 as shown in Figure 12. For more accurate results we need to use RLS. But RLS is computationally complex and the estimate is more accurate to the unknown system. The performance comparison of LMS, NLMS and RLS is tabulated in Table 1.

Table 1: Performance Comparison of LMS, NLMS & RLS Algorithms

Algorithm	MSE	Complexity	Stability
LMS	1.5*10-2	2N+1	Less Stable
NLMS	9.0*10-3	3N+1	Stable
RLS	6.2*10-3	4N2	More Stable
N : Order of the Filter			

5. Conclusion

The Adaptive scheme is used to understand the FIR filters parameters, which is the weights of unknown undefined system. There are many adaptive techniques which are realized to determine the unknown function. The simpler way for understanding and configurable for hardware and software is LMS algorithm. But for higher input accuracy and performance is very hard to predict. In order to overcome this problem many other algorithms are used such as NLMS, RLS, LMS-GA. Hence the choice of algorithm can be made based on the application, for example for an application involving the estimate to be highly accurate with cost and computationally complexity not being an issue RLS algorithm can be used, but for applications where approximate result is sufficient keeping the complexity simple then LMS algorithm is preferred. Therefore, for laboratory application where the accuracy is not an issue but requires simplicity in the LMS algorithm is used.

6. References

[1] I. Dorean, M. Topa, B. Sandor Kirei, E. Szopos, "Interdisciplinarity in Engineering" *Scientific International Conference*, TG.MURES – ROMÂNIA, 15-16 November 2007.

[2] S. A. Ghauri, M. F. Sohail, "System identification using LMS, NLMS and RLS," *2013 IEEE Student Conference on Research and Developement*, 2013, pp. 65-69, doi: 10.1109/SCOReD.2013.7002542.

[3] Ibraheem, I. Kasim. "Adaptive System Identification Using LMS Algorithm Integrated with Evolutionary Computation." arXiv preprint arXiv: 1806.01782 (2018).

[4] T. Jia, Z. J. shu, W. Jie, "An Improved Variable Step Size LMS Adaptive Filtering Algorithm and Its Analysis," *2006 International Conference on Communication Technology*, 2006, pp. 1-4, doi: 10.1109/ICCT.2006.341916.

[5] Y. Chen, Y. Gu and A. O. Hero, "Sparse LMS for system identification," *2009 IEEE International Conference on Acoustics, Speech and Signal Processing*, 2009, pp. 3125-3128, doi: 10.1109/ICASSP.2009.4960286.

[6] Q. Yan-Bin, M. Fan-Gang and G. Lei, "A New Variable Step Size LMS Adaptive Filtering Algorithm," *2007 IEEE International Symposium on Industrial Electronics*, 2007, pp. 1601-1605, doi: 10.1109/ISIE.2007.4374843.

[7] R. Yu, Y. Song and S. Rahardja, "LMS in prominent system subspace for fast system identification," *2012 IEEE Statistical Signal Processing Workshop (SSP)*, 2012, pp. 209-212, doi: 10.1109/SSP.2012.6319662.

[8] C. Lai, "NLMS algorithm with decreasing step size for adaptive IIR filters," *Signal Processing*, Volume 82, Issue 10, October 2002, pp. 1305–1316, https://doi.org/10.1016/S0165-1684(02)00275-X.

[9] G. Akgün, H. u. Hasan Khan, M. Hebaish and D. Gohringer, "System Identification using LMS, RLS, EKF and Neural Network," *2019 IEEE International Conference on Vehicular Electronics and Safety (ICVES)*, 2019, pp. 1-6, doi: 10.1109/ICVES.2019.8906339.

[10] I. K. Ibraheem, Adaptive IIR and FIR Filtering using Evolutionary LMS Algorithm in View of System Identification, *International Journal of Computer Applications* (0975 – 8887), Volume 182 – No. 11, August 2018.

[11] S. C. Douglas, "Analysis of the multiple-error and block least-mean-square adaptive algorithms," *in IEEE Transactions on Circuits and Systems II: Analog and Digital Signal Processing*, vol. 42, no. 2, pp. 92-101, Feb. 1995, doi: 10.1109/82.365348.

[12] G. Ryu, D. Kim, J. Choe, D. Kim, H. Bae, "Adaptive system identification using fuzzy inference based LMS algorithm," *Proceedings of Third International Conference on Signal Processing (ICSP'96)*, 1996, pp. 587-590 vol.1, doi: 10.1109/ICSIGP.1996.567332.

[13] E. Szopos, M. Topa, N. Toma, "System identification with adaptive algorithms," *2005 IEEE 7th CAS Symposium on Emerging Technologies: Circuits and Systems for 4G Mobile Wireless Communications*, 2005, pp. 64-67, doi: 10.1109/EMRTW.2005.195681.

[14] M. Nakamoto, N. Shimizu, T. Yamamoto, "A system identification approach for design of IIR digital filters," *IECON 2013 - 39th Annual Conference of the IEEE Industrial Electronics Society*, 2013, pp. 2360-2365, doi: 10.1109/IECON.2013.6699500.

[15] Archana Sarangi, S. K. Sarangi, Siba Prasada Panigrahi, "An approach to identification of unknown IIR systems using crossover cat swarm optimization," *Perspectives in Science*, Volume 8, 2016, Pages 301-303, https://doi.org/10.1016/j.pisc.2016.04.059.

Dr. Sudheesh K V, has received the B. E in Electronics and Communication Engineering and M. Tech in Digital Electronics and Communication from Visvesvaraya Technological University, Belagavi, INDIA. He has received Ph.D. degree in the field of Image Processing from the Visvesvaraya Technological University, Belagavi, INDIA. He is currently working as an Associate Professor in Electronics and Communication Engineering Department, Vidyavardhaka College of Engineering, Mysuru, INDIA.
His research interests include Pattern Recognition, Image Processing, Signal Processing, Machine Learning and Brain Abnormality Detection. He has published 10 technical papers in international journals and conferences. He serves as a reviewer for several international conferences.

Kiran is working as Assistant Professor in department of Electronics and Communication engineering at Vidyavardhaka college of Engineering, Mysuru, Karnataka, India. Kiran received his M. Tech in Digital Electronics and Communication Systems at Malnad College of Engineering - Hassan affiliated to Visvesvaraya Technological University, Belgaum, Karnataka, India. He is currently pursuing his Ph. D at Visvesvaraya Technological University, Belgaum, Karnataka, India. His research interests are related to Human Computer Interaction and medical Image security. He has published several research papers at national and international journals, conference proceedings.

Dr. Naveen Kumar H N, has received the B. E in Electronics and Communication Engineering and M. Tech in Digital Electronics and Communication from Visvesvaraya Technological University, Belagavi, INDIA. He has received Ph.D. degree in the field of Image Processing from the Visvesvaraya Technological University, Belagavi, INDIA. He is currently working as an Associate Professor in Electronics and Communication Engineering Department, Vidyavardhaka College of Engineering, Mysuru, INDIA.
His research interests include Pattern Recognition, Image Processing, Signal Processing, Automatic Facial Expression Recognition and Machine Learning. He has published 8 technical papers in international journals and conferences. He serves as a reviewer for several international conferences.

Dr. Mahadevaswamy, has received the B. E in Electronics and Communication Engineering and M. Tech in Digital Signal Processing from Visvesvaraya Technological University, Belagavi, INDIA. He has received Ph.D. degree in the field of Speech Processing from the Visvesvaraya Technological University, Belagavi, INDIA. He is currently working as an Associate Professor in Electronics and Communication Engineering Department, Vidyavardhaka College of Engineering, Mysuru, INDIA.
His research interests include Pattern Recognition, Speech Processing and Signal Processing. He has published 10 technical papers in international journals and conferences. He serves as a reviewer for several international conferences.

JENRS

Received: 20 February 2022, Revised: 12 March 2022, Accepted: 13 March 2022, Online: 12 April 2022

DOI: https://dx.doi.org/10.55708/js0104011

Methodology for Learning Mathematics Based on Collaborative Work with the Support of ICT Tools and Virtual Environments of the UCN Campus

Carlos Esteban Huerta Briones *

North Catholic University, Department of Mathematics, Antofagasta, 1240000, Chile

*Corresponding author: Carlos Esteban Huerta Briones, Piedras Negras 9557, 968369367 & chuerta@ucn.cl
Corresponding author ORCID: 0000-0002-1825-0097

ABSTRACT: The article indicated basically showed the autonomous collaborative work of the students and no direct reference was made regarding the work in remote classroom, this time what is presented is a methodology of direct work of the teacher with the students during the teaching sessions, which last 60 minutes in times of pandemic, which allowed to establish more solid bases for both direct and indirect work of students from the point of view of their learning. The lecture sessions were developed following the following scheme: Active-participatory class, Collaborative Activity with the support of the teacher and Assistantship would complete. Regarding the evaluations and qualifications, these were carried out considering processes of direct feedback to the groups formed as indicated in. The evaluations were carried out through the Moodle-based platform of the UCN Virtual Campus, which considered, multiple choice questions, short answer and a development exercise.

KEYWORDS: Training process, evaluation, feedback, collaborative learning, mathematics

1. Introduction

The work that is presented incorporates actions and activities for the learning of mathematics of first-year students of the university, within which is developed in the article "Methodologies of collaborative learning and peer evaluation in virtual educational environments"[1].

The continuation of the pandemic forces all teachers to implement adaptations and improvements in learning strategies during distance classes, even more than studies show, according to [2]. Students conceive that teacher are not prepared for the virtual context in which classes take place, they perceive activities as tasks that accumulate; adding to this a poor communicative quality, either by the connectivity or by the form of expression of both actors [3]. Regarding the participation of students during distance classes, this is very scarce to say nothing, only some of them participate or consult with monosyllables through chat, rarely a student participates through their microphone. In any case for students, intervening directly in this type of classes is equivalent to going out to the blackboard in a face-to-face class. By virtue of the above is that we implemented a modality of classes that achieved a better participation by the students, in fact, the students were grateful to be able to develop exercises immediately during the classes and thus also for the implementation of the feedback processes of the applied evaluations. It is important to note that the subject where this model was applied was the subject of Calculus.

I for students recently entered the university to careers in Engineering. 2 parallels were formed with 35 and 37 students respectively, so it was necessary to train and guide in the work to be done to the second teacher who taught the indicated subject, in this sense it was important to have previously elaborated a didactic planning of the subject. The topics that were worked on in this symbol were: Inequations, Conics, functions and differential calculus.

2. Ease of Use Applied methodology model

To improve the participation of the students it was important to show examples and propose related exercises to be developed by them with the support of the teacher and end with an assistantship work that in the training process sought to consolidate what was developed during the recently finished class.

For the subject of assistantships, we had the support of the academic success program that the university has, they assigned us two assistants as tutors, one for each parallel, who worked with the students in the third block of 30 minutes and supported the autonomous collaborative work of the students following the guidelines indicated in the aforementioned article.

Coordination meetings were held between teachers and assistants, in order to properly guide the work to be done and specify what their role was in this new way of working. They were provided with the guides for collaborative work and didactic planning, in which the links to be used are found.

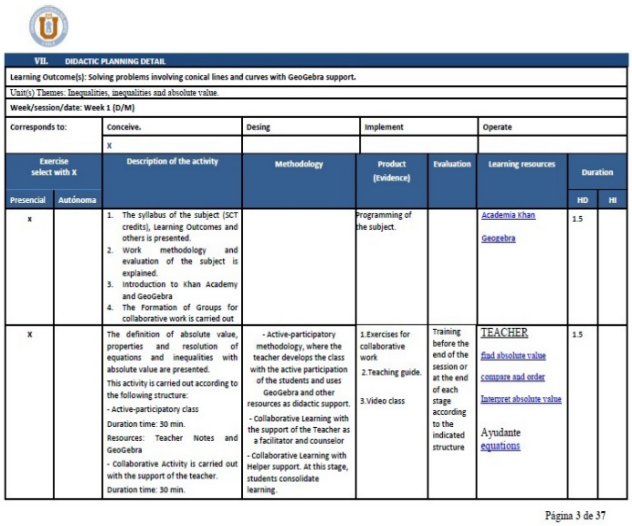

VII. DIDACTIC PLANNING DETAIL

Learning Outcome(s): Solving problems involving conical lines and curves with GeoGebra support.

Unit(s) Themes. Inequalities, inequalities and absolute value.

Week/session/date: Week 1 (D/M)

Corresponds to:		Conceive.	Desing	Implement		Operate		
		x						
Exercise select with X		Description of the activity	Methodology	Product (Evidence)	Evaluation	Learning resources	Duration	
Presencial	Autónoma						HD	HI
x		1. The syllabus of the subject (SCT credits), Learning Outcomes and others is presented. 2. Work methodology and evaluation of the subject is explained. 3. Introduction to Khan Academy and GeoGebra 4. The Formation of Groups for collaborative work is carried out		Programming of the subject.		Academia Khan Geogebra	1.5	
x		The definition of absolute value, properties and resolution of equations and inequalities with absolute value are presented. This activity is carried out according to the following structure: - Active-participatory class Duration time: 30 min. Resources: Teacher Notes and GeoGebra - Collaborative Activity is carried out with the support of the teacher. Duration time: 30 min.	- Active-participatory methodology, where the teacher develops the class with the active participation of the students and uses GeoGebra and other resources as didactic support. - Collaborative Learning with the support of the Teacher as a facilitator and counselor - Collaborative Learning with Helper support. At this stage, students consolidate learning.	1.Exercises for collaborative work 2.Teaching guide. 3.Video class	Training before the end of the session or at the end of each stage according to the indicated structure	TEACHER find absolute value compare and order Interpret absolute value Ayudante equations	1.5	

Página 3 de 37

Figure 1: Partial view Didactic Planning

It is valid to note that in the traditional model of face-to-face classes and the current program of the subject contemplates 2 sessions of chair and a session of assistantship, regarding the assistantship both in the face-to-face and at a distance, finally the teacher ends up doing all the exercises and the effect on the student in terms of learning is ineffective and the role of the students is passive, which goes in the opposite direction to the guidelines declared in the institutional educational project.

On this occasion we carried out the 3 sessions as a chair with the exception that the last 30 minutes were dedicated to an assistantship, this fact was key to the consolidation of the students' learning, since they immediately reinforced what was developed during the chair.

This class model was developed according to the following 3 stages:

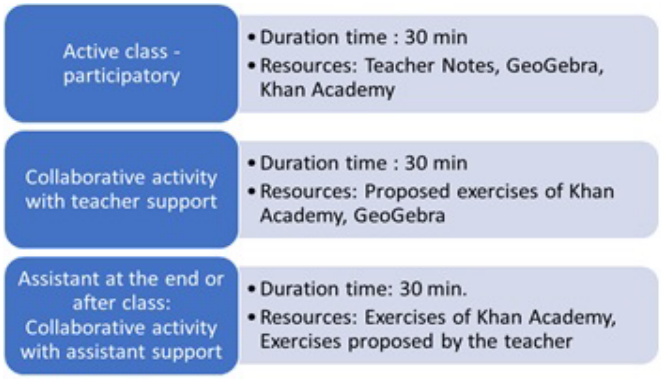

Figure 2: Session Structure

3. Evaluation process

The evaluation of the learning process has always been a complex process [4], above all, because it has a very relevant influence on the quality of the process. If we do not evaluate correctly, learning will not be of quality and we will have lost a lot of time and resources to not achieve the main objective of such learning [5].

The above makes note how complex the evaluation process is in general and particularly in online modality classes, in this regard several questions arise in relation to who is really answering the evaluation, there is no control during this process, in addition to the fact that there is a large number of applications that solve the mathematics exercises with enough details.

Along with the rest, it must be considered that online evaluation processes, unless developments are requested, in questions of alternatives only final results are requested, which does not allow evaluating the development processes that students carry out to reach the final result.

In conclusion, it is not possible to identify precisely what the student really knows and what mathematical skills, in this case, he handles with a reasonable capacity.

In response to the above, we implemented an evaluation process that would identify the achievement of students' learning, as indicated in the program of the subject, among others the following are defined:

- Solve problems involving conical lines and curves with the support of GeoGebra.
- Determine bijectivity and its implications in a real variable function.
- Calculate limits of real functions involving indeterminate forms.
- Determine continuity of real functions in a variable.
- Calculate the derivative of real functions in a variable.
- Interpret the derivative in physical and geometric problems.
- Interpret the graph of real functions in a variable with the support of GeoGebra.
- Solve problems of optimizing real functions in a variable.

The work and creativity to elaborate questions that evidence the achievement of the learning, turns out to be an arduous and very extensive work in the elaboration of this type of questions. That is why we chose to carry out a process of presentations that would allow the students to show how they arrived at the results they marked as a correct alternative in this type of questions.

The general idea was to show what the students really knew, the truth that we could only incorporate development questions, however, the interest of insisting on this type of questions, was the feedback process that was generated in the instances of questions and answers

when the students had to expose and thus justify their choices.

This instance allowed the student to identify their errors and thus be able to correct them, in a large case and I would say that it was very recurrent the fact that the students marked the alternative that was closest to the result that they reach when developing the exercise, without clearly identifying which was the error that did not lead to the correct answer, well this instance allowed them to correct and receive from the teacher the corresponding feedback.

This process was framed in the evaluation as an instance for learning and that was very well received by the students, stating that it allowed them to improve and learn from their own mistakes.

For each evaluation, a set of different questions was elaborated that measured the same thing, that is, batteries of questions of the same type were made that appeared randomly for different students.

Below are images of some questions elaborated and considered in summative assessments.

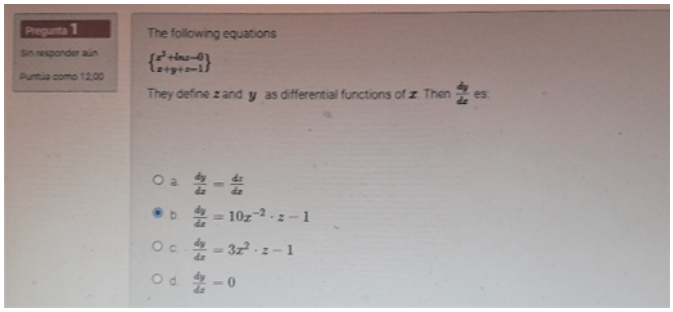

(a)

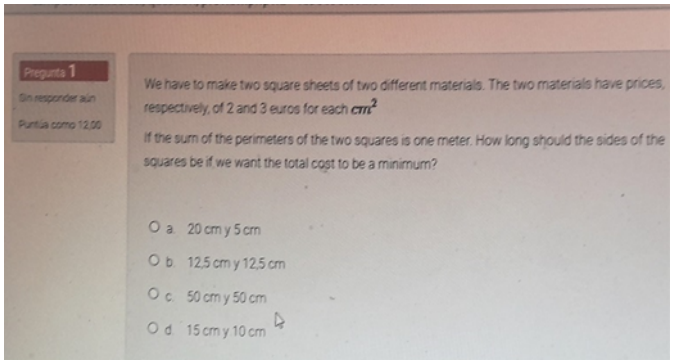

(b)

Figure 2. (a) Single choice question (b) Context question

4. ICT tools and virtual environments of the UCN campus

In the reflection of Ortega and Casillas "Critical perspective of the impact of ICT in the educational context"[6], a different perspective of the use of ICT is addressed by questioning the real impact that technology has had in the educational field. By dismantling some myths created around the use of these technologies, the authors lead us to the understanding that ICTs are not by themselves the infallible solution to all kinds of problems.

Specifically, in the field of education, they show how it is not possible to place all hopes in technologies to solve educational problems. They claim that technological instruments alone will not improve work within the classroom; a greater effort is required that considers training and content aspects that involve the participants. According to the reflection, it is true that the use of ICT does not generate learning by itself, but that the appropriate, strategic use and how it is used contributes to the understanding of students during the teaching sessions that are taught. Now, in the times of pandemic that we are living, we were forced to use ICT in the training process of students. In our case, the use of GeoGebra contributed significantly in the understanding of the topics discussed, for example, the following problem was developed in the unit of Conics:

"Determine the equation of the circumference passing through the center of the conic $x^2 + y^2 - 2x - 2y + 1 = 0$ and its center is in the center of the parabola $x^2 = 8y$."

In face-to-face classes this type of exercises for students implied a greater complexity when solving them and generally they could not finish it, in fact, when this exercise was proposed to current students, they could not do it algebraically, however, by making the graphs with GeoGebra they could better analyze the exercise and managed to solve it. The fact of having the graphic resource facilitated the analysis and passage from an abstract context to a friendlier context, where they were allowed to see more clearly the way to find the solution.

Notwithstanding the above, the teachers also developed the exercise analytically in such a way that the students had both forms of solution. In any case, the final reflection of the students is that the exercise was simpler than it seemed. In this sense, graphic mathematics contributes to the understanding of the topics to be discussed.

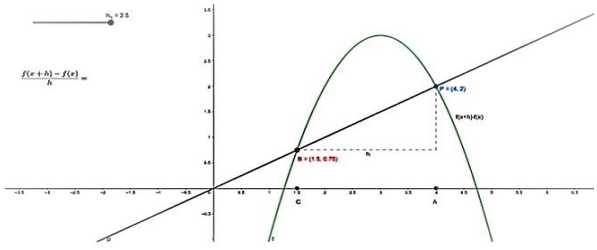

Figure 3. Geometric interpretation of the derivative with GeoGebra

Another classic and important topic of differential calculus is the geometric interpretation of the derivative, to present this topic the teachers elaborated in GeoGebra an interactive activity that allowed the students to intervene modifying parameters and thus visualize the

geometric meaning of the derivative relating it to the delivered definition of the derivative [7].

The new virtual platform based on Moodle that was implemented at the university was a great contribution to the application of evaluations and their respective correction in the case of development exercises. Important, in addition, the writing in latex for the language of mathematics, facilitated the teaching work and improved the means of communication with the students, in this platform all the links of Khan Academic that were used in each class were uploaded.

Interactive activities were incorporated for student support, as well as all recorded classes [8].

Figure 4. Classes recorded on UCN virtual platform

In respect of Khan Academic, of this platform, the proposed exercises that they have in each topic that the subject required were used. The exercises were selected according to the need to carry out practices immediately during the class of chair and during the collaborative work carried out by the teacher and by the assistant, all these links, as already mentioned, were incorporated into the didactic planning of the subject. Another important contribution of this platform is that, if a student makes a mistake in an exercise, it offers help with specific indications or with an explanatory video associated with the topic being evaluated [9].

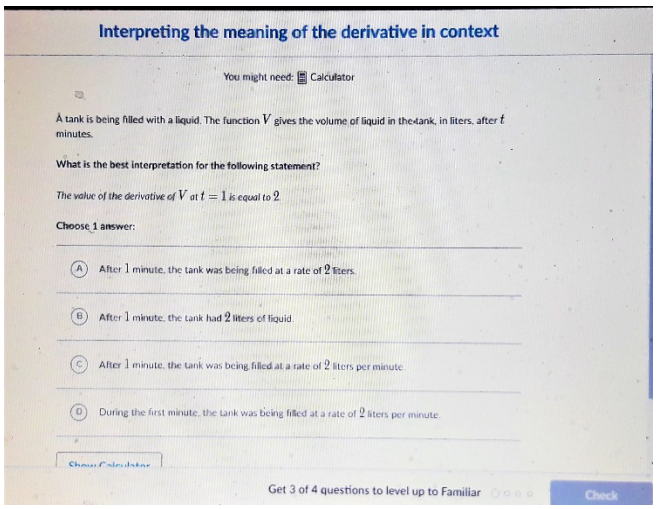

Figure 5. Context question Khan Academic

5. Results

5.1. Closing survey

To know the opinion regarding the innovation implemented in the subject of calculus I, a mixed type questionnaire was developed with closed and open questions, addressing the following areas in its elaboration: the first of them considering the time of dedication to the subject, a second area of general perception of the methodology, a third aspect regarding the disposition to study in the subject and finally an evaluation of the activities developed during the semester.

Closed questions were asked through Five-level Likert scales and 10-level semantic differential.

The survey was carried out through a Google form and applied once the subject was finished, for this the questionnaire was shared on the virtual campus platform of the University.

5.1.1. Time of dedication to the subject

According to the answers of the group of students, they dedicate between 9 and 5 hours a week to the signature, mentioned that only 3% of them dedicate 9 hours, being the lowest percentage of voting. On the other hand, 83% of the sample dedicates between 5, 6 and 7 hours, which translates into 31% who dedicate 5 hours, 28% who dedicate 6 hours and 24% who dedicate 7 hours, which according to what is defined in the subject.

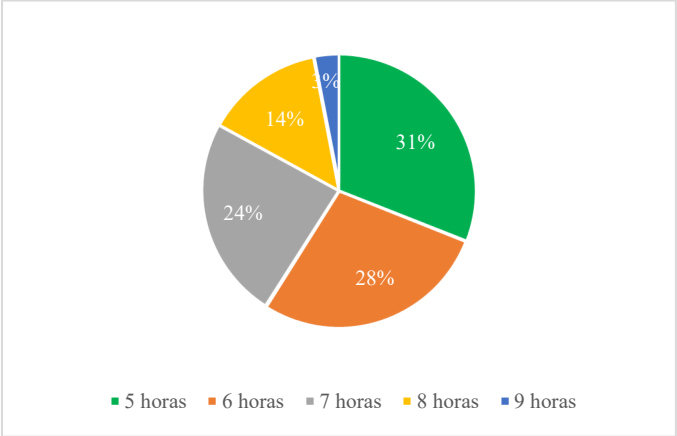

Figure 6. Graph of Dedication to the subject

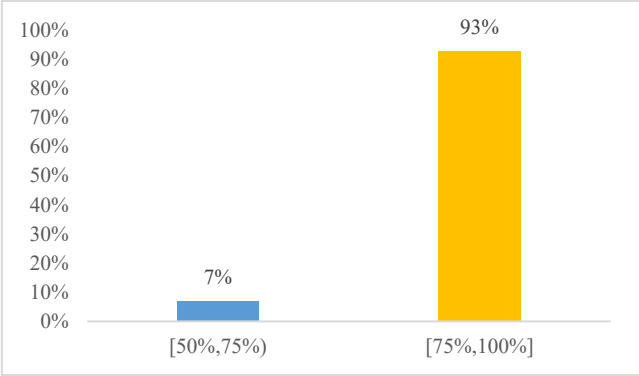

Figure 7. Attendance graph

5.1.2. Attendance Percentage

Of the total number of students who responded to the survey, 93% of them declare to attend classes in an average attendance of 75% to 100% while in a smaller percentage with 7% it does between 50% and 75%.

5.1.3 Evaluation of collaborative work

In relation to the learning experience in the subject, a 4-level assessment scale is proposed, describing whether this experience was a good, very good, regular or bad experience, resulting in 34% of them considering it very good, while 45% rated it at a "good" level, only 21% as regular and none of them as a "bad" experience. That is, 79% of them generated a positive evaluation of the learning experience.

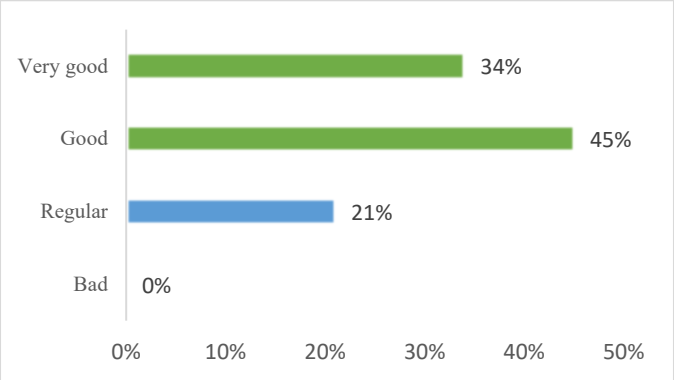

Figure 8. Collaborative work evaluation chart

Then a numerical assessment of the experience is requested, considering a scale of 1 to 10 points, 31% of them rate it with 10, 28% with 9, 10% with 8, 17% with 7, 10% with 6 and 4% of the answers with a rating of 4 points. Considering the scores greater than or equal to 7, 86% of the answers are located, while only 14% of the answers do so with a score of 6 and 4 points.

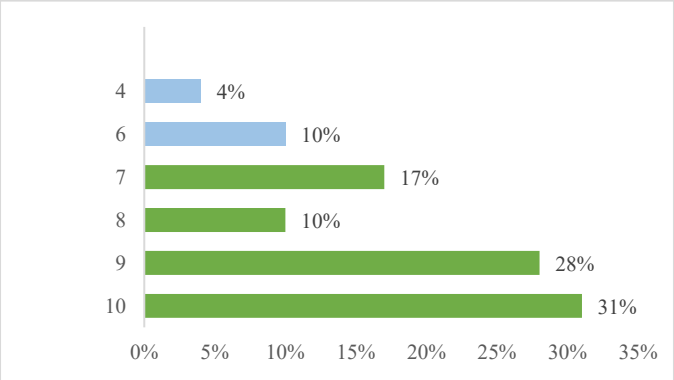

Figure 9. Numerical valuation graph

When consulting regarding the reasons for the score, they comment on different factors regarding the assessment, among them they mention some problems associated with the coordination and equity of the work between students, as well as mention positive aspects of the score mentioning that there are academic benefits, collaboration in learning, time organization, a good relationship with the teacher and a good use of the platform Khan Academy.

5.1.4 Arguments mentioned by the students

Communication problems between students

- Lack of communication with the group
- My group never attended classes
- Lack of notice, that surveys influence grades

Equity and coordination of work

- Equitable, to the point that a guide could be done only by me.
- Since there was not much group work on the part of my team except for some group mates.
- It's hard to work with people you've never worked with before
- As such it is not a bad idea to work that way in a group, but even so you do not work in an "intense" way, the fact that everything is online is a complicated issue to carry and whether we want or not that hinders the work on the part of the students as on the part of the teachers.
- It all depends on the people who touch you in the group
- In theory the collaborative work methodology is good, but in the implementation, there are details that are not always ideal. Such as the fact that not everyone participates, or that there are delays in the delivery of tasks.
- It always depends on the group members the experience in general
- There are times when teamwork was not

Academic benefits

- I had classmates who explained to me when I did not understand some exercises, they were orderly and, on the exercise, guides I find that their contents were complete and useful.
- At first, I had a hard time working with my group, but once organized, it was quite a good experience and we were productive according to the group work plan proposed by the teacher.
- Having a group with which to do work and help each other in case we have doubts has helped me a lot.
- Because I feel that it is somewhat easier to work as a team and share your knowledge and help each other.
- The collaborative work was a different way of being able to understand the subject since there are colleagues who help each other, in addition to allowing them to study before a test.
- I find that it helps too much when it comes to studying, the assigned classmates fulfilled their tasks, plus there was a fairly fluid communication.
- The teacher answers all the doubts that appear and, in my group, we work very well and collaborate all.

Relationship with the teacher

- The teacher is very good

I like the result obtained I thought the result obtained

- Was very decent

Complications

- Good methodologies employed, however, with some complications in the course.

Use of platform

- Because it was possible to understand the subjects and practice of methods through Khan Academy

5.1.5. Learning perception

As for the self-assessment of the learning, the lowest response scores are found in the item associated with the previous learning of the subject, while the highest of the scores is assigned to the item associated with each teacher in charge, obtaining a score of 4.1 points.

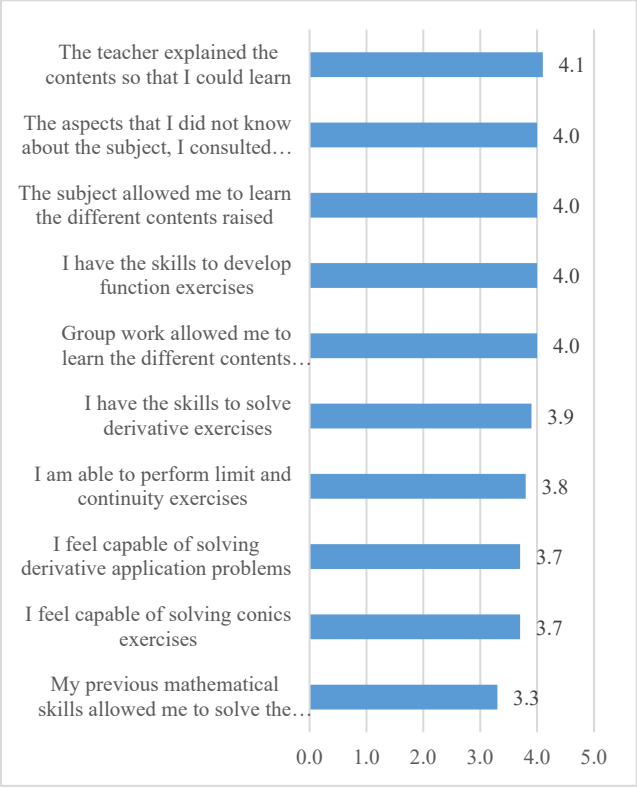

Figure 10: Student Learning Perception Graph

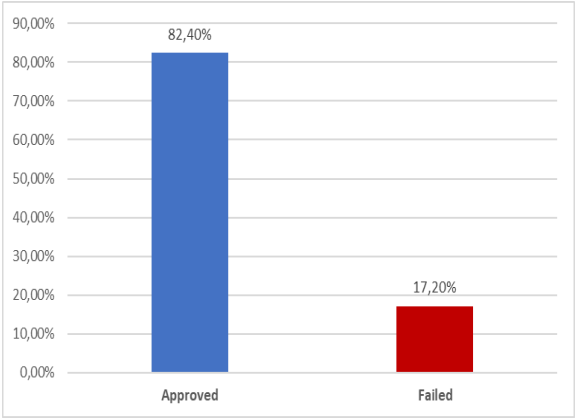

Figure 11: Percentages de approbation

5.2. Overall Performance

Considering the two parallel courses, the total number that participated in this subject were 72 students and whose general results are shown in the following graph:

Finally indicate that the average course grade was 5.4 on a scale of 1 to 7.

References

[1] C. H. Briones, C. Pon Soto, "Collaborative learning methodologies and peer assessment in virtual educational environments", *Proceedings - International Conference of the Chilean Computer Science Society, SCCC*, vol. 2020-Novem, 2020, doi:10.1109/SCCC51225.2020.9281201.

[2] J. A. Miguel Román, "La educación superior en tiempos de pandemia: una visión desde dentro del proceso formativo", *Revista Latinoamericana de Estudios Educativos*, vol. 50, no. ESPECIAL, pp. 13–40, 2020, doi:10.48102/rlee.2020.50.especial.95.

[3] S. Tejedor et al., "Education in times of pandemic: Reflections of students and teachers on virtual university education in Spain, Italy and Ecuador", *Revista Latina de Comunicacion Social*, vol. 2020, no. 78, pp. 1–21, 2020, doi:10.4185/RLCS-2020-1466.

[4] T. York, et.al, "Defining and measuring academic success", *Practical Assessment, Research a.alnd Evaluation*, vol. 20, no. 5, pp. 1–20, 2015. DOI: https://doi.org/10.7275/hz5x-tx03.

[5] D. Camacho, C. Alarcón et al. "Educación superior en tiempos de pandemia". Ciencia Latina Revista Científica Multidisciplinar, vol. 5, pp. 13955–13968, 2021 doi:10.37811/cl_rcm.v5i6.1368.

[6] J. Ortega, M. Casillas. Perspectiva crítica del impacto de las TIC en el contexto educativo. En A. Ramírez y M. A. Casillas, *Háblame de TIC: Tecnología digital en la Educación Superior*, pp. 71-84, 2014. Córdoba, Argentina: Brujas. *ISBN: 9789875914223*

[7] J. Pabón , Z. Nieto Sánchez, C. A. Gómez Colmenares, "Modelación matemática y GEOGEBRA en el desarrollo de competencias en jóvenes investigadores", Revista Logos, Ciencia & Tecnología, vol. 7, no. 1, 2015, doi:10.22335/rlct.v7i1.257.

[8] M. Rizo Rodríguez, "Aprendizaje con MOODLE", Revista Multi-Ensayos, vol. 4, no. 8, pp. 18–25, 2019, doi:10.5377/multiensayos.v4i8.9448.

[9] A. Salvatierra , S. Romero, L. Flores, "Khan Academy: Fortalecimiento del aprendizaje de Cálculo I en estudiantes universitarios", Propósitos y Representaciones, vol. 9, no. 1, 2021, doi:10.20511/pyr2021.v9n1.1042.

CARLOS HUERTA BRIONES has done his bachelor's degree from UNIVERSIDAD DE TALCA in 1990. He has done his master's degree from UNIVERSIDAD CATOLICA DEL NORTE in 1994.

Received: 19 January 2022, Revised 24 February 2022, Accepted: 26 February 2022, Online: 12 April 2022

DOI: https://dx.doi.org/10.55708/js0104012

Image Processing and Data Storage for Fire Alarm

Muhammad Zia ur Rahman*[1], Saba Waseem[1], Sidra Riaz[2], Zainab Riaz[1], Aneeq Asif[1], Ayesha Siddiqa[1], Ali Asghar[1]

[1] Department of Mechanical, Mechatronics and Manufacturing Engineering, University of Engineering and Technology Lahore, Faisalabad Campus, Faisalabad, Pakistan

[2] Department of Aerospace and Engineering, Politecnico di Bari, Bari Italy

*Corresponding author: Muhammad Zia ur Rahman, ziaurrahman@uet.edu.pk

Corresponding author ORCID: https://orcid.org/0000-0003-2304-8392

ABSTRACT: This paper explains the algorithm for fire alarm for the purpose of safety from any loss and property damage. Here, the designed algorithm is for the comparison of captured pictures. The purpose of comparison is to validate our results. In captured pictures, there may exist fire colour in pictures, which is the indication of fire in that specific area. Captured pictures are stored in folder and its path is stored in excel. We observed the indication of fired picture through fire alarm. When the fire is diminished, we used to reset button to stop the buzzer and to monitor the system again. The path of those pictures as well as the time and date of captured pictures will remain store in excel for later study of the failure of the system and also for the record purposes.

KEYWORDS: Fire Detection, Fire Safety, Image Processing, Data Storage

1. Introduction

Nowadays, conventional smoke detectors are widely used, however they take charge of a limited area. In large buildings, it may take time for the detection of smoke particles. Image-based smoke and fire detection is a latest technique, which can serve the requirement of fire detection in large buildings and outdoor environment.

Few researchers have done work on this latest technique. However, most of methods of fire detection are based on blurriness of image and geometry. Early studies about fire detection began with video based fire detection using colour indication. In [1], described algorithm of fire detection based on the temporal fluctuation of data of fire and used colour information. Another method, that was utilized in this paper, was the colour histogram to create a colour lookup table of flame pixels and thereafter took advantage of variation of pixels to predict whether it was a fire pixel or not. In [2], it is defined the process to detect the fire flame, however this algorithm used pixel information that cannot indicate fire pixels in appropriate way when there exist objects of same colour distribution as flame.

In [3], elaborated the technique of face recognition technique that employs the available databases of two different datasets in face recognition literature. Eigen faces and Fisher faces are applied to extract the relevant information from the images that are relevant for fire recognition in image processing. T.X. Truong [4] used the multi stage pattern recognition techniques to detect fire flame in video sequences. In the detailed description of visual analysis for the detection of fire flames in surveillance video, fire region is determined by colour ratio and motion of fire flame [5]. In [6], detailed explanation of the image processing technique to determine availability of free space for parking in a wireless device grid area, is provided.

In [7], it was not considered real time detection and combined tree-structured transform and occurrence of gray level matrices to predict the texture feature of flame and smoke. Yuan [8] provided the model of block motion and orientation to analyze real time smoke detection, and model can eliminate the disturbance created by artificial lights and moving objects. Research on smoke and flames were both show irregular motion of particles, create complex and turbulent phenomena that might be characterized by a dimensionless edge or surface measure [9].

In [10], it is employed the colour dynamic video sequences, which obtained from stationary camera to detect smoke and flame in sensitive areas. Fire safety

journal [11] used the logistic regression and temporal smoothing for fire flame detection in inspection video.

The tool that is being used in this research work, is image processing. Using this, an algorithm is designed to detect the fire flame. When flame is detected through captured image, it is stored in Excel sheet, which will help the workers for further manipulation. A reset button is used, which help to reactivate the system after the fire flame detection but if problem is not terminated properly due to which the sparks occurs then it stops whenever it detects the spark and the image in which fire or spark is detected is stored in the computer for the use of the operator or master of the machine to detect the error with in no time and it remained the part of the history until operator delete it. In this the time whenever fire is detected the time is also noted and stored if any component detects repeatedly then operator has to inform its supervisor to replace that component [12–17].

In this algorithm, we are working on online Arduino to operate and reset the buzzer. According to our knowledge, this work is not done in all open literature. This algorithm may applicable in industries, to monitor fire sensitive devices and domestic purposes. Main advantage of our project is security of sensitive areas, where fire flame may occur and there is a danger for the lives of the worker as well [18]. In it you not need to check each element or component, you have to check only that region which is detected by the camera. So, it is also time saving as well as cost saving.

2. Methodology

In MATLAB, one cannot write code for arduino and use camera until libraries of arduino and USB camera are not added.

First of all, add the arduino library and USB camera library to MATLAB to use arduino and camera.

- Connect the Buzzer and the reset button to arduino as shown in the Figure 1.

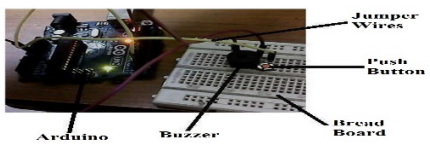

Figure 1: Apparatus or Experimental setup

- In this algorithm, when the program runs, camera captures the images of that specific area where we want to detect the fire, instantly and repeatedly [19].
- The colour detection method is used to detect the fire image, we use the RGB ratio to detect the flame of the fire (if you have different flame just change the value of RGB and detect the fire) the ratio we use is as follows:

Flame = Red(100%) + Green(95.7%) – Blue(100%)

- When the fire in the image detected, it creates a folder "fired_data_pics" in PC at specified location as shown in the Figure 2.

Figure 2: Folder of the fired pics

- A subfolder of that date (when fire detected) is created in the "fired_data_pics" folder in which all the detected fired images are stored as shown in the Figure 3. The command used to create folder is as follows:

M-File:

```
t=fix(clock); d=int2str(t(:,3));
mo=int2str(t(:,2));
y=int2str(t(:,1));
day= [ d'_'mo'_'y]
g='fire_data_pics'
l=sprintf(day)
file=fullfile(g,l)
mkdir (file)
```

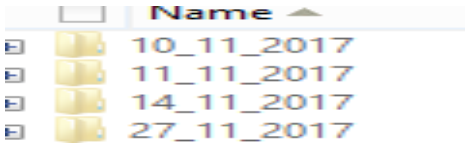

Figure 3: Folder of the fired pictures according to days

- In this subfolder, the pictures are saved with their numbers arranged in an ascending order as shown in Figure 4.

M-File:

```
path=fullfile('F:\ProgramFiles\MATLAB\R2
015a\ fire_data_pics',day);
name = 'image_%04d.tif';
 i = i + 1;
image_name = sprintf(name,i);
fullnamed=fullfile(path,image_name);
imwrite(fireimg, fullnamed);
```

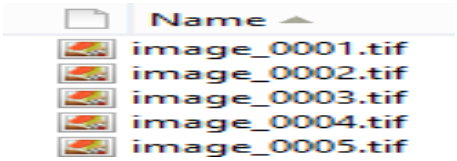

Figure 4: Fired pictures captured in a day at different time

- Similarly, an excel sheet is created for record as shown in the Figure 5. The command used to create excel file is as follows:

  M-File:

  header='NO.','Fired image','Time';

  xlswrite('firealarm_data',header,day,'B2')

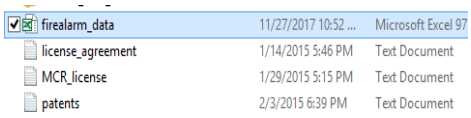

Figure 5: Excel sheet for record

- Sheets of the different days are also generated in it as similar as the subfolders are created earlier as shown in the Figure 6.

Figure 6: Excel sheets with respect to days

- Time of fire indication is then noted and stored in created excel sheet as shown in Figure 7.

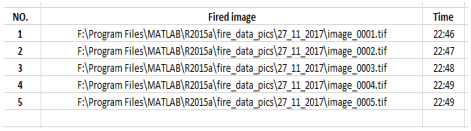

NO.	Fired image	Time
1	F:\Program Files\MATLAB\R2015a\fire_data_pics\27_11_2017\image_0001.tif	22:46
2	F:\Program Files\MATLAB\R2015a\fire_data_pics\27_11_2017\image_0002.tif	22:47
3	F:\Program Files\MATLAB\R2015a\fire_data_pics\27_11_2017\image_0003.tif	22:48
4	F:\Program Files\MATLAB\R2015a\fire_data_pics\27_11_2017\image_0004.tif	22:49
5	F:\Program Files\MATLAB\R2015a\fire_data_pics\27_11_2017\image_0005.tif	22:49

Figure 7: Record of the day on Excel sheet

- The path of that image is stored in the excel sheet to help the user to find the fired image as shown in Figure 8.

  M-File:

```
timec=fix(clock);
mins=int2str(timec(5));
hrs=int2str(timec(4));
if timec(5)<10
mins= ['0}, mins];
end
time= [hrs ':' mins];
inform={t,fullnamed,time};
 t=t+1;
xlswrite('firealarm_data', inform, day, k(i,:))
```

- As the fire detected, the buzzer will on as an indicator of fire alarm.
- Detected image then stored in created folder for the user to detect the origin of the fire and hence, the monitoring system is stopped.
- When the user clears the defects, then he has to press the reset button.
- When buzzer is alarmed after troubleshooting, a reset button is pressed to reactivate the system and the system starts monitoring and the buzzer is stopped.
- Our method is real time processing method and uses simple algorithm based on fire colour detection.

3. Proposed system architecture

The fire was detected at the start and a folder is created to store the image that was captured instantly by the system at the time of detection [20–23]. The date and time of fire detection, was stored in an excel file to see when the last event occurred. Buzzer was turned on from the start when the fire was detected and will remain in that state till the reset button was pressed and the system was reactivated [24].

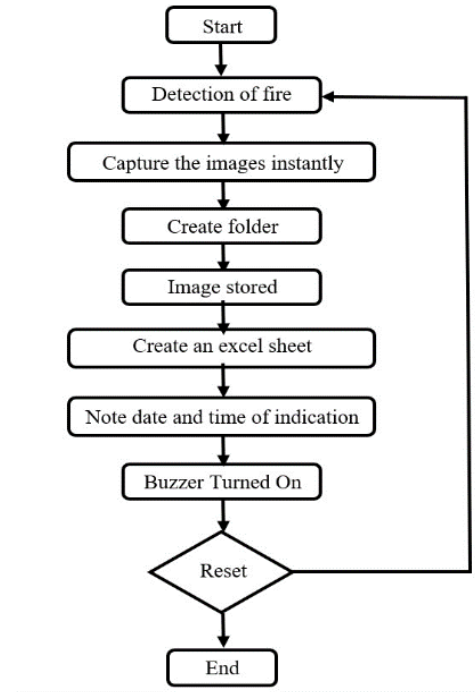

Figure 8: Complete Block Diagram

4. Results

When the algorithm runs camera, it continuously monitor the specific area by capturing the images regularly [25] but it seemed like that a video of the specific area is formed.

Following Figure 9 is taken, when no fire is detected.

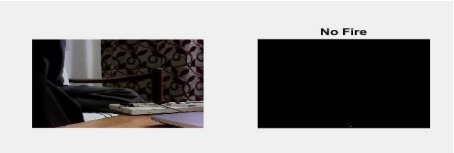

Figure 9: Monitoring during the system running

As the fire detected, the Figure 10 displays and the program stopped monitoring and the buzzer started as an indication of the fire alarm until the reset button is not pressed. The system starts working again after pressing the resetting button. Hence, it once again starts monitoring and the buzzer is 'OFF' if the fire is not terminate then it again stops and buzzer become 'ON'. So, you have to completely repair the system before resetting the system.

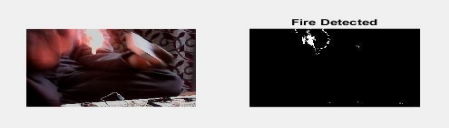

Figure 10: Fire detected Test

Similarly, the same procedure can be used to detect the fire in some real scenarios such as in the room to any appliance such as computers, refrigerators, [26–30] circuit breakers and different electrical circuits. Burning of computer is shown in the Figure 11. Therefore, in this method, we can detect fire in its starting period and we can save ourselves from such extensive fire. In this way we will able to overcome the fire and save most of the part of the appliance.

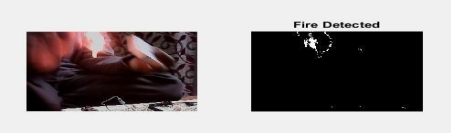

Figure 11: Fire detected from appliances

Another example where we can use this type of fire detector is in the mines or tunnels. This can be very helpful in saving the lives of the laborers working in the mines. Whenever there exists some unfortunate event such as fire due to short circuits and no one examined it but camera caught that fire and alerts the workers to be attentive and active with the help of buzzer and showing the image of sparking area, so you the repair the damaged area and origin of the fire properly.

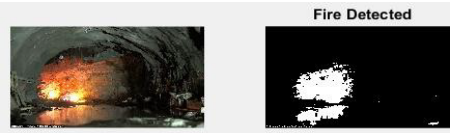

Figure 12: Fire detected in the mines

This type of method can also be use useful in industries or firms to detect the fire in the machinery.

Suppose [31], in a cloth factory the first step is to remove pilling from cloth this can be done through fire we can use this there as well, if the intensity of the fire increases from the set value then burner will stop [32] [33]. In this way we can save a lot of cloth and lives of the workers.

In the mill or factory there are many machines through which many functions are performed to run the factory or to build the products. There is a lot of chances that any machine or any component of the machine is overloaded and it burns then there is a chance that this spark may harm the machine and product as well [34–39].

If we use this method then sparks of the components are being noticed and form data and picture collection necessary steps are easy to be taken with in the right time. In the Figure 13 the same agenda is shown as I described.

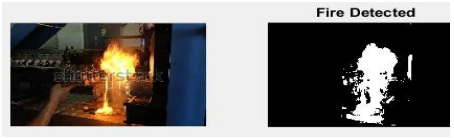

Figure 13: Fire detected from processing machines

5. Conclusions

Keeping in view the importance of time nowadays, this method could be considered the most helpful and affordable technique for fire detection as it takes less time [40–42] to detect the fire and takes images instantly. Additionally, it is the most convenient and useful method in the sense that it stores the detected image for the user to troubleshoot the defected area in no time and replace or manage the load for the specific part or component of the machine. Information like the path of detected image and time at which fire was detected is stored in an excel file which is helpful to check the history of the machine for workers and managers.

This system is economical, simple, and easy to introduce in industry and a public area with the end goal of safety [43–46]. It is obvious that our results are better than previously introduced techniques. Every system in the world has some pros and cons [47]. The limitation associated with this working phenomenon includes that it cannot be utilized in an open-air environment, as it uses a color detection method to detect fire. Consequently, it is relevant just for some particular monitoring such as monitoring process of the machinery, fire monitoring in the mines, and for the monitoring of appliances [48] [49]. We can additionally work on this system by attaching a fire extinguisher with it so that it can diminish the fire whenever fire is detected [50]. This is exceptionally useful in making the lives of individuals safe. Hence, the designed algorithm is unique and very simple for controlling.

References

[1] H. Yamagishi, J. Yamaguchi, "A contour fluctuation data processing method for fire flame detection using a color camera," *2000 26th Annual Conference of the IEEE Industrial Electronics Society. IECON 2000. 2000 IEEE International Conference on Industrial*

Electronics, Control and Instrumentation. 21st Century Technologies , vol. 2, pp. 824–829 , 2000, doi: https://doi.org/10.1109/IECON.2000.97222.

[2] S.-J. Wang et al., "Video-based early flame detection for vessels by using the fuzzy color clustering algorithm," *Proc. Int. Computer Symp*, vol. 3, pp. 1179–1184, 2006.

[3] W. Zhao et al., "Face recognition: A literature survey," *ACM computing surveys (CSUR)*, vol. 35, no. 4, pp. 399–458, 2003.

[4] T. X. Truong, J.-M. Kim, "Fire flame detection in video sequences using multi-stage pattern recognition techniques," *Engineering Applications of Artificial Intelligence*, vol. 25, no. 7, pp. 1365–1372, 2012, doi: https://doi.org/10.1016/j.engappai.2012.05.007.

[5] M. Li et al., "Review of fire detection technologies based on video image," *Journal of theoretical and applied information technology*, vol. 49, no. 2, pp. 700–707, 2013.

[6] D. B. L. Bong, K. C. Ting, K. C. Lai, "Integrated Approach in the Design of Car Park Occupancy Information System (COINS).," *IAENG International Journal of Computer Science*, vol. 35, no. 1, 2008.

[7] Y. Cui, H. Dong, E. Zhou, "An early fire detection method based on smoke texture analysis and discrimination," *2008 Congress on Image and Signal Processing*, vol. 3, pp. 95–99, 2008, doi: https://doi.org/10.1109/CISP.2008.397.

[8] F. Yuan, "A fast accumulative motion orientation model based on integral image for video smoke detection," *Pattern Recognition Letters*, vol. 29, no. 7, pp. 925–932, 2008.

[9] Z. Xiong et al., "Video-based smoke detection: possibilities, techniques, and challenges," *IFPA, fire suppression and detection research and applications—a technical working conference (SUPDET), Orlando, FL*, 2007.

[10] Y. H. Habiboğlu, O. Günay, A. E. Cetin, "Flame detection method in video using covariance descriptors," *2011 IEEE International Conference on Acoustics, Speech and Signal Processing (ICASSP)*, pp. 1817–1820, 2011, doi: https://doi.org/10.1109/ICASSP.2011.5946857.

[11] S. G. Kong et al., "Fast fire flame detection in surveillance video using logistic regression and temporal smoothing," *Fire Safety Journal*, vol. 79, pp. 37–43, 2016, doi: https://doi.org/10.1016/j.firesaf.2015.11.015.

[12] J. Sang et al., "Joint image compression and encryption using IWT with SPIHT, Kd-tree and chaotic maps," *Applied Sciences*, vol. 8, no. 10, pp. 1963, 2018, doi: https://doi.org/10.3390/app8101963.

[13] A. Mateen, M. Azeem, M. Shafiq, "AZ model for software development," *arXiv preprint arXiv:1612.08811*, 2016.

[14] M. A. Akbar et al., "Investigation of Project Administration related challenging factors of Requirements Change Management in global software development: A systematic literature review," *2018 International Conference on Computing, Electronic and Electrical Engineering (ICE Cube)*, pp. 1–7, 2018, doi: https://doi.org/10.1109/ICECUBE.2018.8610966.

[15] M. A. Akbar et al., "Improving the quality of software development process by introducing a new methodology–AZ-model," *IEEE Access*, vol. 6, pp. 4811–4823, 2017.

[16] M. A. Akbar et al., "A fuzzy analytical hierarchy process to prioritize the success factors of requirement change management in global software development," *Journal of Software: Evolution and Process*, vol. 33, no. 2, pp. e2292, 2021.

[17] M. A. Akbar et al., "A robust framework for cloud-based software development outsourcing factors using analytical hierarchy process," *Journal of Software: Evolution and Process*, vol. 33, no. 2, pp. e2275, 2021, doi: https://doi.org/10.1002/smr.2275.

[18] M.Z. Rahman et al., "The Prescribed Fixed Structure Intelligent Robust Control of an Electrohydraulic Servo System", Mathematical Problems in Engineering, vol. 2022, 12, 2022. Doi: 10.1155/2022/5144602

[19] U. Farooq et al., "A Reliable Approach to Protect and Control of Wind Solar Hybrid DC Microgrids," 2019 IEEE 3rd Conference on Energy Internet and Energy System Integration (EI2), Changsha, China, 348-353, 2019. doi: 10.1109/EI247390.2019.9062101.

[20] M. Taiyaba et al., "Secure V2X Environment using Blockchain Technology." In Proceedings of the Evaluation and Assessment in Software Engineering, pp. 469-474. 2020. DOI: https://doi.org/10.1145/3383219.3383287

[21] M. Shafiq et al., "Towards successful global software development." In Proceedings of the Evaluation and Assessment in Software Engineering, 445-450. 2020. DOI: 10.1145/3383219.3383283

[22] S. Akram, M. Shafiq, M. A. Akbar, "Automated risk analysis model for software development enhancement," *International Journal of Multidisciplinary Sciences and Engineering*, vol. 7, no. 8, pp. 23–27, 2016.

[23] N. Nasrullah et al., "Reversible data hiding in compressed and encrypted images by using Kd-tree," *Multimedia Tools and Applications*, vol. 78, no. 13, pp. 17535–17554, 2019.

[24] J. Ahmad et al., "The deep neural network based classification of fingers pattern using electromyography," *2018 2nd IEEE Advanced Information Management, Communicates, Electronic and Automation Control Conference (IMCEC)*, pp. 455–461, 2018, doi: https://doi.org/10.1109/IMCEC.2018.8469534

[25] M. A. Akbar et al., "AZ-Model of software requirements change management in global software development," *2018 International Conference on Computing, Electronic and Electrical Engineering (ICE Cube)*, pp. 1–6, 2018.

[26] M. A. Akbar et al., "Organization type and size based identification of requirements change management challenges in global software development," *IEEE Access*, vol. 8, pp. 94089–94111, 2020.

[27] A. A. Khan, M. A. Akbar, "Systematic literature review and empirical investigation of motivators for requirements change management process in global software development," *Journal of Software: Evolution and Process*, vol. 32, no. 4, pp. e2242, 2020.

[28] M. A. Akbar et al., "Prioritizing Management Success Factors in Offshore Software Development," *Arabian Journal for Science and Engineering*, vol. 45, no. 12, pp. 10163–10184, 2020.

[29] T. Kamal, Q. Zhang, M. A. Akbar, "Toward successful agile requirements change management process in global software development: a client–vendor analysis," *IET Software*, vol. 14, no. 3, pp. 265–274, 2020.

[30] M. A. Akbar et al., "An empirical study investigation of task allocation process barriers in the context of offshore software development outsourcing: An organization size based analysis," *International Journal of Computing and Digital Systems*, vol. 8, no. 04, pp. 343–350, 2019, doi: http://dx.doi.org/10.12785/ijcds/080403.

[31] M. A. Akbar et al., "Prioritization of global software requirements' engineering barriers: An analytical hierarchy process," *IET Software*, vol. 15, no. 4, pp. 277–291, 2021, doi: https://doi.org/10.1049/sfw2.12022.

[32] M. A. Akbar et al., "Success factors influencing requirements change management process in global software development," *Journal of Computer Languages*, vol. 51, pp. 112–130, 2019, doi: https://doi.org/10.1016/j.cola.2018.12.005.

[33] M. A. Akbar et al., "Investigation of the requirements change management challenges in the domain of global software development," *Journal of Software: Evolution and Process*, vol. 31, no. 10, pp. e2207, 2019, doi: https://doi.org/10.1002/smr.2207.

[34] M. T. Riaz et al., "Wireless android based home automation system," *Adv. Sci. Technol. Eng. Syst. J*, vol. 2, no. 1, pp. 234–239, 2017, doi: 10.25046/aj020128.

[35] M. T. Riaz et al., "A wireless controlled intelligent healthcare system for diplegia patients," *Mathematical Biosciences and Engineering*, vol. 19, no. 1, pp. 456–472, 2022, doi: https://doi.org/10.3934/mbe.2022022.

[36] H. A. Javaid et al., "Classification of Hand Movements Using MYO Armband on an Embedded Platform," *Electronics*, vol. 10, no. 11, pp. 1322, 2021, doi: https://doi.org/10.3390/electronics10111322.

[37] M. T. Riaz et al., "The Intelligent Transportation Systems with Advanced Technology of Sensor and Network," *2021 International Conference on Computing, Electronic and Electrical Engineering (ICE Cube)*, pp. 1–6, 2021.

[38] M. T. Riaz et al., "Design and Experimental Validation of a Small-Scale Prototype Active Aerostatic Thrust Bearing," *2021 International Conference on Computing, Electronic and Electrical*

Engineering (ICE Cube), pp. 1–6, 2021.
[39] M. T. Riaz et al., "Wireless model for high voltage Direct Current measurement using Hall sensor," *2021 International Bhurban Conference on Applied Sciences and Technologies (IBCAST)*, pp. 642–647, 2021. doi: https://doi.org/10.1109/IBCAST51254.2021.9393186.
[40] M. T. Riaz et al., "Analysis and Evaluating the Effect of Harmonic Distortion Levels in Industry," *2021 4th International Conference on Energy Conservation and Efficiency (ICECE)*, pp. 1–7, 2021, doi:10.1109/ICECE51984.2021.9406283.
[41] M. T. Riaz et al., "Steady state analysis of HVDC transmission system based on MATLAB/SIMULINK," *2019 International Conference on Electrical, Communication, and Computer Engineering (ICECCE)*, pp. 1–6, 2019, doi: 10.1109/ICECCE47252.2019.8940745.
[42] M. T. Riaz et al., "Research on the Protection of Hybrid HVDC System," *2018 International Conference on Power Generation Systems and Renewable Energy Technologies (PGSRET)*, pp. 1–6, 2018, doi:10.1109/PGSRET.2018.8686007.
[43] M. T. Riaz et al., "Investigation of Electrical Properties of Epoxy Resin Composite with the Surface Modification of SiO 2 Nanoparticles," *2021 International Conference on Computing, Electronic and Electrical Engineering (ICE Cube)*, pp. 1–5, 2021, doi: https://doi.org/10.1109/ICECube53880.2021.9628354.
[44] M. T. Riaz et al., "Design of a Free Energy Generator using Gravity Wheel & Dynamo," *2021 4th International Conference on Energy Conservation and Efficiency (ICECE)*, pp. 1–5, 2021.
[45] M. Idrees et al., "Fuzzy logic based calculation and analysis of health index for power transformer installed in grid stations," *2019 international symposium on recent advances in electrical engineering (RAEE)*, vol. 4, pp. 1–6, 2019.
[46] M. A. Akbar et al., "Requirement change management challenges in GSD: An analytical hierarchy process approach," *Journal of Software: Evolution and Process*, vol. 32, no. 7, pp. e2246, 2020.
[47] M. A. Akbar et al., "Multicriteria decision making taxonomy of cloud-based global software development motivators," *IEEE Access*, vol. 8, pp. 185290–185310, 2020, doi: https://doi.org/10.1109/ACCESS.2020.3030124.
[48] H. A. Raza et al., "Analysis the effect of 500kv High-Voltage Power Transmission Line on the Output Efficiency of Solar-Panels," *2019 International Conference on Electrical, Communication, and Computer Engineering (ICECCE)*, pp. 1–6, 2019, doi:10.1109/ICECCE47252.2019.8940803.
[49] L. Hanwu et al., "Regularity of Current Dispersal in Different Kinds of Grounding Electrode," *2018 IEEE International Conference on High Voltage Engineering and Application (ICHVE)*, pp. 1–4, 2018, doi:10.1109/ICHVE.2018.8642240.
[50] M. A. Akbar et al., "Towards successful agile development process in software outsourcing environment: a systematic literature review," *International Journal of Business Innovation and Research*, vol. 23, no. 2, pp. 141–167, 2020.

MUHAMMAD ZIA UR RAHMAN is working as a Lecturer in the department of mechatronics and control engineering at university of engineering and technology Lahore, Faisalabad Campus, Pakistan since May 2016. He received his bachelor degree in Electronics Engineering from COMSATS Abbottabad in 2013 and Master degree in Control System from University of engineering and technology Taxila Pakistan in 2015. His current research interests include robust and optimal control systems.

SIDRA RIAZ is recently doing Ph.D. Degree from Politechnico di Bari University of Italy.

Her current research interests include aerospace engineering, plasma physics and optimal control systems.
.

SABA WASEEM is doing B.Sc. in Mechatronics and Control Engineering from University of Engineering and Technology Lahore (Faisalabad Campus).

Currently, she is working on a project whose title is Porosity Measurement of Woven Fabric using Light Through Methodology.

JENRS

Received: 07 February 2022, Revised: 11 March 2022, Accepted: 03 April 2022, Online: 12 April 2022

DOI: https://dx.doi.org/10.55708/js0104013

An Elaborate Breakdown of the Essentials of Biogas Production

Abdulhalim Musa Abubakar * [1], Kiman Silas [2], Mohammed Modu Aji [2]

[1] Department of Chemical Engineering, Faculty of Engineering, Modibbo Adama University (MAU), P.M.B 2076, Yola, Adamawa State, Nigeria
[2] Department of Chemical Engineering, Faculty of Engineering, University of Maiduguri (UNIMAID), P.M.B 1069, Maiduguri, Borno State, Nigeria

*Corresponding author: Abdulhalim Musa Abubakar, +2347050244277 & Email: abdulhalim@mautech.edu.ng
Corresponding author ORCID: 0000-0002-1304-3515

ABSTRACT: World search for ways to properly manage rural and urban waste generated on daily basis from domestic and industrial buildings, perhaps leads to the adoption of the anaerobic digestion (AD) systems. The system utilizes microorganisms such as viruses, fungi, helminths, bacteria and protozoa to degrade waste so as to generate useful by-products such as biogas, used in heating, lighting and as fuel. Research on ways to effectively generate biogas from different feedstock had been serious in recent years, especially the study of the process kinetics to maximize production. This review seeks to provide details on feedstock type, pretreatment, substrate degradation, biogas properties, biogas utilization and factors influencing its production. Conclusion is drawn, noting that maximum biogas yield can only be obtained if the production parameters are carefully selected. Pressure being among the factors affecting the microclimate of digesters, is often uncontrolled in most biogas production facilities being slightly above the atmospheric pressure. Recent findings shows that biogas/methane amounts is increased with decreased internal gas pressure and could be a new efficient and effective process control strategy together with pH and temperature. This work will equip researchers and biogas plant developers with the rudiments of the technology which will eliminate the lack of technological know-how often experienced in some realms; in order to breach the gap in production and create a balance between waste generation, recycle and reuse.

KEYWORDS: Biogas, Biodigester, Pretreatment, Anaerobic digestion, Feedstock type

1. Introduction

In the 17th century, Robert Boyle and Stephen Hale produced for the first time, biogas from decaying organic matter [1]. Sir Humphry Davy identified methane in the gas generated from cattle manure decomposition in 1808; however, methane was first identified via experimentation in 1776 by Alessandro Volta [1–3]. Five decades later, at Bombay, India, the first anaerobic digester was built in 1859. Though China is presently leading in the development of the technology, it all began in 1920, when Luo Guorui built the first hydraulic digester called 'Chinese Guorui Natural Gas Stove'. In 1930s, the discovery gained academic recognition leading to scientific research [1]. Germany's main feedstock for biogas production in 1945 was agricultural products. With increasing awareness of the technology, the 1950s witnessed an upsurge in the development of biogas plants [2]. Early biogas plant builders in Africa are Algeria, followed by Kenya and Tanzania, between 1930s and 1950s. Up till this present time, more and more plants are been built as part of policy strategy of government of some countries and/or local and international organizations with aims including, poverty

reduction, economic growth, electricity generation, improve agricultural yield, solution to pollution problems and to arrest the menace of desertification.

By 2050, a 70% rise in world waste generation, triggered by industrialization and population growth is predicted [2]. This will increase the demand for energy and fuel of which biogas is a good candidate. Currently, thousands of biogas plants are being in operation in Africa, North America, Europe and Asia [4–6]. Germany with 4000 biogas plants occupies the leading position in Europe in biogas production, majorly utilizing farm residue for coproduction [7]. Sweden has ≅ 233 biogas facilities while Austria in 2008, a report, puts the number of biogas plants for green electricity production at 294 [7]. Europe is the leading continent in biomethane production (2.4 billion m^3), with 18,943 plants feeding 725 biomethane plants and producing 15.8 billion m^3 of biogas [8]. Authors like [9], [10] and [11] gave insight on cooking preferences of biogas, potentials of livestock and agricultural waste for biogas production, and the energy potentials of biogas in their respective countries, which are India, Greece, China and Ukraine. In the Mekong Delta region of Vietnam, super-intensive shrimp aquaculture is becoming prominent and the AD of shrimp sludge with other biomass gives promising result [12]. Indonesia targets 16.9% increase in biogas exploitation for power generation by 2025 [13]. Other Asian countries have the following numbers of digesters: China, 20 million family size type; India, 100, 000 digesters; Korea, 24000; and Taiwan, 7,500 biofermenters [9–11]. In Africa, lack of technical know-how is one of the reasons that puts most of the biogas plants in the continent out of operation, especially in Zimbabwe, where this gases are been flared [14]. Egyptians use underground biodigesters; Ethiopia employs fixed dome bioreactor in about 4500 household utilizing kitchen waste; while it has been reported that biogas potential in Mauritania is 520-258.7 $(\pm 125.8)\times 10^6$ m^3/year [5, 15–17]. Guinea witnessed their first digester in Kindia and Macenta in 1977 and from 1981-1999, 90 more plants was installed, which died out as a result of non-monitoring [3]. But in 2016, 2000 digesters was reported by the same author to have been constructed by the government. East and North Africa could boost of 3.2 million m^3/h of biogas generation according to [5, 15–18].

The larger the volume of useful organic waste generated by a country, the higher its potential for biogas production. In developing countries, 93% of waste generated are dumped at road-sides, open lands and waterways or burned/incinerated – but world over, almost 40% of waste goes to landfills [19]. Despite the fact that Nigeria, Africa's most populous country, generates massive amounts of trash, the government have made little effort to develop a biogas plant to benefit from any of its products. However, various bench-scale biodigester investigations have been conducted in Nigerian polytechnics and universities solely for research purposes [18]. In addition, Canada's waste generation is estimated to reach 35.5 million tonnes [8]. But the potential in Canada is below countries that can boost of huge number of industries generating degradable byproducts, large hectares of land yielding high agricultural residue, large animal population or whose human population has the potential of generating enormous municipal waste, such as China, India Indonesia, Nigeria, Brazil, United States and Germany.

Setting up a biogas plant to be operated for large scale production of biogas or a small size one for domestic use, all require expertise and adherence to conditions that suits the manufacturing process. Research is ongoing to find ways of achieving optimum production by combining certain constraint parameters of production. In essence, the versatility of the process is increasing due to new findings often reported. In 2010, Mohamed Samer, developed a software to facilitate the planning, design, dimensioning and estimating the amount of materials needed for biogas plant construction together with cost analysis capability [20]. In the internet, many experts have tried to replicate this using Excel Spreadsheet or through the development of a PC or android software (e.g. BiogasApp, India) that gives the biogas and energy output of some feedstock in their locality [21]. Existing softwares are Anessa AD.A used for biogas plant feasibility assessment and operation, SMART BIOGAS, SIMBA#Biogas for biogas plant simulation and the software for biogas research by S.D. Hafner (2018). Also, the study on biogas production using ASPEN by process engineers is scanty [22, 23]. In this work, the various type of digesters for anaerobic decomposition, the feedstock type, feedstock preparation, degradation stages, variables influencing production, biogas characteristics and cleaning are highlighted.

2. Biodigester

Bioreactors is also termed digesters – an airproof reactor tank or vessel that is simple, cheap, robust, easy to operate and maintain [24–26]. Biogas digesters or simply biodigesters are considered small-scale if subjected to domestic use and large-scale, as in industrial digesters [27]. They are flexible because they are made of plastics such as polyvinyl chloride (PVC) and low-density polyethylene (LDPE) or high-density polyethylene (HDPE) [28]. Microorganisms such as fungi, bacteria and protozoa can

survive in an oxygen-void environment, degrading the feedstock to produce biogas and digestate. The process is identical to what happens in a cow's stomach, where stomach bacteria convert food into dungs and biogas as shown in Figure 1 (a mixture of methane and carbon dioxide gas) [29].

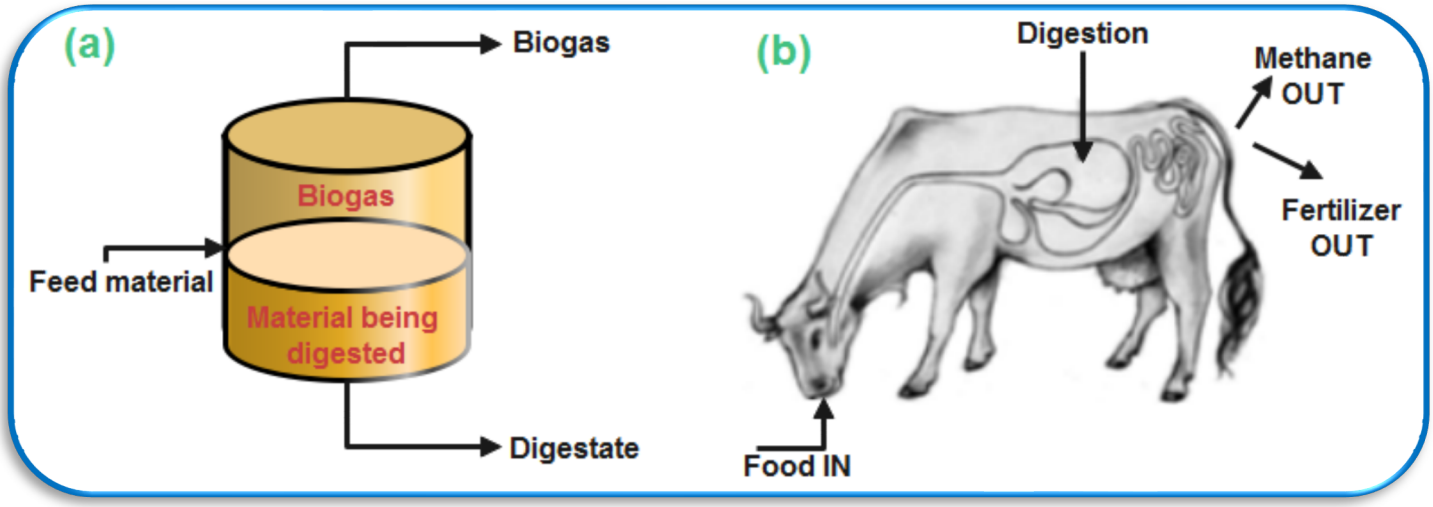

Figure 1: Biodigester (a) Flow Diagram and (b) Cow's Stomach [21, 29]

Not only methane as shown in Figure 1b is produced, but several other gases constitute the biogas end-product. The more the waste is degraded, the more the gas is produced [30]. The decomposed substrate is the residue called the digestate which is rich in macro- and micro nutrients, and used as biofertilizer [25, 31, 32]. The digestate will have little or no smell if the digester is working perfectly [29].

2.1 Biogas Composition and Properties

Biogas is a colorless and odourless gas composed of methane (CH_4), carbon dioxide (CO_2), hydrogen (H_2), hydrogen sulphide (H_2S), ammonia (NH_3), nitrogen (N_2), oxygen (O_2) and water vapor (H_2O) in varying proportions. Main compound present is CH_4; in some cases reaching up to two-third of the whole composition, and referred to as the energy component of the biogas [21, 33, 34]. Second most-highest concentration in biogas is CO_2, which could diminish it's energy value [6]. Hydrogen sulphide (H_2S) is noxious and toxic when in high concentration in biogas, whereas siloxanes: a silicon derivative gotten from decomposition of cosmetics is rarely present [33, 35]. Table 1 shows typical biogas compositions reported from biogas analyzers such as Gas Chromatography (GC), Fourier Transforms Infrared (FTIR) spectroscopy and Gas Chromatography-Mass Spectrometry (GC-MS), Gas Chromatograph coupled with a Thermal Conductivity Detector (GC-TCD) among others [36].

Table 1: Typical Biogas Composition [4, 15, 21, 24, 25], [33–35, 37–41]

Component	Percentage (%)
CH_4	35-75
CO_2	15-65
H_2	0-7
H_2S	0-3
NH_3	0-2
N_2	0-10
O_2	0-2
H_2O	1-7
Trace gases	< 2

Despite the multitude of gaseous compounds present in biogas, it is still 20% lighter than air [14, 42]. Yield and composition of biogas depends on digestion condition, feedstock and co-substrate type [15, 34]. Biomethane are upgraded biogas where composition of more than 40% CH_4 will be responsible for the characteristic flammability of the gas [29, 43, 44]. This flame is hotter than fire and is clear, similar to liquefied petroleum gas (LPG) blue [15, 42, 45, 46]. Biogas are characterized with low energy density, slow flame speed and partial combustion; a property that is considered negative [34]. In addition, ignition temperature is in the range of 650-750^{0}C [14, 42]. Gaseous compounds including NH_3, H_2S and CO_2 in biogas are poisonous, which is the main reason biogas can suffocate anyone exposed to it in an enclosed area [29]. Removal or reduction of these poisonous gas, brings biogas to the level of natural gas or fuel grade CH_4, especially using the pressure swing adsorption (PSA) technique, as reported by [47]. For instance, CO_2 content could be brought to desirable level

during upgrading process by scrubbing as well as the use of recent technology known as the microbial electrochemical to reduce CO_2 [48]. [49] stated that biogas recirculation is cost-effective when it comes to enhancing the quality of biogas in AD reactors while [50] explains biogas up-gradation into syngas via dry reforming. Mega joules (MJ) is the energy units of biogas and 1 m^3 of raw biogas at STP containing 60% CH_4 will give a heating value of 21.5 MJ (5.97 kW h) [27, 34].

Dangers faced in the use of biogas comes from the CH_4 content and is the reason for the hazardous characteristic of biogas. The safety measures to be taken while operating biogas plants on either large-scale, small or household size basis are the wearing of protective equipment, avoidance of contact with digester content through the use of gloves and regular hand washing [11, 29]. Electric spark triggering explosion, fire when naked flame is brought closer to gas or through smoking, risk of diseases such as malaria, cholera and typhoid especially while handling livestock waste, H_2S poisoning (up to 10-150ppm causing lungs irritation), smell when digester is dysfunctional and asphyxiation due to inadequate ventilation are potential dangers associated with biogas production [17, 29, 33, 51]. Threshold percentage resulting in explosion is observed in two cases; when 10-30% of the gas is diluted with air and when the biogas containing 60% of CH_4 mixes with air [51]. The same author reported that, even though CH_4 is non-toxic, concentrations between 5-15% is explosive.

2.2. Categories of Feedstock for Anaerobic Digestion (AD)

Organic wastes are the main feedstock for AD and is divided into three broad categories including agricultural, municipal and industrial waste [4, 43, 52]. Agricultural wastes are livestock residue, garden waste, harvest residue, energy crops, vegetable by-products, grasses (e.g. steamed lemon grass and sudan grass) and algae (e.g. *Spirogyra neglecta* and *Cladophora glomerata*) [12, 18]. In [53], it was reported that 1 kg of water hyacinth will generate approximately 0.014 m^3 of biogas. Livestock residues are obtained from slaughter houses, ranges, pisciculture, insect farms and poultry houses, which are fish residue (e.g. shrimp sludge, fish meal, fish maw and isinglass), insects and worms, poultry litter, keratin-rich waste and manures [12, 39]. 1 kg of cattle dung, pig dung, chicken droppings and chicken manure will generate approximately 0.04 m^3, 0.06 m^3, 0.07 m^3 and 0.065-0.116 m^3 of biogas respectively from 1:1 water-to-feedstock ratio [53, 54]. Volume of 1 kg of fresh cattle dung is about 0.9 litres, containing 8% dry biodegradable mass. Over 250 million cattle population in India is a promising potential for biogas and energy generation [7]. If manures are not properly handled, they can result in emission of nitrous oxide (N_2O) to the atmosphere, whose negative effect on the climate is 265-298 times greater than CO_2, contributing to about 10% of global non-CO_2 emissions [55, 56].

Insect farming technology breeding silkworm and caterpillar excreta generates biogas comparable to animal waste; specifically silkworm excreta was reported to generate 331.97 m^3/Mg TS [57]. Poultry litter are lignocellulosic bedding materials containing wasted water, spilled feed (e.g. grains, peanut hulls and pine straw), wood shavings, poultry manure, feathers and sawdust [58, 59]. Keratin-rich waste are fibrous protein in the form of skin, wool, chicken feather, horns, mixture of borns, hooves, beaks, hair, nails, organs, hard tissues and claw produced by fish, meat and wool industry, in large quantity [60]. Manures are animal droppings which is a mixture of H_2O, straw, excreta (faeces and urine), livestock bedding, sand and wasted feed, that is rich in NPK and fiber; and is obtained from elephant, cattle, sheep, goat, chicken, camel, donkey, pig, rabbit, deer, horses and duck [48, 49, 61, 62]. Manures can be used to produce biogas, biofuel and synthetic gas – while on the other hand, manure fibers can be used to produce building materials, plant growth medium identical to peat moss, paper, seed starter pots and fertilizer garden sculptures, thereby changing its environmental liability status to a useful product. Carbohydrate, fat, protein, crude fiber and ash contents in pig, cow and chicken manures are respectively, "38, 4, 19, 20 & 19%", "20, 4, 15, 40 & 21%" and "25, 4, 29, 15 & 27%", according to [7]. Taiwan have constructed over 7,500 CH_4-generating devices, that utilizes pig manure in Taiwan while Poland produces 112 million Mg of manures yearly making it the largest producer in Europe, but utilizes < 1% to manufacture biogas [56].

Municipal wastes are divided into municipal solid waste (MSW) and liquid waste, including food waste (FW), municipal waste water, landfill waste, papers, green waste, urban sanitation and aquatic biomass, gotten from diverse sources such as domestic, educational, industrial and medical facilities [8, 63, 64]. Annually, 2 billion tons of MSW is generated worldwide, which is projected to rise to 3.4 billion tons by 2050 [19]. FW is defined as a variable substrate, uneaten, discarded or lost during stages of production, processing, distribution and consumption of foods including rice, yam, noodles, nuts, pasta, eggs, fish, bagasse, vegetables, oil waste, fruits, meat, potato, and sweets [65–70]. Huge amounts of FW are products from restaurants, canteens, markets, hotels, hostels, food

processing industries and households coming from kitchen's of the listed buildings and locations [34, 60, 71]. Dirty water and remains of different food types are generated in the kitchen, and are for example, tuber peels (e.g. potato peels), vegetable residue, fruits peel, cooked food leftovers and spices [71, 72]. Spices including red chili, black pepper, cinnamon, coriander, garlic, turmeric, cardamom and clove are unsuitable for AD process [73]. Waste oils such as cooking oil, essential oils, microalgal oil, fish waste oil, fat, grease and palm oil are feedstock for biogas production [74]. Presently, Indonesia remains the largest palm oil producer in the world and more production will balance the gap between increasing demand for the product (rose by 186% from 2010-2025) [75]. Municipal waste water like sewage sludge and water from gutters are typified by low recovery of biogas [45, 76, 77]. In developing nations where there are no good drainage systems, the waste waters cannot be easily tapped and harnessed. Potentials of human faeces for biogas production have also been experimented [13]. Depending on the climate, diet, food and water intake, biogas production rate of human excreta is 0.02-0.07 m^3/kg day, while daily production of this waste from an average adult human is 1-1.3 kg of urine and 0.2-0.4 kg of faeces as reported by [54].

Landfill site receives almost all types of waste, grouped into organic and inorganic sub-types of which typical example is MSW disposed at landfill via composting or open dumping and leachate formed at landfill sites which yields considerable percentage of biogas during AD [4, 45, 63, 78]. A linear statistical model had been developed by [79] to model the energy potential of the MSW comprising of woods, grasses, papers, leaves, food remnants, plastics, metals and glasses in nine densely populated Northern states in Nigeria to serve as a tool for setting up energy policy that will aid waste management in the region. Waste recovery in one of the state (Maiduguri), such as metals, plastics, bottles, ceramics, paper and magazines from waste collection points and dumpsites is an activity that would be responsible for poverty alleviation and job creation, especially when paper and magazines recovered are channeled to biogas generation [80]. Also, analysis of leachate samples in four dumpsites of the same location (Ajaganaram, Bulabulin, Gwange & Monday Market) is reported to be rich in metallic nutrients that would support AD if exploited by the locales [81]. Paper sludge, with potential of 14.7 mL/gVS of biogas, emanates from the paper mill primary clarifier in the water treatment unit of the industry [82]. Generally, papers contain two types of structural carbohydrate (cellulose and hemicellulose), which are ideal AD substrate found in paper and pulp industry, printing press and learning institutions, including cardboard, filter paper, waste paper, newspaper, tissue paper and magazine [83, 84].

Aquatic biomass are possibly aquatic weeds such as floating weeds (e.g. water hyacinth or *Eichhornia crassipes*, *Azolla pinnata*, duckweeds or *Lemna perpusilla*, *Pistia stratiotes*, *Neptunia oleracea*, *Pandanus helicopus*, etc), emergent weeds (e.g. *Nymphae spp.*, *Nelumbo nucifera*, *Myriophyllum aquaticum*, etc), algal weeds (e.g. *Microcystis aeuginosa*, *Dinoflagellates spp.*, *Oscillatoria*, etc), marginal weeds (e.g. *Marsilia mutica*, *Typha angustifolia*, *Colocasia esculenta*, *Cyperus papyrus*, etc), submerged weeds (e.g. *Myriophyllum spicatum*, *Vallisneria spiralis*, *Ceretophyllum demersum*, *Hydrilla verticillata*, chara/muskgrass or skunkweed, etc) and water primrose (*Ludwigia hyssopifolia*), which are rich lignocellosic biomass [18, 24, 66, 67, 85, 86]. Invasive aquatic weeds are found in India, Indonesia, Australia, Brazil, North America, New Zealand, Central America, Malaysia, South-East Asia and Africa (places include Rivers of Southern Mozambique, South Africa, Kenya, Ghana, Mali, Egypt, Benin Republic, Volta River of Burkina Faso, Niger Republic, Sudan and Nigerian coastal creeks and lagoons); but it is most-abundant in Indonesia [85–93]. They are found in almost every part of the world and had been reported to be a good source of biogas generation with potential for power generation in Kenya [92]. In the literature, water hyacinth is the most used aquatic biomass for biogas production because it is abundant, having the capacity to double their number in just 2 weeks, constituting a pollution to water bodies [94, 95]. It originated in Brazil and was 1st seen in 1984 around Badagry Creek in Lagos; River Benue at Makurdi in 1988; and River Niger and Kainji Lake in 1992, all in Nigeria [89, 96]. In [97], the potentials of water hyacinth's application for biogas synthesis by communities living near the Lake Chad Basin in North Eastern Nigeria had been highlighted. In addition, communities living near River Niger, River Kaduna, River Benue, Kainji Dam and the Kaduna River in Nigeria can also make use of the available biomass. Using conical flasks as digesters, [95] studied the possibility of reaping considerable volume of biogas from floating aquatic weeds. Other aquatic biomass are *Elodea canadensis*, considered as the most widespread plant in Europe; *Azolla filiculoides* ranks second followed by *Vallisneria spiralis* and *Elodea nuttallii* in the same continent; *Typha angustifolia*, whose infestation in the wetlands of Hadejia-Jama'are, Lake Chad Basin and Sokoto-Rima river basins in Northern Nigeria constitutes a major problem; and water fern (*Salvinia molesta*) which produces (on average) 6.7 l/kg of

biogas from 1st ever recorded research carried out by Abbasi & Nipaney in 1984 [86, 88, 96, 98, 99].

Industries processing food and agricultural products, pharmaceutical industries, fodder and brewery industry, sugar industry, fruit processing, textile industry and wastewater treatment plants (WWTPs) are some of the industries generating semi-solid and liquid organic waste for anaerobic digesters [26, 68, 69, 100, 101]. WWTPs generate semi-solid waste by-products known as sludge, which is sub-divided into settled primary sludge or waste activated sludge (WAS) generated during biological treatment of which >18,000 of these plants are in Europe alone [31, 59, 70, 102]. Domestic and municipal wastewater produced worldwide is around 360,000 m^3 yearly out of which 52% is mostly treated in WWTPs according to Utrecht University and the United Nations (UN)'s findings [103]. Two types of waste are gotten from fruit processing facilities which are solid waste consisting of stones, skin, seeds and peels, and liquid waste from juice and wash-waters [60, 104–109]. In [110], MSW (FW inclusive) is predicted to rise to about 72,146 tons/day in South Africa by 2025 as a result of population growth. Pharmaceutical wastewater is the least exploited source of biogas production compared to the textile and beverage industry effluents. Tetracycline antibiotic has been shown to enhance production in a lab-scale anaerobic baffled reactor (ABR), whereas herbal pharmaceutical wastewater could generate about 43.3% CH_4 when digested [111, 112]. Cotton yarn wastes and textile wastes (of which globally, ≅ 75% is disposed of in landfills) could be reused or recycled back into clothing or channeled into bioenergy manufacture [113, 114]. This venture might not be easy as effluent from textile industries are characterized by toxicity, lower pH and carbon-to-nitrogen (C/N) ratio [115, 116]. The beverage industry has been given the desired concern by researchers, especially in the application of soft drink beverage waste, native beverage vinasse and alcoholic wastewater [100, 117, 118].

It is possible to distinguish two major types of waste that can be digested into liquid effluent waste (e.g. wastewater, manure slurry, sewage sludge, agro-food effluents, etc) and organic solid waste (e.g. agricultural, industrial and municipal waste) [33, 76]. It is advisable, most times, to opt for substrates looking at its sustainability, energy recovery, digestibility, yield potential, environmental and economic values [15, 18, 69].

2.3. Feedstock Preparation

Certain amount of inorganic contaminants (e.g. debris, grits, glass, sticks and metals) are advised to be removed prior to subjecting them to AD to produce biogas [15, 47]. Pretreatment, addition of additives, degradation stages and biogas storage and utilization must also be considered. Pretreatment breaks down the lignin layer and chemical properties of lignocellulosic matter, increasing its resistibility to degradation by enzymes and bacteria during AD [24, 60]. Untreated lignocellulosic raw matter are bulky and difficult to feed into conventional biogas digesters [119]. It is highly required to select appropriate pretreatment process for a sustainable conversion into bioenergy [120]. Table 2 shows the advantages of subjecting organic feedstock to pretreatment stages.

Table 2 Advantages of Substrate Pretreatment

S. No.	Merit of Pretreatment	Reference
1.	It enhances degradation of substrates and increase process efficiency	[34]
2.	Reason for sustainable conversion of feedstock into renewable energy source	[120]
3.	Remove potential inhibitors in feedstock, decrease crystallinity of cellulose and increase its porosity	[60]
4.	Lowering the degree of polymerization	[40]
5.	Reduce the required retention time (RT) for AD	[69]
6.	Accelerate hydrolysis	[121]
7.	Increase the accessible surface area and consequently improve CH_4 production	[31, 122]

Ideally, pretreatment methods are grouped into physical, chemical, biological and combined methods [31, 34, 59, 84, 100, 123].

2.3.1. Physical Pretreatment

Alternatively, physical pretreatment is known as mechanical pretreatment. Since substrate particle sizes directly influence AD, the sole aim of carrying out physical pretreatment is to reduce the sizes of raw materials, thereby increasing the surface area for hydrolyzing enzymes, enhancement of heat and mass transfers and in knowing the viscosity of the slurry [15, 34, 124–126]. The technique is popular and involves the use of knives, blades and hammers to grind, chip, mill, crumble, cut and shred biomass into small particles before AD [6]. Mechanical pretreatment method is a technique applied to change the appearance or structure of the biomass by mechanical means including extrusion, comminution/milling (e.g. ball

milling), steam explosion, liquid hot water pretreatment, microwave irradiation and ultrasonic treatment [47, 84, 122]. Figure 2 shows a shredded paper before and after pretreatment.

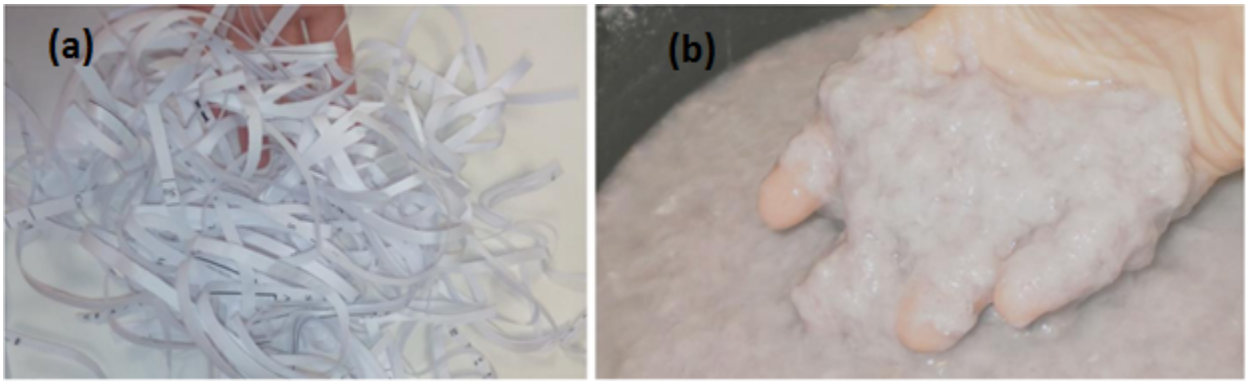

Figure 2: Paper Pretreatment: (a) Shredded Paper Before Pretreatment and (b) Paper Pulp After Pretreatment [84]

Extrusion involves the use of an extruder which subjects the lignocellulosic biomass to a series of treatments, such as sudden pressure drop, heating and mixing [127]. Thermal pretreatment involves the use of steam or hot water at 50–250°C to effect cell wall disintegration through the breaking of the hydrogen bonds that maintain mechanical strength of the biomass [128, 129]. This can further be sub-divided into low temperature (< 110°C) and high temperature (> 110 °C) reactions [6]. Another type of thermal pretreatment technique is high pressure steam explosion, required for disrupting the lignocellulosic structure of substrates [38]. It requires a very high pressure (5-60 bar) and temperature in the range of 160–250°C [127]. Liquid hot water pretreatment uses elevated temperature (140-220°C) and pressure to keep H_2O in liquid state [130]. Also called hydrothermal or pressurized hot water pretreatment, with benefits such as reduction in the risk of inhibitors production (e.g. furfural), increase enzyme accessibility and the ability to efficiently solubilize hemicellulose and lignin [15, 16, 131]. Microwave irradiation is quick in disintegrating sludge, as well as ensuring its solubilization and degradability. It destroys the faecal coliforms and *Salmonella spp.* and also increase the hydrolysis rate of lignocellulosic matter, especially straw. Other physical pretreatment approaches for sludge disintegration such as pulse electric fields, grinding, high-pressure homogenization, microwave irradiation, lysis centrifuges and ultrasonication were highlighted by [31]. Microwave irradiation heating and ultrasonic pretreatment can transform the internal microstructure of straw [130] as depicted in Figure 3.

Figure 3: Wheat straw (a) Before and (b) After Physical Treatment [30]

2.3.2. Chemical Pretreatment

Chemical pretreatment is based on the application of acid or base to improve raw material degradation rate as well as to break down the covalent bond of the lignocellulose [100, 130]. Acid treatment disrupts the Van der Waals, hydrogen and covalent bonds that bind the molecules of the organic matter before decomposition using either sulfuric (H_2SO_4), hydrochloric (HCl), formic, nitric acid (HNO_3), phosphoric acid (H_3PO_4), hydrogen peroxide (H_2O_2) and/or ethanoic acid (CH_3COOH) [38, 127, 132]. High-concentration acid pretreatment is done at low temperature whereas low-concentration pretreatment is carried out at high temperatures [68]. Alkali treatment method causes swelling of the fibers thereby conditioning the biomass to efficiently serve the AD process at different concentrations of lime ($Ca(OH)_2$), sodium hydroxide (NaOH), sodium carbonate (Na_2CO_3), sodium bicarbonate ($NaHCO_3$), aqueous ammonia ($NH_3{\cdot}H_2O$), potassium hydroxide (KOH), urea or NH_3 solution by soaking or spraying on the raw material surface [24, 132–134]. Alkaline pretreatment with ozone (O_3) (ozonolysis) and H_2O_2 has been reported to have the same effect with the forgone base compounds [31, 120, 132].

In general, chemical pretreatment are limited in application due to high cost of chemicals and pose environmental side effect [34, 59]. It is fact, that chemical pretreatment with alkali is better than acid pretreatment. Volume of acid/base, time and reaction temperature cannot be the same for all feedstock, as mass of feedstock taken for pretreatment is based on researcher's discretion. For instance, [135] had tested 3 different chemical pretreatment techniques, namely organosolv, N-methyl morpholine N-oxide (NMMO) and alkaline pretreatment for 15g, 7.5g and 16g of wheat straw respectively, at different temperature, molarity of chemicals and reaction time.

2.3.3. Biological Pretreatment

Biological pretreatment entails applying micro-organisms (fungi, archaea, protozoa and bacteria) and enzymes to organic matter to break down lignin and hemicellulose [100, 136]. Growth and metabolism of anaerobic fungi (*Piromyces spp.*, phylum *Neocallimastigomycota*, *Saccharomyces cerevisiae*, white and soft rot fungi) are crucial factors to their effective utilization [127]. White rot fungi is the most prominent microbe extracted from decaying wood that is used in biological pretreatment [6]. Source of *Neocallimastigomycota* are faeces and digestive tracts of various large mammal herbivores (e.g. elephants, goats, rhinoceros, horses, buffalos, cows, camels, and sheep) as well as reptiles and mice. Glycoside hydrolases, carbohydrate esterases and polysaccharide lyases are various enzymes used for this technique [136]. [137] also views the utilization of insect gut bacteria as a promising tool to enhance biogas generation.

Biological pretreatment is a slow process requiring longer RT, but beneficial, as it accelerates the hydrolysis process, has less energy consumption, long pretreatment cycle, has mild reaction conditions, needs efficient biological bacterium agent and cover large area [68, 130]. Application of biological pretreatments has been patronized in recent years because of the complex composition of lignocellulosic resources persistent in anaerobic environments, desire to reduce hydraulic retention times and the wish to increase the net carbon conversion rates [138]. Biological pretreatments can be divided into three parts including enzymatic, anaerobic and aerobic [70]. Biological pretreatment effect the necessary changes much better than physical and chemical pretreatment, but needs efficient bacterium agent [130]. Huge operational cost and high energy demands are the major disadvantages associated with physical, chemical and thermal pretreatments, which make those pretreatment technologies unsuitable and almost impractical [120].

2.3.4. Combined Pretreatment Method

Sometimes one substrate is subjected to two pretreatment methods simultaneously, implying a combined pretreatment procedure. Often times, a combination of physical and chemical methods are applied because they are faster and easier to implement [70, 84, 100]. Such combinations has synergistic pretreatment effect and functions better than single method given that an environmentally friendly pretreatment method is desired [121, 122]. But combinations sometimes, comes with unique disadvantages; for instance, chemical treatment has pollution consequences while biological treatment is challenging to monitor; but a combination of the two carries the two drawbacks together [139]. Pretreatment period beyond 3-30 days is not conducive according to [24]. Objectives, any disintegration/pretreatment technology is poised to achieve are basically, release of organic substrate (increase in COD solubilization), elimination of foaming in digestion chambers and secondary settling tanks, increase in the biogas yield, and access to trapped organic substances inside the biomass [121].

Composting could also be applied as a pretreatment technique prior to biogas production, but composting may lead to organic matter degradation and consequently reduced biogas yield during the AD process and so, partial composting has been suggested to avoid organic matter loss [140]. Major reasons why some feedstock are not ideal for biogas production is that they are difficult to digest by microorganisms, they exhibit slow digestion rate and are contaminated by inhibitors [60]. The goal of the pretreatment steps is to facilitate the digestion process by removing these barriers.

2.3.5. Additives

Certain adsorbents, enzymes or catalyst may be added to the bioreactor housing the feedstock for AD to optimize the yield of CH_4 as well as stabilize the process. Pectin, silica gel, bentonite, tale powder, activated carbon, kaolin, gelatin and polyvinyl alcohol are examples of adsorbents that can work the talk [69]. Examples of

biological catalysts are plants, crop residues, weeds, microbial culture, powdered leaves, legumes and cellulolytic strains of bacteria. Among these legumes are *Acacia auriculiforms*, *Eucalyptus tereticonius*, *Gulmohar*, *Dalbergia sisoo* and *Leucacena leucocephala* – capable of stimulating 18-40% increase in biogas production [141]. Production was also reported to grow up to 8.4-44% using cattle dung plus cellulolytic bacterial strains like actinomycetes [141]. Rumen fluids are rich in cellulolytic and methanogenic bacteria which are used as biostarters to shorten maximum biogas production time and increase production [87]. Enzymes are typically biocatalyst such as lyases, oxidoreductases, hydrolysases, transferases, ligases and isomerases for enhancing biomass disintegration biologically [121]. The most commonly explored catalyst are magnetite, silica gel, zeolite, and natural clinoptilolite [48]. In [142], guar gum's ability to enhance biogas production from coal has been demonstrated.

2.4. Stages of Degradation

AD process consist of four stages, which are in the order of hydrolysis, acidogenesis, acetogenesis and methanogenesis, transitioned by various set of microbes [45, 59, 67, 73, 115, 129, 143–145]. The acidogenesis and acetogenesis stages are sometimes coupled together as the acidification step making it a three stage process of hydrolysis, acidification and methanogenesis [131]. Two stage AD involves two separate bioreactors for acidogenesis and methanogenesis [69, 128].

2.4.1. Hydrolysis

Hydrolysis is the first step as well as the rate-limiting step of the AD process [4, 16, 58, 129]. Here, insoluble complex organic hydrocarbon polymers (such as carbohydrates, lipids, polysaccharides, proteins and nucleic acids) are converted or depolymerized into simple, soluble, low molecular weight simple sugars or monosaccharides, long chain fatty acids, amino acids, purines and pyrimidines by hydrolytic bacteria (e.g. *Clostridium*, *Micrococci*, *Bacteroides*, *Butyrivibrio*, *Fusobacterium*, *Selenomonas*, and *Streptococcus*, among others) by secreting enzymes such as cellobiase, amylase, lipase, cellulose, xylanase and protease [34, 45, 49, 69]. In the process, cellulose is hydrolyzed to glucose while hemicellulose are decomposed to monosaccharides like xylose, glucose, galactose, arabinose and mannose [77]. If the feedstock contains carbohydrate, hydrolysis stage is just few hours, but if the substrate is composed of fats and protein, it takes a few days [4]. It is often said that hydrolysis is the limiting step, specifically, when a high lignin feed material is used.

2.4.2. Acidogenesis

Usually, acid production is the second step in all AD process of organic waste. It is possible to divide this stage into acidogenesis and acetogenesis [4]. The fastest reaction is the acidogenesis phase [31, 127]. In this stage monomers or long chain molecules from hydrolytic stage are degraded into volatile fatty acids (VFAs) (e.g. acetic, butyric, propionic and valeric acids), acetate, alcohol and other short-chain fatty acids, H_2, alcohols and CO_2 by fermentative microorganisms (e.g. *Streptococcus*, *Lactobacillus*, *Bacillus*, *Escherichia coli*, *Salmonella*, *Clostridium*, *Ruminococcus*, *Bacillus*, *Escherichia*, *Bacteroïdes*, *Enterobacter*, etc) [15, 138]. These microorganisms are called acidogens or acidogenic bacteria. The precursors for CH_4 production in the process are acetic and butyric acids [45, 49]. Acidogenesis is primarily characterized by the buildup of lactate, ethanol, propionate, butyrate and higher VFAs called electron sink or intermediate products [49, 145]. Therefore, bacterium responsible for the hydrolysis and acidogenesis are facultative and obligate anaerobic bacteria [38]. Acidogenesis is followed by acetogenesis, a sub-stage where organic acids and alcohols are converted to acetate together with CO_2 and H_2 by two co-existing groups of acetogens including, syntrophic acetogenic bacteria producing H_2, acetate and CO_2 from VFAs and homoacetogens converting CO_2 and H_2 to acetate [31, 127, 146]. Again, it can be said that *Syntrophobacter* are propionate-utilizing acetogens while *Syntrophomonas* are butyrate-utilizing acetogens which are bacteria belonging to the genera *Acetobacterium woodii* and *Clostridium aceticum* [15, 49, 146]. Normally, bacteria require time (delay period known as dead time) before processing materials fed to digester tanks before biogas/methane is produced [21]. This period is technically referred to as the lag phase and had been incorporated to almost all microbial growth kinetic models in the literature to estimate the length of time microorganisms spend in reactors before growth and biogas production is observed.

2.4.3. Methanogenesis

Methanogenesis is the most critical as well as rate-limiting stage, all through the AD process that result in

long start-ups of up to 3 months step [138, 145]. It constitutes the last stage of AD in which methanogens generate CH_4 from the final products of acetogenesis [42]. As CH_4 is produced, stability and performance of the process is considered up to par. Methane yield from various feedstock can be measured in m^3/kg VS, dm^3/kg TS or any simple unit of volume as shown in Table 3.

Table 3: Summary of Biomass and Their Methane Yield [4, 42, 145]

Substrate type	Methane yield (m^3/kg VS)	Substrate type	Methane yield (m^3/kg VS)
Iponnoea stem	0.426	Grass	0.190-0.467
Poplar wood	0.33	Clover grass	0.290-0.390
Hemp	0.355-0.409	Switchgrass	0.140-0.298
Sunflower	0.154-0.400	Hay	0.236-0.281
Oilseed rape	0.240-0.340	Peanut hull	0.112-0.182
Potatoes	0.275-0.426	Cauliflower stems	0.331
Potato skin	0.267	Beet leaves	0.231
Sugar beet	0.236-0.381	Citrus waste	0.137
Fooder beet	0.420-0.500	Orange peel	0.230-0.332
Barley	0.353-0.658	Maize	0.259
Triticale	0.337-0.555	Onion skin	0.4
Alfalfa	0.340-0.500	Cucumber waste	0.309
Ryegrass	0.390-0.410	Fluted pumpkin peel	0.161-0.164
Nettle	0.120-0.420	Cattle slurry	0.156-0.240
Straw	0.242-0.324	Water hyacinth	0.362
Leaves	0.417-0.453	Pulp and paper mill sludge	0.429
Cattle manure	0.2-0.25	Food waste	0.440-0.480
Pig manure	0.25-0.35	Kitchen waste	0.7
Poultry manure	0.3	*Arthrospira platensis*	0.293
Carrot waste	0.417	*Chlamydomonas reinhardtii*	0.387
Carrot petioles	0.309	*Chlorella kessleri*	0.218
Banana fruit and stem	0.529	*Dunaliella salina*	0.42
Banana peeling	0.277-0.411	*Dunaliella salina*	0.323
Tomato waste	0.42	*Spirulina sp.*	0.424
Sorghum	0.42	Green algae	0.31
Corn stover	0.36	*Chlorella sp.*	0.264
Paddy straw	0.367	*Monoraphidium sp.*	0.264
Millet straw	0.39	*Chlorella vulgaris*	0.150-0.350
Wheat straw	0.270-0.383	*Isochrysis galbana*	0.338
Vegetable waste	0.19-0.40	*Selenastrum capricornutum*	0.209
POME	0.5-0.55	*Scenedesmus sp.*	0.351

Methanogens needs nitrogen to make up for their protein requirements, leading to the production of CH_4 by three groups of methanogens, namely acetotrophic, methylotrophic and hydrogenotrophic [129]. Acetotrophic methanogens (include, *Methanonococcus mazei*, *Methanothrix soehngenii* and *Methanosarcina barkeri*) decompose acetate into CH_4 and CO_2 [45, 69, 127] via the Equation (1).

$$CH_3COOH \rightarrow CH_4 + CO_2 \quad (1)$$

Hydrogenotrophic bacteria such as *Methanospirillum hungatei* and *Methanoculles receptaculi* consume H_2 to yield CH_4 [34] via Equation 2 and 3.

$$CO_2 + 4H_2 \rightarrow CH_4 + 2H_2O \quad (2)$$
$$4CO + 2H_2O \rightarrow CH_4 + 3CO_2 \quad (3)$$

Methylotrophic methanogens changes methyl or trimethylamine specie of a given substrate into CH_4 through Equation 4 and 5 pathway [129]:

$$3CH_3OH + 3H_2 \rightarrow 3CH_4 + 3H_2O \quad (4)$$
$$4(CH_3)_3N + 6H_2O \rightarrow 9CH_4 + 3CO_2 + 4NH_3 \quad (5)$$

Majority of components of biogas are generated during the methanogenic phase, which is seriously affected by temperature, pH, substrate type and feeding rate [4]. Other factors, namely, substrate complexity, process complexity, low productivity, poor stability and inefficient biodegradability impede CH_4 production from AD [67, 69]. AD is not the only area bacteria has economic advantage. Oil-eating bacteria can help degrade oil spilled on the environment, a process known as bioremediation [147].

3. Equations to Estimate Biogas Yield

The methane production rate (MPR) and gas production rate (GPR) are two main defining factors of AD performance. To measure biogas yield, inlet tap of a graduated burette containing paraffin oil and the outlet pipe of a biodigester connected to the top of the burette are open. The generated gas will then displace some volume of the paraffin oil in the graduated burette – thus volume of gas produced can then be taken as the volume of biogas yield. By implication, volume of paraffin oil displaced is proportional to the volume of gas yield as described by [131]. In large biogas plants, this volume is recorded daily in m³/day (SI units). In 2016, IRENA computed gas production across a wide range of RTs and temperatures and came up with Equation (6) to evaluate biogas yield per day.

$$G = \frac{Y \times V_d \times S}{1000} \quad (6)$$

Where, G = biogas production (m³/day), V_d = digester volume (m³), S = initial conc. of volatile solids in the slurry (kg/m³) and Y = yield factor (based on temperature and feedstock RT). If the yield value is measured in terms of volatile solids, it can be corrected to m³/day units by multiplying it by mass flowrate of the volatile solids in the feed, in accordance with [21] and as given in Equation (7).

$$\dot{V}_{BG} = \dot{m}_{VS} \times Y_{BG} \quad (7)$$

Where $\dot{V}_{BG}$ = estimated biogas production rate (m³ biogas/day), $\dot{m}_{VS}$ = mass flow rate of volatile solids contained in feed material (kg volatile solid/day), Y_{BG} = biogas yield (m³ biogas/kg volatile solid) and V = recorded volume of the biogas (ml). Normalized volume of biogas ($mLgVS_{substrate}^{-1}day^{-1}$) measured from water displacement method, similar to paraffin oil displacement method by [131] can be estimated base on Equation 8 [66],

$$V_N = \frac{V \times 273 \times (760 - P_w)}{(273+T) \times 760} \quad (8)$$

$$P_w = P(T) = 0.61121 \times 7.500617 \times \exp\left[\left(18.678 - \frac{T}{234.5}\right)\left(\frac{T}{257.14+T}\right)\right] \quad (9)$$

where, V_N = volume of the dry biogas at standard temperature and pressure (mL_N), $P(T)$ = vapor pressure (mmHg), T = temperature at the ambient space (⁰C), and P_w = water vapour pressure can be estimated according to the modified Buck equation or Equation (9). Digital biogas flowmeters is more easier to use compared to the displacement method; or the Hohenheim Biogas Yield Test method reported by [148].

3.1. Biogas Yield from Livestock and Crop Residue

Equations to estimate biogas yield for specific feedstock like manures, livestock waste and crop residue has also been presented. For instance, volume of biogas generated annually for manures analyzed in Brazil was estimated using Equation 10 [149],

$$Q_{BGM} = \frac{I_M . NA . f_M . \varepsilon}{1000} \quad (10)$$

where, I_M = manure generation rate of the animal herd (kg/hr), NA = number of animal herds in all territory, f_M = factor of biogas production (m³/t), 1000 = factor for unit adjustment, ε = collection efficiency in bio-digester {[149] adopted a value of 90%}, and Q_{BGM} = biogas flow produced by AD of manure (m³/yr). Alternatively, theoretical biogas produced from animal manures can be estimated based on Equation (11) [5, 32, 150],

$$TPB = M \times AC \times TS \times EB_{TS} \quad (11)$$

where, TPB = biogas production (m³/yr), M = amount of manure available from the animals (kg/yr), TS = percentage of total solids that can be found in animal manure, AC = coefficient of availability and EB_{TS} = predicted biogas production per kilogram of the total solids (m³/kg TS). Though the content of the livestock waste is not defined, the theoretical biogas production from livestock waste can be predicted using Equation 12 [16],

$$\mathrm{BP} = \frac{\mathrm{N_T \times VS \times B_0 \times CV \times 365}}{10^6} \quad (12)$$

where, BP = theoretical biogas potential (TJ y^{-1}), N_T = total population of the livestock, VS = volatile solid part of the waste (kg d^{-1}), B_0: CH_4 potential of the livestock waste (m³ kg^{-1}), and CV = caloric value of biogas assuming 60% CH_4 composition (MJ m^{-3}). Biogas potential from crop residue can be determined using equations 13, 14 and 15 [16],

$$\mathrm{R} = \mathrm{C_p} \times \mathrm{RPR} \quad (13)$$

$$\mathrm{RPR} = \frac{\mathrm{R}}{\mathrm{Y}} \quad (14)$$

$$\mathrm{M} = \mathrm{R} \times \mathrm{TS} \times \mathrm{VS} \times \mathrm{MP} \quad (15)$$

where, R = total available crop residue (tonnes, t), C_p = amount of crop produced (t y^{-1}), RPR = residue to yield ratio, Y = yield of product (t ha^{-1} y^{-1}), M = CH_4 produced (m³ y^{-1}), TS = total solid (%), VS = volatile solid (%) and MP = methane potential (m³ kg^{-1} VS). Moles of CH_4 gas or biogas produced can be evaluated using the simple ideal gas equation if the pressure, volume and temperature (PVT) conditions are known [151] and is evaluated using Equation (16).

$$\mathrm{n} = \frac{\mathrm{PV}}{\mathrm{RT}} \quad (16)$$

where, n = number of moles of gas, P = pressure (hPa), V = volume of gas (ml), R = molar gas constant (8.314 J/mol K), and T = temperature (K). Metric volume capacity of CH_4 gas production (specific yield) is given in Equation 17 [28].

$$\mathrm{V_s} = \frac{\mathrm{B_0 S_0}}{\mathrm{HRT}}\left[1 - \frac{\mathrm{K}}{\mathrm{HRT}(\mu_{\mathrm{max}}) - 1 + \mathrm{K}}\right] \quad (17)$$

Where V_s = CH_4 gas metric volume capacity (specific yield) (m³/day), K = kinetic coefficient, B_0 = the highest CH_4 gas production capacity (m³/kg), S_0 = the concentration of volatile solid in the input material (kg/m³), HRT = Hydraulic Retention Time (day), and μ_{max}: maximum specific growth rate of organisms per day.

3.2. Biogas Energy Potential

It is also possible to estimate the amount of electricity that can be generated from biogas, knowing the CH_4 content of the gas and the amount of biogas produced yearly. The biogas-generated energy potential can be calculated according to Equation 18 [12],

$$\mathrm{E_{biogas}} = \mathrm{C} \times \mathrm{CH_4} \times \mathrm{BP} \times \eta \quad (18)$$

where, E_{biogas} = quantity of electricity or heat energy produced (kWh year^{-1}), C = lower calorific value of methane (MJ/m³), CH_4 = methane content (%), BP = amount of biogas produced per year or the biogas potential (m³ year^{-1}) and η = overall efficiency of the conversion of biogas (%). Most potent GHG is CH_4 with a greenhouse effect that is 25 times more powerful than CO_2 [68]. In the Literature, the main source of greenhouse gas emission of CH_4 from AD technology happens as a result of leakage of the reactor and it is up to 5%. The GHG methane emission due to leakage (M_{CH_4}) is presented in Equation 19 [32],

$$\mathrm{M_{CH_4}} = 0.05 \times \mathrm{CH_4(AD)} \times 0.717 \quad (19)$$

where, 0.717 kg/m³ = density of CH_4 and $CH_4(AD)$ = actual volume of CH_4 produced from the AD plant. Methane leakage can also be determined using Equation 20 [16],

$$\mathrm{CH_4} = \mathrm{CH_{4_{produced}}} \times \left(\frac{1}{\mathrm{CE}} - 1\right) \quad (20)$$

where, $CH_{4_{produced}}$ = annual biogas production per digester (m³ y^{-1}) and CE = CH_4 collection efficiency. Quantity of CO_2 emissions from biogas are predicted according to Equation 21 [16],

$$\mathrm{CF_B} = \mathrm{Q_{B_i}} \times \mathrm{C_i} \times \mathrm{EF_c} \times \frac{44}{12} \quad (21)$$

where, CF_B = CO_2 emission from biogas consumption (tonne of CO_2), Q_{B_i} = quantity of biogas consumed (m³), C_i = calorific value of biogas per unit volume released (TJ m^{-3}), and EF_c = carbon emission factor for biogas (tonne TJ^{-1}). A spreadsheet calculator to estimate biogas production and the operational revenue and costs for UK-based farm-fed anaerobic digesters has been developed by [21]. The calculator is first compared with literature

reported data, and then applied to the digester unit on a UK Farm to demonstrate its use in a practical setting [21].

4. Utilization of Biogas

The cell gas or typically biogas is employed domestically, locally or for an entire nation in multitude of areas or applications [144]. The gas can be transformed and valorized into diverse forms of energy including power, heat, liquefied natural gas, compressed natural gas or may perhaps be considered as a fuel [152]. Crude biogas is purified using methods including water washing, pressure swing absorption, selexol adsorption, amines gas treatment [1, 143] and/or a simple laboratory setup illustrated in [153]. Particular gaseous species can also be removed, in the case of moisture removal using analytical grade sodium sulphate (Na_2SO_4), CO_2 removal using 15% NaOH solution or iron oxide removal of H_2S [92]. Table 4 gives two major areas biogas finds applications.

Table 4: Applications of biogas in the Energy Sector and Biotechnology [21, 39, 70, 154]

Domain	Uses
Renewable and sustainable energy	✓ Methanol, ethanol, higher alcohols ✓ Biohydrogen ✓ Compressed biogas ✓ Heat and electricity ✓ Diesel ✓ Gasoline ✓ Jet fuels ✓ Fuel cells ✓ Stirling engines ✓ Dual fuel engines ✓ Micro-gas turbines
Biotechnology	✓ Paraffins, naphthenes, aromatics ✓ Organic silicon compounds ✓ Digestate as organic fertilizers

Renewable natural gas (RNG) or biomethane is a methane-rich biogas or biogas that has been upgraded or refined to get rid of CO_2, water vapor and traces of other gases to meet natural gas standards [45, 50, 147, 149, 151, 155]. Such gas will then be a substitute for natural gas in applications and can also be upgraded catalytically to synthesis gas [34, 156]. Apart from heating in Table 4, as refined fuel, it finds application in cooking, lighting and running vehicles [27, 34, 136, 145, 157]. For instance, the service of a biogas-powered train named 'Biogastaget Amanda' has been employed since 2005 in Sweden; and by 2007, the number of vehicles fueled with upgraded biogas is around 12,000 worlwide. Around 1800s, Louis Pasteur discovered that biomethane could be deployed for lighting and heating; though doing that is wasteful and constitute a pollution [40, 41]. It is fitting to apply biogas for cooking as it is faster than firewood or charcoal stoves [144].

In the chemical industry, upgraded biogas also replaces biogas for chemical production [15, 139]. To minimize cost, gas generators or biogas-powered electricity plants are ambitiously targeted by rural and urban areas of developing and developed countries, especially European nations as alternative renewable energy [15, 28, 137]. Worldwide, installed capacity of biogas for electricity generation is estimated to reach 22,040 megawatts (MW) by 2025 even though economic feasibility is still a major barrier [5, 139]. The co-byproduct of the AD process is the digestate, a slurry which can be sold as fertilizer, specifically called biofertilizer for additional revenue [27, 135]. All these are advantages associated with the production of biogas. Table 5 presents the merits and demerits linked to biogas use and synthesis.

Table 5: Advantages and Disadvantages Governing Production and Utilization of Biogas [15, 41, 45]

Merits	Demerits
[1]. Substitute for other fuels	[1]. Involves seeding
[2]. Plant occupy small area	[2]. Microbes are temperature sensitive
[3]. Limits greenhouse gases (GHGs)	[3]. Weather sensitive (limited output below 15℃)
[4]. Avert deforestation	[4]. Not attractive industrially (not economically feasible)
[5]. Cheaper technology	
[6]. Diverse feedstock	
[7]. Long service years (up to 20 years)	

[8]. Can be locally built
[9]. Sanitation and waste management
[10]. As organic fertilizer
[11]. Energy for rural and urban inhabitants
[12]. Employment creation

It is obvious that disadvantages associated with the use and production of biogas or biomethane is not one that limit its manufacture as more and more plants are built yearly across continents of the globe, because those challenges can easily be addressed.

5. Factors Affecting Biogas Yield

Biogas yield is simply the resulting biogas output per unit mass of substrate or volatile solid [21]. Factors influencing the production of biogas are feedstock type, pH, VFAs, tank volume, RT, pressure, organic loading rate (OLR), chemical oxygen demand (COD), temperature, trace elements/nutrients, carbon to nitrogen (C/N) ratio, inoculation ratio, moisture content, microbial proliferation, pretreatment, additives, alkalinity and particle size [27, 28, 38, 42, 64, 121, 136, 137, 158]. Normally, how these parameters are carefully chosen is crucial to optimizing AD for biogas production [129].

5.1. pH

The most significant parameter affecting the digestion of organic waste feedstock is pH [68]. The alkalinity is a critical indicator of stability and survival of microorganisms in AD process, as it has a great stimulating effect and should be kept within 2500 to 5000 mg/l [141, 145]. A ±0.5 pH fluctuation can significantly affect reaction kinetics and gas yield. Hence, in modern plants, pH controllers are installed to check possible fluctuations.

AD occurs at optimum neutral pH of 7 [11, 68, 69]. The fraction of CO_2 in the digester gas, concentration of VFA, alkalinity of the system and bicarbonate concentration are compounds/agents causing pH change in digesters [73, 145]. Low pH can inhibit bacterial growth and gas generation causing system failure or low buffering capacity [42]. High pH is no different. Therefore, pH should be kept within a range of 6.0-8.0 [47]. [31] and [38] all reported a value of pH within the range affirmed by [67]. The 3 bacterial degradation stages discussed earlier, functions at specific pH range. Microorganisms involved in hydrolysis require a pH of around 6.0 [68]. Acidogenic bacteria operates at optimum pH of 5.5-6.5 [73, 127]. Acetogenic bacteria survive at pH range of 6.0-7.0 while slow growing methanogenic bacteria requires an optimum pH of 6.5-8.2 [66, 134].

5.2. C/N Ratio

Carbon (C) and nitrogen (N) are one of the most crucial nutrients/elemental compositions to watch during AD fermentation and are scientifically presented as ratios, termed carbon to nitrogen (C/N) ratio [42, 124]. Nitrogen-containing compounds such as nucleic acid, urea or uric acid and proteins are often converted to NH_3 during microbial decomposition [33, 58, 69]. In that case, the level of NH_3 in the biodigester plays a critical role in the stability of the process [159]. It can act as a pH neutralizer against VFAs. On the contrary, high amount of NH_3 intoxicate the microorganisms and increase pH which then inhibit further growth [34, 58, 68].

It is necessary therefore, to examine the effect of low and high C/N ratio in the fermentation process. High C/N ratio depletes nitrogen desired by the AD process, causes slow degradation and result in reduced biogas yield [43, 73, 141]. FW is known to be rich in nitrogen [151]. Low C/N ratio in FW lead the digester to a 'sour' situation, reduce pH in the AD system and accumulate inhibitors such as NH_3 [43, 51, 141]. For hydrolysis, optimum C/N ratio is between 16/1 and 45/1 while C/N ratio is in the range of 20–35 or 20-30 for methanogenesis [4, 37, 123, 160]. To adjust the C/N ratio, FW from slaughterhouses, MSW and food processing industries that are partly rich in protein and fat can be mixed and fed to the reactor [129]. Natural clinoptilolite have also been used as means to adjust the C/N ratio in AD system [47]. The C/N ratio of some raw materials for AD has been detailed in Table 6.

Table 6: C/N ratio Levels of Various Feed Materials [4, 54, 59, 60, 123, 126, 131]

Substrates/materials	C/N ratio	Substrates/materials	C/N ratio
Cow dung	16-25	Rice straw	51-67
Poultry manure	5-15	Wheat straw	50-150
Pig manure	6-14	Straw (rice, wheat)	70
Sheep dung	30-33	Whole grain	20-24
Elephant dung	43	Whole plant ensilage	35-70
Horse manure	20-40	Sugar cane bagasse	140-150
Rabbit manure	17.9	Corn stalks/straw	50-56
Deer manure	25.72-30.06	Oat straw	48-50
Kitchen waste	25-29	Sugar beet/sugar foliage	35-40
Fruits and vegetable waste	7-35	Fallen leaves	50-53
Food waste	3-17	Seaweed	70-79
Peanut shoots/hulls	20-31	Algae	75-100
Waste cereals	16-40	Sawdust	200-500
Grass/grass trimmings	12-16	Potatoes	35-60
Grass ensilage (meadow grass, clover)	14-22	Waste from sawmills	511
Alfalfa	12-17	Paper	173
Slaughterhouse waste	22-37	Human excreta	8
Goat manure	10-20	Water hyacinth	25
Mixed FW	15-32	Municipal solid waste	40
Sludge	6	Mulberry leaves	14.85
Saw dust	>200	Mushroom residue	21.96-23.11
Silkworm	11.28		

5.3. Retention Time

In carrying out design and optimization of AD systems, retention time (RT) is one of the parameters to consider [129]. It is divided into a hydraulic retention time (HRT) taking care of the liquid phase or solid retention time (SRT) denoting the time spent by the microbial culture in the digester [68]. By definition, HRT or hydraulic loading rate (HLR) is the mean time spent by the feedstock in the biofermenter, whereas SRT is the mean time the solid bacteria or microorganism spend in the digester [40, 44, 57, 58, 73]. If the feedstock and microbial mixed cultures are available in the same phase, then HRT = SRT [129]. Mathematically, RT can be evaluated based on the active volume of the digester tank and the volume feed flow rate [21, 27]. Both RTs are presented in Equation 22 and 23,

$$HRT = \frac{V_{DT}}{Q_{feed}} \quad (22)$$

$$SRT = \frac{V_{DT} \times X}{Q_{feed} \cdot X_x} \quad (23)$$

where, V_{DT} = active volume in the digester tank (m^3), Q_{feed} = influent flow rate (m^3/day), X = cell concentration in the reactor (mg/l), and X_x = concentration in flow out of the reactor (mg/l). Equation 22 is based on [4, 34, 140, 150] while Equation 23 is according to [64]. RT should not be too short or too long. Short RTs constitute a risk of flushing out unfermented feedstock, cell intoxication, accumulation of VFAs, low CH_4 yield and even process failure [48]. Long RTs causes slow gas yield, death of microorganisms due to depleted nutrients and insufficient usage of the feedstock [34, 40, 123]. Longer RTs has been reported by [46] to be about 250 days in Austria and 150 days in Germany by law. RTs are sometimes selected based on the ambient temperature condition of the host environment or bacterial survival temperature. The RTs are 10-50 days for mesophilic, 60–120 days in psychrophilic and 14-16 days in thermophilic conditions [68, 77, 161]. Mean RT for animal waste is 20–40 days while for organic waste, it is 60–90 days [42]. Based on the weather condition of tropical and cold countries, RTs fluctuates [68]. Therefore, factors that determines the required RT are process temperature, type of technology and waste composition [161].

5.4. Temperature

Temperature influence the survival of microbes in AD system and affects the rate of biological reactions [120, 128, 141]. It has a direct effect on microbial performance as each bacterial group has a specific temperature range they are active in [21, 162]. Again, the choice of temperature is gravely influenced by the climatic considerations [42]. Bacteria can survive in four different temperature conditions, namely; psychrophilic (10-25℃), mesophilic (20-45℃), thermophilic (45-70℃) and hyperthermophilic (~70℃) temperature regimes [4, 31, 37, 49, 57, 58, 67, 127, 150, 163].

Higher temperature, especially those between mesophilic and thermophilic regimes is a perfect environment for biological decomposition [68, 141]. Mesophilic enzymes functions at an optimum temperature of 37℃ [159]. Sometimes too high a reactor temperature leads to process failure and could denature sensitive enzymes. Very low digester temperature slows down AD and may not enhance an optimal catalytic efficiency of the enzymes [37, 67]. For ideal fermentation, the temperature should be kept above 30℃ [42]. The weather condition is capable of fluctuating the digester temperature, as such, in 2022, Ibrahima Toure developed a digital console to monitor temperature and humidity in bioreactors [3]. Sawdust to serve as insulators to digester tank bodies to maintain a room temperature for digestion had been studied using cotton yarn waste by [114].

Table 7 compares the merits and demerits of the two most common temperature regimes.

Table 7: Mesophilic Versus Thermophilic Process [49, 58, 69, 73, 127, 141]

	Advantages	**Drawbacks**
Mesophilic process	➢ Better process stability ➢ Less nitrate concentration in the sludge ➢ Decreasing free NH_3 ➢ Requires less thermal energy	➢ Low CH_4 yield ➢ High retention time (30-50 days) ➢ More clogging risk ➢ Bigger digester size ➢ High viscosity of influent ➢ Less degradation efficiency
Thermophilic process	➢ Less clogging risk ➢ Lower retention time (15-16 days) ➢ Lower viscosity ➢ Small size of digesters	➢ Larger investment ➢ Higher free NH_3 concentration ➢ Decreased stability process ➢ Higher thermal energy required

➢ Higher pathogen removing from substrate	➢ More sensitive to environmental changes
➢ Higher organic load-bearing capacity	➢ High nitrate concentration in the sludge
➢ Higher biogas production rate	
➢ Higher efficiency of degradation	

Generally, thermophilic range is advantageous over mesophilic range due to its faster degradation rate, high OLR and greater efficiency. The two are however tolerable to ±3℃ temperature fluctuation. But however, requires a continuous reacting system if OLR is the most important factor to the operator. Equation 24 [34, 69] is a correlation between the reaction rate and the biological process with temperature while the Arrhenius equation or Equation 25 [34, 164] gives the temperature dependency on CH_4 emission.

$$k_T = k_{20}\,\theta^{(T-20)} \quad (24)$$

$$\ln k = \ln A - \frac{E_a}{RT} \quad (25)$$

Where k_T = reaction rate constant at temperature, T, k_{20} = reaction rate constant at 20℃, θ = temperature activity constant, T = temperature (℃ or K), A = pre-exponential (frequency) factor, E_a = activation energy (J mol^{-1}), k = CH_4 emission rate (g CH_4 / kg VS/d), and R = universal gas constant (8.314 J/mol/K).

5.5. Organic Loading Rate

OLR is defined as the amount of biomass fed into the anaerobic digester per day per unit volume of the system during continuous feed [73, 141]. It is commonly expressed in terms of volatile solids, VS/m^3 day, COD, kg/m^3 day and total solid, TS/L day [150]. It is possible to calculate OLR using Equation 26 [31, 50], Equation 27 [162] or Equation 28 [159].

$$OLR = \frac{C}{HRT} \quad (26)$$

$$OLR = \frac{Q \times S_0}{V_l} \quad (27)$$

$$OLR = \frac{m \times c}{V_R \times 100} \quad (28)$$

where, C = feed concentration (g. VS/L), HRT = hydraulic retention time, V_l = volume of liquid in the reactor (l), Q = flow rate (l/h), S_0 = influent substrate concentration (g COD/L), m = amount of substrate in a unit time (kg d^{-1}), c = concentration of organic dry matter (% oDM), and V_R = volume of reactor (m^3). [38] and [67] have given a satisfactory detail on OLR. A very high OLR can cause process inhibition by rising the VFAs content, there causing irreversible acidification and failure of the process [69, 161, 162].

5.6. Pressure, COD and Inoculation Ratio

Literature report on the effect of pressure in AD systems is scanty, because majority of biogas storage systems, tank vessels and their covers are limited to holding low pressures (near atmospheric pressure) [129]. Except during compression to be stored in LPG cylinders, after purification and/or H_2O removal, that a pressure of up to 4 bar is maintained. However, during co-digestion of cow dung and Tofu liquid waste, [165] noticed that by controlling the internal gas pressure of the bioreactor, CH_4 output is found to be higher than the uncontrolled scheme. In another research carried out by [166], when a piston is used to maintain a reduced constant internal gas pressure, amount of CH_4 was observed to increase, thereby reducing the cost of chemical addition to maintain a stable pH. The measure of the amount of oxygen needed to oxidize all organic materials present to H_2O and CO_2 by titrimetric and photometric methods is known as COD [167]. COD content of several feedstock can be determined, in order to optimize the procedure, produce accurate result and improve efficiency of the process [167]. COD:N:Phosphorus (P) ratio had also been reported in the range of 300–600:5:1, which are needed to maintain the digester operation [168]. Inoculum supply to digesters undergoing AD, will help improve the overall gas yield, increase the CH_4 volume in biogas and reduce the retention period [169]. The inoculation ratio in AD is described as the substrate-to-microbe (S/M), feedstock-to-inoculum (F/I), or substrate-to-inoculum (S/I) ratio [170]. It can be calculated on the basis of volatile solids, total solids or loading rate. A greater inoculation ratio can lessen the start-up time and enhance the CH_4 yield [120].

5.7. Micro and Macro-nutrients

Sufficient amount of both macro- and micronutrients are vital for the continuous performance of the biogas process [150]. Heavy metals or macronutrients have very little effect on VFA composition but pose a major hazard to microbial activity and population [135]. For survival of microbes and stable multistage AD process, low concentrations of trace elements or micronutrients such as tungsten, cobalt, zinc, iron, chromium, nickel, molybdenum, magnesium and selenium are needed [58, 73]. In energy crops, nutrient concentration are inadequate causing problems such as acidification, low CH_4 yield and process instability in those crops [150].

5.8. Agitation/mixing

In order to create a homogeneous physical, chemical and biological environment in the anaerobic biodigester, mixing is necessary. Improper mixing destroys microbial cells, disturb the symbiosis of acetogens and methanogens, forms anaerobic granules, and make the process too costly [58, 73]. High speed mixing depletes biogas yields whereas low velocity mixing allows reactor to absorb the disruption due to shock loading [120]. It is beneficial when it is done properly to keep the temperature evenly distributed throughout, maintain a good mass transfer within the system, minimize hydraulic dead zone and foaming in the digester, dilute toxic and inhibitory agents in the reactor bringing them to a uniform composition, balance pH levels and prevent deposition of solids and scum in the AD process, and supply microorganisms with nutrients [4, 28, 58, 141, 145].

Several mixing techniques depending on digester design and substrate type had been described in the literature. Large-scale biogas plants uses pneumatic, mechanical and hydraulic mixing technologies [159]. Mechanical mixers uses shaft in which either impellers or propellers are attached [28]. They are however difficult and costly when installing them for FW. Main advantage of pneumatic mixing technology in which gas sparging is an example is that it decreases the complexity, requires no moving parts and low cost of maintenance [64]. It has the disadvantage of inability to mix around top and bottom of the digester. Installation of mixing devices, such as piston, nozzles and scrapers is another alternative used in some plants; as in Schmidt-Eggersgluss German-type of biogas plant, where nozzle is incorporated to flush slurry so as to achieve a desired mixing effect [169]. Optimal stirring inside the reactor depends on several factors such as size of the digester, mixing technology, operating temperature, the feedstock used and dry matter value of the substrate [159].

5.9. Inhibitors

Examples of inhibitors of detrimental effect to AD process are spices, detergents, mineral ions, oxygen and sulphide. Sulphides are output of sulphate-producing bacteria (SRB). These sulphides, will inhibit SRB or methanogens, accelerate oxidation of organics, decrease CH_4 formation, alter the pH value and reduce the efficiency of the methanogenic stage [159]. One example is H_2S which is considered poisonous in large quantity but acceptable in low amounts [64]. Heavy metals (iron, nickel, molybdenum, cadmium, lead, mercury, chromium, copper, cobalt and zinc) and light metals (potassium, magnesium, sodium, calcium and aluminum) are among nutrients crucial for survival of microbes in right concentrations [58, 150]. Smaller concentrations have stimulatory effect on microbes while higher concentration inhibit bacterial growth by disrupting the structure and function of the enzymes [58, 147]. Soluble salts of light and heavy metals are toxic substances [42].

Detergents, oxygen and spices could also inhibit AD systems. Detergents in small quantity is safe in anaerobic digesters but lead to death of microbes when in large quantity [120]. Anaerobic mediums require no oxygen; since oxygen are toxic to microorganism surviving in oxygen-free environment [150]. Spices are antimicrobial materials due to the presence of biochemical components such as thymol in thyme and oregano and eugenol in clove, carvacrol in oregano, allicin in garlic, vanillin in vanilla, cinnamic aldehyde in cinnamon and allyl isothiocyanate in mustard [73]. Other toxics are alkylbenzenes, halogenated benzenes, nitro benzenes, phenol, alkylphenols, nitrophenols, halogenated phenols, alcohols, halogenated alcohols, alkanes, aldehydes, ethers, ketones, halogenated aliphatics acrylates, carboxylic acids, amines, nitriles, amides, pyridine and its derivatives, as well as long-chain fatty acids [159].

5.10. VFA Concentration

VFAs are transitional output of CH_4 production pathway. The principal acids produced from AD are acetic acid, propionic acid and butyric acid [37, 38, 42, 168]. Accumulation of VFAs lowers the pH level and could occur when the speed of fermentation throughput is much slower compared to their formation [69, 159, 160]. Elevated levels of VFA levels are obviously linked to unconverted organic matter coming along with bad smells [11, 33, 171].

5.11. Moisture Content

Moisture content or H_2O content are relevant, in that they aid metabolism and activities of microorganisms. Based on moisture content, there are three types of feedstock used for AD of organic waste, which are wet, semi-dry and dry AD [43, 58]. Dry AD doesn't require substrate pretreatment into watery pulp and is simpler compared to wet AD [155]. When the moisture content exceeds 20%, dry digestion technology is preferable, especially for FW [150, 155]. A semi-dry AD process is employed for municipal waste recycling plants while wet fermentation technique is engaged in WWTPs. Also, based on the above moisture content type, the feedstock may be in form of high solids, thick slurry and thin slurry [50, 151].

Figure 4 summarily presents the review steps or pivotal headings in the text as formerly captured by [172].

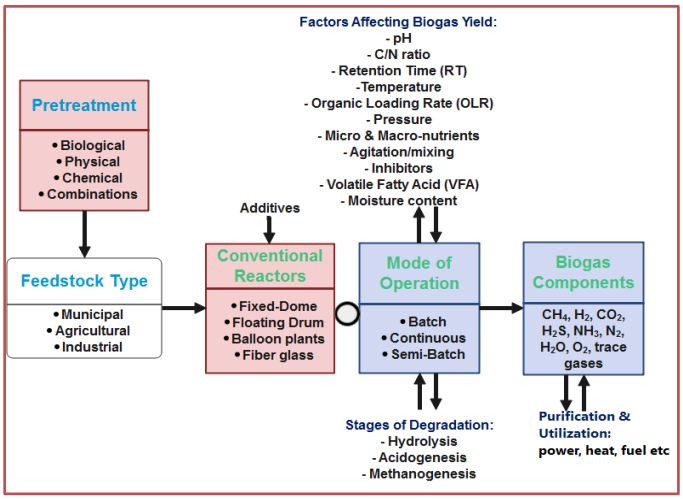

Figure 4: Important Basics in Biogas Production

Figure 4 also lists four types of digesters, among which is the floating gas holder type. Versions of the floating drum bioreactor is the Khadi Village Industries Commission (KVIC) model, Deenbandhu model (developed by Action for Food Production (AFPRO) in 1984) and the Pragati model (a combination of Deenbandhu and KVIC designs), all regarded as the Indian digesters [20, 54]. Utilization of the Deenbandhu model in India is around 90% over other models and a $2m^3$/day capacity of this plant costs ≅ $105.36, whereas KVIC will cost ≅ $184.38. Different balloon digester development technologies is prominent in application in countries like Belize, Kenya, Peru, Uganda, Bolivia and South Africa which are modifications to the first developed ones in the 1960s in Taiwan [168]. Biogas produced in large scale establishments is mostly stored in double membrane gas storage balloons, with a pressure of 25 bar and total volume of either 1040 m^3, 3000 m^3 or 4040 m^3 [19].

6. Conclusion

From the essential ingredients for a successful transition from biowaste to biogas presented here, it is obvious that lots of expertise is required before venturing into the process and while the process is ongoing. Hence, biogas production is a versatile aspect that requires adequate feasibility studies before setting up a plant and routine laboratory test to maintain a desired environment in the system. Perhaps, that explains the reason why countries that cannot survive the demanding nature and dynamics involve in the process, are yet to find the technology profitable and possibly the reason most of them became non-operational after few years of commissioning. The failure cannot be blamed only on the absence of expertise but also the lack of political will to address the energy needs in those areas, probably attributed to the low economic fortune of those countries. Researchers are however providing enormous inputs in almost all universities in the world to make government see the effectiveness of the process in addressing their energy needs.

The use of aquatic biomass apart from water hyacinth and pharmaceutical wastes are not that prominent compared to other biomass. Further studies are needed to eliminate pharmaceutical waste and invasive aquatic biomass from land and water bodies respectively, in order to solve pollution problems they pose. Modelling and simulation in this area has gained the needed

recognition from experts but can still be tabled for further concerns from researchers in relevant fields where limitations are highlighted. Already, several kinetic models of biogas production that can be used to forecast the potentials of a particular substrate for biogas production has been developed. The world is in the 10th decade since the inception of academic research in biogas production, but as old as biogas technology is, only few softwares had been developed so far to facilitate sensitivity analysis, optimization and better simplify the understanding of the process.

Conflict of Interest

The authors declare no conflict of interest.

References

[1] O. S. Joshua et al., "Fundamental principles of biogas product," *International Journal of Scientific Engineering and Research (IJSER)*, vol. 2, no. 8, pp. 47–50, 2014.

[2] S. Harirchi et al., "Microbiological insights into anaerobic digestion for biogas, hydrogen or volatile fatty acids (VFAs): A review," *Bioengineered*, vol. 13, no. 3, pp. 6521–6557, 2022, doi:10.1080/21655979.2022.2035986.

[3] I. Toure et al., "Design and realization of digital console for monitoring temperature and humidity in a biodigester," *International Advance Journal of Engineering Research (IAJER)*, vol. 5, no. 2, pp. 1–6, 2022.

[4] M. R. Atelge et al., "Biogas production from organic waste: Recent progress and perspectives," *Waste and Biomass Valorization*, vol. 11, pp. 1–22, 2018, doi:10.1007/s12649-018-00546-0.

[5] M. M. Ali et al., "Mapping of biogas production potential from livestock manures and slaughterhouse waste: A case study for African countries," *Journal of Cleaner Production*, vol. 256, no. 120499, pp. 1–18, 2020, doi:https://doi.org/10.1016/j.jclepro.2020.120499.

[6] T. M. Thompson, B. R. Young, S. Baroutian, "Advances in the pretreatment of brown macroalgae for biogas production," *Fuel Processing Technology*, vol. 195, no. 106151, pp. 1–12, 2019, doi:10.1016/j.fuproc.2019.106151.

[7] S. Alexopoulos, *Biogas systems: Basics, biogas multifunction, principle of fermentation and hybrid application with a solar tower for the treatment of waste animal manure*, vol. 5, no. 4, (Kavala Institute of Technology, 2012).

[8] O. Norouzi, A. Dutta, "The current status and future potential of biogas production from Canada's organic fraction municipal solid waste," *Energies*, vol. 15, no. 475, pp. 1–17, 2022, doi:https://doi.org/10.3390/en15020475.

[9] M. Talevi et al., "Speaking from experience: Preferences for cooking with biogas in rural India," *Energy Economics*, vol. 107, no. 105796, pp. 1–10, 2022, doi:https://doi.org/10.1016/j.eneco.2021.105796.

[10] V. P. Aravani et al., "Agricultural and livestock sector's residues in Greece & China: Comparative qualitative and quantitative characterisation for assessing their potential for biogas production," *Renewable and Sustainable Energy Reviews*, vol. 154, no. 111821, pp. 1–10, 2022, doi:https://doi.org/10.1016/j.rser.2021.111821.

[11] O. Kucher et al., "Energy potential of biogas production in Ukraine," *Energies*, vol. 15, no. 5, pp. 1–22, 2022, doi:https://doi.org/10.3390/en15051710.

[12] T. S. Nam et al., *Lab-scale biogas production from co-digestion of super-intensive shrimp sludge and potential biomass feedstocks*, vol. 6, no. 1, (2022).

[13] I. Syofii, D. P. Sari, "Production of biogas based on human fesses as an alternative energy for remote areas application," *Indonesian Journal of Engineering and Science*, vol. 3, no. 1, pp. 1–6, 2022, doi:https://doi.org/10.51630/ijes.v3.i1.29.

[14] P. Mukumba et al., "A possible design and justification for a biogas plant at Nyazura Adventist High School, Rusape, Zimbabwe," *Journal of Energy in Southern Africa*, vol. 24, no. 4, pp. 12–21, 2013.

[15] L. Ioannou-ttofa et al., "Life cycle assessment of household biogas production in Egypt: Influence of digester volume, biogas leakages, and digestate valorization as biofertilizer," *Journal of Cleaner Production*, vol. 286, no. 125468, pp. 1–14, 2021, doi:10.1016/j.jclepro.2020.125468.

[16] E. W. Gabisa, S. H. Gheewala, "Potential, environmental, and socio-economic assessment of biogas production in Ethiopia: The case of Amhara regional state," *Biomass and Bioenergy*, vol. 122, pp. 446–456, 2019, doi:10.1016/j.biombioe.2019.02.003.

[17] H. Gebretsadik, S. Mulaw, G. Gebregziabher, "Qualitative and quantitative feasibility of biogas production from kitchen waste," *American Journal of Energy Engineering*, vol. 6, no. 1, pp. 1–5, 2018, doi:10.11648/j.ajee.20180601.11.

[18] A. M. Abubakar, "Biodigester and feedstock type: Characteristic, selection, and global biogas production," *Journal of Engineering Research and Sciences (JENRS)*, vol. 1, no. 3, pp. 170–187, 2022, doi:https://doi.org/TBA.

[19] S. Gençoğlu, M. S. Bilgili, "Management of liquid digestate in biogas plants," *9th Global Conference on Environmental Studies (CENVISU-2021) Antalya, Turkey*, no. 14, pp. 51–62, 2021.

[20] Mohamed Samer, "Biogas plant constructions," in *Biogas*, (Cairo, Egypt: , 2012), 344–368, doi:10.5772/31887.

[21] A. Wu et al., "A spreadsheet calculator for estimating biogas production and economic measures for UK-based farm-fed anaerobic digesters," *Bioresource Technology*, vol. 220, pp. 479–489, 2016, doi:10.1016/j.biortech.2016.08.103.

[22] K. Rajendran et al., "A novel process simulation model (PSM) for anaerobic digestion using Aspen Plus," *Bioresource Technology*, 2014.

[23] J. A. Arzate, "Modeling and simulation of biogas production based on anaerobic digestion of energy crops and manure," (Technischen Universitat Berlin, Berlin, 2019).

[24] H. T. T. Nong et al., "Development of sustainable approaches for converting the agro-weeds Ludwigia hyssopifolia to biogas production," *Biomass Conversion and Biorefinery*, pp. 1–9, 2020, doi:https://doi.org/10.1007/s13399-020-01083-4.

[25] O. Khayal, "Main types and applications of biogas plants," *Nile Valley University*, pp. 1–11, 2019, doi:10.13140/RG.2.2.32559.69287.

[26] R. Jyothilakshmi, S. V Prakash, "Design, fabrication and experimentation of a small scale anaerobic biodigester for domestic biodegradable solid waste with energy recovery and

sizing calculations," *Procedia Environmental Sciences*, vol. 35, pp. 749–755, 2016, doi:10.1016/j.proenv.2016.07.085.

[27] IRENA, "Measuring small-scale biogas capacity and production." Abu Dhabi, United Arab Emirates, 2016.

[28] M. A. Fahriansyah, Sriharti, "Design of conventional mixer for biogas digester," *IOP Conference Series: Earth and Environmental Science*, pp. 1–8, 2019, doi:10.1088/1755-1315/277/1/012017.

[29] Z. Lenkiewicz, M. Webster, "How to convert organic waste into biogas: A step-by-step guide." wasteaid.org.uk/toolkit . (accessed: 14-Aug-2021).

[30] M. M. Jaffar, A. M. Rehman, "Wheat straw optimization via its efficient pretreatment for improved biogas production," *Civil Engineering Journal*, vol. 6, no. 6, pp. 1056–1063, 2020, doi:http://dx.doi.org/10.28991/cej-2020-03091528.

[31] D. Elalami et al., "Pretreatment and co-digestion of wastewater sludge for biogas production: Recent research advances and trends," *Renewable and Sustainable Energy Reviews*, vol. 114, no. 109287, pp. 1–23, 2019, doi:10.1016/j.rser.2019.109287.

[32] T. Chowdhury et al., "Latest advancements on livestock waste management and biogas production: Bangladesh's perspective," *Journal of Cleaner Production*, vol. 272, no. 122818, pp. 1–20, 2020, doi:https://doi.org/10.1016/j.jclepro.2020.122818.

[33] Y. Lahlou, *Design of a biogas pilot unit for Al Akhawayn University* (School of Science and Engineering, 2017).

[34] B. Bharathiraja et al., "Biogas production – A review on composition, fuel properties, feed stock and principles of anaerobic digestion," *Renewable and Sustainable Energy Reviews*, vol. 90, pp. 570–582, 2018, doi:10.1016/j.rser.2018.03.093.

[35] EIA, "Biomass explained." www.eia.gov-energyexplained-biomass-landfill-gas-and-biogas-php . (accessed: 14-Aug-2021).

[36] P. M. Njeru, P. Njogu, "Conversion of water hyacinth derived biogas to biomethane for electricity generation in Kenya: A waste to energy (WtE) approach," *Proceedings of 2014 International Conference on Sustainable Research and Innovation*, vol. 5, pp. 79–81, 2014.

[37] W. Fuchs et al., "Tackling ammonia inhibition for efficient biogas production from chicken manure: Status and technical trends in Europe and China," *Renewable and Sustainable Energy Reviews*, vol. 97, pp. 186–199, 2018, doi:10.1016/j.rser.2018.08.038.

[38] S. A. Neshat et al., "Anaerobic co-digestion of animal manures and lignocellulosic residues as a potent approach for sustainable biogas production," *Renewable and Sustainable Energy Reviews*, vol. 79, pp. 308–322, 2017, doi:10.1016/j.rser.2017.05.137.

[39] E. M. M. Esteves et al., "Life cycle assessment of manure biogas production: A review," *Journal of Cleaner Production*, vol. 219, pp. 411–423, 2019, doi:10.1016/j.jclepro.2019.02.091.

[40] I. V Yentekakis, G. Goula, "Biogas management: Advanced utilization for production of renewable energy and added-value chemicals," *Frontiers in Environmental Science*, vol. 5, pp. 1–16, 2017, doi:10.3389/fenvs.2017.00007.

[41] R. L. Granado et al., "Technology overview of biogas production in anaerobic digestion plants: A European evaluation of research and development," *Renewable and Sustainable Energy Reviews*, vol. 80, pp. 44–53, 2017, doi:10.1016/j.rser.2017.05.079.

[42] I. A. Raja, S. Wazir, "Biogas production: The fundamental processes," *Universal Journal of Engineering Science*, vol. 5, no. 2, pp. 29–37, 2017, doi:10.13189/ujes.2017.050202.

[43] HomeBioGas, "What is Biogas? A Beginner's Guide." www.homebiogas.com/what-is-biogas-a-beginners-guide- . (accessed: 13-Aug-2021).

[44] M. Parsaee et al., "A review of biogas production from sugarcane vinasse," *Biomass and Bioenergy*, vol. 122, pp. 117–125, 2019, doi:10.1016/j.biombioe.2019.01.034.

[45] S. M. A. Abuabdou et al., "A review of anaerobic membrane bioreactors (AnMBR) for the treatment of highly contaminated land fill leachate and biogas production: Effectiveness, limitations and future perspectives," *Journal of Cleaner Production*, vol. 255, no. 120215, pp. 1–12, 2020, doi:10.1016/j.jclepro.2020.120215.

[46] B. Stürmer et al., "Agricultural biogas production: A regional comparison of technical parameters," *Renewable Energy*, vol. 164, pp. 171–182, 2021, doi:10.1016/j.renene.2020.09.074.

[47] A. A. Abd, M. R. Othman, "Biogas upgrading to fuel grade methane using pressure swing adsorption: Parametric sensitivity analysis on an industrial scale," *Fuel*, vol. 308, no. 121986, pp. 1–10, 2022, doi:https://doi.org/10.1016/j.fuel.2021.121986.

[48] N. Aryal et al., "Microbial electrochemical approaches of carbon dioxide utilization for biogas upgrading," *Chemosphere*, vol. 291, no. 132843, pp. 1–10, 2022, doi:https://doi.org/10.1016/j.chemosphere.2021.132843.

[49] T. Yuan et al., "A review on biogas upgrading in anaerobic digestion systems treating organic solids and wastewaters via biogas recirculation," *Bioresource Technology*, vol. 344, no. 126412, pp. 1–10, 2022, doi:https://doi.org/10.1016/j.biortech.2021.126412.

[50] S. Jung et al., "Upgrading biogas into syngas through dry reforming," *Renewable and Sustainable Energy Reviews*, vol. 143, no. 110949, pp. 1–10, 2021, doi:https://doi.org/10.1016/j.rser.2021.110949.

[51] P. A. Westenbroek, J. I. Martin, "Anaerobic digesters and biogas safety." https://farm-energy.extension.org/anaerobic-digesters-and-biogas-safety/ . (accessed: 11-Mar-2021).

[52] S. K. Sheryazov et al., "Study of the parameters of biogas plants," *IOP Conference Series: Earth and Environmental Science, DAICRA 2021*, vol. 949, no. 012108, pp. 1–11, 2022, doi:10.1088/1755-1315/949/1/012108.

[53] M. F. I. Al Imam et al., "Development of biogas processing from cow dung, poultry waste, and water hyacinth," *International Journal of Natural and Applied Science*, vol. 2, no. 1, pp. 13–17, 2013.

[54] Oxfam, "Design, construction and maintenance of a biogas generator." Oxfam Technical Briefs, : 1–10, 2015.

[55] H. B. Møller et al., "Agricultural biogas production — Climate and environmental impacts," *Sustainability*, vol. 14, no. 1849, pp. 1–24, 2022, doi:https://doi.org/ 10.3390/su14031849.

[56] J. Mazurkiewicz, "Energy and economic balance between manure stored and used as a substrate for biogas production," *Energies*, vol. 15, no. 413, pp. 1–17, 2022, doi:https://doi.org/10.3390/en15020413.

[57] Ł. Małgorzata, J. Frankowski, "The biogas production potential from silkworm waste," *Waste Management*, vol. 79, pp. 564–570, 2018, doi:10.1016/j.wasman.2018.08.019.

[58] A. M. Abubakar, M. U. Yunus, "Reporting biogas data from various feedstock," *International Journal of Formal Sciences:*

Current and Future Research Trends (IJFSCFRT), vol. 11, no. 1, pp. 23–36, 2021, doi:10.5281/zenodo.6366775.

[59] K. Chaump et al., "Leaching and anaerobic digestion of poultry litter for biogas production and nutrient transformation," *Elsevier*, vol. 84, pp. 413–422, 2018, doi:10.1016/j.wasman.2018.11.024.

[60] R. J. Patinvoh et al., "Innovative pretreatment strategies for biogas production," *Bioresource Technology*, vol. 224, pp. 13–24, 2016, doi:10.1016/j.biortech.2016.11.083.

[61] H. L. de C. e Silva et al., "Lab-scale and economic analysis of biogas production from swine manure," *Renewable Energy*, vol. 186, pp. 350–365, 2022, doi:10.1016/j.renene.2021.12.114.

[62] G. Grasselli, T. Gal, J. Szendrei, "Possibilities to establish biogas plants in the Northern Great Plain Region, based on cattle and pig manure," *University of Debrecen, Centre for Agricultural Sciences and Engineering*, pp. 85–87, 2008.

[63] A. Aromolaran, M. Sartaj, R. M. Z. Alqaralleh, "Biogas production from sewage scum through anaerobic co-digestion: The effect of organic fraction of municipal solid waste and landfill leachate blend addition," *Biomass Conversion and Biorefinery*, pp. 1–17, 2022, doi:10.1007/s13399-021-02152-y.

[64] S. K. Srivastava, "Advancement in biogas production from the solid waste by optimizing the anaerobic digestion," *Waste Disposal & Sustainable Energy*, vol. 2, no. 2, pp. 85–103, 2020, doi:10.1007/s42768-020-00036-x.

[65] W. Wongarmat et al., "Anaerobic co-digestion of biogas effluent and sugarcane filter cake for methane production," *Biomass Conversion and Biorefinery*, vol. 12, pp. 901–912, 2022, doi:https://doi.org/10.1007/s13399-021-01305-3.

[66] S. Achinas, G. J. W. Euverink, "Elevated biogas production from the anaerobic co-digestion of farmhouse waste: Insight into the process performance and kinetics," *Waste Management & Research*, vol. 37, no. 12, pp. 1240–1249, 2019, doi:10.1177/0734242X19873383.

[67] L. Zhang, K. Loh, J. Zhang, "Enhanced biogas production from anaerobic digestion of solid organic wastes: Current status and prospects," *Bioresource Technology Reports*, vol. 5, pp. 280–296, 2019, doi:10.1016/j.biteb.2018.07.005.

[68] S. K. Pramanik et al., "The anaerobic digestion process of biogas production from food waste: Prospects and constraints," *Bioresource Technology Reports*, vol. 8, pp. 1–38, 2019, doi:10.1016/j.biteb.2019.100310.

[69] S. Mirmohamadsadeghi et al., "Biogas production from food wastes: A review on recent developments and future perspectives," *Bioresource Technology Reports*, vol. 7, no. 100202, pp. 1–37, 2019, doi:10.1016/j.biteb.2019.100202.

[70] U. Brémond et al., "Biological pretreatments of biomass for improving biogas production: An overview from lab scale to full-scale," *Renewable and Sustainable Energy Reviews*, vol. 90, pp. 583–604, 2018, doi:10.1016/j.rser.2018.03.103.

[71] M. Sivaprakash et al., "Analysis of bio-gas from kitchen waste," *International Conference on Advances in Materials, Computing and Communication Technologies 2385*, vol. 090001, no. January, pp. 1–7, 2022, doi:https://doi.org/10.1063/5.0070710 Published.

[72] N. Kaya, M. Bİlgİn, "Biogas production from potato peel," *Acta Biologica Turcica*, vol. 35, no. 1, pp. 49–56, 2022.

[73] N. Sahu et al., "Evaluation of biogas production potential of kitchen waste in the presence of spices," *Waste Management*, vol. 70, pp. 236–246, 2017, doi:10.1016/j.wasman.2017.08.045.

[74] M. M. El-Dalatony et al., "Pig- and vegetable-cooked waste oils as feedstock for biodiesel, biogas, and biopolymer production," *Biomass Conversion and Biorefinery*, pp. 1–11, 2022, doi:10.1007/s13399-021-02281-4.

[75] J. Jupesta, "Using biogas from palm oil residues to enhance energy access in Indonesia," *International Association for Energy Economics*, pp. 33–35, 2015.

[76] J. C. Ortega-bravo et al., "Biogas production from concentrated municipal sewage by forward osmosis, micro and ultrafiltration," *Sustainability*, vol. 14, no. 2629, pp. 1–11, 2022, doi:https://doi.org/10.3390/su14052629.

[77] M. C. Caruso et al., "Recent updates on the use of agro-food waste for biogas production," *Applied Sciences*, vol. 9, no. 6, pp. 1–29, 2019, doi:10.3390/app9061217.

[78] M. F. Al Ajlouni, M. Khattab, "Biogas and compost generated from organic waste at Al-Akaider landfill in Jordan," *Journal of Advanced Sciences and Engineering Technologies (JASET)*, vol. 5, no. 1, pp. 8–22, 2022, doi:https://doi.org/10.32441/jaset.05.01.02.

[79] M. Ben Oumarou et al., "Statistical modelling of the energy content of municipal solid wastes in Northern Nigeria," *Arid Zone Journal of Engineering, Technology and Environment (AZOJETE)*, vol. 12, pp. 103–109, 2016.

[80] M. B. Oumarou, A. M. Kundiri, M. Dauda, "Material recovery from wastes: An employment and poverty alleviation tool," *Arid Zone Journal of Engineering, Technology and Environment (AZOJETE)*, vol. 13, no. 1, pp. 66–76, 2017.

[81] A. M. Kundiri, B. A. Umdagas, M. B. Oumarou, "Characterization of leachate contaminants from waste dumpsites in Maiduguri, Borno State," *Arid Zone Journal of Engineering, Technology and Environment (AZOJETE)*, vol. 13, no. 1, pp. 140–148, 2017.

[82] C. Priadi et al., "Biogas production in the anaerobic digestion of paper sludge," *2013 5th International Conference on Chemical, Biological and Environmental Engineering (ICBEE 2013)*, vol. 9, pp. 65–69, 2014, doi:10.1016/j.apcbee.2014.01.012.

[83] A. Williams, "The production of bioethanol and biogas from paper sludge," (Stellenbosch University, 2017).

[84] C. Rodriguez et al., "Mechanical pretreatment of waste paper for biogas production," *Waste Management*, vol. 68, pp. 157–164, 2017, doi:10.1016/j.wasman.2017.06.040.

[85] S. Patra, "Aquatic weed resources in India and South-East Asia," *International Journal of Current Research (IJCR)*, vol. 5, no. 5, pp. 1343–1345, 2013.

[86] S. N. Ismail et al., "Invasive aquatic plant sciences of Chenderoh Reservoir, Malaysia," *IOP Conference Series: Earth and Environmental Science*, pp. 1–8, 2019.

[87] Winardi Dwi Nugraha, Syafrudin, and Lathifah Laksmi Pradita, "Biogas production from water hyacinth," in *Biogas-Recent advances and integrated approaches*, eds Abd El-Fatah Abomohra et al. (InTech Open, 2020), 15, doi:10.5772/intechopen.91396.

[88] M. Kawaroe et al., "Utilization of aquatic weed Salvinia molesta as a raw material for biogas production," *Jurnal Pengolahan Hasil Perikanan Indonesia (JPHPI)*, vol. 22, no. 2, pp. 209–217, 2019, doi:https://doi.org/10.17844/jphpi.v22i2.27891.

[89] D. O. Ezama, "Impact of water hyacinth infection in Nigeria inland waters: Utilization and Management," (The Maritime Commons: Digital Repository of the World Maritime University, Malmo, Sweden, 2019).

[90] S. D. F. Langa, M. P. Hill, S. G. Compton, "Agents sans

frontiers: cross-border aquatic weed biological control in the rivers of Southern Mozambique," *African Journal of Aquatic Science*, vol. 45, no. 3, pp. 329–335, 2020, doi:https://doi.org/10.2989/16085914.2020.1749551.

[91] Arne Jernelov, "Water hyacinths in Africa and Asia," in *The lon-term fate of invasive species*, (2017), 117–136, doi:10.1007/978-3-319-55396-2_9.

[92] P. Njogu et al., "Biogas production using water hyacinth (Eicchornia crassipes) for electricity generation in Kenya," *Energy and Power Engineering*, vol. 7, pp. 209–216, 2015, doi:http://dx.doi.org/10.4236/epe.2015.75021.

[93] W. D. Nugraha et al., "Biogas production from water hyacinth (Eichhornia crassipes): The effect of F/M ratio," *8th International Conference on Future Environment and Energy (ICFEE 2018)*, pp. 1–6, 2020, doi:10.1088/1755-1315/150/1/012019.

[94] V. B. Barua, A. S. Kalamdhad, "Water hyacinth to biogas: A review," *Pollution Research Paper*, vol. 35, no. 3, pp. 491–501, 2016.

[95] M. A. Enaboifo, O. C. Izinyon, "Potential of biogas production from floating aquatic weeds," *Periodical: Advanced Materials Research*, vol. 824, pp. 467–472, 2013, doi:https://doi.org/10.4028/www.scientific.net/AMR.824.467.

[96] A. A. Jimin, E. I. Magani, H. I. Usman, "Rainy season identification and species characteristics of aquatic macrophytes in the floodplains of River Benue at Markudi," *Journal of Sustainable Development in Africa*, vol. 16, no. 6, pp. 145–165, 2014.

[97] A. A. Eyo, "Review of possibilities of water hyacinth (Eichhornia crassipes) utilization for biogas production by rural communities in Kainji Lake Basin." http://hdl.handle.net/1834/18845 . (accessed: 07-Apr-2022).

[98] A. Hussner, "Alien aquatic plant species in European countries," *Weed Research*, vol. 52, no. 4, pp. 297–306, 2021, doi:https://doi.org/10.1111/j.1365-3180.2012.00926.x.

[99] A. Hussner et al., "Management and control methods of invasive alien freshwater aquatic plants: A review," *Aquatic Botany*, vol. 136, pp. 112–137, 2017, doi:http://dx.doi.org/10.1016/j/aquabot/2016/08.002.

[100] G. Bochmann et al., "Anaerobic digestion of pretreated industrial residues and their energetic process integration," *Bioprocess Engineering*, vol. 19, pp. 1–11, 2020, doi:https://doi.org/10.3389/fbioe.2020.00487.

[101] M. Rasel et al., "Industrial waste management by sustainable way," *Europa Journal of Engineering and Technology Research (EJ-ENG)*, vol. 4, no. 4, pp. 111–114, 2019, doi:http://dx.doi/10.24018/ejers.2019.4.4.1225.

[102] J. Semple, R. Hewett, D. Balzano, "Analysis: Europe's water/wastewater in numbers." waterworld.com/international/utilities/article/16201111/analysis-europes-waterwastewater-in-numbers . (accessed: 07-Apr-2022).

[103] H. E. Macedo et al., "Global distribution of wastewater treatment plants and their released effluents into rivers and streams," *Earth System Science Data*, pp. 1–33, 2022, doi:https://doi.org/10.5194/essd-2021-214.

[104] Budiyono et al., "Production of biogas from organic fruit waste in anaerobic digester using ruminant as the inoculum," *MATEC Web of Conferences*, vol. 156, no. 03053, pp. 1–5, 2018, doi:https://doi.org/10.1051/matecconf/201815603053.

[105] David O Olukanni, Gbemisola I Megbope, and Oluwatosin J Ogundare, "Assessment of biogas generation potential of mixed fruits solid waste," in *Biomethane through resource circularity*, 1st ed. , (CRC Press, 2021), 12.

[106] O. M. Alikhan, S. Khoramnejadian, S. M. Khezri, "Vegetable and fruit market wastes as an appropriate source for biogas production via anaerobic digestion process," *Zeitschrift fur Physikalische Chemie*, vol. 235, no. 11, pp. 1447–1453, 2021, doi:https://doi.org/10.1515/zpch-2020-1723.

[107] T. Aryanto et al., "Utilization of fruit waste as biogas plant feed and its superiority compared to landfill," *International Journal of Technology (IJTech)*, vol. 8, no. 8, pp. 1385–1392, 2017, doi:https://doi.org/10.14716/ijtech.v8i8.739.

[108] S. A. Hammid, N. Aini, R. Selaman, "Anaerobic digestion of fruit wastes for biogas production," *International Journal of Advance Research and Innovative Ideas in Education (IJARIIE)*, vol. 5, no. 4, pp. 34–38, 2019.

[109] A. O. Chinwendu et al., "The potential of biogas production from fruit wastes (watermelon, mango and pawpaw)," *World Journal of Advanced Research and Reviews (WJARR)*, vol. 1, no. 3, pp. 52–65, 2019, doi:https://doi.org/10.30574/wjarr.2019.1.3.0026.

[110] C. J. K. Kell, "Anaerobic co-digestion of fruit juice industry wastes with lignocellulosic biomass," (Stellenbosch University, 2019).

[111] Sharda Dhadse and Shanta Satyanarayan, "Role of microbial and organic amendments for the enrichment of methane production in bioreactor," in *Biogas: Basics, integrated approaches, and case studies [Working Title]*, eds Abd El-Fatah Abomohra and El-Sayed Salama (InTech Open, 2022), doi:10.5772/intechopen.102471.

[112] M. Lu et al., "Biogas generation in anaerobic wastewater treatment under tetracycline antibiotic pressure," *Scientific Report*, vol. 6, no. 28336, pp. 1–9, 2016, doi:10.1038/srep28336.

[113] J. P. Juanga-Labayen, I. V Labayen, Q. Yuan, "A review on textile recycling practices and challenges," *Textiles*, vol. 2, pp. 174–188, 2022, doi:https://doi.org/10.3390/textiles2010010.

[114] M. Twizerimana et al., "Anaerobic digestion of cotton yarn wastes for biogas production: Feasibility of using sawdust to control digester temperature at room temperature," *Scientific Research*, vol. 8, no. 7, pp. 1–15, 2021, doi:10.4236/oalib.1107654.

[115] K. Opwis, J. S. Gutmann, "Generation of biogas from textile waste waters," *Chemical Engineering Transactions (CEt)*, vol. 27, pp. 103–108, 2012, doi:10.3303/CET1227018.

[116] P. Kumar, S. Samuchiwal, A. Malik, "Anaerobic digestion of textile industries wastes for biogas production," *Biomass Conversion and Biorefinery*, vol. 10, pp. 715–724, 2020, doi:https://doi.org/10.1007/s13399-020-00601-8.

[117] A. Cruz-Salomon et al., "Biogas production from a native beverage vinasse using a modified UASB bioreactor," *Portal Komunikacji Naukowej*, vol. 198, pp. 170–174, 2017, doi:10.1016/j.fuel.2016.11.046.

[118] J. Wickham et al., "Anaerobic digestion of soft drink beverage waste and sewage sludge," *Bioresource Technology*, vol. 262, pp. 141–147, 2018.

[119] S. Mirmohamadsadeghi et al., "Pretreatment of lignocelluloses for enhanced biogas production: A review on influencing mechanisms and the importance of microbial diversity," *Renewable and Sustainable Energy Reviews*, vol. 135, no. 110173, pp. 1–19, 2021, doi:10.1016/j.rser.2020.110173.

[120] J. Kainthola, A. S. Kalamdhad, V. V Goud, "A review on

enhanced biogas production from anaerobic digestion of lignocellulosic biomass by different enhancement techniques," *Process Biochemistry*, vol. 84, pp. 81–90, 2019, doi:10.1016/j.procbio.2019.05.023.

[121] S. Wacławek et al., "Disintegration of wastewater activated sludge (WAS) for improved biogas production," *Energies*, vol. 12, no. 21, pp. 1–15, 2019, doi:10.3390/en12010021.

[122] Z. Kong et al., "Large pilot-scale submerged anaerobic membrane bioreactor for the treatment of municipal wastewater and biogas production at 25◦C," *Bioresource Technology*, vol. 319, pp. 1–12, 2021, doi:10.1016/j.biortech.2020.124123.

[123] S. M. M. N. Dehkordi et al., "Investigation of biogas production potential from mechanical separated municipal solid waste as an approach for developing countries (case study: Isfahan-Iran)," *Renewable and Sustainable Energy Reviews*, vol. 119, no. 109586, pp. 1–12, 2020, doi:10.1016/j.rser.2019.109586.

[124] S. Banerjee, N. Prasad, S. Selvaraju, "Reactor design for biogas production: A short review," *Journal of Energy and Power Technology (JEPT)*, vol. 4, no. 1, pp. 1–14, 2022, doi:10.21926/jept.2201004.

[125] K. O. Olatunji et al., "Modelling the effects of particle size pretreatment method on biogas yield of groundnut shells," *Waste Management & Research (WMR)*, pp. 1–13, 2022, doi:10.1177/0734242X211073852.

[126] S. Sarto, R. Hildayati, I. Syaichurrozi, "Effect of chemical pretreatment using sulfuric acid on biogas production from water hyacinth and kinetics," *Renewable Energy*, vol. 132, pp. 335–350, 2019, doi:10.1016/j.renene.2018.07.121.

[127] A. Abraham et al., "Pretreatment strategies for enhanced biogas production from lignocellulosic biomass," *Bioresource Technology*, vol. 301, no. 122725, pp. 1–13, 2020, doi:10.1016/j.biortech.2019.122725.

[128] K. Hagos et al., "Anaerobic co-digestion process for biogas production: Progress, challenges and perspectives," *Renewable and Sustainable Energy Reviews*, vol. 76, pp. 1485–1496, 2017, doi:http://dx.doi.org/10.1016/j.rser.2016.11.184.

[129] S. Sarker et al., "A review of the role of critical parameters in the design and operation of biogas production plants," *Applied Sciences*, vol. 9, no. 9, pp. 1–38, 2019, doi:10.3390/app9091915.

[130] Q. Yu et al., "A review of crop straw pretreatment methods for biogas production by anaerobic digestion in China," *Renewable and Sustainable Energy Reviews*, vol. 107, pp. 51–58, 2019, doi:10.1016/j.rser.2019.02.020.

[131] A. M. Uche et al., "Design and construction of fixed dome digester for biogas production using cow dung and water hyacinth," *African Journal of Environmental Science and Technology*, vol. 14, no. 1, pp. 15–25, 2020, doi:10.5897/AJEST2019.2739.

[132] T. H. Chowdhury, "Review on the pre-treatment methods of waste for anaerobic digestion," *The Seu Journal of Electrical and Electronic Engineering (SEUJEEE)*, vol. 2, no. 1, pp. 46–51, 2022.

[133] T. Liu et al., "Effects of liquid digestate pretreatment on biogas production for anaerobic digestion of wheat straw," *Bioresource Technology*, vol. 280, pp. 345–351, 2019, doi:10.1016/j.biortech.2019.01.147.

[134] F. Almomani, "Prediction of biogas production from chemically treated co-digested agricultural waste using artificial neural network," *Fuel*, vol. 280, no. 118573, pp. 1–13, 2020, doi:10.1016/j.fuel.2020.118573.

[135] G. Mancini et al., "Increased biogas production from wheat straw by chemical pretreatments," *Renewable Energy*, vol. 119, pp. 608–614, 2018, doi:10.1016/j.renene.2017.12.045.

[136] J. Vinzelj et al., "Employing anaerobic fungi in biogas production: Challenges & opportunities," *Bioresource Technology*, vol. 300, no. 122687, pp. 1–10, 2020, doi:10.1016/j.biortech.2019.122687.

[137] B. K. Show et al., "Insect gut bacteria: A promising tool for enhanced biogas production," *Reviews in Environmental Science and Bio/Technology*, pp. 1–25, 2022, doi:https://doi.org/10.1007/s11157-021-09607-8.

[138] A. O. Wagner, P. Illmer, "Biological pretreatment strategies for second-generation lignocellulosic resources to enhance biogas production," *Energies*, vol. 11, no. 1797, pp. 1–14, 2018, doi:10.3390/en11071797.

[139] A. A. Rajput, C. Visvanathan, "Effect of thermal pretreatment on chemical composition, physical structure and biogas production kinetics of wheat straw," *Journal of Environmental Management*, vol. 221, pp. 45–52, 2018, doi:10.1016/j.jenvman.2018.05.011.

[140] M. Tabatabaei et al., "A comprehensive review on recent biological innovations to improve biogas production, Part 1: Upstream strategies," *Renewable Energy*, vol. 146, pp. 1204–1220, 2019, doi:https://doi.org/10.1016/j.renene.2019.07.037.

[141] O. Raymond, U. Okezie, "The significance of biogas plants in Nigeria's energy strategy," *Journal of Physical Sciences and Innovation*, vol. 3, pp. 11–17, 2011.

[142] H. Guo et al., "Biodegradation of guar gum and its enhancing effect on biogas production from coal," *Fuel*, pp. 1–9, 2021, doi:10.1016/j.fuel.2021.122606.

[143] A. Pigosso et al., *Fundamentals of anaerobic digestion, biogas purification, use and treatment of digestate* (Concordia, SC: Brazilian Agricultural Research Corporation-Embrapa Swine & Poultry, 2022).

[144] B. K. McCabe, T. Schmidt, *Integrated Biogas Systems: Local Applications of Anaerobic Digestion Towards Integrated Sustainable Solutions* (Queensland, Australia: IEA Bioenergy, 2018).

[145] B. Singh, Z. Szamosi, Z. Siménfalvi, "Impact of mixing intensity and duration on biogas production in an anaerobic digester: A review," *Critical Reviews in Biotechnology*, vol. 40, no. 4, pp. 508–521, 2020, doi:10.1080/07388551.2020.1731413.

[146] C. P. C. Bong et al., "The characterisation and treatment of food waste for improvement of biogas production during anaerobic digestion– A review," *Journal of Cleaner Production*, vol. 172, pp. 1545–1558, 2017, doi:10.1016/j.jclepro.2017.10.199.

[147] A. M. Abubakar, M. Alhassan, "History, adverse effect and clean up strategies of oil spillage," *International Journal of Applied Sciences: Current and Future Research Trends (IJASCFRT)*, vol. 11, no. 1, pp. 31–51, 2021, doi:10.5281/zenodo.5557307.

[148] I. V Miroshnichenko, N. V Nikulina, "Designing a biogas plant for an educational and scientific livestock complex," *8th Scientific and Practical Conference "Biotechnology: Science and Practice"*, pp. 151–163, 2022, doi:10.18502/kls.v7i1.10117.

[149] I. F. S. dos Santos et al., "Assessment of potential biogas production from multiple organic wastes in Brazil: Impact on energy generation, use, and emissions abatement," *Resources, Conservation & Recycling*, vol. 131, pp. 54–63, 2018, doi:10.1016/j.resconrec.2017.12.012.

[150] N. Sawyerr et al., "An overview of biogas production: Fundamentals, applications and future research," *International*

Journal of Energy Economics and Policy, vol. 9, no. 2, pp. 105–116, 2019, doi:10.32479/ijeep.7375.

[151] J. Maroušek et al., "Advances in nutrient management make it possible to accelerate biogas production and thus improve the economy of food waste processing," *Energy Sources, Part A: Recovery, Utilization, and Environmental Effects*, pp. 1–10, 2020, doi:10.1080/15567036.2020.1776796.

[152] M. Tabatabaei et al., "A comprehensive review on recent biological innovations to improve biogas production, Part 2: Mainstream and downstream strategies," *Renewable Energy*, vol. 146, pp. 1392–1407, 2019, doi:https://doi.org/10.1016/j.renene.2019.07.047.

[153] D. Oladejo et al., "Pretreatment and optimization strategy for biogas production from agro-based wastes," *The International Journal of Engineering and Science (IJES)*, vol. 11, no. 3, pp. 14–20, 2022, doi:10.9790/1813-1103011420.

[154] B. Venturin et al., "Effect of pretreatments on corn stalk chemical properties for biogas production purposes," *Bioresource Technology*, vol. 266, pp. 1–36, 2018, doi:10.1016/j.biortech.2018.06.069.

[155] M. Khalil et al., "Waste to energy technology: The potential of sustainable biogas production from animal waste in Indonesia," *Renewable and Sustainable Energy Reviews*, vol. 105, pp. 323–331, 2019, doi:10.1016/j.rser.2019.02.011.

[156] N. Schiaroli et al., "Catalytic upgrading of clean biogas to synthesis gas," *Catalysts*, vol. 12, no. 109, pp. 1–28, 2022, doi:https://doi.org/10.3390/catal12020109.

[157] A. Z. Abdul, A. M. Abubakar, "Potential swing to natural gas-powered electricity generation," *International Journal of Natural Sciences: Current and Future Research Trends (IJNSCFRT)*, vol. 10, no. 1, pp. 27–36, 2021.

[158] A. Rafiee et al., "Biogas as an energy vector," *Biomass and Bioenergy*, vol. 144, no. 105935, pp. 1–10, 2021, doi:https://doi.org/10.1016/j.biombioe.2020.105935.

[159] A. Nsair et al., "Operational parameters of biogas plants: A review and evaluation study," *Energies*, vol. 13, no. 15, pp. 1–27, 2020, doi:10.3390/en13153761.

[160] J. Maroušek et al., "Advances in the agrochemical utilization of fermentation residues reduce the cost of purpose-grown phytomass for biogas production," *Energy Sources, Part A: Recovery, Utilization, and Environmental Effects*, pp. 1–11, 2020, doi:10.1080/15567036.2020.1738597.

[161] M. N. Usman, M. A. Suleiman, M. I. Binni, *Anaerobic digestion of agricultural wastes: A potential remedy for energy shortfalls in Nigeria*, vol. 4, no. 1, (Scholarena, 2021).

[162] M. Bakraoui et al., "Biogas production from recycled paper mill wastewater by UASB digester: Optimal and mesophilic conditions," *Biotechnology Reports*, vol. 25, pp. 1–8, 2020, doi:10.1016/j.btre.2019.e00402.

[163] S. O. Cinar et al., "Long-term assessment of temperature management in an industrial scale biogas plant," *Sustainability*, vol. 14, no. 612, pp. 1–17, 2022, doi:https://doi.org/10.3390/su14020612.

[164] A. H. Bhatt, L. Tao, "Economic perspectives of biogas production via anaerobic digestion," *Bioengineering*, vol. 7, no. 74, pp. 1–19, 2020, doi:10.3390/bioengineering7030074.

[165] A. R. I. Utami et al., "Analysis of the effect of internal gas pressure of an anaerobic digester on biogas productivity of a mixture of cow dung and tofu liquid waste," *The 9th National Physics Seminar-AIP onference Proceedings 2320*, vol. 2320, pp. 1–9, 2021, doi:https://doi.org/10.1063/5.0037446.

[166] B. R. Prajapati, R. K. Sharma, I. M. Amatya, "Effect of reduced gas pressure on yield of biogas and other physicochemical parameters," *International Journal of Energy and Environmental Engineering*, vol. 12, pp. 31–37, 2021, doi:https://doi.org/10.1007/s40095-020-00351-3.

[167] C. M. W. Harnadek, N. G. H. Guilford, E. A. Edwards, "Chemical oxygen demand analysis of anaerobic digester contents," *STEM Fellowship Journal*, vol. 1, no. 2, pp. 1–5, 2015, doi:10,17975/sfj-2015-008.

[168] Y. Y. Choong, K. W. Chou, I. Norli, "Strategies for improving biogas production of palm oil mill effluent (POME) anaerobic digestion: A critical review," *Renewable and Sustainable Energy Reviews*, vol. 82, pp. 2993–3006, 2018, doi:10.1016/j.rser.2017.10.036.

[169] K. V. Kumar et al., "A review on production of biogas, fundamentals, applications and its recent enhancing techniques," *Elixir International Journal*, vol. 57, pp. 14073–14079, 2013.

[170] A. Khadka et al., "Effect of the substrate to inoculum ratios on the kinetics of biogas production during the mesophilic anaerobic digestion of food waste," *Energies*, vol. 15, no. 834, pp. 1–16, 2022, doi:https://doi.org/10.3390/en15030834.

[171] M. Ghiandelli, "Development and implementation of small-scale biogas balloon biodigester in Bali, Indonesia," (KTH School of Industrial Engineering and Management, 2017).

[172] A. Mishra et al., "Multidimensional approaches of biogas production and up-gradation: Opportunities and challenges," *Bioresource Technology*, vol. 338, no. 125514, pp. 1–14, 2021, doi:https://doi.org/10.1016/j.biortech.2021.125514.

ABDULHALIM MUSA ABUBAKAR was awarded Degree (B.Eng.) in Chemical Engineering from University of Maiduguri (UNIMAID)-Nigeria on 27 September, 2018.

He works as graduate assistant (GA) with Modibbo Adama University (MAU), Yola-Nigeria. Other qualifications, some of which adds to his skill set are Certificate of Proficiency in Word Processing Packages (Computer Appreciation) (2016), Certificate of Completion in AutoCAD (2016 & 2017), Diploma Certificate in Oil & Gas Management (2017), Certificate of IT Training Course Completion (2018), Certificate of National Service (2019), Certificate of Learning in Occupational Health & Safety (2020), Data Science, Excel, Project Management Skills (2021) and Information Security (2022) . He is also a

member of reputed Engineering Bodies, such as IAENG and O3GP. He is also interested in C++ programming application in numerical problem solving in Chemical Engineering and had published papers in that regard.

KIMAN SILAS attended University of Maiduguri in Borno state, Nigeria and graduated with Bachelor's degree in Chemical Engineering in 2007. He obtained Master degree in Chemical Engineering in 2012 in University of Maiduguri in Borno state, Nigeria. He joined Universiti Putra Malaysia and obtained his PhD in Chemical Engineering in 2019.

He published many journal papers and is presently lecturing at the Department of Chemical Engineering, University of Maiduguri in Borno state, Nigeria. His specialty is in Renewable Energy and Environmental Engineering and an expert in CO_2 Capture, Waste Utilization, Biomass Conversion and Gas Cleaning. He is a registered member of the Council for the Regulation of Engineering in Nigeria (COREN) and Nigerian Society of Engineers (NSE).

Received: 19 January 2022, Revised: 18 February 2022, Accepted: 26 February 2022, Online: 12 April 2022

DOI: https://dx.doi.org/10.55708/js0104014

Human-Computer Interaction for Older Adults - a Literature Review on Technology Acceptance of eHealth Systems

Awais Ahmad [*,1], **Peter Mozelius** [2]

[1] Uppsala University, Department of Information Technology, Uppsala, 751 05, Sweden
[2] Mid Sweden University, Department of Computer and System Science, Östersund, 831 25, Sweden

*Corresponding author: Awais Ahmad, Stamvagen 70, 831 73, Östersund, Sweden , 0046 76 527 91 62, awais.ahmad@it.uu.se

ABSTRACT: The population of older adults globally increased during the last couple of decades. Due to these demographic changes, the need for medical care has also significantly increased. Despite the age-related disabilities and chronic diseases, most older adults prefer independent living in their home environment. Technology-enhanced systems and eHealth applications seem to provide some promising solutions for older adults' well-being and independent living. However, the adoption and acceptance of these applications for older adults are unclear and further research is needed in this area. This study was carried out as a literature review, to meet the aim of identifying and discussing important factors in the Human-computer interaction of eHealth for older adults. The overall research question for this study was: *What are the critical factors to consider for an improved human-computer interaction in technology-enhanced health care systems for older adults?* Findings indicate some important factors to address: personal integrity, trust, technology acceptance, accessibility of ICT and eHealth literacy. If the presented factors are considered and addressed, it would be easier to achieve the desired aim of independent living. The authors recommend a human-computer interaction that is older adults centred, with the involvement of older adults users in the design process. Proper education and training on the use of eHealth services are also of great importance. Finally, the technology-enhanced system should also provide good social and technological support to the users.

KEYWORDS: eHealth, Human-Computer Interaction, HCI, Older adults, Ageing well, Independent living

1. Introduction

In most parts of the world, the percentage of older adults increases rapidly, where the fastest growth can be identified in low- and middle-income countries [1, 2]. Today there are globally between 5-600 million people that are 65 years or older, with an estimated increase to around 1.5 billion by the year 2050 [3]. The older people get, the more they will be dependent on medical and social care. In the contemporary society, many older adults are living alone without any support from friends and family members [4].

There are a number of different terms used for the idea of older adults' right to stay healthy, and to have a rich and joyful life. Some of the most frequently used are successful ageing, active ageing, healthy ageing, positive ageing, productive ageing, competent ageing, and ageing well. These terms have often been combined with the concept of independent living, and the aim of a more cost-effective healthcare [5]. In a strive for consistency, this study has used the terms ageing well and independent living.

The rapid technological development in the 21st century has opened up many new opportunities for eHealth and home care. However, as highlighted by [6], new technology also creates new challenges and critical factors for user acceptance among older adults. Facilitated by an improved human-computer interaction (HCI), eHealth could offer a promising enhancement to traditional healthcare when the percentage of older adults further increases. This study, which builds on our earlier publication [7], has kept the same focus on investigating research studies on eHealth and their findings regarding critical HCI factors for older adults.

The aim of the study was to identify, analyse and discuss important factors in human computer interaction

of eHealth for older adults. The overall research question to answer was: *What are the critical factors to consider for an improved human computer interaction in technology enhanced health care systems for older adults?* For the more long-term objective, the results in this study could hopefully be used as a checklist in the development of eHealth services for older adults.

2. Ageing Well

As found in the large scale cross-sectional study by [8], older adults are concerned about how to age well. In a survey, respondents were asked if they ever had thought about ageing well, and whether their thoughts about ageing well had changed during the previous 20 years. In this respondent group where all persons were aged above 65 years, 90 % had previously thought about ageing well, and about 60% of the respondents said that their thoughts had changed during the previous 20 years. The conclusion of the study was that ageing well is a complex matter encompassing not only physical and functional health, but also psychological and social health [8].

Growing old involves multiple chronic diseases and age-related changes, where endocrine, inflammatory or immune, cardiovascular, and neuroanatomical factors also can cause depression. Late life depressions can have severe consequences, but in general depressions are less prevalent among older adults than what is the case for younger adults [9]. Furthermore, older adults' social isolation caused by living alone, having small social networks, and infrequent participation in social activities have also been identified as severe health risks [10].

Considering the rapid growth of older adults, several research studies have emphasised the importance of developing new user-friendly eHealth services to support the idea of ageing well [11]. Some recent research articles have pointed out that most older adults prefer to age in their home environments [12]. However, the involved contextual and psychosocial factors must be thoroughly investigated if the new e-health services should be successful, and add value for the well-being of older adults [13,14].

3. Method

The study design is inspired by the six-step method for literature reviews that has been outlined by [15]. The six ingoing steps are: 1. Selecting a review topic, 2. Developing the tools of argumentation, 3. Searching for literature, 4. Surveying the literature, 5. Critique and analysis of the found literature, and finally 6. Writing up the review with a presentation of results. The first step was carried out during intermissions of a seminar on eHealth, and the second step was a brainstorm session with ideas jotted down on a whiteboard. Step 3 to 6 were carried out iteratively including backward searches on interesting and relevant references in the found articles. In [16], the authors described the term backward search as "reviewing older literature cited in the articles yielded from the keyword search".

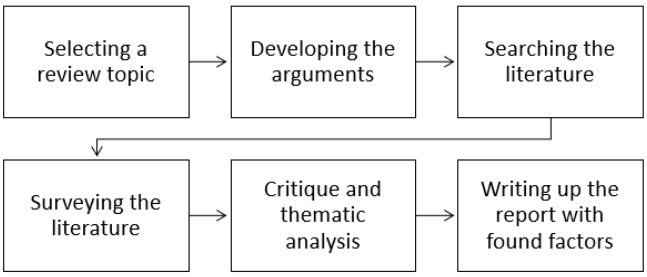

Figure 1: The used six-step method for literature reviews

To investigate the current state of Interaction design and HCI for older adults in the area of eHealth, Boolean searches were carried out, using different combinations of the keywords: 'Human Computer Interaction', 'HCI', 'eHealth', 'eServices', and 'Older adults'. The databases for the searches were and Google scholar and Scopus, and with a focus on articles published after 2010. However, some older articles were included when they had findings that could contribute to answer the research question [7]. Furthermore, in this new updated version the earlier result set has been updated with some relevant and more recent publications.

In the first search, with combinations of the keywords above, 456 articles were retrieved. Then authors conducted a screening and read all the article abstracts, with the result that 225 articles were excluded. The common denominator for exclusion was that the articles did not have a direct relationship to the aim and the research question. Later, the remaining 231 articles were further scrutinised to find out if they had a potential to answer the research question. 208 articles were classified as non-relevant and excluded in this step. The remaining 22 articles from the original search were then further categorised into primary articles and secondary articles. The criterion for a primary article is that it must address all important keywords, while a secondary article does not need to contain all the keywords. However, a secondary article had to contain specific and detailed information that would contribute to meet the research aim.

As a part of step 5 in the literature review, results have been thematically analysed and grouped with the aim of finding interesting themes to answer the research question, and to inspire future research. The thematic analysis was conducted as outlined in the article by [17] following the six phases that are listed in Table 1 below.

The first step in this process had the recommended focus of familiarising with the data [17], This immersion process was carried out by reading and rereading the retrieved articles and at the same time taking notes for the

further analysis, and to get ideas for the initial coding. Step two involved the start of the systematic analysis, and the initial coding. In [18], the authors have illustrated a thematic analysis as "a brick-built house with a tile roof, your themes are the walls and roof and your codes are the individual bricks and tiles".

Table 1: The six phases of the thematic analysis

Phase 1	Articles were read and reread while taking notes
Phase 2	Initial codes were generated in the selected articles
Phase 3	Codes were collated into preliminary themes
Phase 4	Themes were reviewed and cross-checked
Phase 5	Definitions and names were generated for all themes
Phase 6	Writing up the analytic narrative with found themes

In the next third step, the code bricks were aggregated into preliminary wall elements, with the idea of capturing "something important about the data in relation to the research question, and represents some level of patterned response or meaning within the data set" [17]. The following fourth involved the recommended quality checking, where the found codes and elements were checked for consistency, and for their potential to contribute to answer the research question. For this fourth step, [18] have facilitating five control questions to support the process:

1. Is this an element, a category, or just a code?
2. If it is an element or a category, what is the quality of this element or category?
3. What are the boundaries of the element or category?
4. Are there enough meaningful data to support this element or category?
5. Is the element or category coherent?

When the elements and themes or categories were checked, the fifth step handled the definition and naming of the themes. Finally, the sixth remaining step was to write up the presentation of the findings in the thematic analysis, a presentation that can be found below under 'Results and discussions'.

4. Selected Publications

Table 2 here below shows a chronological listing of the set of selected publications, with information about author(s), study location, and the column for the main study: findings and critical factors. The objective was to provide an up-to-date analysis of Interaction design and HCI in the area of eHealth services for older adults, which in this new version has been updated. At the same time, several relevant and interesting older articles were retrieved in the direct searches, and in the complementary backward searches.

Table 2: Primarily articles in the literature review

Authors	Location	Findings/factors
Henkemans et al. [19]	Netherlands United States	Visual sensing devices, video monitoring, Ethical considerations, Privacy, Sense of false confidence
Jung & Loria [20]	Sweden	Compatibility with citizen needs, User's trust in service provider
Rogers & Fisk [21]	United States	Understanding older adultism's needs, preferences, and desires for technology in their lives
Stojmenova et al. [22]	Slovenia	Technological experience, Education level, Lifestyle characteristics, Cognitive changes, Sensory processes
Lee & Coughlin [23]	Global-Literature review	Confidence, Emotion, Technical and social support, Affordability, Usability, Usefulness
Fischer et al. [24]	Global-Literature review	Privacy vs. Utility, Trust, Internet access, Assistive Technology
Vines et al. [25]	United Kingdom	Embracing alternative measures of success. An HCI research agenda shaped by older people
de Veer et al. [26]	Netherlands	Awareness, Internet skills, The role of social influence, Ease of use
Peek et al. [12]	Netherlands	Independent living, behavioural options, personal thoughts on technology use, influence of the social network, influence of organisations and the

		role of the physical environment
Axelsson & Wikman [13]	Sweden	Independence was critical among older adults in the sense of control and choice, when older persons use e-health services.
Ahmad et al. [27]	Sweden	Due to lack of IT literacy and experience, older adults have less acceptance of eHealth applications
Ma et al. [28]	Malaysia	Social influence, trust, familiarly of a given technology are the main factors of technology acceptance.
Bong et al. [29]	Norway	Older adults' participation and involvement in design of digital games is critical for technology acceptance.

In Table 2, all the listed articles have a direct relationship to both the aim and the research question, which qualify them to be 'primarily'. Many articles were found irrelevant for this study and excluded, but articles containing interesting details, or with an indirect relation, have been included in the analysis to get more details and to add nuances to the discussion. These 'secondary articles' have been listed separately below in Table 3.

Table 3: Secondary articles in the literature review

Authors	Location	Findings/factors
Rudd et al.[30]	United States	Patient Prospective, Cognitive changes affect the ability to use technology
Courtney et al. [31]	United States	Self-perception of health, physical condition, mental and emotional condition, anticipatory living, environmental influences, the perceived
		redundancy of the technology
Charness & Boot [32]	United States	Attitudinal barriers, Cognitive barriers, Privacy concerns, Age-related changes affecting technology use
Wagner et al. [33]	Canada	The impact of Person on Environment and the impact of Environment on Person.
Heart et al. [34]	Israel	Perceived usefulness, perceived impact, Perceived ease of use, Technological issues, Personal traits, Social issues, Facilitating issues
Xie et al. [35]	United States	e-health literacy and participatory design
Young et al. [36]	United States	Technological discomfort, Home-based health information technology, electronic health records, data security and confidentiality,
Latulipe et al. [37]	Korea	Behavioural intention, Data security and accuracy, Socio-Technological environment
Christopho rou et al. [11]	Cyprus	Usefulness, satisfaction and motivation

5. Findings and Discussions

This study had the aim of identifying, analysing and discussing determinant HCI factors in eHealth services for older adults.

An important main finding in the analysis was the identification of independent living as an overall key concept in designing eHealth systems for older papulation. Many of the selected studies have emphasised the importance of considering older adults' independence [12, 13, 9, 38, 39]. Independent living is the suggested overall umbrella concept that also has a relation to the other identified factors. In order to accomplish this independence, older adults must have a genuine control over their eHealth services [27, 29, 37, 39, 40]. Moreover, older adults using eHealth services have expressed that activities such as, voluntary work and hobbies are

significant determinants of independent living [12]. Figure 2 illustrates the main critical factors that may affect older adults' independent living.

Other identified factors that support independent living are to facilitate socialisation, communication, and to consider eHealth user's safety [2, 11, 41]. The study by [13], recommends that eHealth services should be implemented with the aim to strengthen older adults' mobility and self-management. Moreover, the analysis in this study identified independent living as the major aim for eHealth design for the elderly population. However, in the successful implementation of eHealth services, all the critical factors that are listed below have to be considered.

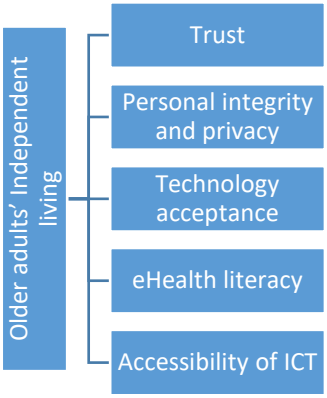

Figure 2: The critical factors that affect older adults' independent living

5.1. Trust

Findings clearly show that various forms of trust are a critical factor in HCI design for eHealth systems for older adults. One major factor is users' trust in the eHealth service providers. eHealth has some identified problems such as the misinterpretation of provided information, technical difficulties, and security and privacy issues. For these matters, the users' trust in the service provider has been pointed out as the main factor in several studies [20, 42]. Older adults' confidence in the interaction with high-technology devices seems to be generally lower if compared to younger people [43]. There are for various reasons a need for support, and a support that includes both technical and social aspects [23]. Trust was also established as a crucial factor in another study on eHealth systems in rural Bangladesh [44].

5.2. Personal integrity and privacy

As discussed in the study by [19], the perceived benefits of using eHealth interventions must be weighed against the perceived privacy concerns. The recommendation from this study is to minimise duration of monitoring technologies, and to never use more monitoring than the actual needs. As an example, a so-called point light camera can transmit images where activities can be distinguished without revealing any personal identity. This can be compared to the more detailed images captured with a video camera, where personal integrity definitely is an issue [19]. Not a surprising finding, but it has been pointed out that users are more willing to use the relatively non-intruding monitoring systems [39].

On the other hand, when the usefulness of eHealth services is perceived as high, users are willing to compromise on privacy. This is an important balance to handle for healthcare providers, the one between the implementation of monitoring systems, and older adults' privacy [31]. Without respect for personal integrity, the aim of independent living will never be achieved.

5.3. Technology acceptance

Older adults' attitudes towards the use of eHealth services are strongly dependent on the services' usefulness, the ease of use, and the general attitude toward using eHealth services [20, 24, 45]. This is not surprising since these are the major factors in the technology acceptance model (TAM). This study also found that the TAM model did not include the dependencies on the quality of internet connection, and on adequate information. The conclusion from the study on technology acceptance carried out by [19], is close to what was discussed in the previous section on trust. Older adults can definitely perceive the benefits of technology in their homes, but the acceptance is related to integrity issues related to monitoring technologies.

The older standpoint that the adoption of technology among older adults mainly is a matter of only costs and performance efficiency has been revised. In [23], the authors highlighted technology acceptance should be seen as a complex issue that is affected by several other factors. Other than usefulness and usability, the most important identified factors were support, emotion, independence, affordability, accessibility, experience and confidence. Regarding the more general eHealth services, a known hypothesis is the preparedness to use eHealth services is increasing for users with high level of ICT proficiency, however, a study by [46] determined that a better ICT experience might increase the intention to use the eHealth services. An explanation might be that older adults with a higher ICT proficiency, also have a good understanding in the risks involved in using eHealth services.

5.4. eHealth literacy

To design user-friendly and inclusive eHealth servises and systems, it is of utmost importance to understand the deficits that come with ageing. eHealth services must be easy to learn and use also for the target group of older adults [25, 47, 48]. However, even with an older adult centred design, eHealth services will hardly be self-explanatory and eHealth literacy is also dependent on proper training [35, 47]. The recommendation from the study by [32], is that the training initiatives for ageing

adults ought to consider the age-related changes in ability in the target group.

As brought up by many researchers in the field, an improved education with proper training is considered a fundamental factor for successful eServices for older adults [49, 50]. In an extension of this fundament, the author in study [30] had the remark that education and training is not enough even for adults that have graduated from high school. Furthermore, this study also suggested that new and modern technology such as touch screens and voice activation could be involved to facilitate older adults' use of eHealth services [30].

In the study [51], the authors observed that ageing has a direct relationship to the ability of understanding information. Older adults often have a reduced ability to use eHealth services and a generally low eHealth literacy. The presented recommendation in the study is to redesign eHealth systems, and that the related eHealth literacy issue should be addressed [51].

Relevant education with a pre-training that involves exercises related to the actual eHealth applications, would certainly improve older adults' intention and ability to use them. What also seems to be a plausible prediction is that the future will have a growing number of older adults who have used internet services on a regular basis. Persons that have started to use eServices early in life, will probably continue to use them as older adults [26].

5.5. Accessibility of ICT

As highlighted in the study [20], reliable internet access is a crucial factor, and there are a large number of variations of ICT infrastructures in different parts of the world. Stable access to technology has sometimes been neglected in eHealth design for older adults [23, 52]. When the underlying infrastructure that is taken for granted is missing, services can entirely fail. In many countries, this can be a barrier to solutions that have been successful in other parts of the world. Countries with low-income populations often have an internal digital division that demands specific design solutions to address technological obstacles [37]. Finally, as highlighted in the study [34], eHealth systems for older adults should preferably have a simple and user-friendly technical design and have a straightforward focus on demonstrating the valuable benefits.

6. Conclusion

This study shed light on the major determinants of acceptance and adoption of eHealth systems for older adults. Trust in technology and personal ability to use the eHealth systems, personal integrity and privacy, fear to use new technology, eHealth education and literacy, and accessibility of ICT infrastructure and services are of utmost importance.

Findings also highlighted that independent living and human well-being should be the overall aim of future eHealth, which also was a recommendation in the study by [45]. In order to accomplish this aim, the suggestion is, as highlighted in the studies [22] and [25], a human-centred eHealth design, where the older adults should be actively involved, and empowered in the design and development of eHealth systems and services. Finally, proper education and training on the use of eHealth services is also of great importance.

7. Future Work

This study shed light on the main critical factors for human-computer interaction in the area of eHealth services for older adults. The interesting next step would be to investigate in which sub-fields older adults have the largest need for eHealth services and telecare. Further research is needed to investigate if the identified factors are general for all diseases, or how might their significance be changed depending on different types of diseases?

Acknowledgement

We would like to thank Pär-Ove Forss, Head of the Computer and System Science Department at Mid Sweden University, for his kind support throughout this research process.

Conflict of Interest

The authors declare no conflict of interest.

References

[1] M. Tonelli and M. Riella, "Chronic kidney disease and the aging population," *Brazilian Journal of Nephrology*, vol.36, pp.1–5, 2014.

[2] F. P. Tajudeen, N. Bahar, T. Maw Pin, and N. I. Saedon, "Mobile technologies and healthy ageing: A bibliometric analysis on publication trends and knowledge structure of mHealth research for older adults," *International Journal of Human–Computer Interaction*, vol.38, no. 2, pp.118–130, 2022.

[3] K. A. Kline and D. M. Bowdish, "Infection in an aging population," *Current opinion in microbiology*, vol.29, pp.63–67, 2016.

[4] V. N. Stroetmann, T. Hüsing, L. Kubitschke, and K. A. Stroetmann, "The attitudes, expectations and needs of elderly people in relation to e-health applications: results from a European survey," *Journal of Telemedicine and Telecare*, vol.8, no. 2_suppl, pp.82–84, 2002.

[5] L. Foster and A. Walker, "Active and successful aging: A European policy perspective," *The gerontologist*, vol.55, no. 1, pp.83–90, 2015.

[6] C. Botella, E. Etchemendy, D. Castilla, R. M. Baños, A. García-Palacios, S. Quero, M. Alcaniz, and J. A. Lozano, "An e-health system for the elderly (Butler Project): A pilot study on acceptance and satisfaction," *CyberPsychology & Behavior*, vol.12, no. 3, pp.255–262, 2009.

[7] A. Ahmad and P. Mozelius, "Critical factors for human computer interaction of ehealth for older adults," Proceedings of the 2019 the 5th International Conference on e-Society, e-Learning and e-Technologies, pp.58–62, 2019.

[8] E. A. Phelan, L. A. Anderson, A. Z. Lacroix, and E. B. Larson, "Older adults' views of 'successful aging'—how do they compare with researchers' definitions?," *Journal of the American Geriatrics Society*, vol.52, no. 2, pp.211–216, 2004.

[9] A. Fiske, J. L. Wetherell, and M. Gatz, "Depression in older adults," *Annual review of clinical psychology*, vol.5, pp.363–389, 2009.

[10] E. Y. Cornwell and L. J. Waite, "Social disconnectedness, perceived isolation, and health among older adults," *Journal of health and social behavior*, vol.50, no. 1, pp.31–48, 2009.
[11] C. Christophorou, S. Kleanthous, D. Georgiadis, D. M. Cereghetti, P. Andreou, C. Wings, E. Christodoulou, and G. Samaras, "ICT services for active ageing and independent living: identification and assessment," *Healthcare technology letters*, vol.3, no. 3, pp.159–164, 2016.
[12] S. T. Peek, K. G. Luijkx, M. D. Rijnaard, M. E. Nieboer, C. S. van der Voort, S. Aarts, J. van Hoof, H. J. Vrijhoef, and E. J. Wouters, "Older adults' reasons for using technology while aging in place," *Gerontology*, vol.62, no. 2, pp.226–237, 2016.
[13] S. Wiklund Axelsson and A. Melander Wikman, "Ready for eHealth. Older Swedes' perceptions of eHealth Services: Using the PIADS scale as a predictor for readiness," *Technologies*, vol.4, no. 3, p.29, 2016.
[14] C. Robert, M. Erdt, J. Lee, Y. Cao, N. B. Naharudin, and Y.-L. Theng, "Effectiveness of eHealth nutritional interventions for middle-aged and older adults: Systematic review and meta-analysis," *Journal of medical Internet research*, vol.23, no. 5, p.e15649, 2021.
[15] L. A. Machi and B. T. McEvoy, "The literature review: Six steps to success (Third)," SAGE Publications, Inc, 2016.
[16] J. vom Brocke, A. Simons, B. Niehaves, B. Niehaves, K. Reimer, R. Plattfaut, and A. Cleven, "Reconstructing the giant: On the importance of rigour in documenting the literature search process," 2009.
[17] V. Braun and V. Clarke, "Using thematic analysis in psychology," *Qualitative research in psychology*, vol.3, no. 2, pp.77–101, 2006.
[18] V. Braun and V. Clarke, "Thematic analysis.," 2012.
[19] O. B. Henkemans, K. E. Caine, W. A. Rogers, A. D. Fisk, M. A. Neerincx, and B. D. Ruyter, "Medical monitoring for independent living: user-centered design of smart home technologies for older adults," Proc. Med-e-Tel Conf. eHealth, Telemedicine and Health Information and Communication Technologies, pp.18–20, 2007.
[20] M.-L. Jung and K. Loria, "Acceptance of Swedish e-health services," *Journal of multidisciplinary healthcare*, vol.3, p.55, 2010.
[21] W. A. Rogers and A. D. Fisk, "Toward a psychological science of advanced technology design for older adults," *Journals of Gerontology Series B: Psychological Sciences and Social Sciences*, vol.65, no. 6, pp.645–653, 2010.
[22] E. Stojmenova, B. Imperl, T. Zohar, and D. Dinevski, "User-Centred E-Health: Engaging Users into the e-Health Design Process.," Bled eConference, p.38, 2012.
[23] C. Lee and J. F. Coughlin, "PERSPECTIVE: Older adults' adoption of technology: an integrated approach to identifying determinants and barriers," *Journal of Product Innovation Management*, vol.32, no. 5, pp.747–759, 2015.
[24] S. H. Fischer, D. David, B. H. Crotty, M. Dierks, and C. Safran, "Acceptance and use of health information technology by community-dwelling elders," *International journal of medical informatics*, vol.83, no. 9, pp.624–635, 2014.
[25] J. Vines, G. Pritchard, P. Wright, P. Olivier, and K. Brittain, "An age-old problem: Examining the discourses of ageing in HCI and strategies for future research," *ACM Transactions on Computer-Human Interaction (TOCHI)*, vol.22, no. 1, pp.1–27, 2015.
[26] A. J. De Veer, J. M. Peeters, A. E. Brabers, F. G. Schellevis, J. J. J. Rademakers, and A. L. Francke, "Determinants of the intention to use e-Health by community dwelling older people," *BMC health services research*, vol.15, no. 1, pp.1–9, 2015.
[27] A. Ahmad, K. Ahlin, and P. Mozelius, "Technology Acceptance of an Online Speech and Language Assessment Application for Stroke Patients-the Medical Caregivers' Viewpoints," Tenth International Conference on Global Health Challenges (GLOBAL HEALTH 2021), Barcelona, Spain, October 3-7, 2021., 2021.
[28] Q. Ma, A. H. Chan, and P.-L. Teh, "Insights into older adults' technology acceptance through meta-analysis," *International Journal of Human–Computer Interaction*, vol.37, no. 11, pp.1049–1062, 2021.
[29] W. K. Bong and I. Bronshtein, "Designing Digital Games with & for Home-dwelling Older Adults' Social Interaction under Sheltering Measures," 2021.
[30] C. for D. Control and Prevention, "Improving health literacy for older adults: Expert panel report 2009," *Atlanta, GA: US Department of Health and Human Services*, 2009.
[31] K. L. Courtney, G. Demeris, M. Rantz, and M. Skubic, "Needing smart home technologies: the perspectives of older adults in continuing care retirement communities.," 2008.
[32] N. Charness and W. R. Boot, "Aging and information technology use: Potential and barriers," *Current Directions in Psychological Science*, vol.18, no. 5, pp.253–258, 2009.
[33] N. Wagner, K. Hassanein, and M. Head, "Computer use by older adults: A multi-disciplinary review," *Computers in human behavior*, vol.26, no. 5, pp.870–882, 2010.
[34] T. Heart and E. Kalderon, "Older adults: are they ready to adopt health-related ICT?," *International journal of medical informatics*, vol.82, no. 11, pp.e209–e231, 2013.
[35] B. Xie, T. Yeh, G. Walsh, I. Watkins, and M. Huang, "Co-designing an e-health tutorial for older adults," in Proceedings of the 2012 iConference, 2012, pp.240–247.
[36] R. Young, E. Willis, G. Cameron, and M. Geana, "'Willing but unwilling': attitudinal barriers to adoption of home-based health information technology among older adults," *Health informatics journal*, vol.20, no. 2, pp.127–135, 2014.
[37] C. Latulipe, A. Gatto, H. T. Nguyen, D. P. Miller, S. A. Quandt, A. G. Bertoni, A. Smith, and T. A. Arcury, "Design considerations for patient portal adoption by low-income, older adults," Proceedings of the 33rd annual ACM conference on human factors in computing systems, pp.3859–3868, 2015.
[38] A. Bowes and G. McColgan, "Telecare for older people: promoting independence, participation, and identity," *Research on Aging*, vol.35, no. 1, pp.32–49, 2013.
[39] A. Melander-Wikman, Y. Fältholm, and G. Gard, "Safety vs. privacy: elderly persons' experiences of a mobile safety alarm," *Health & social care in the community*, vol.16, no. 4, pp.337–346, 2008.
[40] Y. van Hierden, T. Dietrich, and S. Rundle-Thiele, "Designing an eHealth Well-Being Program: A Participatory Design Approach," *International Journal of Environmental Research and Public Health*, vol.18, no. 14, p.7250, 2021.
[41] M. Jovanović, A. De Angeli, A. McNeill, and L. Coventry, "User requirements for inclusive technology for older adults," *International Journal of Human–Computer Interaction*, vol.37, no. 20, pp.1947–1965, 2021.
[42] T. Wang, S. R. Mazanec, and J. G. Voss, "Needs of Informal Caregivers of Patients With Head and Neck Cancer: A Systematic Review," Oncology Nursing Forum, vol.48, no. 1, pp.11–29, 2021.
[43] Z. Zhou, J. Zhou, and F. Liu, "Fewer Steps the Better? Instructing Older Adults' Learning and Searching in Smartphone Apps," *International Journal of Human–Computer Interaction*, pp.1–12, 2021.
[44] M. N. Hossain, H. Okajima, H. Kitaoka, and A. Ahmed, "Consumer acceptance of eHealth among rural inhabitants in developing countries (A Study on Portable Health Clinic in Bangladesh)," *Procedia computer science*, vol.111, pp.471–478, 2017.
[45] L. T. Vassli and B. A. Farshchian, "Acceptance of health-related ICT among elderly people living in the community: A systematic review of qualitative evidence," *International Journal of Human–Computer Interaction*, vol.34, no. 2, pp.99–116, 2018.
[46] N. Bhatnagar, H. Madden, and Y. Levy, "Initial empirical testing of potential factors contributing to patient use of secure medical teleconferencing," *Journal of Computer Information Systems*, vol.57, no. 1, pp.89–95, 2017.
[47] N. Davis, K. Shiroma, B. Xie, T. Yeh, X. Han, and A. De Main, "Designing eHealth tutorials with and for older adults," *Proceedings of the Association for Information Science and Technology*, vol.58, no. 1, pp.92–103, 2021.
[48] R. Verma, C. Saldanha, U. Ellis, S. Sattar, and K. R. Haase, "eHealth literacy among older adults living with cancer and their caregivers: A scoping review," *Journal of Geriatric Oncology*, 2021.

[49] K. Oberschmidt, C. Grünloh, F. Nijboer, and L. van Velsen, "Best Practices and Lessons Learned for Action Research in eHealth Design and Implementation: Literature Review," *Journal of Medical Internet Research*, vol.24, no. 1, p.e31795, 2022.
[50] M. Thapliyal, N. J. Ahuja, A. Shankar, X. Cheng, and M. Kumar, "A differentiated learning environment in domain model for learning disabled learners," *Journal of Computing in Higher Education*, pp.1–23, 2021.
[51] M. S. Wolf, J. A. Gazmararian, and D. W. Baker, "Health literacy and functional health status among older adults," *Archives of internal medicine*, vol.165, no. 17, pp.1946–1952, 2005.
[52] C. Scheerens, J. Gilissen, A. M. Volow, J. L. Powell, C. M. Ferguson, D. Farrell, B. Li, C. Berry, and R. L. Sudore, "Developing eHealth tools for diverse older adults: Lessons learned from the PREPARE for Your Care Program," *Journal of the American Geriatrics Society*, vol.69, no. 10, pp.2939–2949, 2021.

AWAIS AHMAD is a PhD candidate at Uppsala University Sweden. He also works as a lecturer at the Mid Sweden University.
Awais Ahmad have several years of research experience in eHealth and human-computer interaction(HCI) has 18 publications in the field of computer science, HCI and eHealth

PETER MOZELIUS is an Associate Professor and Researcher, working at the Department of Computer and Systems Sciences at the Mid Sweden University in Östersund, Sweden. Research interests are in the areas of Technology enhanced learning, eHealth, Game-based learning, and Programming education.

Received: 12 January 2022, Revised: 31 March 2022, Accepted: 09 April 2022, Online: 12 April 2022

DOI: https://dx.doi.org/10.55708/js0104015

Determining the Parameters of the Sine-Wave Filter Factors Affecting Filtration Quality

Pustovetov Mikhail *

Department of Engineering Technology Technological Institute (Branch) of Don State Technical University in the City of Azov, 346780, Russia

* Corresponding author: Pustovetov Mikhail, +79885651027, mgsn2006@yandex.ru

ABSTRACT: The paper deals with proposals for the procedure of selecting the parameters of the sine-wave filter in case of increased voltage frequency (400—600 Hz) on the output of frequency converter, which is an element of power supply system. Author describes in article the structure of the power supply system for an unmanned underwater vehicle, which contains a sine-wave filter connected to frequency converter output. The system's simulator has a block structure. As blocks previously developed computer models of electrical devices (transformer, autonomous voltage inverter, L-shaped filter, rectifier) are used. The subject of sine-wave filter output voltage quality and contribution to this of input voltage's modulation index is also described at 100—200 Hz.

KEYWORDS: Sine-wave filter, Electromagnetic compatibility, Frequency converter, Pulse width modulation, Modulation index, Simulation

1. Introduction

Computer simulation today is one of the most popular and wide-spread information technologies used for the analysis and synthesis of technical systems, the consideration of electromagnetic, mechanical, thermal and other processes in them (sometimes under conditions that are difficult or impossible to apply to a real technical device). Computer simulation allows us to reduce the cost of devices development, reducing the materials and time consumption, but at the same time as above consider many different options of construction and modes. This allow specialists to recognize unsuccessful technical solutions before failure occurs or other negative impact during operation and apply acceptable methods to fix them at various stages of the device lifecycle.

For a contemporary electric drive based on frequency controlled AC motors and for a power supply systems (PSS) which include a frequency converter (FC), the problem of electromagnetic compatibility is one of the most ones due to the features of technology of voltage generation by pulsed converters based on semiconductor switches. The output voltage of pulsed converters is formed as a sequence of pulses of trapezoidal shapes. Every pulse has very steep fronts. Such a voltage contains a wide range of higher time harmonics. An additional losses of energy for all elements of the electric circuit from the FC output to the load occurs because of this. One way to reduce the influence of higher time harmonics is the EMC filters installation [1, 2] to suppress them. The sine-wave filter (SF) [3, 4] is one of filter types for FC output voltage.

Author should like to describe and gradually consider have applied by him procedure of the SF parameters selection for increased up to 400—600 Hz frequency of voltage. Proposed parameters selection procedure takes into account the possibility of operating the SF in the fundamental harmonic's frequency range. On other hand, the subject of SF output voltage quality and factors contributes to it is interesting.

2. The Initial Data and Limitations

The authors of [5-10] articles propose description of the PSS used for powering unmanned underwater vehicles. Figure 1 presents an example of underwater vehicle MCC-3000 produced by LLC Marine Geo Service (Moscow, Russia). Underwater vehicle's PSS contain (Figure 2): a source of balanced three line-to-line voltage of 380 V RMS value at 50 Hz frequency; FC structure contains a 3-phase input rectifier 1 (diodes D7 – D12), DC voltage link 1 (L_{d1} , C_{d1} as an L-shaped filter) and a 3-

phase two-level autonomous voltage inverter (AVI) pulse width modulated (PWM) output voltage with frequency control (diodes D1 – D6 and IGBT T1 – T6), the FC's output voltage fundamental harmonic frequency is f_1 = 400—600 Hz in steady-state operation; SF (R_{LSF}, L_{SF}, C_{SF}, R_{CSF} as 3-phase L-shaped filter); 3-phase step-up transformer (PT1); cable-umbilical (R_C, L_C, C_C); 3-phase step-down transformer (PT2); 3-phase rectifier 2 (diodes D13 – D18); DC voltage link 2 (L_{d2}, C_{d2} as an L-shaped filter) and an equivalent load in the form of resistance R_{load}. The DC voltage link 2 and the rectifier 2 represent the head part of another FC, which also includes another AVI, from which the wide speed range frequency controlled electric drive of propellers based on 3-phase synchronous AC motors is powered. In Figure 2 instead of these electric drive and AVI the resistor R_{load} drawn.

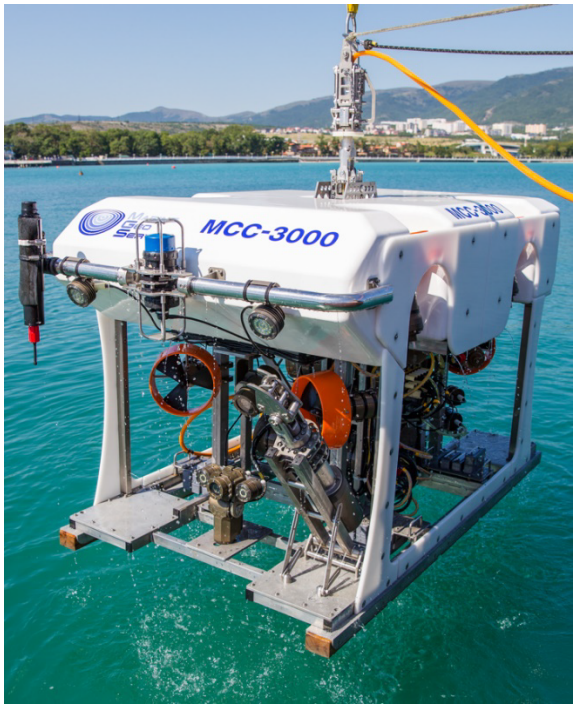

Figure 1: Unmanned underwater vehicle MCC-3000 produced by LLC Marine Geo Service (Moscow, Russia)

f_{PWM} = 14 kHz – is the PWM carrier frequency. The FC's power is limited. That is the value of FC's output current at long-term mode is limited. The same value $I_{L\Sigma}$ will have a current through inductance L_{SF} of the SF phase. The L_{SF} value is limited by the permissible voltage drop on it (percent impedance (short-circuit voltage v_{sc}, %, equation (1))) caused by the current at long-term mode (for example, 10 % of the phase voltage fundamental harmonic RMS value). Needless to say, that FC's output current $I_{L\Sigma}$ will contain wide harmonic spectrum. The voltage drop on the inductance caused by each current harmonic will be proportional to this harmonic frequency. Therefore, it is convenient to assume that the permissible voltage drop should occur from the flow through the inductor of only fundamental (first) current I_{L1} harmonic as a limitation for L_{SF} calculations. The RMS value of the FC output current fundamental harmonic we can define through the usage of the power supplied by the primary 3-phase voltage source, the rated load power, the efficiency of devices (cables, transformers, rectifiers) series connected in the PSS. The resistance R_{LSF} of the SF inductor phase L_{SF} can be determined approximately in accordance with [1].

3. The Adopted Values for Parameters of Devices During Simulation

The SF of type Schaffner FN5020-75-35 parameters, being measured by the specialists of LLC Marine Geo Service (Moscow), in addition to the characteristics published in [11], are represented in Table 1, where V_{p-p} - the line-to-line voltage rated RMS value, f_0 - the SF resonance frequency, I_{rated} - the current through R_{LSF}, L_{SF} branch rated RMS value (FC rated output current).

$$v_{sc},\% = \frac{\sqrt{3} I_{rated} \sqrt{\left(2\pi f_1 L_{SF}\right)^2 + R_{LSF}^2}}{V_{p-p}} \cdot 100\% . \quad (1)$$

$$f_0 = \frac{1}{2\pi\sqrt{L_{SF} C_{SFY}}} . \quad (2)$$

In equation (2) as C_{SFY} we mean Y connection of SF phases capacitances. In case of Δ connection of capacitances will be true equation (3)

$$C_{SF\Delta} = \frac{C_{SFY}}{3} . \quad (3)$$

For the cable-umbilical type KG (3x3,0+1x0,75+2x3E)-190-60 with a length of 3.4 km, based on its geometric dimensions, during simulation the parameters $R_C = 21.964\ \Omega$, $L_C = 0.108$ mH and $C_C = 0.168$ μF have used. Author has used concentrated parameters for cable simulation. In accordance with data published in [6] it gives a slight discrepancy in the load voltage results compared to the model with distributed parameters (<6 %) and experimental data (within 5 %).

Both PT1 and PT2, which are part of the PSS, are constructed as a transformer group of three toroidal single-phase transformers inside the common protective shell. PT1 is the type OSM T 380/1900-12.0-400. PT2 is the type OSM T 1900/240-10.0-400. Each phase of PT1 and PT2 has a separate magnetic circuit. Because of this fact, a mathematical model of a 3-phase transformer without magnetic coupling between the phases (3 connected to each other models of single-phase transformer) has used. The approximate parameters of the T-shaped equivalent circuit of transformer [12] and characteristics used for the

simulation of PT1 and PT2 are presented in Table 2. Magnetic saturation [13, 14] not taken into account.

For the AVI simulation, the computer model based on idealized switches has used, similar to published in [1, 14], with the difference that in the control system had to reduce the capacitance of the capacitors from 10 nF (the value used in [1, 15] at $f_{\text{PWM}} = 1 - 2.5$ kHz) to 1 nF at $f_{\text{PWM}} = 14$ kHz (you can find $C_1 = C_2 = 1$ nF in Figure 3).

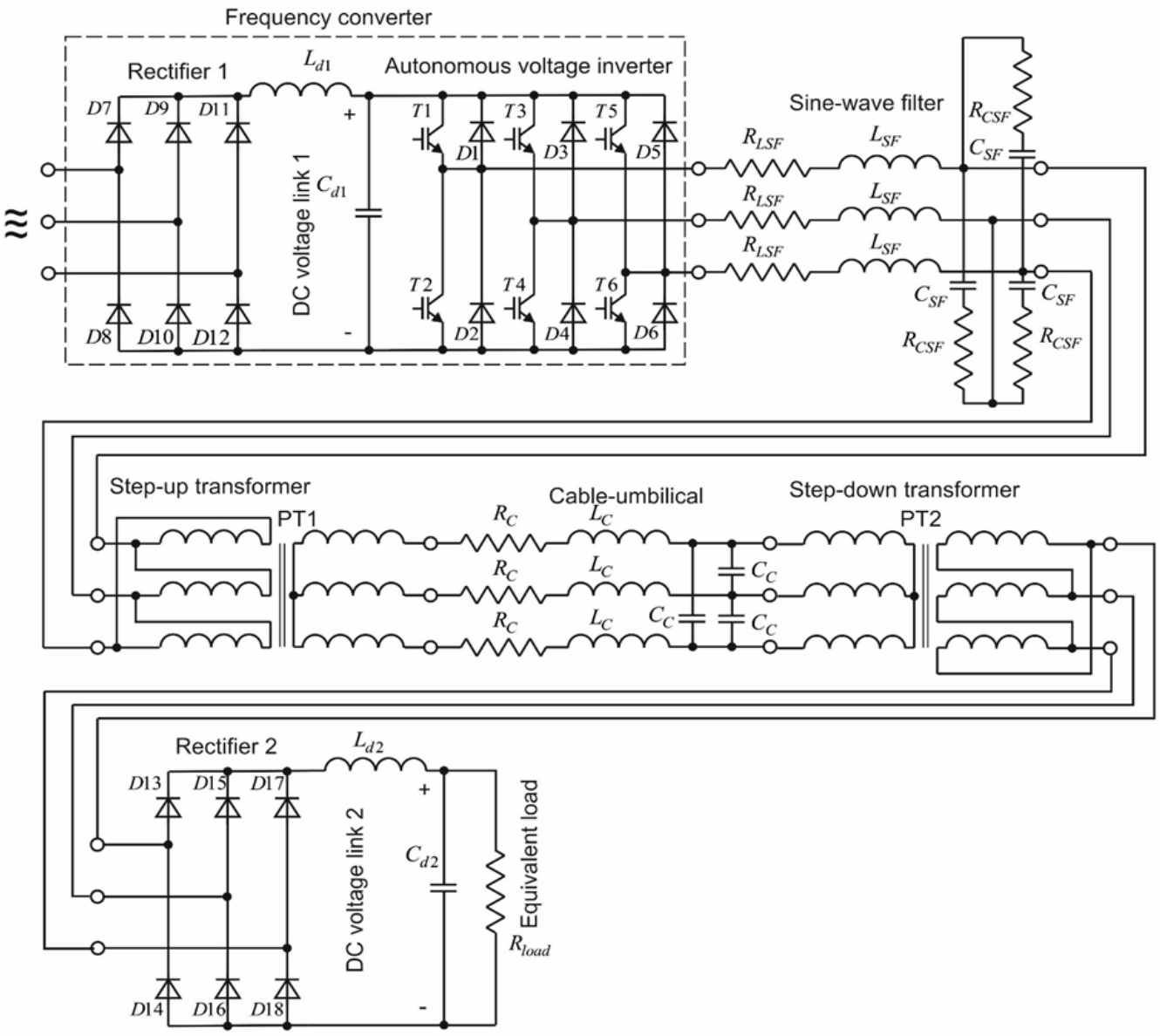

Figure 2: The scheme of PSS for unmanned underwater vehicle

Table 1: Characteristics and Parameters of SF Type Schaffner FN5020-75-35

f_1	I_{rated}	V_{p-p}	L_{SF}	R_{LSF}
Hz	A	V	mH	mΩ
400	75	500	0.195	8.62
600				

C_{SF}	R_{CSF}	f_0	f_{PWM}	$\frac{f_{\text{PWM}}}{f_0}$	v_{sc}
μF	mΩ	kHz	kHz	p.u.	%
8.5	10	2.3	14	6.2	13
					19

Table 2: Characteristics and Parameters for Simulation of 3-Phase Transformers

Name or symbol			Dimension	Value	
				for PT1	for PT2
T-shaped equivalent circuit parameters	$L_{\sigma 1}$		mH	0.0191	1.286
	$L'_{\sigma 2}=\left(\frac{w_1}{w_2}\right)^2 L_{\sigma 2}\approx\left(\frac{V_{1phase}}{V_{2phase}}\right)^2 L_{\sigma 2}$				
	r_1		mΩ	5.7712	0.26
	r_2			8.6567	0.173
	Connected in series	L_m	H	0.0456	1.368
		r_m	Ω	21.83	654.875
The rated mode characteristics when powered by pure sinus voltage		V_{1phase} - RMS value of primary winding phase voltage	V	380	1900
		V_{2phase} - RMS value of secondary winding phase voltage		1900	240
		Power on secondary winding terminals	kVA	36	30
		f_1	Hz	400	
Transformer's current amplitude value at no load mode (close to magnetization current amplitude value at the rated mode)			A	4.675	0.45

This shortens the pauses between switching off one and turning on the other switches at the same phase of the AVI model (for example, T2 and T1 in Figure 1a), and necessary to avoid the loss of short voltage pulses at the AVI output during simulation at high f_{PWM} . The computer model of PSS implemented by means of PSpice [16-18]. For the DC voltage link simulation parameters of L-shaped filters shown in Table 3. These parameters determined according [15]. The load of the PSS (dissipates on R_{load}) can vary from no-load mode to 45 kW overload. The rated power of PT1 is 36 kVA and 30 kVA for PT2.

4. The Suggested Sequence of Sine-Wave Filter Parameters Selection

1. Let's derive L_{SF} from equation (1) on the base of permissible voltage drop caused by the I_{L1}. Generally recommended $v_{sc},\% = 10$ %. R_{LSF} may be neglected.

Table 3: Parameters values for L-shaped Filters of DC Voltage Links Simulation

L_{d1}	L_{d2}	C_{d1}	C_{d2}
mH		μF	
0.36	0.44	10700	9000

2. Set the frequency multiplicity $\frac{f_{\text{PWM}}}{f_0}$. For previously specified in this article f_{PWM} and f_1 values $\frac{f_{\text{PWM}}}{f_0}=5-7$ is suitable. Generally, the frequency multiplicity should be such that the AVI's output voltage higher harmonic components caused by f_{PWM} (they have high amplitudes) would be damped. After that let's find f_0 .

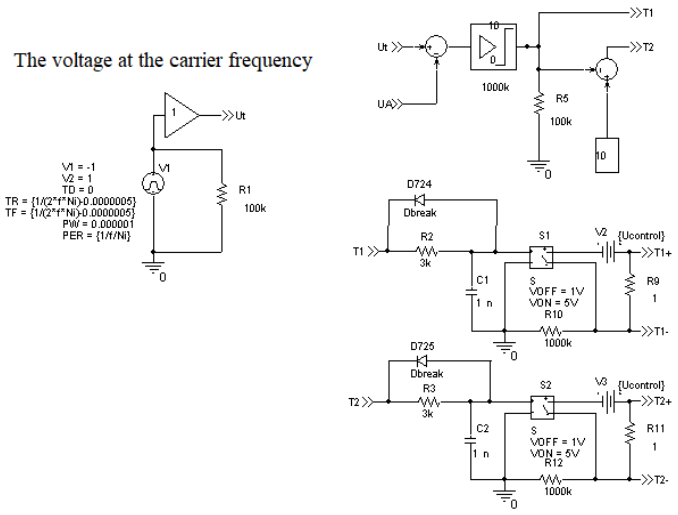

Figure 3: The control system of AVI's phase A - by OrCAD tool designed computer model [16]

3. Knowing L_{SF} and f_0 values we'll derive from equation (2) the capacitance C_{SFY} per phase of the SF if there is the Y connection. When there is the Δ connection we'll find $C_{SF\Delta}$ from equation (3).

Table 4: Bode Diagram for the SF of Type Schaffner FN5020-75-35

f, Hz		400	2000	2800	600	3000	4200
# of time harmonic		1	5	7	1	5	7
Output SF voltage/ input SF voltage, p.u.	at no load condition	1.03	5.21	1.87	1.08	1.30	0.40
	at rated load	1.03	3.57	1.70	1.07	1.23	0.39

Table 5: Simulation Results for the SF of Type Schaffner FN5020-75-35, Characterizing the Voltages Harmonic Composition

f, Hz	400	2000	2800	600	3000	4200
Time harmonic's #	1	5	7	1	5	7
Output SF voltage/ input SF voltage, p.u.	1.036	2.374	2.401	1.129	1.095	0.622
$\frac{THD_{VoutputSF},\%}{THD_{VinputSF},\%}$ (taken into account HTH till 240 kHz)	$\frac{6.017}{42.143}$			$\frac{4.235}{45.232}$		

4. Next step author suggests to provide simulation for checking the SF with previously calculated parameters for the absence in the f_1 operating range of resonant phenomena associated with a significant increase in the filter's output voltage amplitude. For this purpose, PSS's simulator building recommended. Let's make computational experiment fulfillment during which the FC's output voltage and frequency firstly increases to a maximum value (ascending part of the graph 1 in Figures 4 and 5), followed by a steady state (horizontal part of graph 1), lastly at the fixed maximum output voltage of the AVI, the frequency is slowly reduced to the lower f_1 boundary (the slope of the graph 1). Figures 4 and 5 use the following notation: 1 - graph of $2f_1$, Hz; 2 - graph of SF's output line-to-line instantaneous voltage. First of all, the computational experiment should be performed at no load condition - in this case, the resonant phenomena, if they exist, are manifested to the greatest extent. In addition, it is possible to perform the similar simulation under load. If resonant phenomena detected, to move them out of the frequency f_1 operating range, it is appropriate to increase the inductance L_{SF}. If this is not desirable, you can reduce the filter capacity C_{SF}. We need to remember that for the same inductor reduction in capacity leads to a deterioration of filtering properties, and the increase in capacity, although approximating the shape of the filter's output voltage to sinusoidal, but results to an increase of the current through the capacitance, including by increasing of the fundamental harmonic, and hence increase the SF's inductor current, that is, FC's output current, which can lead to overload and shutdown of the FC. Simultaneous increase of capacitance and inductance results to an increase in the denominator of the equation (2), that is, to f_0 decrease and its shift toward f_1. This can cause the fundamental voltage harmonic amplification, which, under constant load, will lead to an increase in $I_{L\Sigma}$ and I_{L1}.

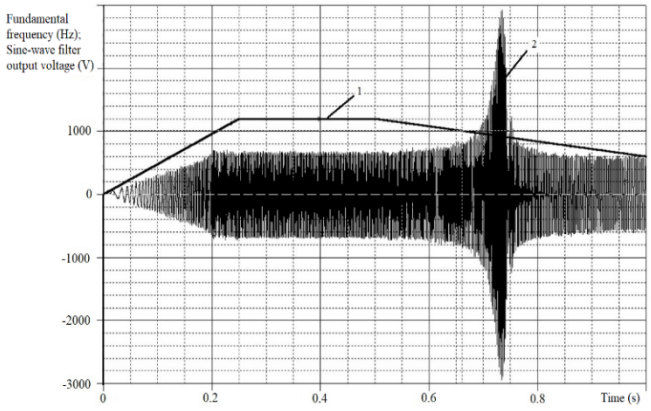

Figure 4: Results of simulation test for output voltage resonant phenomena in case of SF with $L_{SF} = 0.776$ mH, $C_{SF\Delta} = 20$ μF and no load mode

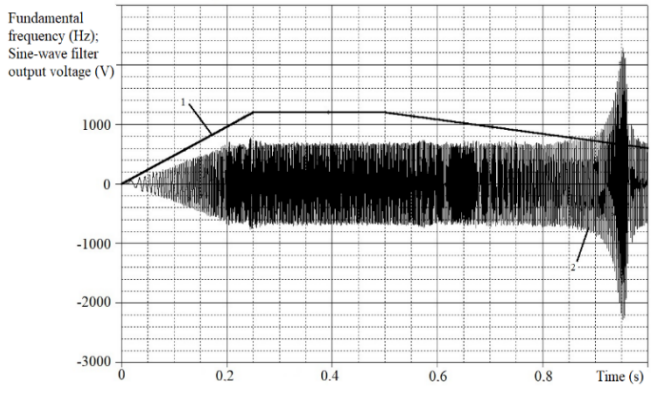

Figure 5: Results of simulation test for output voltage resonant phenomena in case of SF with $L_{SF} = 0.15$ mH, $C_{SF\Delta} = 20$ μF and no-load mode

5.After all checking of the losses in the SF's elements and the total power losses can be done. If the damping resistors in branches with capacitances are absent, we can estimate the series resistance connected with the phase capacitance of the order of units or tenths of $\mu\Omega$ (best - in accordance with the catalog data of capacitors). The focus on energy efficiency of equipment achievement, for example, in [19] is formulated as follows: "For two-level converters in the absence of various types of filters, these (additional due to non-sinusoidal supply voltage) losses can be ... 1-2 % of the rated power of the motor. ... there are losses in the filter, but they will be lower than the reduction of additional losses due to power from the converter. Thus, the total efficiency of the electric drive is increased."

5. Justification of the Possibility of Increasing the Sine-Wave Filter's Inductance Value

As we can see from Table 1, the SF type Schaffner FN5020-75-35 has $v_{sc},\% > 10$ %. Let's find out why this is allowed. In Figure 6 we can see the Bode diagram calculated for the SF type Schaffner FN5020-75-35. Table 4 contains the values of the same Bode diagram for some characteristic frequencies. From the Figure 6 and data Table 4 it follows that the SF voltage fundamental harmonic falls into the signal amplification region. One or both of the voltage's lowest-frequency 5th and 7th highest time harmonics (HTH) also fall into there.

Bode diagram gives us a possibility to clarify the requirement to limit the voltage drop $v_{sc},\%$ in the SF's phase inductor, which was limited to 10 % earlier, prohibiting voltage's fundamental harmonic excessive weakening. Taking into account the SF output voltage's fundamental harmonic gain, if necessary, we can assume $v_{sc},\% > 10$ %, which has implemented for the SF type Schaffner FN5020-75-35 in accordance with Table 4 data.

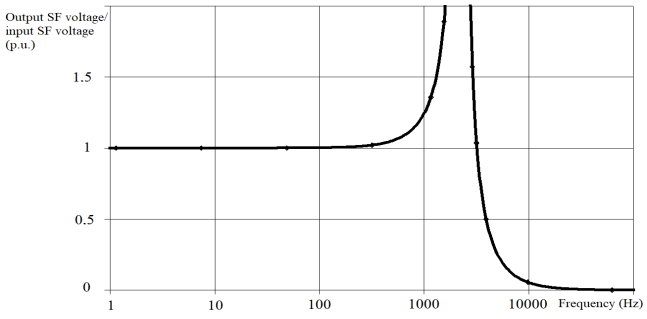

Figure 6: Bode diagram of the SF type Schaffner FN5020-75-35

6. Simulated Voltages for Different Blocks of PSS

The results of steady state mode voltages simulation for different blocks of the PSS under load with SF type Schaffner FN5020-75-35 we can see in Figure 7 and Figure 8. The following notation have adopted: 1 – line-to-line voltage at the FC output (SF input); 2 – phase-to- phase output voltage of SF; 3 – line-to-line voltage of the low voltage (secondary) winding of PT2; 4 – voltage on C_{d2} and on $R_{load} = 4.8\ \Omega$; 5 – rectifier 2 output voltage.

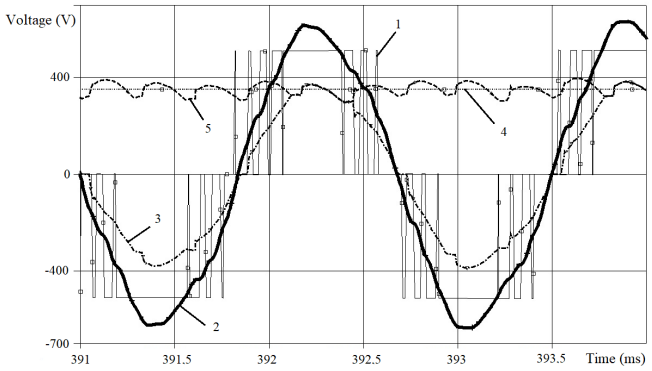

Figure 7: Simulated voltages for PSS at $f_1 = 600$ Hz at 27.75 kW equivalent load

For the SF's effectiveness demonstration Figure 9 and Figure 10 represent the spectral compositions of the line-to-line voltages at the SF's input and output for the case shown in Figure 8.

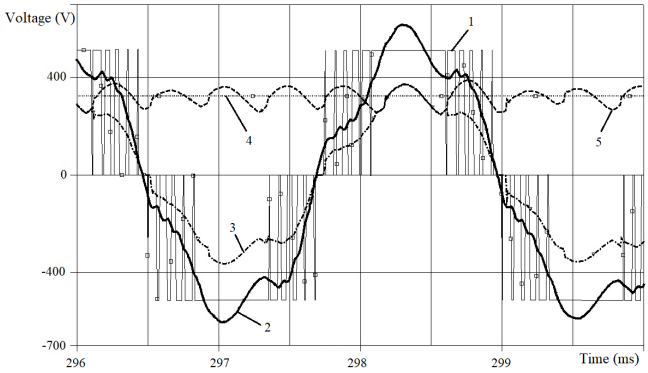

Figure 8: Simulated voltages for PSS at $f_1 = 400$ Hz at 21.8 kW equivalent load

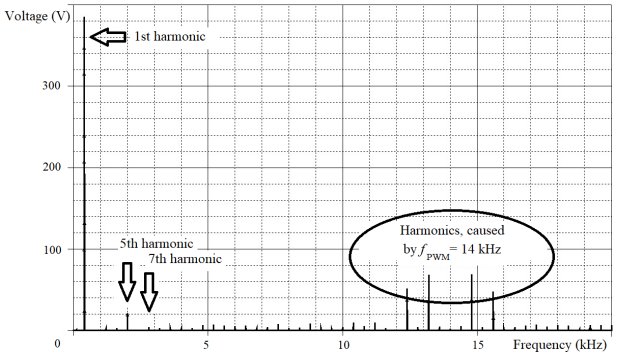

Figure 9: Harmonic composition of the SF's input line-to-line voltage RMS values in Figure 8 case

The comparison of Figure 9 and Figure 10 confirms that SF suppresses noticeably the HTH caused by f_{PWM}, but, in accordance with Table 4 prediction, SF strengthens the 5th and 7th HTH, which causes the deformation of graphs 2 and 3 in Figure 8 especially. Also we can see that the voltage fundamental harmonic has amplified (Figure 10).

In Table 5 author summarize the processed results of Figure 7 and Figure 8 for the input and output line-to-line SF's voltages. Needless to say, that results which Table 5 contains, in satisfactory agreement with the data of the Table 4 and Figure 6.

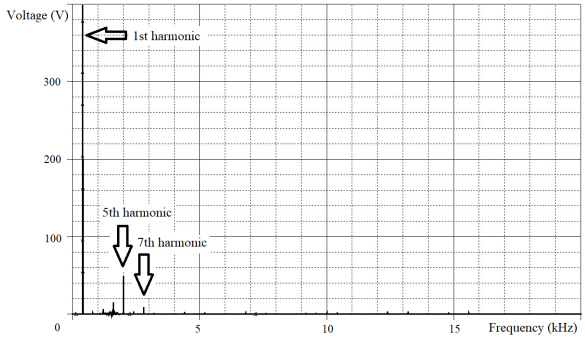

Figure 10: Harmonic composition of the SF's output line-to-line voltage RMS values in Figure 8 case

7. Impact Investigation of the DC Choke L_{d2}

We know, that the DC choke L_{d2} may be absent in PSS. How does the voltage shape react to such a technical solution? In this case, the shape of voltages (graphs 2 and 3 in Figure 11, Figure 12) is close to pure sinus only at no load mode. While the load increases, the graph 2 shape deviates from the sine wave more and more. As we can understand from the harmonic analysis results, this occurs because of an increase of HTH with the 5th and 7th numbers in the voltage harmonic composition. At the same time, graph 3 will have flat (cut off) vertex.

Furthermore, the absolute value of the amplitude of graph 3 (the flat vertex) coincides with the graph 4 parts. Simulation results in Figures 11 and 12 developed at $L_{SF} = 0.16$ mH and $C_{SF\Delta} = 13$ μF. We can make a conclusion, that when the output rectifier 2 loaded directly by the capacitance, it is possible that SF will provide a close to pure sinus output voltage wave shape, but at no load mode only. In Figure 13 presented the confirmation of this conclusion by voltage waveforms of the experimental PSS (got by specialists of LLC Marine Geo Service (Moscow, Russia)).

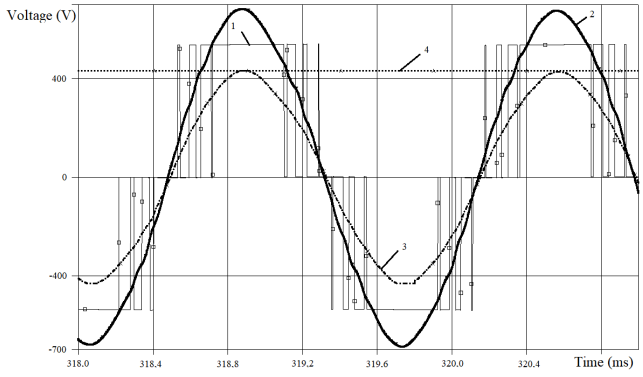

Figure 11: Simulated voltages for PSS without L_{d2} at $f_1 = 600$ Hz at no load mode

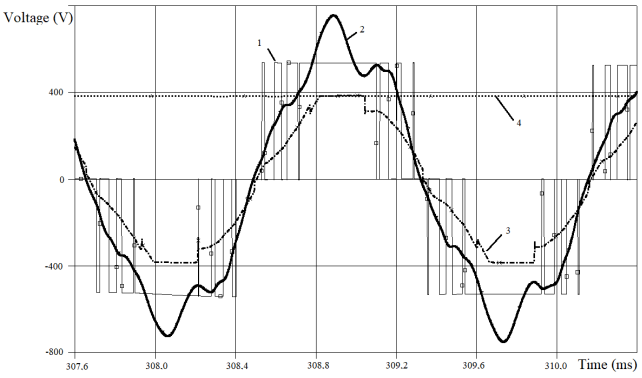

Figure 12: Simulated voltages for PSS without L_{d2} at $f_1 = 600$ Hz and 30.6 kW equivalent load value

The experimental results in Figure 13 got for $L_{SF} = 0.09937$ mH and $C_{SF\Delta} = 12$ μF at an equivalent load of 10 kW. Figure 13 (a) demonstrates the line-to-line voltage on the secondary winding of a step-down transformer PT2 at $f_1 = 504$ Hz; (b) line-to-line SF output voltage at 401 Hz.

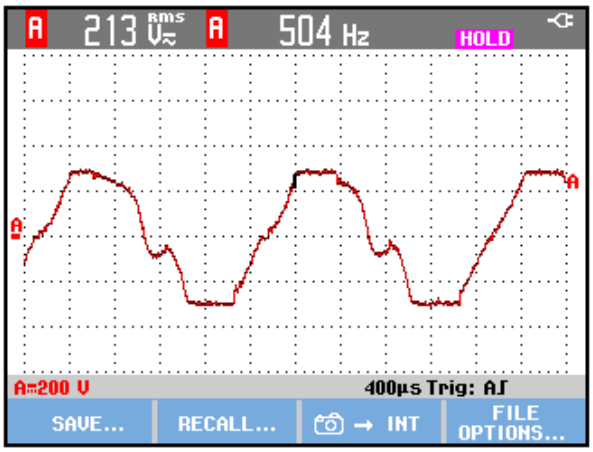

(a)

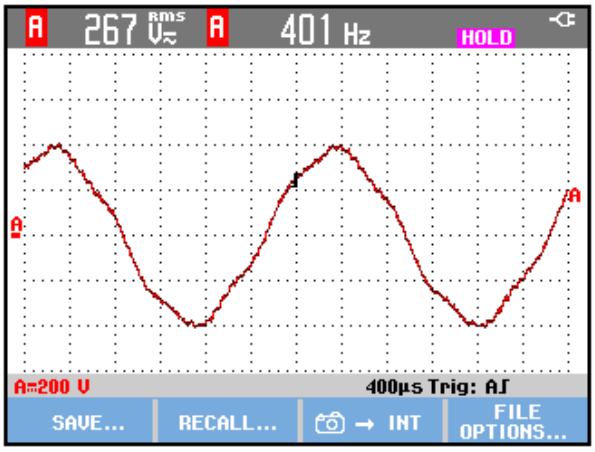

(b)

Figure 13: Experimental PSS voltages waveforms

8. FC Output Voltage Modulation Index Contribution to SF Output Voltage Quality

Currently, FC with SF connected at the output are also used as a regulated power supply for testing electrical equipment [20, 21]. For example, for conducting

experiments of open circuit (no load) and short circuit of power transformers.

It is known that the no-load test is carried out at the rated voltage. Otherwise the short-circuit test of the transformer is carried out at a reduced supply voltage in order to limit the currents through the windings. That is, the FC, for example, can form rated output line-to-line voltage of 690 V RMS. The same FC has to form output line-to-line voltage of 200 ... 250 V RMS at the transformer short circuit test mode. This is 29 ... 36% of the rated voltage (rounded to 1/3). This is actually the PWM modulation index, the duty cycle of the pulses averaged over the period of the modulating voltage. Therefore, 2/3 of the time in the voltage period is occupied by pauses (see in Figure 14 and Figure 15 the experimental graphs of line-to-line output voltage for the 3-phase FC of type GoodDrive GD300 (manufactured in China) with rated power of 1000 kW).

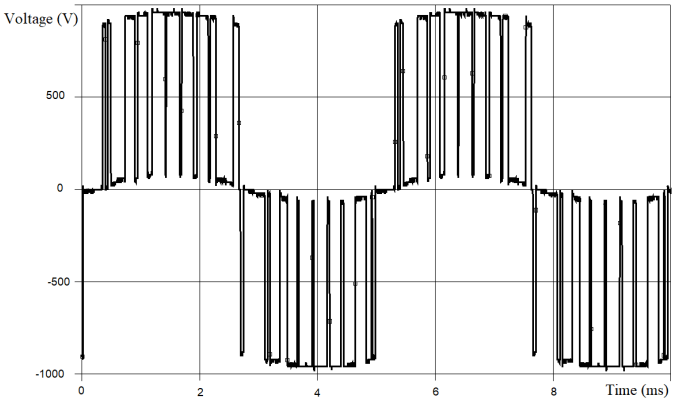

Figure 14: Experimental line-to-line voltage graph at the inverter output (1st harmonic frequency 200 Hz, set RMS value of 1st harmonic 600 V)

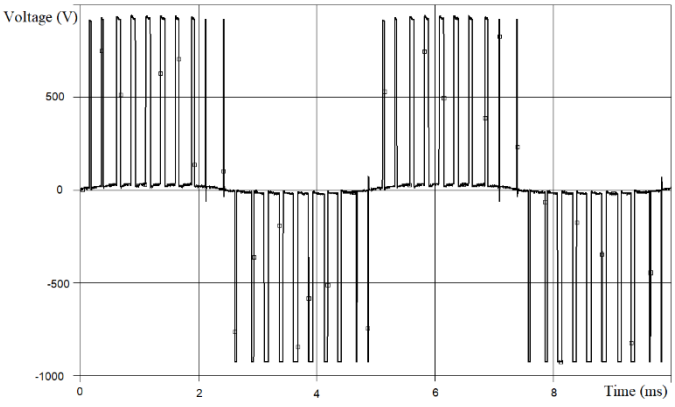

Figure 15: Experimental line-to-line voltage graph at the inverter output (1st harmonic frequency 200 Hz, set RMS value of 1st harmonic 200 V)

Figure 16 and Figure 17 show an experimental graphs of the line-to-line voltage at the SF's output (SF equivalent parameters are $L_{SF} = 0.1$ mH, $C_{SF\Delta} = 240$ μF (capacitances of SF phases connected in Δ scheme)). In all the experiments discussed in section 8 of this article, the PWM carrier frequency $f_{\text{PWM}} = 2$ kHz.

Tables 6 and 7 show the results of harmonic analysis for the experimental graphs of line-to-line voltage at the FC output and at the SF output, respectively. In the tables 6 and 7 the HTH up to 1.6 MHz taken into account.

Test data for analysis provided by specialists of LLC Scientific and Production Enterprise "Electromash" (Novocherkassk, Russia).

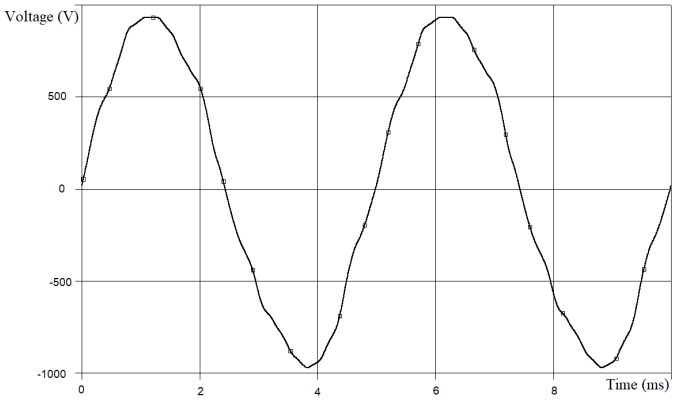

Figure 16: Experimental line-to-line voltage graph at the output of the SF (frequency of the 1st harmonic is 200 Hz, the RMS value of the 1st harmonic is 663.9 V)

Table 6: $THD_{VinputSF}$, % Depending on the RMS Value of 1st Harmonic Line-to-line Voltage Specified for the Inverter Output

Fundamental frequency f_1, Hz	RMS value of the 1st harmonic line-to-line voltage specified for the inverter output, V	$THD_{VinputSF}$, %
50	200	164.5
100	200	161.3
150	200	160.5
200	200	162.0
50	600	59.9
100	600	60.1
150	600	60.5
200	600	61.8

Table 7: $THD_{VoutputSF}$, % Depending on the RMS Value of 1st Harmonic Line-to-line Voltage at the SF Output

Fundamental frequency f_1, Hz	RMS value of the 1st harmonic of line-to-line voltage at the SF output, V	$THD_{VoutputSF}$, %
100	260.4	8.5
200	239.1	8.0

100	662.2	5.0
200	663.9	5.7

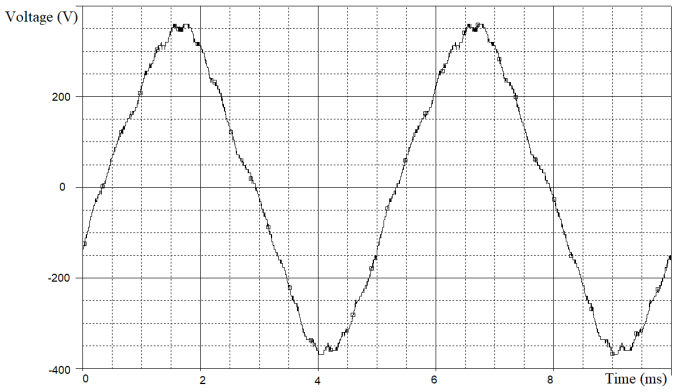

Figure 17: Experimental line-to-line voltage graph at the output of the SF (frequency of the 1st harmonic is 200 Hz, the RMS value of the 1st harmonic is 239.1 V)

9. Conclusion

Basing on predeveloped computer models of L-shaped filter, transformer, AVI, for which the necessary characteristics and parameters are defined and set, the simulator of PSS for an unmanned underwater vehicle has assembled. This computer model has got us an opportunity of electromagnetic processes simulation and studying at different power characteristics and loads. By means of simulation quantitatively and qualitatively has confirmed proper functioning of the SF of type Schaffner FN5020-75-35 in this PSS. This type of SF provides the sufficient filtering action and the resonant phenomena, which could lead to an output voltage's significant increase, absence.

Author suggests provide simulation for checking the SF for absence of resonant phenomena, associated with a significant increase in the filter's output voltage amplitude, within the f_1 operating range. For this purpose, it is recommended computational experiment fulfillment in which, at first, FC's output voltage and frequency increases to a maximum value, at second, a steady state follows, at third, the frequency is reduced slowly to the lower boundary at the fixed maximum AVI's output voltage.

The Bode diagram usage gets an opportunity to refine the quantity requirement for the voltage drop limitation in SF's phase inductor. Taking into account the gain of SF's output voltage fundamental harmonic, if necessary, it is possible to assume $v_{sc}, \% > 10\ \%$.

When using SF loaded by rectifier, a simple way to minimize the SF's output voltage distortion and voltage distortion at the terminals of an equivalent load over the wide range of load is an inclusion of DC choke L_{d2} to DC voltage link 2 of PSS. In case of its absence, it is possible to achieve a sinusoidal SF's output voltage shape only at no load mode. While load turned on, the SF's output voltage and the voltage at load terminals shapes can have noticeable distortions. The L_{d2} usage gives an additional positive effect, decreasing the voltage amplitude at the C_{SF} terminals.

With a reduced value of the FC's output voltage fundamental harmonic, as occurs in the short-circuit load mode, the harmonic composition of the FC output voltage is much more noisy than at no-load conditions, when the voltage of the fundamental harmonic of the FC is close to the rated value. That is, at a reduced voltage of the fundamental harmonic (low modulation index), the operating conditions of the SF are much more complicated than at the rated voltage of the fundamental. Namely: SF will, as expected, provide in the case of a reduced output voltage of the FC a worse harmonic composition of the voltage across the load than at the rated voltage of the FC.A particular problem arises if the SF must provide high-quality filtering over a wide range of output voltage values. This problem is further complicated if it is required to receive a voltage at the output of the inverter not of any one fixed frequency, but a certain range of voltage frequencies. In these conditions, it is practically impossible to cut out certain unwanted harmonics from the spectrum using passive filters without damaging the voltage waveform in any part of the regulated frequency range of the fundamental harmonic. Therefore, when formulating the requirements for the SF's output voltage quality, it is advisable to clarify which mode of operation of the FC they correspond to, and whether an increase of voltage $THD_{VoutputSF}, \%$ is permissible when deviating from this mode.

References

[1] M.Yu. Pustovetov, S.A. Voinash, "Analysis of dv/dt Filter Parameters Influence on its Characteristics. Filter Simulation Features," *2019 International Conference on Industrial Engineering, Applications and Manufacturing (ICIEAM)*, pp. 1-8, 2019, doi:10.1109/ICIEAM.2019.8743007.

[2] C.F. Post, "EMC design considerations for medium to large variable speed drives in industry," *2014 XXXIth URSI General Assembly and Scientific Symposium (URSI GASS)*, 2014, doi:10.1109/URSIGASS.2014.6929538.

[3] Baek Seunghoon, Choi Dongmin, Bu Hanyoung, Cho Younghoon 2020, "Analysis and Design of a Sine Wave Filter for GaN-Based Low-Voltage Variable Frequency Drives," *Electronics*, vol. 9 no. 345, pp. 76-89, 2020, doi:10.3390/electronics9020345.

[4] E. Dresvianskii, M. Pokushko, A. Stupina, V. Panteleev, V. Yurdanova, "Control of high-voltage pump motor using a frequency sinewave filter converter," *IOP Conf. Ser.: Mater. Sci. Eng.*, vol. 450, p. 072003, 2018, doi:10.1088/1757-899X/450/7/072003.

[5] O. Sulaiman, A.H. Saharuddin, "Power Integrity Requirement of New Generation of ROV for Deep Sea Operation," *Global Journal of Researches in Engineering Automotive Engineering*, vol. 12, no. 3, pp. 16-28, 2012.

[6] V.M. Rulevskiy, V.G. Bukreev, E.O. Kuleshova, E.B. Shandarova, S.M. Shandarov, Yu. Z. Vasilyeva, "The power supply system model of the process submersible device with AC power

transmission over the cable-rope," *IOP Conf. Ser.: Mater. Sci. Eng.*, vol. 177, no.1, p. 012098, 2017, doi:10.1088/1757-899X/177/1/012098.
[7] V.M. Rulevskiy, V.G. Bukreev, E.B. Shandarova, E.O. Kuleshova, S.M. Shandarov, Yu.Z. Vasilyeva "Mathematical model for the power supply system of an autonomous object with an AC power transmission over a cable rope," *IOP Conf. Ser.: Mater. Sci. Eng.*, vol. 177, no. 1, p. 012073, 2017, doi:10.1088/1757-899X/177/1/012073.
[8] V.M. Rulevskiy, V.A. Chekh, Y.A. Shurygin, A.A. Pravikova, "Voltage stabilizer in power supply of underwater vehicle," *IOP Conf. Ser.: Mater. Sci. Eng.*, vol. 327, p. 022018, 2018, doi:10.1088/1757-899X/327/2/022018.
[9] M.Yu. Pustovetov, "The Procedure of Sine-Wave Filter Parameters Selection Including Simulation in Case of Increased Frequency of Voltage," *2020 International Multi-Conference on Industrial Engineering and Modern Technologies (FarEastCon)*, 2020, doi:10.1109/FarEastCon50210.2020.9271606.
[10] V.M. Rulevskiy, A.A. Pravikova, D.Yu. Lyapunov, "Autonomous Inverters' PWM Methods for Remotely Controlled Unmanned Underwater Vehicles," *2016 International Conference on Industrial Engineering, Applications and Manufacturing (ICIEAM)*, 2016, doi:10.1109/ICIEAM.2016.7911641.
[11] Sine wave filters FN 5020 - SCHAFFNER Group - PDF Catalogs. https://pdf.directindustry.com/pdf/schaffner-group/sine-wave-filters-fn-5020/15134-878671.html
[12] M.Yu. Pustovetov, "A universal mathematical model of a three-phase transformer with a single magnetic core," *Russian Electrical Engineering*, vol. 86, no. 2, pp.98-101, 2015, doi: 10.3103/S106837121502011X.
[13] M.Yu. Pustovetov, "Method for Taking into Account of Magnetization Curve Nonlinearity at Variable Frequency of Feeding Voltage," *2018 International Conference on Industrial Engineering, Applications and Manufacturing (ICIEAM)*, 2018, doi:10.1109/ICIEAM.2018.8728613.
[14] M. Pustovetov, "An Inductive Coil Simulation," *International Journal of Power Systems*, vol. 6, pp. 90-93, 2021, https://www.iaras.org/iaras/filedownloads/ijps/2021/010-0010(2021).pdf.
[15] M.Yu. Pustovetov, "Determination of the Sufficient Inductance of AC Line Reactor at the Input of Frequency Converter," *Journal of Modeling and Optimization*, vol. 11, no. 1, pp. 25-29, 2019, doi:10.32732/jmo.2019.11.1.25.
[16] J. Keown, *OrCAD PSpice and Circuit Analysis*, Upper Saddle River: Prentice Hall, 2001.
[17] M.H. Rashid, *SPICE for power electronics and electric power*, CRC Press, 2012.
[18] A. Şchiop, V. Popescu, "PSpice simulation of power electronics circuit and induction motor drives," *Rev. Roum. Sci. Techn. – Électrotechn. et Énerg.*, vol. 52, no. 1, pp. 33–42, 2007.
[19] IEC TS 60034-25:2014 Rotating electrical machines — Part 25: AC electrical machines used in power drive systems — Application guide
[20] B. Leelachariyakul, P. Yutthagowith, "Resonant Power Frequency Converter and Application in High-Voltage and Partial Discharge Test of a Voltage Transformer," *Energies*, vol. 14, no. 7, p. 2014, 2021, doi:10.3390/en14072014.
[21] T. Prombud, P. Yutthagowith, "Development of High-voltage Testing System Based on Power Frequency Converter Used in Partial Discharge Tests of Potential Transformers," *Sensors and Materials*, vol. 32, no. 2, pp. 573–585, 2020.

PUSTOVETOV MIKHAIL has done his engineering degree (electrical machines) in 1992 from Rostov-on-Don Institution of Railway Engineering. Theme of the diploma paper: "Linear induction motor with the development of technology for its production".

He has completed his Ph.D. degree (candidate of engineering sciences degree (electromechanics)) in 2000 from Platov South-Russian State Polytechnic University (NPI), Novocherkassk, Russia. Theme of the dissertation: "Traction induction motors calculation methods advancement with the aim of motor's energy performance improving and the torque ripples reduction".

Work experience:

Electrical Design Engineer for the RIF Shipyard (currently);

Acting Head of Department of Engineering Technology (Technological Institute (Branch) of Don State Technical University in the City of Azov) (2020);

Associate Professor of Smart Electric Grids Department (Don State Technical University) (2016 - 2019);

Director of Science-investigating and testing center "Cryotransenergo" at Rostov State Transport University (2012 - 2016);

Chief of Department of Automation and electric drive of machine-tool systems (Don State Technical University) (2007 - 2012);

Engineer-researcher in All-Russian Research and Design Institution of Electrical Locomotives Building (VELNII, Novocherkassk) (2000 - 2011).

Has written and coauthored more than 160 papers (mainly in russian). Holds eight patents (RUS).

JENRS

Received: 15 February 2022, Revised: 01 April 2022, Accepted: 16 April 2022, Online: 22 April 2022

DOI: https://dx.doi.org/10.55708/js0104016

Utilization of Date Tree Leaves Biomass for the Removal of Heavy Metals from Water

Kiman Silas*, Aliyu B. Ngulde, Habiba D. Mohammed

Department of Chemical Engineering, University of Maiduguri, Bama Road, PMB 1069 Maiduguri, Borno State
*Corresponding author: silaskiman@imaid.edu.ng, +2347033539116

ABSTRACT: Cadmium (Cd) is known to have adverse effects on the kidney, liver, bones and cardio-pulmonary system, this heavy metal is usually consumed from drinking water with higher Cd acceptable limits. In this study, Activated Carbon (AC) is produced from Date Tree Leaf (DTL) and impregnated with Zinc Oxide catalyst, where an adsorbent (ZnO/DTL) was developed and used in the adsorption of heavy metals from water samples from three areas of Maiduguri, Nigeria where there are reported kidney problems caused by Cd. The highest concentration of Cd from Dala Kwanan Osi is of Maiduguri (0.017 mg/l) is observed to be completely remove even less than the maximum permitted limits of 0.003 mg/l. The outcomes from SEM, EDXRF, FTIR spectra and XRD patterns revealed the characteristics of the adsorbents. Also, the isotherm study indicated that Langmuir isotherm supersedes (0.9684) the characteristics shown by Freundlich isotherm (0.8479) hence it is more suitable to explicate the correlation of experimental results. It is proven for the first time in Maiduguri, Nigeria that the DTL can now be considered as a waste-to-wealth commodity suitable for the cheap and simple means of removing Cd contamination and other heavy metals from borehole water.

KEYWORDS: Heavy Metals, Date Tree, Adsorbent, Activated Carbon, Metal Oxide

1. Introduction

Water is a very basic source for the existence of life on earth however, the increase in industrialization and modernization has contributed negatively to clean water resources. Many substances such as heavy metals, dyes, pharmaceuticals, surfactants, pesticides, personal care products, and others have contaminated the water resources [1]. These pollutants are environmentally hazardous to human beings and animals [2]. The excess quantity of heavy metals in water causes irritation of the central nervous system and damage to the kidney and liver, Lead (Pb) and Cadmium (Cd) are the most toxic heavy metals which cause many diseases [2,3].

Biomass is abundantly available from several sources all over the world and has numerous roles to play in sustainable development. In addition, to being a food source and renewable raw material, biomass can be used for energy production, carbon sequestration, and as an essential element to produce biochars and activated carbon [4,5].

The conventional technologies for heavy metal contaminated water are precipitation, electrochemical treatment, ion exchange, membrane separation, and adsorption. However, adsorption has been proven to be one of the most suitable and universal methods, which offers remarkable advantages such as fast water treatment, ease of operation, availability, and efficiency [6]. Various adsorbents have been employed in adsorption, ranging from natural products to synthetic materials, carbon materials, such as activated carbon, graphene, and fullerene, were found to be promising adsorbents for removing heavy metals from aqueous solutions due to their stability and large surface area [6-7]. Date Palm fibers are lignocellulosic materials that consist of three vital components: Cellulose (40-50 %), hemicellulose (20-35 %) and lignin (15-35 %) [8] and may be used as adsorbent to remove heavy metal ion from water.

Each date palm tree produces 20 kg of dry leaves yearly [9] while the area under date palm cultivation in Nigeria was estimated at over 1,466.00 ha with an annual production of nearly 20,000 tons of date fruit per annum

[10]. The Date Tree Leaves (DTL) stems and branches are waste and are being burnt while in most cases, they are thrown to liter the environment to become the part of teaming solid waste. As of now, there are no sustainable long-term management strategies to utilize the DTL towards an economical and practical approach to environmental cleanup however, other study [11] reported that AC produced from waste biomass can be utilized to that effect.

AC can be used as a support of Metal Oxides (MO) in the adsorption of heavy metals and are impregnated on the AC as an active catalyst phase due to their low production cost [12]. Wheat Straw Biochar (WSB) was activated for cadmium removal from contaminated water, they found that WSB is a cost-effective and environmentally friendly strategy for the removal of metals from contaminated water [13] however, there is no detailed adsorption time study that is expected to be high due absence of a catalyst. A review on the removal of Cd(II) and other heavy metal ions from aqueous solution by Zinc Oxide (ZnO) nanoparticles as adsorbent was reported [14] however, the shortfall of unsupported MO catalyst involves high cost. The ZnO/activated carbon adsorption capacity (96 mg/g) for the adsorption of Cd^{2+} ions was reported [15] but AC is expensive, therefore, there is a need for developing AC from a cheap local source. Many studies of the removal of heavy metals from contaminated water using AC/MO can be found in the literature [16]–[18]. Hence, ZnO is cheap, and be easily synthesized with AC.

The objective of this work is to produce Activated Carbon using DTL and to impregnate the AC with Metal Oxide (ZnO) also, to characterize the adsorbents before and after adsorption by FTIR, XRD, SEM, EDXRF techniques. The developed adsorbent (ZnO/DTL) will be used to remove heavy metals from three water samples obtained from some areas in Maiduguri, Nigeria. Furthermore, the adsorption isotherms based on Langmuir and Freundlich will be used for the description of the adsorption of the heavy metals over the adsorbents.

2. Materials and methods

2.1. Material

Zinc Oxide (ZnO), Hydrochloric acid (HCL) and deionized water were purchased from Sigma-Aldrich. All the chemicals and reagents used were of analytical reagent (AR) grade or as specified.

2.2. Adsorbent preparation and impregnation

The DTL were collected from a date palm plantation in Moduganari, Maiduguri, Nigeria. the collected leaves were crushed to smaller particle size and washed with distilled water several times to remove dirt particles and water-soluble materials. The washing process is continued until the wash water contained no color. The washed material is then dried in an oven at 50 ^{o}C for 24 h. The sample obtained from the pretreatment process above was then heated in furnace at 600 ^{o}C for 1h and left in the furnace for 24 h to cool in the absence of oxygen. The result obtained from this process is the carbonized sample otherwise known as the Non-impregnated Date Tree Leaves (NIDTL) adsorbent as used in this work. The NIDTL adsorbent produced was activated in accordance to the literature [19] to obtain an activated carbon material Non-impregnated Date Tree Leaves Activated Carbon (NIDTLAC). Further, the NIDTLAC is impregnated with an appropriate aqueous solution of ZnO to develop ZnO/DTLAC adsorbent. The impregnation is simple and easy to carry out [12] unlike other synthesis methods which require specialized equipment such as microscopic/spectroscopic technique as explained in another study [15].

The adsorbent was heated with constant stirring at 70 ^{o}C and 300 rpm until the entire liquid is evaporated and then dried at 110 ^{o}C for 24 h. After which the obtained samples were later calcinated at 400 ^{o}C for 2 h to bind the ZnO catalyst to the AC surface.

2.3 Adsorption activity

The water sample collected from the wash borehole in Maiduguri is analyzed via Atomic Adsorption Spectroscopy (AAS) to detect the presence of arsenic, cadmium, chromium, copper, and lead. After the adsorption, water sample is tested again to check the reduction/ removal of heavy metal initially present in the water sample. water samples collected at three different borehole water points within Maiduguri metropolis.

2.4. Characterization techniques

The characterization of the samples was carried out with; SEM analysis (JSM-6010LA, JEOL, Japan); XRF analysis (X-ray Fluorescence Spectrometer-EDX7000, SHIMADZU Corporation, Japan; FTIR spectra, Bruker Alpha infrared spectrophotometer) with a resolution of 4 cm^{-1} (range 400–4000 cm^{-1}); XRD analysis (BRUKER X-ray Diffraction).

3. Results

3.1. SEM morphology

The structural properties of activated carbon are effective at adsorption capacity, also the interactions of adsorbate/adsorbent play an important role in the adsorption process however, the improvements of the activated carbon properties is realized by impregnating the ZnO over its surface. The ZnO/DTLAC shows that the morphology contains many pores and caves, which may

be due to ZnO evaporation during the carbonization step, similar finding has been reported [11]. The surface of the adsorbents is rough with particles and with amorphous nature of carbon in accordance with previous researchers [20]. Large blocks containing regular channel arrays can be observed with larger pores, this can indicate that the DTLAC preserved the original structure, even after calcination these pores can facilitate the diffusion of the organic molecules inside the composite. This observation was found to favorably agree with other study [21]. Previous SEM analysis after surface modification, showed that the surface structure remained porous with ZnO nanoparticles [22]. The morphology of the ZnO/ DTLAC and NIDTLAC adsorbents are shown in Figure 1.

Also, there are visible pores on the adsorbent that necessitate the adsorption to occur, similar morphological structure can be seen for all the adsorbents. Large blocks containing regular channel arrays can be observed with larger pores, this can indicate that the DTLAC preserved the original structure even after calcination.

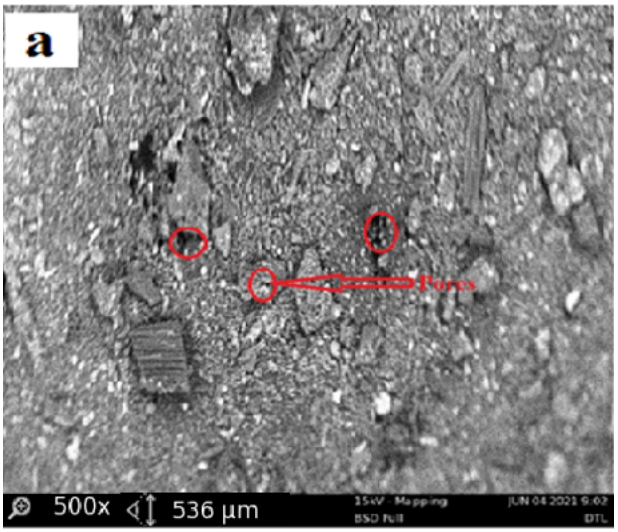

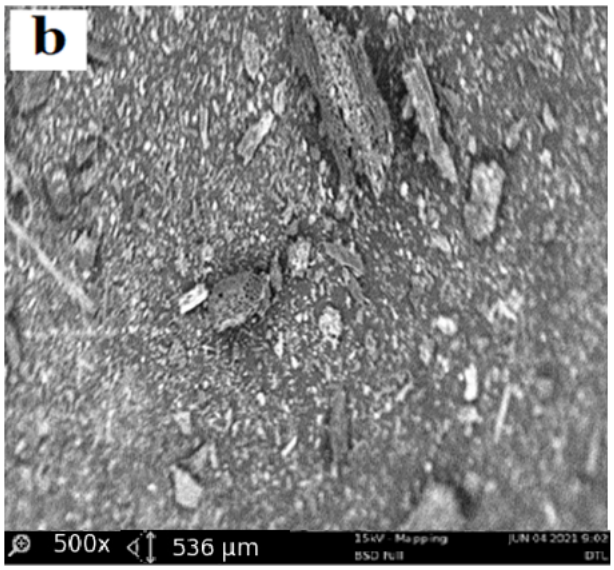

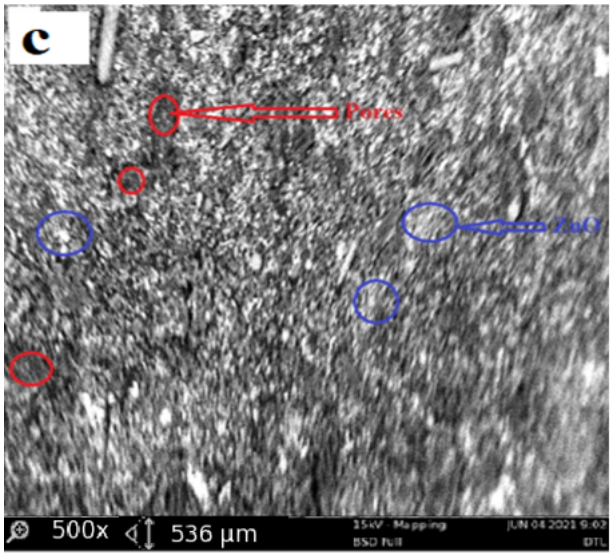

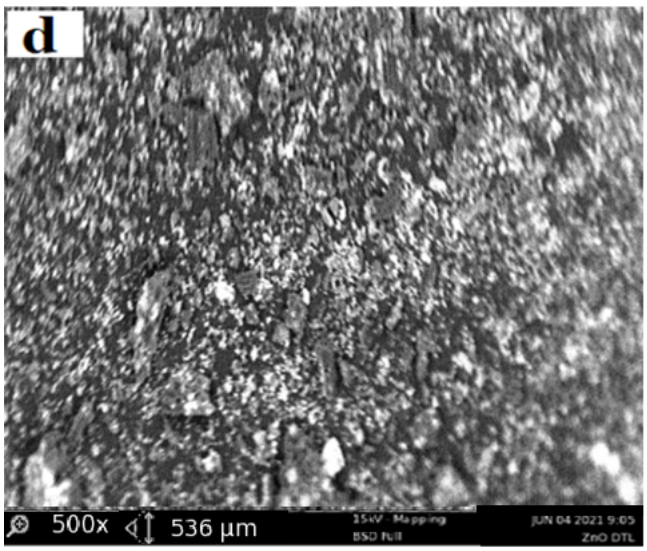

Figure 1: NIDTLAC (a) before and (b) after adsorption; ZnO/DTLAC Adsorbent (c) before and (d) after adsorption

Furthermore, the porous nature of DTLAC can be seen to have provided a more possibility of additional loading space for ZnO nanoparticles, this agrees with a study [23]. Figure 1 showed many white spots distributed over the surface of DTLAC, confirming the presence of ZnO nanoparticles, reported similar morphological study can be found in the literature [11,21]. Also, the SEM images of TiO_2/kaolinite nanocomposite is presented [24] that shows the white spots of TiO_2.

The outcomes of the current SEM images demonstrated that after the heavy metal removal, the surface became relatively smooth however with visible pores and white spots of nanoparticles which suggests that occupation of the adsorbent sites by the adsorbates are partial and there is room for further adsorption activity. From the discussions, an evident change occurred for the morphology of ZnO/DTLAC and NIDTLAC adsorbents before and after adsorption. The same behavior of morphological transformation has been revealed previously [25].

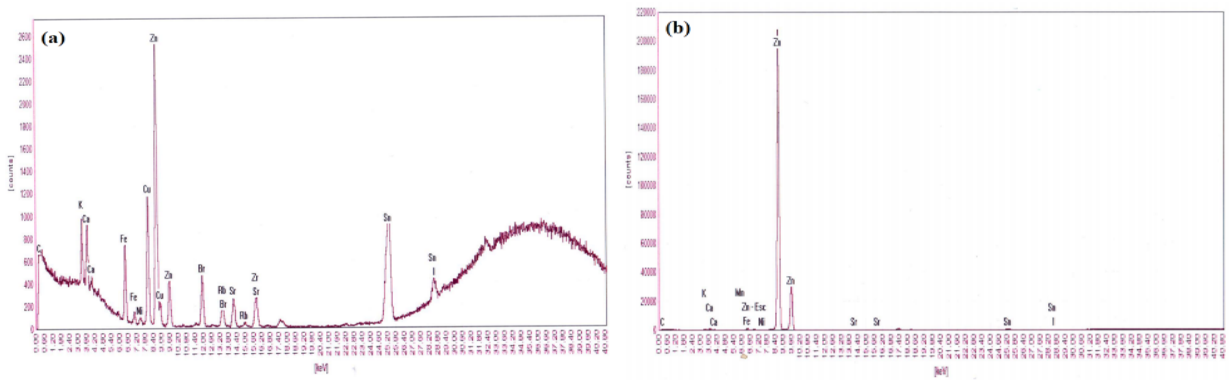

Figure 2: EDXRF of ZnO/DTLAC (a) Before adsorption (b) After adsorption

3.2. Elemental analysis

Characterization of EDXRF shows the chemical composition of the adsorbent which indicates the formation of nanocomposites for ZnO/DTLAC with the visible presents of Zn on the spectra while there is none of these metal oxides on NIDTLAC adsorbent since it is not impregnated with any of the metal oxide, similar XRF result previously can be found elsewhere [26]. Figure 2 shows the EDRF spectrum.

The EDXRF spectra show also that the higher peaks correspond to a greater quantity of the corresponding element in the sample [27]. Table 1 shows the EDXRF elemental analysis.

Table 1: EDXRF Elemental Analysis

Element	ZnO/DTLAC (%) before adsorption	ZnO/DTLAC (%) after adsorption	NIDTLAC
Zn	37.167	27.876	0.5608
Cu	-	-	0.3243
Sn	8.586	9.458	16.512
Cd	0	-0	0
LOI	32.49	41.74	68.15

LOI=Loss in ignition by EDXRF spectroscopy

The importance of the knowledge of the LOI can also be employed as an indicator in monitoring the quality of the final product, it is the amount of weight loss through raising the temperature of the material to a predetermined level [28]. Many studies showed the loss on ignition by EDXRF spectroscopy [29-31]. Characterization of the ZnO/activated carbon nanocomposites in Cd sequestration was reported [15] for FTIR, SEM and XRD without elemental study. It is observed that the intensity peaks of Zn with respect to the other elements is higher for ZnO/DTLAC while the other elements are in very low quantities, so they are not significant for the composition of materials. This finding agrees with a literature [32] however, Sn is also a major element in the composition of DTL and can be seen to be present in all the samples. The amount of Zn reduces after the adsorption which can be attributed to the blockage of Zn nanoparticles dispersed on the DTLAC by the adsorbed heavy metals. The Cd element in the water sample is totally adsorbed and due to its minor amount, it does not show in the peaks of the adsorbents after adsorption. Loss on ignition value of the adsorbents are high indicates high carbonaceous matter [31].

3.3. FTIR analysis

The peak position on the spectra illustrates the presence of a certain functional group with the form of vibration it exhibited. Figure 3 shows the FTIR spectra of NIDTLAC and ZnO/DTLAC adsorbents.

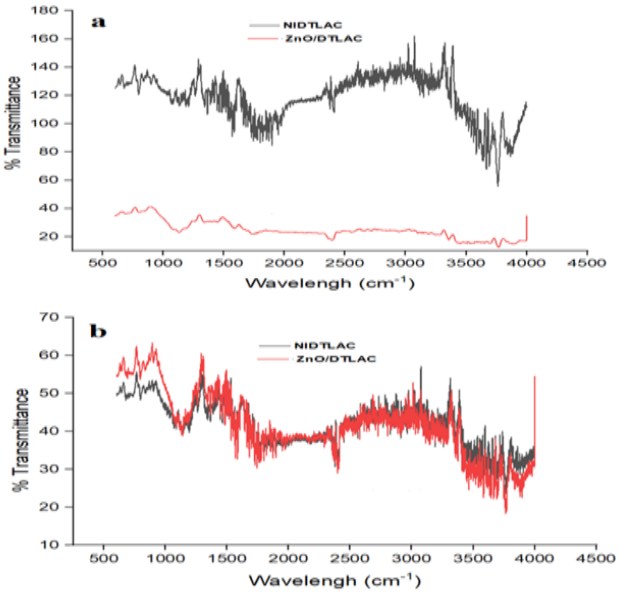

Figure 3: FTIR spectra of NIDTLAC/ ZnO/DTLAC adsorbent (a) before and (b) after adsorption

The shifting of peaks to higher wavenumber and appearance of new peaks showed successful adsorption of the heavy metals [33] and may be due to the interaction of the heavy metals with the functional group [34]. The absorption band at 1578 cm^{-1} arising from aromatic group (C-C), is indicating the formation of carbonaceous material [31]. Table 2 shows the functional groups on the FTIR peak positions and their vibration forms.

Table 2: Functional groups on the FTIR peak positions and their vibration forms

Peak position (cm^{-1})	Functional groups	Vibration form	Reference
38062[a] 3864[b]	—OH and—NH	Stretching vibrations	[35-37]
3761[a] 3763[b] 3768[c,d] 3870[c,d] 3358[c, d] 3355[d] 3431[d]	O—H	Stretching vibrations	[36-37]
3271[b]	C–O	stretching vibrations	[38]
3036[b,d] 3133[d]	O—H	Stretching vibrations	[39]
2905[b]	C -H	stretching vibration	[33]
2838[a] 2840[b] 2713[c,d] 2830[c,d]	C-H	stretching vibrations	[39]
1951[a,d] 1959[b]	C–C	Stretching	[40]
1568[a,b,c,d] 1584[c] 1574[d]	C-C	Stretching	[31]
1197[a] 1186[b]	C–N	Stretching	[34]
694[a,b]	C – H	bending vibration	[39]
687[c]	Si–O	Stretching and bending vibrations	[41-42]

[a]FTIR peak of NIDTLAC before absorption, [b]FTIR spectrum of NIDTLAC after adsorption
[c]FTIR spectrum of ZnO/DTLAC before absorption, [d]FTIR spectrum of ZnO/DTLAC after adsorption

3.4. XRD minerology

The XRD patterns show the diffraction peaks of several phases according to the non-impregnated date tree leaf activated carbon adsorbent. Again, the activated carbon pattern showed an amorphous halo centered at $2\theta = 23^{O}$, which is refers to the reflection of the plane (002) [43], a common feature of non-crystalline structures such as activated carbon. The plane (002) corresponding to activated carbon is confirmed in other studies [39,44]. XRD pattern shows the diffraction peaks of many phases. It indicates the type of XRD peaks belonging to amorphous structure of activated carbon changes into some degree of crystalline nature, previous research shows similar trend [11,45]. Figure 4 shows the XRD analysis of the adsorbents which NIDTLAC showed a highly amorphous nature of the adsorbent in absence of any of the heavy metals, similar conclusion was reported [42]. The intense (100), (002), and (110) peaks can be ascribed to crystalline ZnO with the hexagonal structure (JCPDS card No. 36-1451) [46].

This study suggests an increasing of crystallinity for ZnO/DTLAC adsorbent attributed to the much lower DTLAC amount when compared to the NIDTLAC and same pattern was observed [43]. The phases are presented in Table 3 for the adsorbents.

The change in chemical composition of the adsorbent after adsorption occurred due to the catalyst activity. At the XRD peaks, Cd and Cr appeared at $2\theta = 36.4$ and 58.7^{O} respectively. The ability of the adsorbent to remove the metals from water is depicted by the present of those metal on the diffraction peaks and the corresponding absence of the metals in the AAS analysis after adsorption. The result indicated that Cd and Cr are attached onto ZnO/DTLAC adsorbent after adsorption furthermore, the XRD spectra with the presence of Cd and other heavy metals indicated the formation of partially amorphous solids [42,47]. The study of activated carbons adsorption of heavy metals [48] showed the present of elements and not compounds on the XRD diffractions also, in this study there is no obvious single compound on the XRD diffraction.

3.5. Water Analysis

The source of Cd is from the drinking water (0.017 mg/l) at Dala kwanan Osi while the maximum consumable amount is 0.003 mg/l. Table 4 shows the AAS analysis results before the adsorption of the heavy metals.

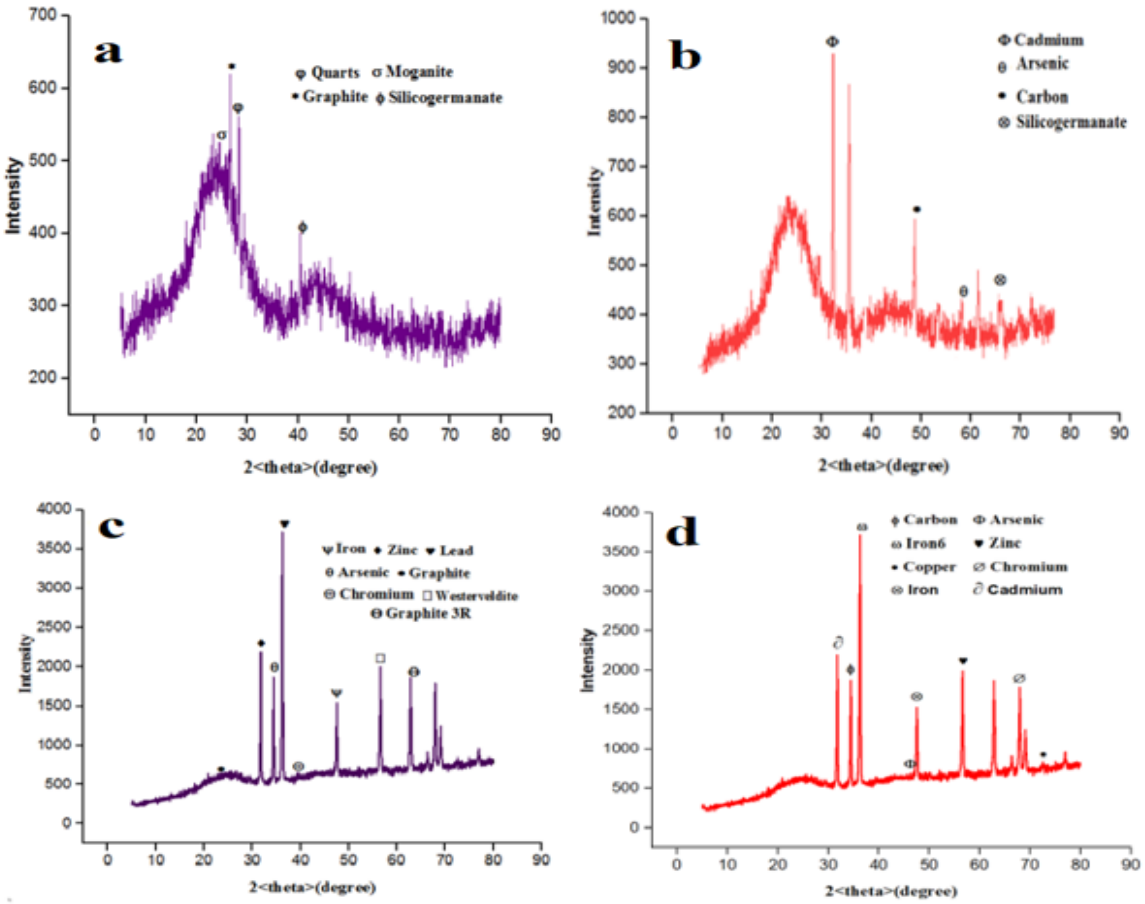

Figure 4: XRD pattern of of NIDTLAC adsorbent (a) before and (b) after adsorption; ZnO/DTLAC adsorbent (c) before and (d) after adsorption

Table 4: AAS analysis Results Before Adsorption

Sample	Arsenic mg/l	Cadmium mg/l	Chromium mg/l	Copper mg/l	Lead mg/l
Sample A (Police college)	0.000	0.002	0.003	0.169	0.009
Sample B (Modaganari bypass)	0.000	0.000	0.001	0.038	0.010
Sample C (Dalakwanan Osi)	0.001	0.017	0.014	0.060	0.010
WHO standard	-	0.003	0.050	1.500	0.010

Table 3: Phases, Chemical Formulae and Quantifications of Adsorbent Before and After Adsorption

Before Adsorption	Chemical Formula	After Adsorption	Chemical Formula/ (%)
NIDTLAC			
Graphite	C6.00 (20.2)	Cadmium	Cd2.00 (2.4)
Quartz	Si3.00 O6.00 (7.1)	Silicogermanate	Si152.00 O304.00 (50.1)
Moganite	Si12.00 O24.00 (14.1)	Arsenic	As6.00 (3.5)
Silicogermanate	Si152.00 O304.00 (58.6)	Carbon	C16.00 (44)
ZnO/DTLC			
Zinc	Zn2.00 (3)	Cadmium	Cd2.00 (6)
Graphite	C16.00 (8.1)	Zinc	Zn2.00 (21)
Chromium	Cr2.00 (3)	Chromium	Cr2.00 (7)
Iron	Fe2.00 (1)	Copper	Cu4.00 (1)
Westerveldite	Fe4.00 As4.00 (1)	Iron	Fe2.00 (1)
Graphite 3R	C6.00V(79.8)	Arsenic	As6.00 (10)
		Iron	Fe6.00 (33)
		Carbon	C16.00 (21)

The heavy metal Cd is a toxic non-essential transition metal that poses a health risk for both humans and animals, its exposure is known to have adverse effects on the kidney, liver, bones and cardio-pulmonary system, but the kidney is the critical organ, where chronic exposure to Cd often causes renal dysfunction [3,49]. Chromium (Cr), Copper (Cu) and lead (Pb) are known to cause cancer, gastrointestinal disorder, poor mental development respectively was found at maximum concentrations of 0.014mg/l, 0.169mg/l and 0.012mg/l respectively as against the maximum acceptable benchmark of 0.050mg/l, 1.00mg/l and 0.010mg/l respectively for Cr, Cu and Pb thereby indicating that all the three metals existed below the maximum permitted in all the three (3) borehole water sample. However, Cd which is known to be toxic to the kidney was the only heavy metal which was found to be existing at a concentration higher than that permitted for portable drinking water and thus if not significantly reduced in the water, it may pose a great danger to the consumer. Table 5 shows the AAS analysis after adsorption.

Table 5: AAS Analysis Result After Adsorption

	Dosage (g)	Arsenic (mg/l)	Cadmium (mg/l)	Chromium (mg/l)	Copper (mg/l)	Lead (mg/l)
Sample A (Police college)	1.0 ZnO/DTL	0.000	0.000	0.004	0.000	0.000
	1.0 NI/DTL	0.000	0.005	0.005	0.011	0.030
Sample B (Modaganari byepass)	1.0 ZnO/DTL	0.000	0.000	0.000	0.020	0.000
	1.0 NI/DTL	0.000	0.000	0.017	0.013	0.002
Sample C (Dala Kwanan Osi)	1.0 ZnO/DTL	0.000	0.000	0.005	0.007	0.035
	1.0 NI/DTL	0.000	0.003	0.007	0.017	0.090
WHO standard		-	0.003	0.050	1.500	0.010

The water samples A, B and C, is have shown a significant change of heavy metals based on the AAS result hence, Ar is completely removed from the water samples as a result. Cd which is queried has been removed significantly in Samples A, B and C with the most efficient adsorbent being ZnO/DTLAC further confirming that adsorbents impregnation improves the efficiency of the adsorbent, this finding agrees with other studies [50-52]. In sample C, which was initially harboring the highest concentration of Cd, it can be observed that the concentration is within the maximum permitted limits of 0.003 mg/l from Table 5.

Moreover, Cr, Cu and Pb has shown significant reduction in concentration where Cu and Pb were completely removed from water sample A by using the ZnO/DTLAC adsorbent. Cr and Pb were also completely removed from water sample B respectively. Also, Cr, Cu and Pb has also been significantly removed in sample C by the ZnO/DTLAC adsorbent. From Table 5, Cd was removed completely using impregnated adsorbent and reduced significantly by the application of non-impregnated adsorbent.

3.6 Adsorption isotherm study

The description of the ZnO/DTLAC adsorbent, was studied for the adsorption behavior using adsorption isotherm models where the adsorption capacity is explained by the models. The Langmuir is formulated as follows [53]:

$$qe = \frac{qmKLCe}{1+KLCe} \quad (1)$$

where, qe is the equilibrium adsorption capacity (mg/g), qm and KL are the maximum adsorption capacity to form a complete monolayer on the surface (mg/g), and the Langmuir constant related to the energy of adsorption (bonding energy of sorption in (L/g), respectively. The linearized form of Langmuir equation is:

$$\frac{Ce}{qe} = \frac{1}{qmKL} + \frac{Ce}{qm} \quad (2)$$

The dimensionless characteristic of Langmuir isotherm referring to the separation factor (RL) is useful in predicting the adsorption efficiency of the adsorption process. It is an indicator of Langmuir isotherm suitability as either unfavorable (RL > 1), linear (RL = 1), favorable (0 < RL< 1), or irreversible (RL = 0); RL can be express as:

$$RL = \frac{1}{1+KL.Co} \quad (3)$$

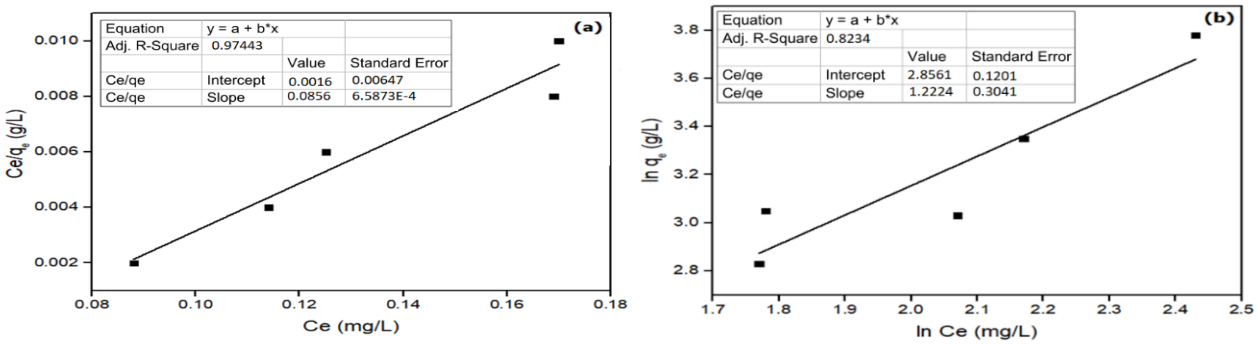

Figure 5: The plot of (a) Langmuir Isotherm (b) Freundlich isotherm

where Co is the highest initial concentration of the adsorbate (mg/L), and KL (L/mg) is the Langmuir constant. The Freundlich model is defined as:

$$qe = K_f Ce^{1/n} \quad (4)$$

where K_f and 1/n are the Freundlich constants related to sorption capacity and sorption intensity, respectively. The linearized form of equation 1 can be obtained by taking logarithms on both sides:

$$\log\ qe = \log Kf + \frac{1}{n}\log Ce \quad (5)$$

The applicability of an isotherm may be determined by the coefficient of determination (R^2) [54] thus, the R^2 value for adsorbent was found to be high in the Langmuir isotherm (0.9684) while that of Freundlich isotherm showed lower R^2 (0.8479). Previous similar study can be found in the literature [55].

A dimensionless characteristic of Langmuir isotherm termed as the separation factor (R_L) [50] is useful to predicts the adsorption efficiency of the adsorption process and shows the suitability of Langmuir isotherm as unfavorable (R_L>1), linear (R_L=1), favorable (0 < R_L< 1) or irreversible (R_L=0) [47]. Moreover, the Langmuir isotherm suitability was indicated by the favorable separation factor (R_L) values gotten as 0.27. The heterogeneity factor (1/n) describing the adsorption capacity by Freundlich isotherm, and its value becomes more heterogeneous as it gets farther to one with the range of favorable adsorption as 1 < n < 10 [56-57].

In this study, the heterogeneity factor is 0.8180 which is not favorable. Therefore, the Langmuir isotherm supersedes the characteristics shown by the Freundlich isotherm hence it is more suitable to explicate the correlation of experimental results, similar work has been reported earlier [54,56,58]. Figure 5 shows the plot of (a) Langmuir Isotherm (b)Freundlich isotherm.

The Langmuir assumptions stated that at maximum adsorption, only a monolayer of adsorbed material is formed. Also, the molecules of adsorbate do not deposit on each other while the adsorption sites were identical. Secondly, under constant temperature, the adsorbed molecules do not interact. Thirdly, there are equal adsorption sites, and the surface of the adsorbent was uniform. Fourthly, the adsorption occurs through the same mechanism. By implication, these assumptions are applicable to the ZnO/DTLAC adsorbent, this finding agrees with the previous work [57].

4. Conclusion

The adsorption capacity of the activated carbon metal oxide impregnated (ZnO/DTLAC) and non-impregnated (NIDTLAC) adsorbents were studied, and the adsorbents were able to remove the heavy metals from three water samples to the required consumable standard. The micrograph by SEM showed that the surface structures are porous, with distributed pores over the carbonaceous matrix, while EDXRF showed the chemical composition of the adsorbent indicating the formation of nanocomposites and the loss on ignition value of the depicts high carbonaceous matter. The absorption band at 1578 cm^{-1} due to aromatic group (C-C), indicated the formation of carbonaceous in composite. XRD spectra of the showed a highly amorphous nature in absence of any of the heavy metals and the activated carbon pattern showed an amorphous halo centered at $2\theta = 23^{O}$, which refers to the reflection of the plane (002), a common feature of non-crystalline structures such as activated carbon. The adsorbents developed are suitable for the decontamination of heavy metals from borehole water in some areas of Maiduguri, Nigeria.

References

[1] T. Rasheed, S. Sha, M. Bilal, T. Hussain, F. Sher, and K. Rizwan, "Surfactants-based remediation as an effective approach for removal of environmental pollutants — A review," *Journal of Molecular Liquids*, vol. 318, pp. 1–15, 2020.

[2] A. A. Siyal, M. R. Shamsuddin, M. I. Khan, N. M. Zulfiqar, Z. Man, J. S. Khairul, A. Azizli, "A Review on geopolymers as emerging materials for the adsorption of heavy metals and dyes," . *Journal of Environmental Management.*, vol. 224, pp. 327-no. 339, 2018.

[3] G. Genchi, M. S. Sinicropi, G. Lauria, and A. Carocci, "The effects of cadmium toxicity," *International Journal of Environment Resource and Public Health*, vol. 17, no. 3782, pp. 1–24, 2020.

[4] W. P. Cheng, J. G. Yang, and M. Y. He, "Evaluation of crystalline structure and SO_2 removal capacity of a series of MgAlFeCu mixed oxides as sulfur transfer catalysts," *Catalysis Communications*, vol. 10, no. 6, pp. 784–787, 2009.

[5] A. Jain, R. Balasubramanian, and M. P. Srinivasan, "Hydrothermal conversion of biomass waste to activated carbon with high porosity: A review," *Chemical Engineering Journal*, vol. 283, pp. 789–805, 2016.

[6] B. Ni, Q. Huang, C. Wang, T. Ni, J. Sun, and W. Wei, "Competitive adsorption of heavy metals in aqueous solution onto biochar

derived from anaerobically digested sludge," *Chemosphere*, vol. 219, pp. 351-357, 2019.

[7] R. Chakraborty, A. Asthana, A. K. Singh, and B. Jain, "Adsorption of heavy metal ions by various low-cost adsorbents: A review," *International Journal of Environmental Analytical Chemistry*, pp. 1–38, 2020.

[8] M. T. A. Shafiq, A.A. Alazba, "Removal of heavy metals from wastewater using Date Palm as a biosorbent: A Comparative Review," *Sains Malaysiana*, vol. 47, no. 1, pp. 35–49, 2018.

[9] Z. Z. Ismail, "Kinetic study for phosphate removal from water by recycled date-palm wastes as agricultural by-products," *International Journal of Environment.*, pp. 37–41, 2012.

[10] M. Abdullahi, S. A. Yahaya, M. K. Sanusi, B. E. Sambo, S. B. Abba "The potentials of esterblishing date palm plantation in sudano sahelian region of Nigeria." Conference: Farm Management Association of Nigeria (FAMAN) At: General Studies Auditorium, Federal University Dutse, Jigawa State Nigeria. 2015.

[11] M. Kamaraj, N. R. Srinivasan, G. Assefa, A. T. Adugna, and M. Kebede, "Facile development of sunlit ZnO nanoparticles-activated carbon hybrid from pernicious weed as an operative nano-adsorbent for removal of methylene blue and chromium from aqueous solution: Extended application in tannery industrial wastewater," *Environmental Technology and Innovation*, vol. 17, pp. 10–40, 2020.

[12] S. Kiman, G. W. Azlina, C.Thomas, and R. Umer, "Carbonaceous materials modified catalysts for simultaneous SO_2/NO x removal from flue gas: A review," *Catalysis Review*, vol. 61, no. 1, pp. 1–28, 2018.

[13] M. A. Naeem *et al.*, "Batch and column scale removal of cadmium from water using raw and acid activated wheat straw biochar," *Water (Switzerland)*, vol. 11, no. 7, pp. 1–17, 2019.

[14] R. Kumar and J. Chawla, "Removal of Cadmium Ion from water/wastewater by nano-metal Oxides: A review," *Water Quality Exposure and Health*, vol. 5, no. 4, pp. 215–226, 2014.

[15] S. Alhan, M. Nehra, N. Dilbaghi, N. K. Singhal, K. H. Kim, and S. Kumar, "Potential use of ZnO@activated carbon nanocomposites for the adsorptive removal of Cd^{2+} ions in aqueous solutions," *Environmental Resource*, vol. 173, pp. 411–418, 2019.

[16] K. Pyrzynska, "Removal of cadmium from wastewaters with low-cost adsorbents," *Journal of Environmental Chemical Engineering*, vol. 7, no. 1, pp. 1–40, 2019.

[17] W. M. H. Wan Ibrahim, M. H. Mohamad Amini, N. S. Sulaiman, and W. R. A. Kadir, "Powdered activated carbon prepared from Leucaena leucocephala biomass for cadmium removal in water purification process," *Arab Journal of Basic Appllied Science*, vol. 26, no. 1, pp. 30–40, 2019.

[18] M. R. Awual, "A facile composite material for enhanced cadmium(II) ion capturing from wastewater," *Journal of Environmental Chemical Engineering*, vol. 7, no. 5, pp. 1–11, 2019.

[19] K. Silas, W. A. W. Ghani, T. S. Y. Choong, R. Umer , "Breakthrough studies of Co_3O_4 supported activated carbon monolith for simultaneous SO_2/NOx removal from flue gas," *Fuel Processing Technolology*, vol. 180, pp. 155–165, 2018.

[20] T. Tay, S. Ucar, S. Karagöz, "Preparation and characterization of activated carbon from waste biomass," . *Journal of Hazardous Materials*, vol. 165, no. 1–3, pp. 481–485, 2009.

[21] M. Zbair, Z. Anfar, H. Ait Ahsaine, N. El Alem, and M. Ezahri, "Acridine orange adsorption by zinc oxide/almond shell activated carbon composite: Operational factors, mechanism and performance optimization using central composite design and surface modeling," *Journal of Environmental Management, vol.* 206, pp. 383–397, 2018.

[22] M. A. Tariq, M. A. Tariq, M. Nadeem, M. M. Iqbal, M. Imran, M. H. Siddique, Z. Iqbal, M. Amjad, M. Rizwan, S. Ali, "Effective sequestration of Cr (VI) from wastewater using nanocomposite of ZnO with cotton stalks biochar: modeling, kinetics, and reusability," *Environmental Science and Pollution Research*, vol. 27, pp. 33821–33834, 2020.

[23] J. Peternela, M. F. Silva, M. F. Vieira, R. Bergamasco, and A. M. S. Vieira, "Synthesis and impregnation of copper oxide nanoparticles on activated carbon through green synthesis for water pollutant removal," *Research*, vol. 21, no. 1, pp. 1–11, 2018.

[24] A. M. Awwad, M. W. Amer, and M. M. Al-aqarbeh, "TiO_2-kaolinite nanocomposite prepared from the Jordanian Kaolin clay: Adsorption and thermodynamics of Pb(II) and Cd(II) ions in aqueous solution," *Chemistry International* , vol. 6, no. 4, pp. 168–178, 2020.

[25] C. Ma, M. Changchang, H. Hai, G. Xin, W. Tao, Z. Zhi, H. Pengwei, L. Yang, Y. Yongsheng, "Honeycomb tubular biochar from fargesia leaves as an effective adsorbent for tetracyclines pollutants," *Journal of The Taiwan Institute Of Chemical Engineers*, vol. 91, pp. 299–308, 2018.

[26] S. Ilyas, D. Tahir, Suarni, B. Abdullah, and S. Fatimah, "Structural and bonding properties of honeycomb structure of composite nanoparticles Fe_3O_4 and activated carbon," *Journal Of Physics: Conference Series*, vol. 1317, no. 1, pp. 1–8, 2019.

[27] G. B. Adebayo, F. A. Adekola, H. I. Adegoke, S. Fausiyat, and J. Wasiu, "Synthesis and characterization of goethite, activated carbon and their composite," *Journal of Chemical Technology And Metallurgy*, vol. 55, no. 5, pp. 1068–1077, 2020.

[28] O. O. Olubajo, I. Y. Makarfi, and O. A. Odey, "Prediction of loss on ignition of ternary cement containing coal bottom ash and imestone using central composite design," *Path of Science*, vol. 5, no. 8, pp. 2010–2019, 2019.

[29] B. Abdullah, S. Ilyas, and D. Tahir, "Nanocomposites Fe/Activated Carbon/PVA for microwave absorber: Synthesis and characterization," *Journal of Nanomaterials.*, vol. 2018, pp. 1–7, 2018.

[30] A. Kumar and P. Lingfa, "Sodium bentonite and kaolin clays: Comparative study on their FT-IR, XRF, and XRD," *Materials Today: Proceedings*, vol. 22, pp. 737–742, 2020.

[31] D. Tahir, S. Liong, and F. Bakri, "Molecular and structural properties of polymer composites filled with activated charcoal particles," *AIP Conference Proceedings*, vol. 1719, pp. 1–5, 2016.

[32] E. Carpio, P. Zúñiga, S. Ponce, J. Solis, J. Rodriguez, and W. Estrada, "Photocatalytic degradation of phenol using TiO_2 nanocrystals supported on activated carbon," *Journal of Molecular Catalysis A: Chemical*, vol. 228, no. 1–2, pp. 293–298, 2005.

[33] V. K. Gupta, S. Agarwal, R. Ahmad, A. Mirza, and J. Mittal, "Sequestration of toxic congo red dye from aqueous solution using ecofriendly guar gum/activated carbon nanocomposite," . *International Journal of Biological Macromolecules*, vol. 158, pp. 1–33, 2020.

[34] S. Sahu, S. Pahi, J. K. Sahu, U. K. Sahu, and R. K. Patel, "Kendu (*Diospyros melanoxylon Roxb*) fruit peel activated carbon — an efficient bioadsorbent for methylene blue dye: equilibrium, kinetic, and thermodynamic study," *Environmental Science and Pollution Research*, vol. 27, pp. 1–14, 2020.

[35] B. K. Saikia, R. K. Boruah, and P. K. Gogoi, "XRD and FT–IR investigations of sub-bituminous Assam coals," *Material Science*, vol. 30, no. 4, pp. 421–426, 2007.

[36] O. O. Sonibare, T. Haeger, and S. F. Foley, "Structural characterization of Nigerian coals by X-ray diffraction, Raman and FTIR spectroscopy," *Energy*, vol. 35, no. 12, pp. 5347–5353, 2010.

[37] S. Lin, Z. Liu , E. Zhao, J. Qian, X. Li, Q. Zhang, M. Ali "A study on the FTIR spectra of pre- and post-explosion coal dust to evaluate the effect of functional groups on dust explosion," *Process Safety and Environmental Protectio.*, vol. 130, pp. 48–56, 2019.

[38] S. Alshuiael, A. Mohammad, "Multivariate analysis for FTIR in understanding treatment of used cooking oil using activated carbon prepared from olive stone," *PLoS One*, vol. 15, no. 5, pp. 1–25, 2020.

[39] A. H. Wazir, I. U. Wazir, and A. M. Wazir, "Environmental effects preparation and characterization of rice husk based physical activated carbon," *Energy Sources, Part A: Recovery, Utilization, And Environmental Effects*, pp. 1–11, 2020.

[40] P. Jujur, M. Nur, M. Asy, and H. Nur, "SEM, XRD and FTIR analyses of both ultrasonic and heat generated activated carbon black microstructures," *Heliyon*, vol. 6, pp. 1–16, 2020.

[41] D. Gandhi, R. Bandyopadhyay, and S. Parikh, "Structural and composition enhancement of Indian Kachchh kaolin clay: characterisation and application as low-cost catalyst" *Indian Chemical Engineer*, pp. 1–11, 2020.
[42] A. J. Bora and R. K. Dutta, "Removal of metals (Pb, Cd, Cu, Cr, Ni, and Co) from drinking water by oxidation-coagulation-absorption at optimized pH," *Journal of Water Process Engineering*, vol. 31, pp. 1–9, 2019.
[43] S. C. Rodrigues, M. C. Silva, J. A. Torres, and M. L. Bianchi, "Use of magnetic activated carbon in a solid phase extraction procedure for analysis of 2, 4-dichlorophenol in water samples," *Water Air Soil Pollution*, vol. 231, no. 294, pp. 1–13, 2020.
[44] D. Propolsky, E. Romanovskaia, W. Kwapinski, and V. Romanovski, "Modified activated carbon for deironing of underground water," *Environmental Research*, vol. 182, pp. 1–16, 2020.
[45] A. I. Osman, C. Farrell, A. H. Al-muhtaseb, H. John, and D. W. Rooney, "The production and application of carbon nanomaterials from high alkali silicate herbaceous biomass," *Scientific Reports*, vol. 10, no. 2563, pp. 1–13, 2020.
[46] M. K. A. Mohammed, D. S. Ahmed, and M. R. Mohammad, "Studying antimicrobial activity of carbon nanotubes decorated with metal-doped ZnO hybrid materials," *Mater. Res. Express*, vol. 6, no. 5, pp. 1–16, 2019.
[47] Q. Ain, M. U. Farooq, and M. I. Jalees, "Application of magnetic graphene oxide for water puri fication: Heavy metals removal and disinfection," *Journal of Water Process Engineering*, vol. 33, pp. 1–14, 2020.
[48] C. F. Ramirez-gutierrez, R. Arias-niquepa, J. J. Prías-barragán, and M. E. Rodriguez-garcia, "Study and identification of contaminant phases in commercial activated carbons," *Journal Of Environmental Chemical Engineering*, vol. 8, no. 1, pp. 10-36, 2020.
[49] M. B. Arain, T. G. Kazi, J. A. Baig, and H. I. Afridi, "Co-exposure of arsenic and cadmium through drinking water and tobacco smoking: Risk assessment on kidney dysfunction," *Environmental Science Pollution Resource*, vol. 22, pp. 350–357, 2015.
[50] S. S. Shah, T. Sharma, B. A. Dar, and R. K. Bamezai, "Adsorptive removal of methyl orange dye from aqueous solution using populous leaves: Insights from kinetics, thermodynamics and computational studies," *Enviromental Chemistry and Ecotoxicoly*, vol. 3, pp. 172–181, 2021.
[51] M Vakili, H. M. Zwain, A. Mojiri, W. Wang, F. Gholami, Z. Gholami, A. S. Giwa, B. Wang, G. Cagnetta, B. Salamatinia, "Effective adsorption of reactive black 5 onto hybrid hexadecylamine impregnated chitosan-powdered activated carbon beads," *Water*, vol. 12, no. 2242, pp. 1–14, 2020.
[52] K. Azam R. Raza, N. Shezad, M. Shabir, W. Yang, N. Ahmad, I. Shafiq, P. Akhter, A. M. Hussain, "Development of recoverable magnetic mesoporous carbon adsorbent for removal of methyl blue and methyl orange from wastewater," *Environmental Chemistry and Ecotoxicology*, vol. 8, no. 5, pp. 1–20, 2020.
[53] S. Kiman, G. W. Azlina, C.Thomas, and R. Umer, "Monolith metal-oxide-supported catalysts: Sorbent for environmental application," *Catalyst*, vol. 10, pp. 1–25, 2020.
[54] P. Ganguly, R. Sarkhel, and P. Das, "Synthesis of pyrolyzed biochar and its application for dye removal: Batch, kinetic and isotherm with linear and non-linear mathematical analysis," *Surfaces and Interfaces*, vol. 20, pp. 1–16, 2020.
[55] V. P. Singh and R. Singhal, "Optimization of dye removal by diesel exhaust emission soot using response surface methodology," *Environmental Progress Sustainable Energy*, pp. 1–11, 2020.
[56] E. E. Jasper, V. Olatunji, A. Jude, and C. Onwuka, "Nonlinear regression analysis of the sorption of crystal violet and methylene blue from aqueous solutions onto an agro - waste derived activated carbon," *Applied Water Science, vol.* 10, no. 6, pp. 1–11, 2020.
[57] S. Ullah, M. A. Bustam, M. Ali, A. Abdullah, G. Al-Sehemi, G. Gonfa, A. Mukhtar, F. A. Abdul, M. Ayoub, S. Saqib, N. B. Mellon, "Synthesis and characterization of mesoporous MOF UMCM-1 for CO_2CH_4 adsorption; An experimental, isotherm modeling and thermodynamic study," *Microporous Mesoporous Materials.*, vol. 294, pp. 1–44, 2019.
[58] J. Garc, "Biochar from agricultural by-products for the removal of lead and cadmium from drinking water," *Water*, vol. 12, no. 2933, pp. 1–16, 2020.

KIMAN SILAS attended University of Maiduguri in Borno state, Nigeria and graduated with Bachelor's degree in Chemical Engineering in 2007 and Master degree in Chemical Engineering in 2012. He joined Universiti Putra Malaysia and obtained his PhD in Chemical Engineering in 2019. He published many journal papers and is presently lecturing at the Department of Chemical Engineering, University of Maiduguri in Borno state, Nigeria. His specialty is in Energy and Environmental Engineering and an expert in CO_2 Capture, Waste Utilization, Biomass Conversion and Gas Cleaning. He is a registered member of the Council for the Regulation of Engineering in Nigeria (COREN) and Nigerian Society of Engineers (NSE).

ALIYU BUBA NGULDE is a graduate of University of Maiduguri in Borno state, Nigeria, he obtained his Bachelor's of Engineering degree in Chemical Engineering in 2017 and Master of Engineering degree in Chemical Engineering in the year 2021, also of the University of Maiduguri. He is currently admitted at the Universiti Putra Malaysia to study PhD in Chemical Engineering. Presently, he is a lecturer at the Department of Chemical Engineering, University of Maiduguri in Borno state, Nigeria. His research interest Renewable Energy and Environmental Engineering. He is a registered member of the Council for the Regulation of Engineering in Nigeria (COREN) and Nigerian Society of Engineers (NSE) as well as the International Association of Engineering (IAENG).

HABIBA DANJUMA MOHAMMED is a graduate of University of Maiduguri in Borno state, Nigeria with Bachelor's degree in Chemical Engineering in 2008. She obtained Master degree in Environmental Technology and Management in University of Port Harcourt, Rivers state, Nigeria. She is presently pursuing her PhD in Chemical Engineering. She published some journal papers and is presently lecturing at the Department of Chemical Engineering, University of Maiduguri in Borno state, Nigeria. Her specialty is in Renewable Energy, Biochemical and Environmental Engineering, Waste Technology, Biomass Conversion and Environmental Management. She is a registered member of National Registry for Environmental Professionals (NREP), the Council for the Regulation of Engineering in Nigeria (COREN) and Nigerian Society of Engineers (NSE).

Received: 25 February 2022, Revised: 06 April 2022, Accepted: 15 April 2022, Online: 22 April 2022

DOI: https://dx.doi.org/10.55708/js0104017

MC-SPWM and MC-THIPWM Methods for Symmetric and Asymmetric Design of CHB-MLI: A Study

Jigneshkumar Patel *, **Vijay Sood**

Faculty of Engineering and Applied Science, Oshawa, L1G 0C5, Canada
*Corresponding author: jigneshkumar.patel@ontariotechu.net, vijay.sood@ontariotechu.ca

ABSTRACT: Cascaded H-bridge multilevel inverters (CHB-MLI) are employed in a variety of medium/high power applications. These inverters are known to inject unwanted harmonics into the grid, which negatively affects the grid and connected loads. CHB-MLI topology can reduce many of these harmonics by producing multiple output voltage levels and improves the fundamental component using a suitable modulation technique. However, the CHB-MLI topology configuration requires multiple isolated input sources which must be balanced either with the modulation technique or with an additional method. This paper analyzes multi-carrier pulse width modulation (MC-PWM) techniques for CHB-MLIs. In this study, two basic configurations of CHB-MLI symmetrical and asymmetrical are reviewed, followed by their mathematical analysis. Also, this paper analyses multi-carrier based sinusoidal pulse width modulation (MC-SPWM) and multi-carrier based third-harmonic injected pulse width modulation (MC-THIPWM) techniques with phase-shifted (PS) and level-shifted (LS) carrier arrangements for the CHB-MLI. Moreover, a simulation study has been conducted using MATLAB Simulink to analyze the performance of MC-PWM techniques for the symmetrical and asymmetrical type CHB-MLIs. The 7-level and 9-level CHB-MLIs were evaluated for the stated MC-PWM techniques in terms of harmonics and fundamental components. In addition, discharging current of all input sources was checked to verify the ability of all MC-PWM techniques to balance all input sources.

KEYWORDS: Cascaded H-bridge inverter, Harmonics, Power electronic, Pulse width modulation

1. Introduction

High-voltage (HV) converters are used in motor drives [1], static VAR compensators [2], renewable energy systems [3], [4], high-voltage direct current (HVDC) transmission and other similar applications [5–7]. The traditional single-phase inverter generates two or three-levels in the output signal, while MLIs can create multi-levels in the output signal. More levels supply a lower distortion and better-quality output signal. Moreover, the MLI topology provides a precise control of the voltage stresses on each switch [8]. Therefore, the MLI is more suitable for medium/high voltage and high-power applications. Although there are many MLI topologies available [9–11], the most prevalent MLI topologies are neutral point clamped MLI (NPC-MLI) [4], [12], [13], flying capacitor MLI (FCMLI) [14], and cascaded H-bridge MLI (CHB-MLI) [15]. Among these MLIs, the CHB-MLI has acquired special attention in most topologies because of the modular structure and flexible to generate any number of output voltage levels [16–18].

The CHB-MLI is easy to construct and highly dependable. This inverter has either a symmetrical or asymmetrical mode of operation [19], [20]. The symmetrical mode of CHB-MLI utilizes equal-amplitude DC sources. In contrast, the asymmetrical form of CHB-MLI uses the unique amplitude of various DC voltage sources. Also, the asymmetrical form of CHB-MLI utilizes fewer power electronic (PE) switches than the symmetrical type CHB-MLI [21]. All PE converters need a suitable PWM technique for their operation.

The main classifications of PWM techniques are low- and high-frequency (HF) switching modulation techniques to control multi-level inverters [22], [23]. The low-frequency (LF) modulation technique is more suitable for the high-power converter in high voltage applications like HVDC transmission. The nearest-level modulation (NLM) and selective harmonics elimination (SHE) methods are placed in this category [24], [25]. These methods are efficient in reducing the switching losses. The NLM method is also known as the staircase modulation technique since it generates the nearest possible level by comparing a sinusoidal reference with carriers [26]. This method is suitable for implementing with a larger number of modules. The converter's performance diminishes, and total harmonic distortion (THD) improves when fewer modules are obtainable with this method [27]. This method was also combined with the space-vector modulation technique to improve its capability [28], [29].

Another LF method is the SHE method. In this method, the solution of a set of non-linear transcendental equations are the switching angles of the pulses which turn ON/OFF the PE switches [30], [31]. The primary goal of this method is to cut specific lower-order harmonics from the output voltage/current waveforms. Also, this method can control PE switches at the fundamental frequency, which lowers the switching losses [32], [33]. The trigonometric terms are used in this method to express harmonic components.

The number of equations increases because the switching angles increase with the higher number of modules. The authors of [30], [34–36] proposed many equation-solving methods like the Newton-Raphson (NR) method, particle swarm optimization (PSO), and genetic algorithms (GA) to ease the calculation of the switching angles. Regardless, it is challenging to solve these non-linear equations for more modules. Moreover, output signal and dynamic response are weak [30], [37].

The space vector PWM (SV-PWM) is also a LF switching technique. This method is an addition to the basic SV control technique with an expanded number of vectors [38]. This method provides a higher voltage on the AC side [39]. At the same time, it reduces the voltage and current THD compared to the SPWM method. The functional status of the switches can be described by switching states for this method. Yet, it is very complicated to decide the whole the vectors for more modules in HV applications [40], [41].

The carrier-based modulation technique is considered a HF modulation scheme. A single HF triangular carrier wave is compared with the reference wave to generate gate pulses [42]. It is also known as the SPWM technique. It is simple and easy to implement and highly popular.

Some researchers [43–46] replaced the triangular carrier signal with the other carrier signals to develop new modulation techniques. In one technique, the sinusoidal wave replaces the traditional carrier signal. This method is known as sinusoidal-SPWM (S-SPWM). This technique produced more harmonics with a lower fundamental output voltage than the SPWM technique [43]. The inverse sinusoidal carrier PWM (ISCPWM) method is the other technique, which generates switching pulses using an inverse sinusoidal carrier signal. This method increases the fundamental component in the output signal [43], [44], [46], [47]. Later it was changed to the variable frequency inverse sinusoidal PWM (VFSPWM). Both methods require high computational power digital hardware since it needs a smaller time step to generate a complex carrier signal [44]. These carrier signals and modulation signals must be synchronized to control harmonics. Another advanced carrier-based PWM technique, named UN-shape carrier PWM (UNPWM) [43], was proposed to overcome the drawbacks of SPWM and S-SPWM. It can increase the essential component and reduce harmonics in the output signal, though generating an UN-shape carrier signal is not easy with digital controllers.

As in the conventional method, gating pulses result from corresponding multiple carrier signals and sinusoidal reference signals. The MC-PWM technique for the MLI is an extension of this traditional technique. The third harmonic injected PWM (THIPWM) method uses a newly generated reference signal. This reference signal is achieved by injecting the third-order harmonic into the sinusoidal signal [48], [49].

Like the SPWM, switching pulses are produced with the triangle and a new reference signal. In both (SPWM and THIPWM) methods, HF carrier signal transfers the LF harmonics to HF harmonics. The affordable filter can decrease these HF harmonics to the accepted harmonic limits suggested by the IEEE Std 519-1992. According to IEEE Std 519-1992, the total voltage distortion (THD) limit is 5% for the voltage 69 kV and below [50], [51].

Furthermore, the fundamental element becomes lessened in the output by the MC-SPWM technique regarding MC-THIPWM. Therefore, MC-SPWM reduces the inverter's efficiency [52].

There are two ways to arrange carrier signals in the MC-PWM method: phase-shifted (PSPWM) or level-shifted (LSPWM). In the PSPWM, the phase of the one carrier signal displaces the other signal's phase horizontally. In contrast, one carrier signal shifts the other vertically in the LSPWM. Moreover, the carrier signals are placed as alternate-phase-disposition (APOD), in-phase-disposition(IPD), and phase-opposition-disposition(POD) [53–57].

This paper investigates the behavior of a 7-level and 9-level 3-phase symmetric/asymmetric CHB-MLI using MC-based SPWM and THIPWM methods for all carrier signal arrangements. This paper is arranged as follows: Section 2 introduces an H-bridge inverter. Section 3 presents the CHB-MLI topology. The MC-based PWM approach is illustrated in Section 4. Similarly, the execution for the symmetric and asymmetric types of CHB-MLI is presented in Section 5. Then, a qualitative analysis and numerical examination of both kinds of CHB-MLI using different MC-PWM is produced, employing MATLAB/Simulink simulations.

2. H-bridge inverter

The traditional low voltage (LV) inverter (voltage source inverter (VSI)) is a 1-phase, which produces two-level in the output, which is used for LV applications. A classic configuration of a 1-phase H-bridge (HB) inverter is shown inside the orange square in Figure 1. This VSI is simple and effortless to run. A suitable control method can be used with this VSI to generate the 3-level signal in the output. There are 4-switches used to form 2-legs of the HB. The 3-phase inverter (shown in Figure 1 inside the blue box) has 6-switches to build 3-legs for phases A, B & C respectively.

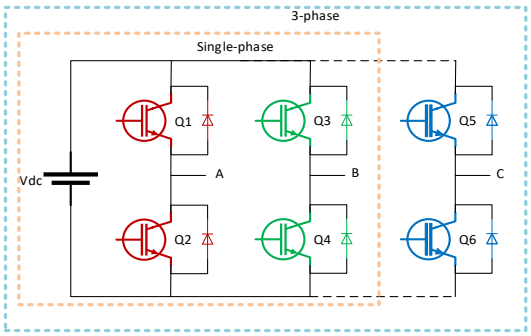

Figure 1: 1-phase and 3-phase VSI [58]

$$v_o = \frac{4V_{dc}}{\pi}\left(sin(\omega t) + \frac{1}{3}sin(3\omega t) + \frac{1}{5}sin(5\omega t) + \cdots\right) \quad (1)$$

Where: V_{dc} is a DC voltage

The peak of the fundamental element is shown in Eq. (2), and the value of the root mean square (RMS) signal is expressed in Eq. (3).

$$V_{o1\_peak} = \frac{4V_d}{\pi} \approx 1.27V_{dc} \quad (2)$$

$$V_{o1\_rms} = \frac{V_{o1p}}{\sqrt{2}} = \frac{2\sqrt{2}V_d}{\pi} \approx 0.9V_{dc} \quad (3)$$

Where: V_{o1_peak} is the highest value of the produced voltage

V_{o1_rms} is RMS voltage

3. Configuration of cascaded h-bridge inverter

The applications of HV cannot use 1-phase LV inverters since the restricted voltage blocking capacity of semiconductor switches. Therefore, the CHB-MLI topology is fitting for these types of applications. Figure 2 illustrates the 3-phase CHB-MLI. This configuration uses several HB modules/cells connected in series to produce an enhanced AC output voltage with lower harmonic contents.

Based on the DC source configuration, there are two ways to implement the CHB-MLI symmetrical or asymmetrical configurations.

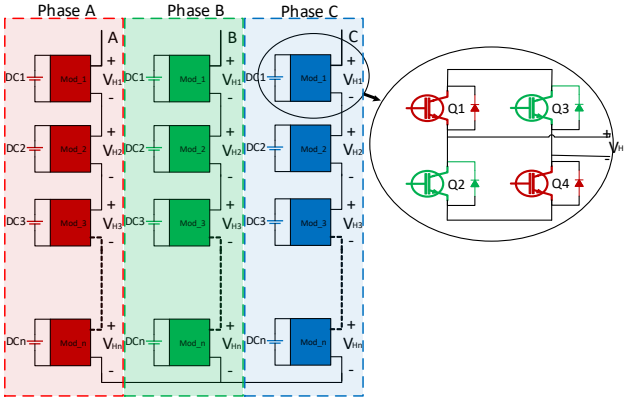

Figure 2: 3-phase CHB-MLI [58]

3.1. Symmetrical configuration

The symmetrical design of CHB-MLI uses multiple isolated DC sources with identical amplitudes. Similarly, a CHB-MLI with 3-series connected cells uses isolated DC input sources of the same amplitudes to produce a 7-level output signal. These 7-levels are measured as *0*, *±E*, *±2E*, *and ±3E*. Usually, the following equation is used to decide the number of levels in this configuration:

$$M = (2H + 1) \quad (4)$$

Where "M" describes the maximum levels in the output signal and "H" relates the number of HB cells per leg.

3.2. Asymmetrical configuration

The asymmetrical type CHB-MLI uses various scale isolated DC sources. Each cell produces 3-different voltage levels in this sort of structure. Therefore, the highest voltage levels depend on the DC sources' peak value. There are binary and trinary systems to figure out DC levels in a CHB-MLI. In the binary method, it uses V_{dc1} = E, V_{dc2} = 2E, and V_{dc3} = 4E. This sequence of input amplitudes of voltages results in 15 levels in the phase-voltage of CHB-MLI. Eq. (5) denotes the output voltage-level in this design.

$$M = (2^{H+1} - 1) \tag{5}$$

In trinary method, all input sources are set as: V_{dc1} = E, V_{dc2} = 3E, and V_{dc3} = 9E. This configuration produces voltages with 27-levels in the output phase signal. Eq. (6) expresses the upper limit of output signal levels.

$$M = 3^H \tag{6}$$

4. Mathematical analysis

In a CHB-MLI, the voltage difference of PE switches is each cell's output voltage. Then, two individual switching functions control each cell and Eq. (7) sets the voltage level in each cell $V_{o\_cell_i}$ as:

$$V_{o\_cell_i} = V_{dc}(Q_{1_{cell_i}} - Q_{3_{cell_i}}) \tag{7}$$

Where switching functions are $Q_{1_{cell_i}}$ and $Q_{3_{cell_i}}$, and V_{dc} is a DC input of each HB.

A switching function, Q_i is defined as Eq. (8) where i =1, 2, ⋯, n..

$$Q_i = \begin{cases} 1; when\ Q_i\ is\ ON \\ 0; when\ Q_i\ is\ OFF \end{cases} \tag{8}$$

The overall output voltage of a CHB-MLI is produced as shown in Eq. (9) for the symmetric structure, and Eq. (10) for the asymmetric configuration.

$$V_o = V_{dc} \sum_{i=1}^{n} (Q_{1_{cell_i}} - Q_{3_{cell_i}}) \tag{9}$$

$$V_o = \sum_{i=1}^{n} (Q_{1_{cell_i}} - Q_{3_{cell_i}}) V_{dc_i} \tag{10}$$

Thus, Eq. (11) shows the 7-level symmetric CHB-MLI's output voltage.

$$\begin{cases} V_{o1} = V_{dc}(Q_{1_{cell_1}} - Q_{3_{cell_1}}) \\ V_{o2} = V_{dc}(Q_{1_{cell_2}} - Q_{3_{cell_2}}) \\ V_{o3} = V_{dc}(Q_{1_{cell_3}} - Q_{3_{cell_3}}) \end{cases} \tag{11}$$

Similarly, Eq. (12) illustrates the output voltage of 15- and 27-level asymmetric CHB-MLIs.

$$\begin{cases} V_{o1} = V_{dc_1}(Q_{1_{cell_1}} - Q_{3_{cell_1}}) \\ V_{o2} = V_{dc_2}(Q_{1_{cell_2}} - Q_{3_{cell_2}}) \\ V_{o3} = V_{dc_3}(Q_{1_{cell_3}} - Q_{3_{cell_3}}) \end{cases} \tag{12}$$

5. MC-PWM methods for symmetric and asymmetric CHB-MLI

The MC-PWM methods are named PSPWM and LSPWM as per classification.

5.1. PS-PWM

A CHB-MLI with "(M-1)" carrier-signals can produce an "M" number of levels in the output voltage. These carrier signals have equal amplitude and frequency. Nevertheless, there is a phase displacement between the two carrier waves. The Eq. (13). helps to decide the phase displacement angle for the carrier signals. The PS-PWM method can be sinusoidal PSPWM (PSSPWM) or third harmonic injected PSPWM (THIPSPWM) based on the reference signal.

$$\emptyset_{cr} = \frac{360}{(M-1)} \tag{13}$$

Figure 3 shows the PS-SPWM method for a 7-level CHB-MLI. In this figure, six carriers (Cr1 - Cr6) are shown. Also, the sinusoidal reference wave is used with carrier waves to create control pulses for the PE switches. Furthermore, the gray color waveform approximates the 7-level CHB-MLI's output voltage.

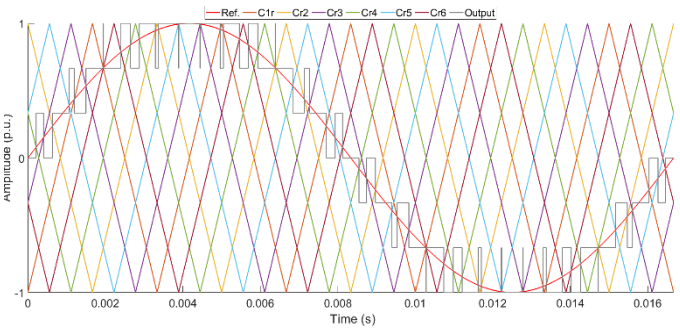

Figure 3: PSSPWM method

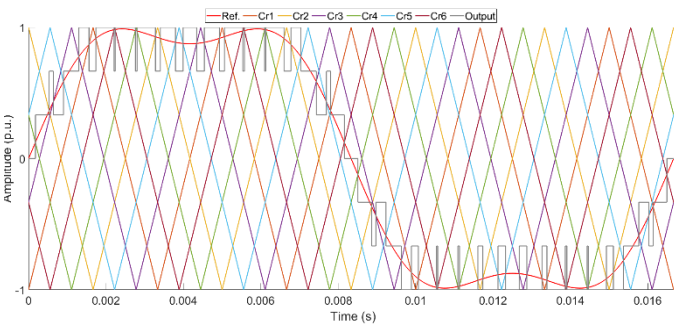

Figure 4: THIPSPWM method

Like the PSSPWM, THIPSSPWM has (M-1) carrier signals for the M-level of CHB-MLI (Figure 4). However, in this method THI signal is used as a modulation signal

to generate switching pulses for the inverter. Also, the signal in gray color estimates the output phase voltage. A 3-phase system is proper for this control method because the triplen harmonics do not appear when a delta-connected transformer is placed.

Also, each HB can produce v_{Hi} output voltage (where i = 1, 2, 3…. N). The Eq. (14) describes 7-level CHB-MLI's output voltage (v_{AN}).

$$v_{AN} = v_{H1} + v_{H2} + v_{H3} \tag{14}$$

Eq. (15) describes the simplified form of CHB-MLI's switching frequency for PSPWM system.

$$f_{inv} = 2Hf_{sw} = (M-1)f_{sw} \tag{15}$$

A symmetrical configuration is suitable for operating using the PS-PWM method because it benefits balancing all DC sources.

5.2. LS-PWM

Like the PSPWM, LSPWM needs "(M-1)" carrier waves that are equal in amplitude to produce "M" levels in the output voltage. Regardless, there is vertical displacement in each other's position such that the bands they inhabit are bordering. Furthermore, LSPWM is classified as LSPWM and THILSPWM. Also, carrier waves can be arranged in various forms, namely, in-phase disposition SPWM (LSIPDSPWM), level shifted alternate phase-disposition SPWM (LSAPODSPWM), and level shifted phase-opposition-disposition (LSPODSPWM). All the above LSPWM techniques are shown in Figures 5 to 10.

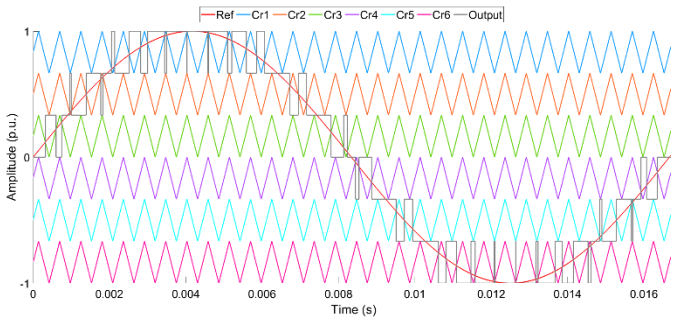

Figure 5: LSIPDSPWM

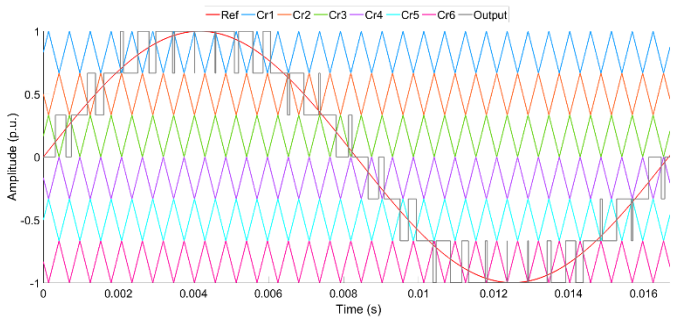

Figure 6: LSAPODSPWM

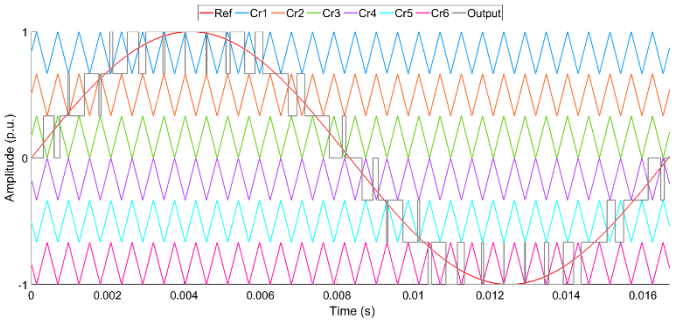

Figure 7: LSPODSPWM

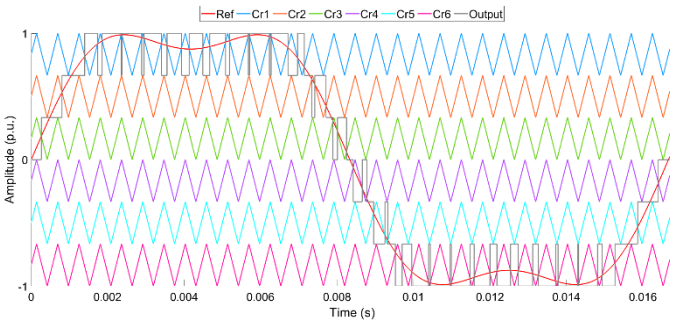

Figure 8: THILSIPDPWM

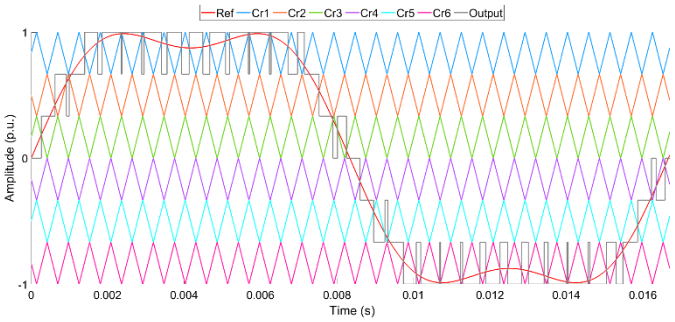

Figure 9: THILSAPODPWM

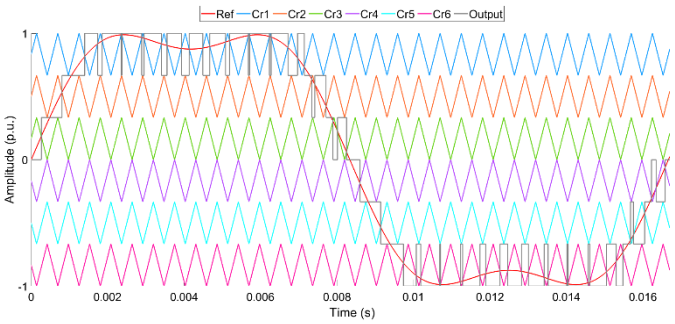

Figure 10: THILSPODPWM

The phase displacement between two carrier waves is zero in the LSIPDSPWM. In contrast, there is 180° phase displacement between every carrier wave in LSAPODSPWM. In the LSPODSPWM, the carrier waves are in phase, placed above zero-reference. Similarly, the carrier waves are in phase, placed beneath zero-reference. However, the 180° phase displacement is seen between the above-zero and below-zero reference lines. A sinusoidal reference wave is used in all three methods. Also, the gray color signal estimates the output voltage.

The control pulses for HB1 can be generated by the uppermost and lowest carrier waves. Similarly, the pulses can be generated for HB3 and HB2 with the innermost carrier waves. The estimation of the output wave and the arrangements for the 7-level CHB-MLI is shown in Figures 5 to 10.

Eq. (16) describes the output voltage of a 7-level CHB-MLI. Also, it shows the peak output voltage for each HB.

$$v_{AN} = v_{H1} + v_{H2} + v_{H3} \quad (16)$$

The operating frequency of PE switches in HB1 is the product of reference wave frequency and the switching pulses per cycle. Furthermore, the switching frequency is different in another HB module. The HB3 can be run at the most subordinate switching frequency.

In general, the operating converter frequency using the LSPWM is equal to the carrier frequency (f_{cr}).

$$f_{sw,conv} = f_{cr} \quad (17)$$

Eq. (18) shows the average value of operating frequency for switches

$$f_{sw,dev} = \frac{f_{cr}}{(m-1)} \quad (18)$$

The PSPWM method generates each HB module's equal amplitude output signal with small phase displacement. Also, the current-carrying time is identical for all switches. In contrast, the output waveforms are not identical when HB modules are controlled by the LS-PWM method because of the different current-carrying times. This issue can be solved with a proper balancing technique to balance losses and conduction time. However, this increased process expands the complexity and price of the design.

6. Realization of MC-PWM for CHB-MLI

MC-PWM technique controls symmetric/asymmetric type CHB-MLI. The "(M-1)" carrier waves can produce "M" level output voltage for both types of CHB-MLI.

The PSPWM technique is applied to the symmetric CHB-MLI only since it balances load current among all isolated inputs. In contrast, the LSPWM method cannot balance the load current among all sources in both types of CHB-MLIs. Still, the load balancing technique is not used in this study.

In the PSPWM method, a 60º phase shift between two carrier waves is needed to produce a 7-levels output voltage for the symmetrical type CHB-MLI configuration. Likewise, a 45º phase shift is needed to generate a 9-level output voltage. A sinusoidal modulation wave is used to form ad PSPWM technique, and a THI modulation wave is considered to create the THIPSPWM method. The THI wave is generated by injecting a third harmonic wave into the 60 Hz frequency sinusoidal wave. The modulation wave is compared with the carrier waves to produce control pulses for the PE switches in both methods.

Both symmetric and asymmetric structure of CHB-MLI model is created considering the LSPWM method. In this method, "(M-1)" carrier waves are vertically displaced to produce an "M" level output signal.

In the LSPWM method, each carrier signal's peak-to-peak value (PPV) can be decided by using Eq. (19).

$$\text{PPV} = \text{“1/(NC/2)”} \quad (19)$$

Where NC is a sum of all carrier waves.

The PPV per carrier wave was 0.33 in symmetrical type 7-level CHB-MLI. Hence, three carrier wave was placed above 0 references, and the remaining three were placed under 0 reference. So, the range of carrier waves is 0.67 to 1 for Cr1, 0.33 to 0.67 for Cr2, and 0 to 0.33 for Cr3. Similarly, the three carriers below 0 reference hold the same values but with negative polarity. Eq. (19) shows that the 9level symmetric type CHB-MLI used a 0.25 PPV value.

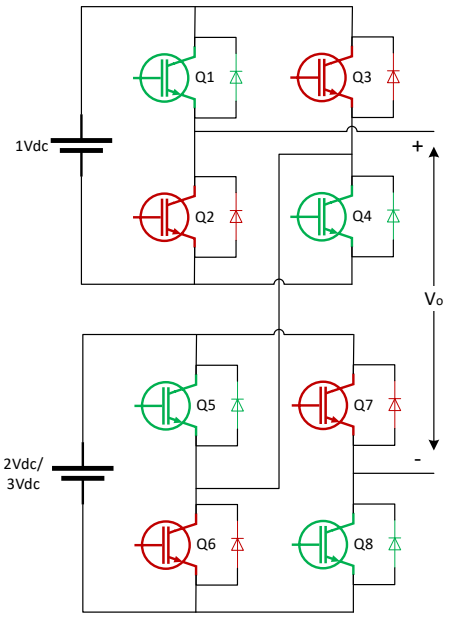

Figure 11: Asymmetric type 7/9level CHB-MLI [58]

Figure 11 shows the asymmetrical configuration of CHB-MLI. This design has fewer switches than symmetrical CHB-MLI despite an equal number of carrier waves being needed. Consequently, an added circuit is

needed for further processing these waves to produce switching pulses. The 7-levels in the output signals are, *+3E, +2E, +E, 0, -E, -2E, and -3E*. These values are output achieved by processing six carrier waves using source formation of 1:2 (V_{dc1}= E, V_{dc2}= $2E$). Figure 12 describes the logic circuit which generates the control pulse for this design. Likewise, the eight carrier waves are used to achieve 9-levels, *+4E, +3E, +2E, +E, 0, -E, -2E, -3E and -4E*, with 1:3 source composition (V_{dc1}= E, V_{dc2}= $3E$). Figure 13 shows the control pulse logic circuit for this design.

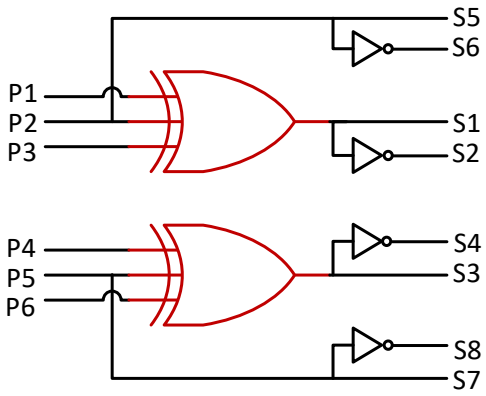

Figure 12: Logic circuit to produce control pulses (7level asymmetric CHB-MLI) [58]

The comparison of carrier and modulation waves produced the switching pulses (P1-P6). As discussed earlier, six carrier waves are used to produce a 7-levels output signal. The modulating wave either be a sinusoidal wave or a THI wave. Figure 12 describes the further processing of these pulses. The pulses P1, P2, and P3 are used as input to the XOR, producing control signal S1 and complimentary signal S2. Thus, S1 and S2 connect to the switches Q1 and Q2. Signal P2 is used for S5 and complementary signal to S6. Another XOR gate used P4, P5, and P6 as input signals. This logic gate produces S4 and complimentary signal S4, which are connected to the switches Q3 and Q4. The signal S7 for switch Q7 is connected to P5, and S8 has used the complementary pulse of P5 for switch Q8.

Asymmetric type CHB-MLI in 9-level design, eight pulse waves P1 to P8 are produced with a single modulating and eight carrier waves. These pulses are further processed using logic gates shown in Figure 13. Signals S1 and complimentary signal S2 are produced with the P1, P3, P4, P6, and P7 input pulses for the NXOR logic. The S1 and S2 drive the switches Q1 and Q2. Likewise, another NXOR logic is used to produce driving pulses S3 and complimentary pulse S4. In this process, P2, P3, P5, P6, and P8 are employed as input signals for the NXOR logic. Also, the driving pulses S5 and S7 are connected to P3 and P6. Moreover, the control pulse S7 is complimentary to S8, and S6 is complimentary to S5.

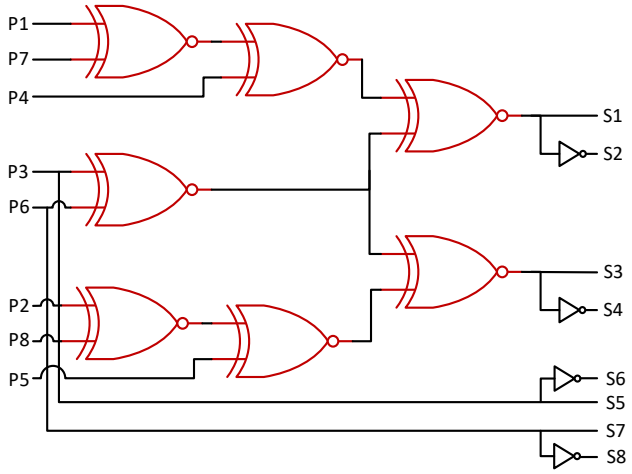

Figure 13: : Logic circuit to produce control pulses (9level asymmetric CHB-MLI) [58]

7. Simulation results

MATLAB/Simulink models are used to study MC-SPWM and MC-THIPWM methods for a symmetrical and asymmetrical design of 3-phase CHB-MLI.

The symmetrical 7- and 9-levels 3-phase CHB-MLI are integrated with MCPWM methods, PSSPWM, PSTHIPWM, LSSPWM, and LSTHIPWM. All MCPWM methods are evaluated by examining the THD and fundamental signals in the line-to-line (L-L) output voltage. The operating frequency of the inverter (f_{sw_inv}) is 96 times the essential frequency of 60 Hz (i.e., 5760 Hz).

Then, asymmetrical 7- and 9-levels 3-phase CHB-MLI operated using variation of LSSPWMs (LSIPDSPWM, LSAPODPWM & LSPODSPWM) and THILSPWM (THILSIPDPWM, THILSAPODPWM & THILSPODPWM) methods. The THD and fundamental components are analyzed using all six various of LSPWM. Furthermore, a qualitative, and quantitative assessment is carried out for all MCPWM methods for both design of CHB-MLI.

The output phase voltage of 7- and 9-levels CHB-MLI is shown in Figure 14 ((a)-(d)) for PSSPWM and THIPSPWM methods. PSPWMs methods generate an output signal that is like the sinusoidal signal in the form of staircase. Additionally, CHB-MLI produces output voltage of 100 V with both control methods. Also, the examination of output signal generated by THIPSPWM shows, the peak voltage created stays constant for an extended time as compared to the signal generated by the PSSPWM method.

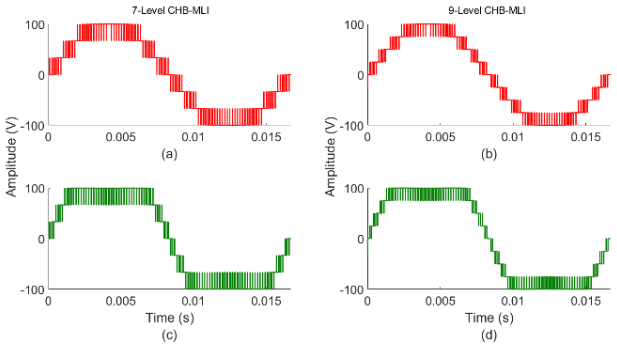

Figure 14: Output phase voltage of symmetrical type CHB-MLI controlled using (a) PSSPWM (7-Level), (b) THIPSPWM (7-Level), (c) PSSPWM (9-Level), (d) THIPSPWM (9-Level)

The L-L voltage of the 7- & 9-levels CHB-MLI is shown in Figure 15 ((a)-(d)). These inverters are run with PSSPWM and THIPSPWM methods like the phase voltage. Both methods produce equal peak voltages.

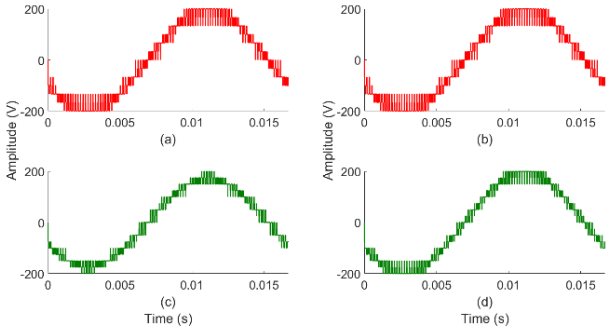

Figure 15: L-L Output voltage of symmetrical type CHB-MLI controlled using (a) PSSPWM (7-Level), (b) THIPSPWM (7-Level), (c) PSSPWM (9-Level), (d) THIPSPWM (9-Level)

The overlaid waveforms of phase voltage (Figure 16 (a)-(f)) produced by symmetrical and their corresponding asymmetrical design of 7- & 9-level CHB-MLIs controlled with each LSPWM method under study. Like the PSPWM method, CHB-MLI create 100 V peak in the output signal with all LSPWM methods.

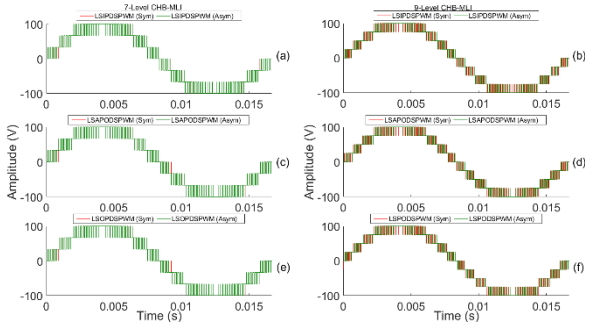

Figure 16: Phase-voltage of symmetrical and asymmetrical CHB-MLI (a) LSIPDSPWM (7-level), (b) LSIPDSPWM (9-level), (c) LSAPODSPWM (7level) (d) LSAPODSPWM (9level)) (e) LSPODSPWM (7level) (f) LSPODSPWM (9level)

The output phase voltage (shown in Figure 16) formed by symmetric and their respective asymmetric design of CHB-MLIs using all LSSPWM method. The information implies both forms of CHB-MLIs results are equivalent to each other. Similarly, the waveform produced by symmetric and their respective asymmetric design of CHB-MLIs using all THILSPWM techniques is denoted in Figure 17. The statistics shows that both sorts of CHB-MLIs outputs are similar.

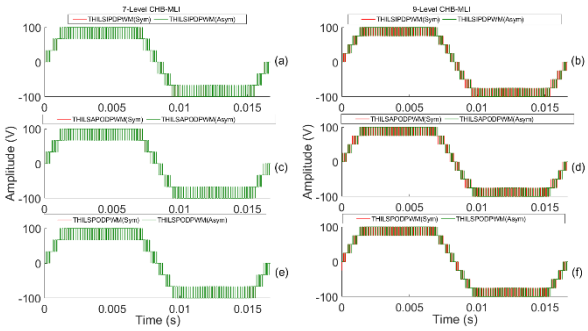

Figure 17: Phase-voltage of symmetrical and asymmetrical CHB-MLI (a) THILSIPDPWM (7-level), (b) THILS IPDPWM (9-level), (c) THILSAPODPWM (7-level) (d) THILSAPODPWM (9-level)) (e) THILS PODPWM (7-level) (f) THILSPODPWM (9-level)

The L-L output voltage produced by symmetric and their respective asymmetric design of CHB-MLIs using all LSSPWM methos is shown in Figure 18. The numbers signify the output voltages are corresponding to each other for both designs of CHB-MLIs. Additionally, the L-L voltage waveform produced by symmetric and their corresponding asymmetric CHB-MLIs applying all THILSPWM method is shown in Figure 19. The results shows that both CHB-MLI's outputs are like each other.

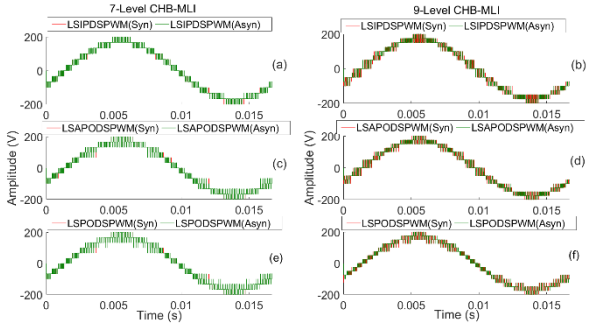

Figure 18: L-L voltage of symmetrical and asymmetrical CHB-MLI (a) LSIPDSPWM (7-level), (b) LSIPDSPWM (9-level), (c) LSAPODSPWM (7-level) (d) LSAPODSPWM (9-level)) (e) LSPODSPWM (7-level) (f) LSPODSPWM (9-level)

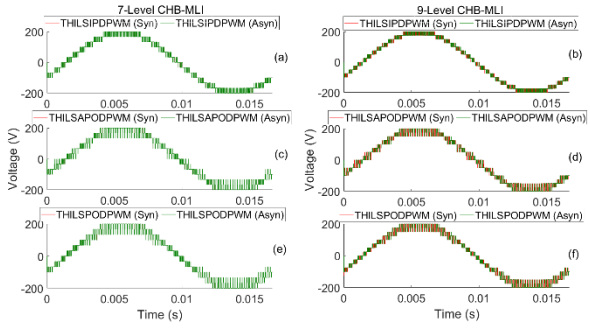

Figure 19: L-L voltage of symmetrical and asymmetrical CHB-MLI (a) THILSIPDPWM (7-level), (b) THILSIPDPWM (9-level), (c) THILSAPODPWM (7l-evel) (d) THILSAPODPWM (9-level)) (e) THILSPODPWM (7-level) (f) THILSPODPWM (9-level)

Figures 20 & 21 shows the THD results of the L-L voltages and phase-voltages waveform of 7- and 9-levels of symmetric/asymmetric design of CHB-MLI for all MCPWM methods, respectively.

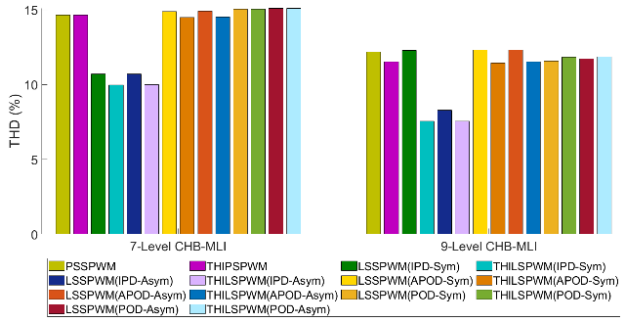

Figure 20: THD in the L-L voltage for 7-and 9-levels CHB-MLI for MCPWM methods

Figure 22 shows the fundamental component produced in the output voltage of 7- and 9-levels of both types of CHB-MLI for all MCPWM methods, correspondingly.

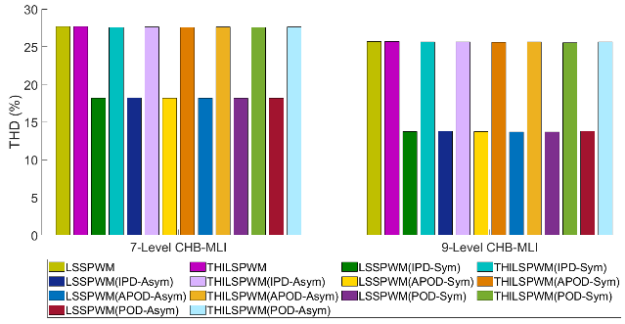

Figure 21: THD in the phase-voltage for 7- and 9-level both types of CHB-MLI applying MCPWM methods

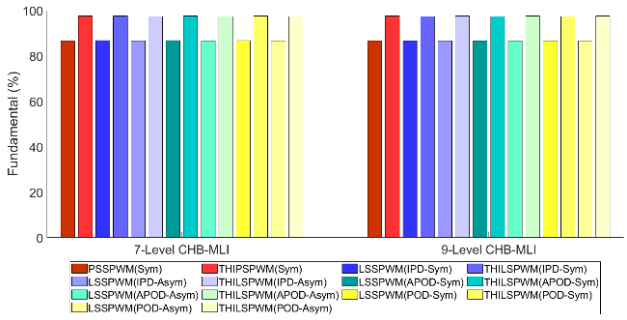

Figure 22: Fundamental freq. component in the output of 7- and 9-levels CHB-MLIs operating with MCPWM methods

Additionally, the PSSPWM and THIPSPWM methods are employed to the 7- & 9-levels symmetrical CHB-MLI to confirm the discharging rate of the input HB sources. The discharging current of all inputs evaluated for PSPWM methods are equal. As depicted in Figure 23, discharging current from all sources in the THIPSPWM modulated CHB-MLI is a bit greater than the PSSPWM controlled CHB-MLI.

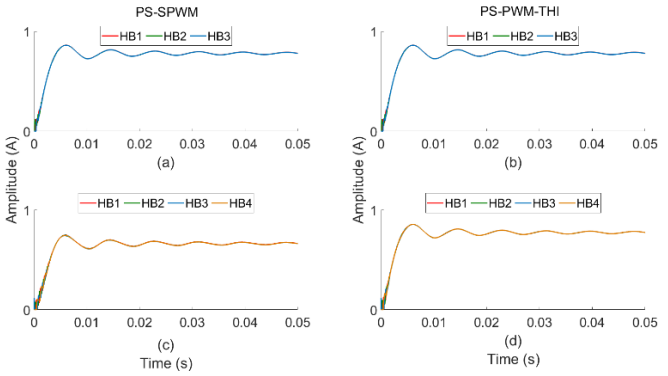

Figure 23: Output current from each HB cell for the (a) PSPWM in 7L, (b) THIPSPWM in 7L, (c) PSPWM in 9L, and (d) THIPSPWM in 9L

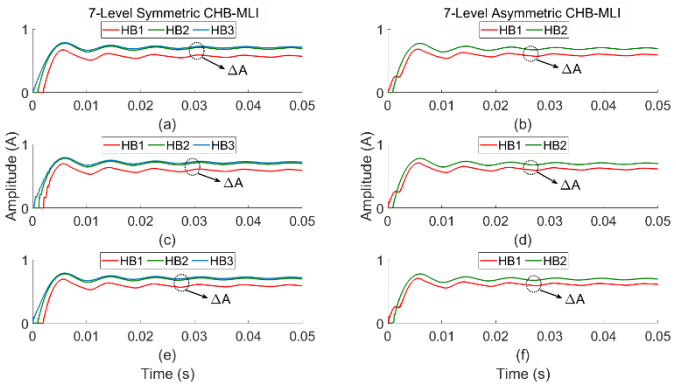

Figure 24: Current for each HB of 7-level symmetric and asymmetric CHB-MLI using (a) LSIPDSPWM (Sym.), (b) LSIPDSPWM (Asym.), (c) LSAPODSPWM (Sym.), (d) LSAPODSPWM (Asym.), (e) LSPODSPWM (Sym.), and (f) LSPODSPWM (Asym.)

Also, the all deviations of LSSPWM and THILSPWM methods are applied to the 7- & 9-levels symmetrical and asymmetrical configuration of CHB-MLI to confirm the discharging of the input source of HB. The RMS value of discharging current of all sources are shown in Figures 24 to 27 ((a)-(f)). The calculated value show that variations of LSPWM method has discharging rate of △A difference. As described in Figures 26 and 27, discharging current of all inputs in the THILSPWM controlled CHB-MLI is slightly greater than the LSSPWM created CHB-MLI. Also, it has similar △A discharging difference in both symmetrical and asymmetrical type CHB-MLIs.

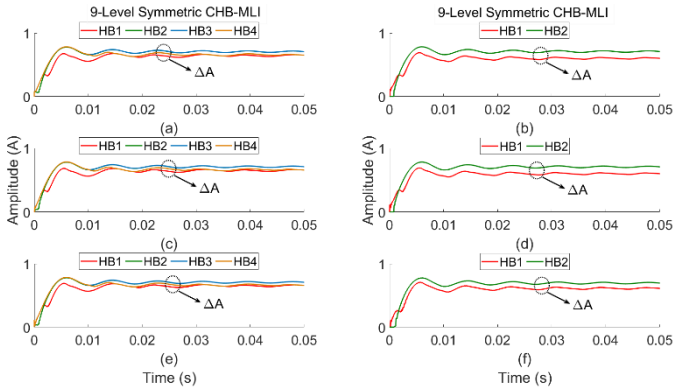

Figure 25: The current from each HB in -level symmetric and asymmetric CHB-MLI applying (a) LSIPDSPWM (Sym.), (b) LSIPDSPWM (Asym.), (c) LSAPODSPWM (Sym.), (d) LSAPODSPWM (Asym.), (e) LSPODSPWM (Sym.), and (f) LSPODSPWM (Asym.)

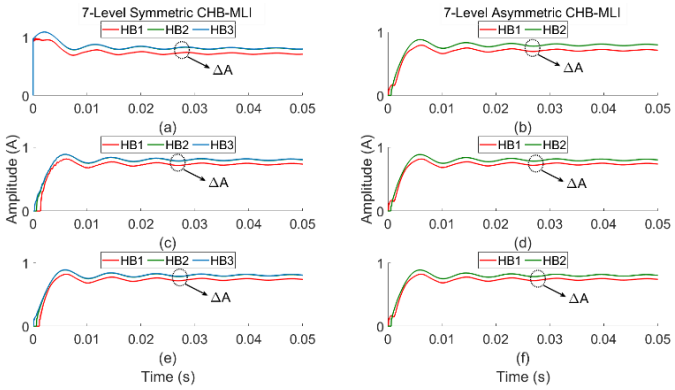

Figure 26: Output current from each HB cell 7-level symmetric and asymmetric CHB-MLI applying (a) THILSIPDPWM (Sym.), (b) THILSIPDPWM (Asym.), (c) THILSAPODPWM (Sym.), (d) THILSAPODPWM (Asym.), (e) THILSPODPWM (Sym.), and (f) THILSPODPWM (Asym.)

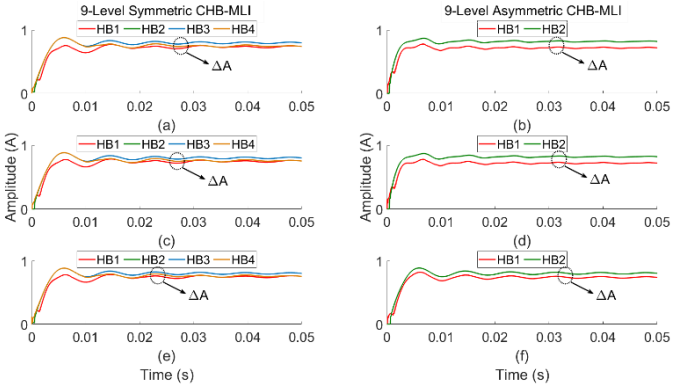

Figure 27: Current of each HB in 9-level symmetric and asymmetric CHB-MLI using (a) THILSIPDPWM (Sym.), (b) THILSIPDPWM (Asym.), (c) THILSAPODPWM (Sym.), (d) THILSAPODPWM (Asym.), (e) THILSPODPWM (Sym.), and (f) THILSPODPWM (Asym.)

Table 1: Fundamental component and THD products of symmetrical CHB-MLI

PWM Methods	Symmetrical type (3-phase)					
	7-Level			9-Level		
	N	THD (%)	F (%)	N	THD (%)	F (%)
PSSPWM	36	14.65	86.60	48	12.19	86.60
THDPSPWM	36	14.65	97.45	48	11.51	97.45
LSIPDSPWM	36	10.72	86.75	48	12.29	86.60
THDLSIPDPWM	36	9.97	97.55	48	7.56	97.40
LSAPODSPWM	36	14.88	86.75	48	12.30	86.60
THILSAPODPWM	36	14.49	97.55	48	11.44	97.40
LSPODSPWM	36	15.05	86.75	48	11.57	86.60
THDLSPODPWM	36	15.05	97.55	48	11.84	97.40

Table 2: Results of essential component and THD of symmetrical CHB-MLI

PWM Methods	Asymmetrical type (3-phase)					
	7-Level			9-Level		
	N	THD (%)	F (%)	N	THD (%)	F (%)
LSIPDSPWM	24	10.70	86.75	24	8.29	86.60
THILSIPDPWM	24	10.01	97.55	24	7.56	97.40
LSAPODSPWM	24	14.91	86.75	24	12.31	86.60
THILSAPODPWM	24	14.53	97.55	24	11.51	97.40
LSPODSPWM	24	15.10	86.75	24	11.74	86.60
THILS-PODPWM	24	15.11	97.55	24	11.86	97.40

The fundamental component and THD are compared for both designs of CHB-MLIs which is summarized in Table 1 and Table 2. In these tables, "N" is the total number of switches used to compose CHB-MLIs. Also, the "F" value showed the essential component in the output signal.

Table 3: THD in the phase voltage of symmetrical CHB-MLI

PWM Methods	Symmetrical type (3-phase)			
	7-Level		9-Level	
	N	THD (%)	N	THD (%)
PSSPWM	36	27.67	48	25.61
THIPSPWM	36	27.67	48	25.61
LSIPDSPWM	36	18.16	48	13.77
THILSIPDPWM	36	27.59	48	25.59
LSAPODSPWM	36	18.16	48	13.74
THILSAPODPWM	36	27.59	48	25.60
LSPODSPWM	36	18.16	48	13.71
THILSPODPWM	36	27.59	48	25.56

Tables 3 & 4 Summaries the THD generated in the phase voltage of the symmetrical/asymmetrical type 7& 9levels CHB-MLIs.

Table 4: THD in the phase-voltage of asymmetrical type CHB-MLI

PWM Methods	Asymmetrical type (3-phase)			
	7-Level		9-Level	
	N	THD (%)	N	THD (%)
LSIPDSPWM	24	18.21	24	13.78
THILSIPDPWM	24	27.61	24	25.64
LSAPODSPWM	24	18.20	24	13.71
THILSAPODPWM	24	27.61	24	25.65
LSPODSPWM	24	18.20	24	13.78
THILSPODPWM	24	27.62	24	25.64

8. Conclusion

This paper analyzed MC-PWM techniques for the symmetric/asymmetric CHB-MLIs. A simulation model for a three-phase symmetric and asymmetric design of CHB-MLI was constructed in MATLAB. The operation of CHB-MLI was brought out at 5760 Hz, which is 96 times of fundamental (60 Hz) frequency inverter switching frequency.

This study discussed the structure of symmetrical and asymmetrical (binary and trinary) type CHB-MLI and the mathematical representation of their output voltages. The simulation results revealed that both types of converters generated equal "M" number levels in the output voltages using (M-1) carrier signals. However, the asymmetrical-trinary CHB-MLI needed the least number of switches and DC sources among symmetrical, asymmetrical (binary), and asymmetrical (trinary) configurations. Therefore, the asymmetrical-trinary configuration used fewer driver circuits, making it simpler, cost-effective, and less vulnerable. Also, the lowest number of switches in conduction per voltage level are needed in an asymmetrical-trinary configuration which shows that the conduction and switching losses are significantly lower leading to the higher efficiency of CHB-MLIs.

Finally, the simulation results revealed that the generated line-to-line and phase voltages by the 9-level (symmetrical and asymmetrical design) of CHB-MLI are much improved compared to the 7-level CHB-MLIs. In addition, it generated a high-quality voltage with the lowest harmonic content, which is 7.56% in line-to-line voltage and 13.71% in phase voltage. Even though, these harmonics are above the accepted limit of IEEE Std 519-1992, it minimizes the harmonic filtering process. That reduces the overall size and cost of the system.

Furthermore, this extensive study shows that the output signal produced by all MCPWM method is equivalent to a similar level of CHB-MLI. In addition, the harmonic study shows that the LSIPDPWM creates noticeably lower distortion (7.56% for 9-level inverter) in the L-L voltage compared to the other methods. The LSIPDPWM technique generated 13.78% THD in the phase-voltage for the 9-level CHB-MLI configuration. Moreover, the different arrangements of carrier signals have different THD in the output signal, which explains the arrangement of carrier signals impacts THD generation.

In addition, results reveal that LSTHIPWM produces nearly 10.8% additional fundamental components in the L-L voltage than the LSPWM, which improves the total productivity of CHB-MLI. That suggests the fundamental component produced in the output of CHB-MLI fit in with MC-design is affected by the choice of modulation signal.

Also, the measurement of source current displays that the PS-PWM technique can balance discharging current of all modules in CHB-MLI. In contrast, all variations of LSSPWM and THILSPWM do not naturally balance the discharging rate of all CHB-MLI modules. Therefore, the carrier rotation algorithm is needed with LSPWMs modulation techniques. This added algorithm increases the computation load on the digital controllers.

References

[1] M. H. Sree Reddy, N. Susheela, P. Malathy, "Sinusoidal tracking method for cascaded multilevel inverter fed induction motor drive," *2021 Emerging Trends in Industry 4.0 (ETI 4.0)*, pp. 1–8, 2021, doi:10.1109/ETI4.051663.2021.9619306.

[2] M. Q. Kasim, R. F. Hassan, "Reduced computational burden model predictive current control of asymmetric stacked multi-level inverter based STATCOM," *2021 IEEE International Conference on Automatic Control & Intelligent Systems (I2CACIS)*, pp. 374–379, 2021, doi:10.1109/I2CACIS52118.2021.9495881.

[3] E. Hallaji, H. M. Kojabadi, "Novel switched-capacitor-based multilevel inverter topology for renewable energy," *2021 12th Power Electronics, Drive Systems, and Technologies Conference (PEDSTC)*, pp. 1–5, 2021, doi:10.1109/PEDSTC52094.2021.9405828.

[4] A. H. Hassanabad, D. Nazeipur, "Design and Simulation of a Control System for Investors in Wind Turbines," vol. 6, no. 3, pp. 6, 2021.

[5] L. Mathe et al., "Battery pack state of charge balancing algorithm for cascaded H-Bridge multilevel converters," *2016 IEEE 16th International Conference on Environment and Electrical Engineering (EEEIC)*, pp. 1–6, 2016, doi:10.1109/EEEIC.2016.7555737.

[6] A. Mittal, K. Janardhan, A. Ojha, "Multilevel inverter-based grid connected solar photovoltaic system with power flow control," *2021 International Conference on Sustainable Energy and Future Electric Transportation (SEFET)*, pp. 1–6, 2021, doi:10.1109/SeFet48154.2021.9375753.

[7] H. Vahedi, A. Dehghanzadeh, K. Al-Haddad, "Static VAr compensator using packed U-cell based multilevel converter," *2018 IEEE 12th International Conference on Compatibility, Power Electronics and Power Engineering (CPE-POWERENG 2018)*, pp. 1–5, 2018, doi:10.1109/CPE.2018.8372576.

[8] Z. Bayat et al., "Provide a new basic unit for cascaded multilevel inverter by reducing the maximum blocking voltage and switches," *2019 27th Iranian Conference on Electrical Engineering (ICEE)*, pp. 576–581, 2019, doi:10.1109/IranianCEE.2019.8786387.

[9] X. Yuan, "Ultimate generalized multilevel converter topology," *IEEE Transactions on Power Electronics*, vol. 36, no. 8, pp. 8634–8639, 2021, doi:10.1109/TPEL.2021.3056646.

[10] M. J. Uddin, Md. S. Islam, "Implementation of cascaded multilevel inverter with reduced number of components," *2021 2nd International Conference on Robotics, Electrical and Signal Processing Techniques (ICREST)*, pp. 669–672, 2021, doi:10.1109/ICREST51555.2021.9331128.

[11] Z. E. Abdulhamed, A. H. Esuri, N. A. Abodhir, "New topology of asymmetrical nine-level cascaded hybrid bridge multilevel inverter," *2021 IEEE 1st International Maghreb Meeting of the Conference on Sciences and Techniques of Automatic Control and Computer Engineering MI-STA*, pp. 430–434, 2021, doi:10.1109/MI-STA52233.2021.9464511.

[12] W. Wan et al., "DC component self-balancing analysis of neutral-point in neutral-point-clamped three-level converters," *2020 IEEE*

9th International Power Electronics and Motion Control Conference (IPEMC2020-ECCE Asia), pp. 1752–1757, 2020, doi:10.1109/IPEMC-ECCEAsia48364.2020.9367804.

[13] N. K. Muthukuri, R. Tagore Yadlapalli, "Comparison of carrier based PWM technique for active neutral point clamping multilevel inverter," *2020 4th International Conference on Intelligent Computing and Control Systems (ICICCS)*, pp. 1288–1292, 2020, doi:10.1109/ICICCS48265.2020.9121130.

[14] X. Jiang, M. L. Doumbia, "Comparative study of grid-connected multilevel inverters for high power phtovoltaic systems," *2019 IEEE 7th International Conference on Smart Energy Grid Engineering (SEGE)*, pp. 184–190, 2019, doi:10.1109/SEGE.2019.8859784.

[15] A. Anthon et al., "Comparative evaluation of the loss and thermal performance of advanced three-level inverter topologies," *IEEE Transactions on Industry Applications*, vol. 53, no. 2, pp. 1381–1389, 2017, doi:10.1109/TIA.2016.2639462.

[16] F. M. Shahir, E. Babaei, "16-level basic topology for cascaded multilevel inverters with reduced number of components," *IECON 2016 - 42nd Annual Conference of the IEEE Industrial Electronics Society*, pp. 3105–3110, 2016, doi:10.1109/IECON.2016.7794068.

[17] A. S. Mohamad, N. Mariun, "Simulation of a 41-level inverter built by cascading two symmetric cascaded multilevel inverters," *2016 7th IEEE Control and System Graduate Research Colloquium (ICSGRC)*, pp. 12–16, 2016, doi:10.1109/ICSGRC.2016.7813293.

[18] B. Rajesh, Manjesh, "Comparison of harmonics and THD suppression with three and 5 level multilevel inverter-cascaded H-bridge," *2016 International Conference on Circuit, Power and Computing Technologies (ICCPCT)*, pp. 1–6, 2016, doi:10.1109/ICCPCT.2016.7530116.

[19] E. Babaei et al., "A new basic unit for symmetric and asymmetric cascaded multilevel inverter with reduced number of components," *IECON 2016 - 42nd Annual Conference of the IEEE Industrial Electronics Society*, pp. 3147–3152, 2016, doi:10.1109/IECON.2016.7793089.

[20] L. Nanda, C. Jena, S. Samal, "Symmetrical and asymmetrical conventional cascaded multilevel inverter with SPWM technique," *2021 International Conference on Intelligent Technologies (CONIT)*, pp. 1–5, 2021, doi:10.1109/CONIT51480.2021.9498417.

[21] A. Moeini, H. Iman-Eini, M. Najjar, "Non-equal DC link voltages in a cascaded H-bridge with a selective harmonic mitigation-PWM technique based on the fundamental switching frequency," *Journal of Power Electronics*, vol. 17, no. 1, pp. 106–114, 2017, doi:10.6113/JPE.2017.17.1.106.

[22] O. V. Nos, E. E. Abramushkina, "The control technique for cascaded H-bridge multilevel converter with faulty cells," *19th International Conference of Young Specialists on Micro/Nanotechnologies and Electron Devices (EDM)*, pp. 6403–6406, 2018, doi:10.1109/EDM.2018.8435054.

[23] N. Ramalingam, M. Saravanan, "Comparison of PWM control techniques for cascaded multilevel inverter," *International Review of Automatic Control (I.RE.A.CO)*, vol. 5, no. 6, pp. 815–828, 2012.

[24] A. R. Kumar et al., "A guide to nearest level modulation and selective harmonics elimination modulation scheme for multilevel inverters," *2019 Innovations in Power and Advanced Computing Technologies (i-PACT)*, pp. 1–8, 2019, doi:10.1109/i-PACT44901.2019.8960205.

[25] A. Perez-Basante et al., "(2N+1) selective harmonic elimination-PWM for modular multilevel converters: A generalized formulation and a circulating current control method," *IEEE Transactions on Power Electronics*, vol. 33, no. 1, pp. 802–818, 2018, doi:10.1109/TPEL.2017.2666847.

[26] Y. Deng, R. G. Harley, "Space-vector versus earest-level pulse width modulation for multilevel converters," *IEEE Transactions on Power Electronics*, vol. 30, no. 6, pp. 2962–2974, 2015, doi:10.1109/TPEL.2014.2331687.

[27] Q. Liu et al., "A modified nearest-level modulation method for modular multilevel converter with fewer submodules," *2017 Chinese Automation Congress (CAC)*, pp. 6551–6556, 2017, doi:10.1109/CAC.2017.8243957.

[28] R. B. Jonnala, N. R. Eluri, S. B. Choppavarapu, "Implementation, comparison and experimental verification of nearest vector control and nearest level control techniques for 27-level asymmetrical CHB multilevel inverter," *2016 International Conference on Control, Instrumentation, Communication and Computational Technologies (ICCICCT)*, pp. 214–221, 2016, doi:10.1109/ICCICCT.2016.7987947.

[29] K. J. Pratheesh, G. Jagadanand, R. Ramchand, "A generalized-switch-matrix-based space vector modulation technique using the nearest level modulation concept for neutral-point-clamped multilevel inverters," *IEEE Transactions on Industrial Electronics*, vol. 65, no. 6, pp. 4542–4552, 2018, doi:10.1109/TIE.2017.2772172.

[30] W. Abd Halim et al., "Selective harmonic elimination based on newton-raphson method for cascaded H-bridge multilevel inverter," *International Journal of Power Electronics and Drive Systems (IJPEDS)*, vol. 8, no. 3, pp. 1193, 2017, doi:10.11591/ijpeds.v8.i3.pp1193-1202.

[31] Y. Sinha, A. Nampally, "Modular multilevel converter modulation using fundamental switching selective harmonic elimination method," *2016 IEEE International Conference on Renewable Energy Research and Applications (ICRERA)*, pp. 736–741, 2016, doi:10.1109/ICRERA.2016.7884431.

[32] M. Ye et al., "Research on current backflow of asymmetric CHB multilevel inverter," *Electronics*, vol. 9, no. 2, pp. 214, 2020, doi:10.3390/electronics9020214.

[33] M. Moranchel et al., "Selective harmonic elimination modulation for medium voltage modular multilevel converter," *2016 IEEE 7th International Symposium on Power Electronics for Distributed Generation Systems (PEDG)*, pp. 1–6, 2016, doi:10.1109/PEDG.2016.7527035.

[34] J. Bindu et al., "Genetic algorithm based selective harmonic elimination in PWM AC-AC converter," *2011 International Conference on Recent Advancements in Electrical, Electronics and Control Engineering*, pp. 393–397, 2011, doi:10.1109/ICONRAEeCE.2011.6129809.

[35] D. Ahmadi et al., "A universal selective harmonic elimination method for high-power inverters," *IEEE Transactions on Power Electronics*, vol. 26, no. 10, pp. 2743–2752, 2011, doi:10.1109/TPEL.2011.2116042.

[36] M. S. A. Dahidah, G. Konstantinou, V. G. Agelidis, "A review of multilevel selective harmonic elimination PWM: formulations, solving algorithms, implementation and applications," *IEEE Transactions on Power Electronics*, vol. 30, no. 8, pp. 4091–4106, 2015, doi:10.1109/TPEL.2014.2355226.

[37] C. Buccella et al., "A selective harmonic elimination method for five-level converters for distributed generation," *IEEE Journal of Emerging and Selected Topics in Power Electronics*, vol. 5, no. 2, pp. 775–783, 2017, doi:10.1109/JESTPE.2017.2688726.

[38] H. Lin et al., "A flexible and fast space vector pulse width modulation technique for multilevel converters," *2019 22nd International Conference on Electrical Machines and Systems (ICEMS)*, pp. 1–4, 2019, doi:10.1109/ICEMS.2019.8921982.

[39] A. Kumar, D. Chatterjee, "A survey on space vector pulse width modulation technique for a two-level inverter," *2017 National Power Electronics Conference (NPEC)*, pp. 78–83, 2017, doi:10.1109/NPEC.2017.8310438.

[40] M. A. Hosseinzadeh et al., "Performance evaluation of cascaded H-bridge multilevel grid-connected converter with model predictive control technique," *2019 IEEE International Conference on Industrial Technology (ICIT)*, pp. 1806–1811, 2019, doi:10.1109/ICIT.2019.8755160.

[41] I. Ahmed, V. B. Borghate, "Simplified space vector modulation technique for seven-level cascaded H-bridge inverter," *IET Power Electronics*, vol. 7, no. 3, pp. 604–613, 2014, doi:10.1049/iet-pel.2013.0135.

[42] J. I. Leon et al., "The essential role and the continuous evolution of modulation techniques for voltage-source inverters in the past, present, and future power electronics," *IEEE Transactions on Industrial Electronics*, vol. 63, no. 5, pp. 2688–2701, 2016, doi:10.1109/TIE.2016.2519321.

[43] P. Vijayarajan, A. Shunmugalatha, H. Habeebullah Sait, "Development of modified carrier based PWM scheme for single phase H-bridge inverter fed isolated wind–PV systems," *Solar Energy*, vol. 126, pp. 208–219, 2016, doi:10.1016/j.solener.2015.12.026.

[44] K. Yodpradit, A. Pichetjamroen, N. Tcerakawanich, "An inverse-sinusoidal PWM technique to improve thermal performance of IGBT module," *2018 IEEE Transportation Electrification Conference and Expo, Asia-Pacific (ITEC Asia-Pacific)*, pp. 1–7, 2018, doi:10.1109/ITEC-AP.2018.8433304.

[45] P. M. Lingom et al., "A single-carrier PWM method for multilevel converters," *2019 IEEE 10th International Symposium on Power Electronics for Distributed Generation Systems (PEDG)*, pp. 122–127, 2019, doi:10.1109/PEDG.2019.8807453.

[46] C. R. Balamurugan et al., "Design of new multilevel inverter topology for various unipolar inverted sine carrier PWM strategies," *i-manager's Journal on Embedded Systems*, vol. 2, no. 4, pp. 37–43, 2014, doi:10.26634/jes.2.4.2806.

[47] R. Nandhakumar, S. Jeevananthan, "Inverted sine carrier pulse width modulation for fundamental fortification in DC-AC converters," *2007 7th International Conference on Power Electronics and Drive Systems*, pp. 1028–1034, 2007, doi:10.1109/PEDS.2007.4487830.

[48] A. S. Rahimi A Subki et al., "Comparative study of sinusoidal PWM and third harmonic injected PWM on three phase cascaded H-bridge multilevel inverter at various amplitude modulation indices," *2018 IEEE PES Asia-Pacific Power and Energy Engineering Conference (APPEEC)*, pp. 520–525, 2018, doi:10.1109/APPEEC.2018.8566478.

[49] M. E. Tamasas et al., "Comparison of different third harmonic injected PWM strategies for 5-level diode clamped inverter," *2017 IEEE Power and Energy Conference at Illinois (PECI)*, pp. 1–6, 2017, doi:10.1109/PECI.2017.7935718.

[50] T. M. Blooming, D. J. Carnovale, "Application of IEEE STD 519-1992 Harmonic Limits," *Conference Record of 2006 Annual Pulp and Paper Industry Technical Conference*, pp. 1–9, 2006, doi:10.1109/PAPCON.2006.1673767.

[51] "IEEE Recommended practice and requirements for harmonic control in electric power systems." IEEE.

[52] A. Aktaibi, M. A. Rahman, A. Razali, "A critical review of modulation techniques," *19th Annual Newfoundland Electrical and Computer Eng. Conference (NECEC 2010)*, 2010.

[53] A. Dekka et al., "Evolution of topologies, modeling, control schemes, and applications of modular multilevel converters," *IEEE Journal of Emerging and Selected Topics in Power Electronics*, vol. 5, no. 4, pp. 1631–1656, 2017, doi:10.1109/JESTPE.2017.2742938.

[54] Y. Li, Y. Wang, B. Q. Li, "Generalized theory of phase-shifted carrier PWM for cascaded H-bridge converters and modular multilevel converters," *IEEE Journal of Emerging and Selected Topics in Power Electronics*, vol. 4, no. 2, pp. 589–605, 2016, doi:10.1109/JESTPE.2015.2476699.

[55] F. Patkar et al., "Performance comparison of symmetrical and asymmetrical six-phase open-end winding drives with carrier-based PWM," *2017 6th International Conference on Electrical Engineering and Informatics (ICEEI)*, pp. 1–6, 2017, doi:10.1109/ICEEI.2017.8312446.

[56] M. Meraj et al., "Novel level shifted PWM technique for unequal and equal power sharing in quasi z-source cascaded multilevel inverter for PV systems," *IEEE Journal of Emerging and Selected Topics in Power Electronics*, vol. 9, no. 1, pp. 937–948, 2021, doi:10.1109/JESTPE.2019.2952206.

[57] K. Thakre, K. B. Mohanty, "Performance improvement of multilevel inverter through trapezoidal triangular carrier based PWM," *2015 International Conference on Energy, Power and Environment: Towards Sustainable Growth (ICEPE)*, pp. 1–6, 2015, doi:10.1109/EPETSG.2015.7510170.

[58] J. Patel, V. K. Sood, "Analysis of symmetric and asymmetric CHB-MLI using MC based SPWM and THI-PWM," *2020 IEEE Electric Power and Energy Conference (EPEC)*, pp. 1–7, 2020, doi:10.1109/EPEC48502.2020.9320041.

JIGNESHKUMAR PATEL completed his bachelor's degree in Power Electronics from Saurastra University, India in 2007. He did his master's degree in Electrical Engineering from California State University, Los Angeles, USA in 2010. He is pursuing his Ph.D. degree in Electrical Engineering from Ontario Tech University, Oshawa, Canada.
He is a student member of the Institute of Electrical and Electronic Engineers (IEEE). His research interests are in power electronic converters and digital controllers. He has published several articles on power electronic converters and digital controllers.

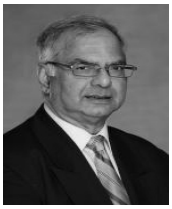

DR. VIJAY K. SOOD obtained his Ph.D. in Power Electronics from University of Bradford, England in 1977. From 1969-76, he was employed at the Railway Technical Centre, Derby, U.K. From 1976-2007, he was a Senior Researcher at IREQ (Hydro-Québec) in Montreal, Quebec. In 2007, he joined Ontario Tech University in Oshawa, Ontario where he is the Department Chair.
He is a Member of the Professional Engineers Ontario, a Life Fellow of the Institute of Electrical and Electronic Engineers (IEEE), a Fellow of the Engineering Institute of Canada (EIC) and Emeritus Fellow of the Canadian Academy of Engineering (CAE). His research interests are in the monitoring, control and protection of power systems using artificial intelligence techniques. Dr. Sood has published over 200 articles, 10 book chapters and written two books on HVDC Transmission.

Received: 07 March 2022, Revised: 05 April 2022, Accepted: 06 April 2022, Online: 23 April 2022

DOI: https://dx.doi.org/10.55708/js0104018

An Extreme Learning Machine for Blood Pressure Waveform Estimation using the Photoplethysmography Signal

Gonzalo Tapia[1], **Rodrigo Salas**[*,1,2,3,4], **Matías Salinas**[1,2,3], **Carolina Saavedra**[1,2], **Alejandro Veloz**[1,2], **Alexis Arriola**[1,2], **Steren Chabert**[1,2,4], **Antonio Glaría**[1]

[1]Escuela de Ingeniería C. Biomédica, Universidad de Valparaíso, Valparaíso, Chile.

[2]Centro de Investigación y Desarrollo en Ingeniería en Salud, CINGS-UV, Universidad de Valparaíso, Valparaíso, Chile.

[3]Programa de Doctorado en Ciencias e Ingeniería para la Salud, Universidad de Valparaíso, Valparaíso, Chile.

[4]Millennium Institute for Intelligent Healthcare Engineering, Santiago, Chile.

[*]Corresponding author: Rodrigo Salas, General Cruz 222, Valparaíso, Chile, rodrigo.salas@uv.cl, ORCID: 0000-0002-0350-6811

ABSTRACT: Blood Pressure (BP) waveform is a result of the response of the arteries to the blood ejection produced by the heart and, therefore, it is an important indicator of the state of the cardiovascular system. Currently, its measurement is performed invasively in critically ill patients who need a continuous and real time monitoring of their treatment response, however, it is possible to measure the BP, continuously and non-invasively, in non-critical patients to detect, monitor and control possible hypertensive events. Nevertheless, current non-invasive techniques can cause discomfort in patients and they are not used in critically ill patients. Consequently, non-Invasive and minimally-Intrusive methodologies (nImI) are required to estimate BP and its waveform. In the current study, the performance of machine learning algorithms, specifically the Extreme Learning Machine (ELM) algorithm, is evaluated to estimate both Blood Pressure and its waveform from the Photoplethysmography (PPG) signal and its first derivative's (VPG) waveforms. A total of 15 healthy volunteers participated in this study. They performed two handgrips, which is isometric maneuver to induce controlled BP rises. The first handgrip is used to train ELM and the second handgrip is used to test the ELM. Our results show that there are high correlation performances (0.98) between the estimated and measured BP waveforms, and a relative error of 3.3 ± 1.4%. An arterial volume-clamp at the middle finger is used as the gold-standard measurement. Meanwhile, BP extreme values estimations, Systolic BP (SBP) and Diastolic BP (DBP), are also performed. ELMs have a performance with an average RMSE of 5.9 ± 2.7 mmHG for SBP and 4.8 ± 2.0 mmHg for DBP and, an average relative error of 5.0 ± 2.7% for SBP and 7.0 ± 4.0% for DBP.

KEYWORDS Extreme Learning Machines, Adaptive Estimation, Biomedical Measurement, Photoplethysmography, Noninvasive treatment, Medical Devices.

1. Introduction

Arterial Hypertension (AHT) is a deadly disease that affects 70 million in the USA and 1,000 million people worldwide. AHT is still the most common risk factor and it is responsible for 54% of strokes and 47% of ischemic heart diseases worldwide [1].

Invasive methods have been used for Blood Pressure (BP) monitoring in critically ill patients for more than 50 years because they facilitate rapid diagnoses and allow us to monitor treatment responses in real-time. Medical procedures are said to be invasive when they require that the external natural protective barriers of the body, such as skin, are pierced, either through cuts or by inserting a medical device into the body. These measurements are more accurate than non-invasive methods because they introduce a cannula in the arterial system to measure BP directly from the artery [2]. Nevertheless, these methods require medical supervision to avoid injuries in the patient.

Medical devices are said to be intrusive when the procedures generate discomfort in patients, decreasing the adherence to the procedure. In particular, non-invasive procedures to measure BP, such as ambulatory blood pressure monitoring, are perceived by the patients as intrusive, the procedure is frequently abandoned, and the detection, monitoring and control of AHT remain elusive [3].

Although the morphology and detail of the arterial pressure waveform can provide useful diagnostic information, modern physicians pay little attention to it [4]. This results in an important waste of a potential diagnostic aid whose usefulness was first recognised over 100 years ago [5]. Mahomed used sphygmography in his studies to analyse the arterial pressure waveform, a technology with levers hooked to a scale-pan in which weights were placed to determine the amount of external pressure needed to stop blood flow in the radial artery [6]. According to [7], sphygmography

lapsed with the introduction of the cuff sphygmomanometer, which only provides the extreme values of the arterial pressure pulse.

Although the measurement of the difference between systolic and diastolic pressures from a single pulse has been used to assess arterial stiffness and cardiovascular risk [8], important additional information is contained within the pressure waveform [9], such as augmentation index, left ventricular workload, cardiac output and, in a lower level, arterial stiffness [10]. Consequently, the use of pulse wave analysis may serve as a guide for physicians when making choices about blood pressure treatment in prehypertensive or hypertensive patients [11].

The pressure wave is generated by the contraction of the left ventricle, which imparts its contractile energy on the blood mass that it contains, raising the pressure to overcome the diastolic pressure in the aorta to open the aortic valve, ejecting the blood and deforming the radius of the aorta lumen [9]. As the ventricle ejects the blood mass into the aorta with each systole, it creates a pulsatile pressure and flow. The pressure wavefront is propagated to most of the peripheral arteries at 8 to 10 m/s, although the blood that leaves the left ventricle takes several cardiac cycles to reach the same distance [7].

The acronym nImI is proposed to summarise a concept that could be applied to medical devices—a device would be nImI if and only if it is non-invasive and it is minimally-intrusive. Non-invasive devices are able to monitor the arterial pressure waveform, such as those based on the volume clamp [12] technique (FINAPRES, CNAP, etc.) and those based in applanation tonometry techniques. Both of these techniques measure blood pressure waveform in a specific point of the body and they then reconstruct brachial and aortic BP waveforms, respectively, with validated algorithms. Nevertheless, analysis from the brachial pressure waveform is not considered to be a suitable indicator for cardiovascular risks [13] and applanation tonometry is not yet a reliable tool to monitor pressure waveform in long-term clinical interventions [14].

Photoplethysmography (PPG) has been studied to estimate and monitor BP non-invasively, measuring the Pulse Transit Time (PTT) and, therefore, the Pulse Wave Velocity (PWV), which are directly related to BP. PTT can be easily measured from a PPG waveform, and it is less expensive and cumbersome than the previously described devices [15]. Nevertheless, the normal use of PPG carries artifacts that interfere with a proper signal preprocessing [16]. However, new clinical applications have been proposed that are supported by computational solutions [17] and novel wearable devices such as smartwatches [18].

The relationship between the PTT and BP is so strong that a device which estimates BP from PTT was patented at the beginning of the 21st century, where two parameters were consider for each subject [19]. Furthermore, the correlation between the BP and PTT has been proven under exercise and drug administration conditions [20]. In previous works by [21] and [22], new approaches were tested to relate PPG and BP. In the first, machine learning has been used to classify PPG waveforms corresponding to high and normal BP in healthy subjects. In the second, PPG is fitted to the finger Arterial Pressure (fiAP).

Recently, some authors have proposed the application of machine learning methods to estimate the BP waveform (see [23]–[25]). In [23], the author proposed an ensemble of support vector regression SVR models to predict the BP [24] have applied SVR combined with genetic algorithms to estimate systolic BP and diastolic BP. In [25], the author proposed the Deep Boltzmann machine to estimate the blood pressure.

The main goal of this work is to validate the mExtreme Learning Machine (ELM) as a model that relates the PPG to fiAP and brachial reconstructed Blood Pressure (reBP) waveforms. This work is structured as follows. In section 2, we introduce the Extreme Learning Machine, the main model used in this article. In section 3, we describe the data acquisition process, the signal processing process and the ELM architectures. The performance results are given in section 4 and we give a discussion in section 5. Finally, some concluding remarks are given in section 6.

2. Theoretical Framework: Extreme Learning Machine (ELM)

ELM [26] has been proposed for training single hidden layer Feedforward Neural Networks (SLFN) [27], as shown in Figure 1. Feedforward Neural Networks (FNN) have been widely used since the introduction of the back propagation algorithm [28], which is essentially a first order gradient method for parameter optimisation and, therefore, has slow convergence problems. In addition, ELM has much lower computational complexity and is particularly attractive for high dimensional and large data applications. In this paper, the ELM algorithm is used for nImI BP estimates from three different inputs PPG and VPG signals, and for a combination of them.

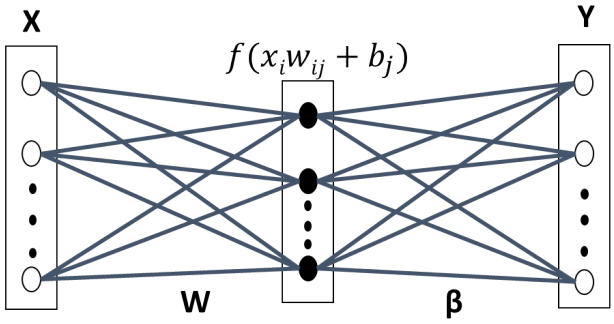

Figure 1: Fully connected architecture of a single hidden layer feed-forward neural network, where the input neurons are fully connected with the hidden layer, and the hidden layer with the output neurons layer.

The main characteristic of ELM is that once the input weights and biases, from input to the hidden layer, are randomly defined, they are not further modified in the learning process. Consequently, ELM has a very short training time. Furthermore, ELM is remarkably efficient and tends to reach global optimum [29]. Various extensions have been made to the original ELM model to make it more efficient and suitable for specific applications [26].

These types of algorithms are suitable for the new era of big data processing, where large amount of data need to be processed in short time. ELM, as a learning technique, is able to provides efficient unified solutions to generalised FNN, including single and multi-hidden layers neural network. This algorithm has both universal approximation and classification capabilities [30].

The input vector is mapped to L-dimensional ELM random feature space, let $\mathbf{x}_i \quad x_1, x_2, ..., x_d$ be the input vector shown in Figure 1, $\mathbf{x}_i \in \chi \subseteq \mathbb{R}^d$ and $\mathbf{T} \quad \mathbf{t}_1, \mathbf{t}_2, ..., \mathbf{t}_N$ the targets values, $(i \quad 1, 2, ..., N)$. The parameters of the j-th hidden node are $\mathbf{w}_j$ corresponding to the weight vector connecting the j-th hidden node to the input nodes, where $\mathbf{w}_j \quad w_{1j}, w_{2j}, ..., w_{Lj}$ and b_j, corresponding to the threshold or bias. $(j \quad 1, 2, ..., L)$ and L is the number of nodes in the hidden layer. These connections are randomly assigned and they remain unchanged during the learning process.

The k-th output function of ELM for generalised SLFN is:

$$y_k\mathbf{x}_i \quad \sum_{j1}^{L} \beta_{jk} h_j \mathbf{w}_j, b_j, \mathbf{x_i} \quad \mathbf{h}\mathbf{x}_i\boldsymbol{\beta}_k, \qquad i \quad 1, ..., N, k \quad 1..K \tag{1}$$

where the vector $\boldsymbol{\beta}_k \quad \beta_{1k}, ...\beta_{Lk}{}^T$ contains the weights between the hidden nodes and the k-th output node. H is the hidden layer output matrix of the neural network, where the i-th column of H is the output of the j-th hidden node with respect to the input $\mathbf{x}_i$:

$$\mathbf{H} \begin{pmatrix} f\mathbf{w}_1, b_1, \mathbf{x}_1 & ... & f\mathbf{w}_L, b_L, \mathbf{x}_1 \\ ... & ... & ... \\ f\mathbf{w}_1, b_1, \mathbf{x}_N & ... & f\mathbf{w}_L, b_L, \mathbf{x}_N \end{pmatrix} \tag{2}$$

where $f\mathbf{w}_j, b_j, \mathbf{x}_i$ is an activation function that satisfies the ELM universal approximation capability theorem [26]. In this paper, the threshold function was used:

$$f\mathbf{w}, b, \mathbf{x} \quad \begin{cases} 1, & \text{if } \mathbf{w} \cdot \mathbf{x} \quad b \leq 0 \\ 0, & \text{otherwise} \end{cases} \tag{3}$$

The ELM learning process consists in solving matrix equation on vector beta:

$$\mathbf{H}\boldsymbol{\beta} \quad \mathbf{T} \tag{4}$$

In theory, if the number of the L neurons in the hidden layer is equal to the number of the possible samples that constitute a problem and, furthermore, $\mathbf{H}$ is invertible, then the solution for $\boldsymbol{\beta}$ will be found multiplying by $\mathbf{H}^{-1}$ at the left-hand of the equation and solving it by linear least squares method [29]:

$$\mathbf{H}^{-1}\mathbf{H}\boldsymbol{\beta} \quad \mathbf{H}^{-1}T \rightarrow \boldsymbol{\beta} \quad \mathbf{H}^{-1}\mathbf{T} \tag{5}$$

Nevertheless, the vector $\mathbf{H}$ will generally not be square and invertible and, for this reason, the values of $\boldsymbol{\beta}$ will be:

$$\boldsymbol{\beta} \quad \mathbf{H}^{\dagger}\mathbf{T} \tag{6}$$

where $\mathbf{H}^{\dagger}$ is the generalised Monroe-Penrose inverse of the matrix $\mathbf{H}$ and, therefore, the values of weights connecting the hidden layer with output neurons layer ($\boldsymbol{\beta}$) can be found multiplying it by the $\mathbf{T}$ vector [31], [29] and [26].

3. Materials and Methods

In this paper, new methodologies are tested to estimate either fiAP and reBP waveforms or SBP and DBP values from PPG. Signals from 15 healthy subjects are recorded and ELM machine learning algorithms are trained to do these BP estimations for each subject.

The required cardiovascular signal acquisition is performed in each subject. The subjects are asked to answer a questionnaire that is adapted from the AHT Clinical Guide of the Chilean Ministry of Health and to sign an informed consent that is approved by Bioethics Institutional Committee for Human Beings Research of the Universidad de Valparaíso (CIBI-SH UV for its acronym in Spanish), accepting to perform the clinical essay.

BP is measured with an oscillometric technique in each subject twice before performing the clinical essay to ensure that the subjects do not have a SBP greater than 140 mmHg or a DBP greater than 90 mmHg. If they declare that they have a cardiovascular disease, then they are excluded from the study.

3.1. The Subjects' Characteristics

Table 1 shows the characteristics of the 15 healthy subjects that participated in this study. Data from these subjects can be found in [32], within the Readme file in section "Getting the Dataset" of "About nImI". Column 2 shows the corresponding code name for each subject of column 1.

In this study, the data were gathered from 10 females and 5 men with a mean age of 31.3 ± 10.8 years old. The youngest subject is 18 years old and the oldest is 50 years old. As is explained on the website, different essays that are performed by volunteers in the project and different configurations for data recordings are used, depending on the essay. Consequently, only those subjects that performed a particular essay are studied in this article. Each subject performs an isometric handgrip maneuver twice to induce BP rises in SBP and DBP while the signals are recorded.

Two oscillometric BP measurements are performed in each subject to obtain their SBP and DBP values for two reason. The main reason is to corroborate that the subject is normotensive and can perform the clinical essay and the second reason is to calibrate the Finapres NOVA.

3.2. Data Acquisition

A detailed description of the data acquisition, signal processing and segmentation is given in [22]. Briefly, PPG and ECG signals are recorded, respectively, in the bandwidth from DC to 10 Hz and from 0.3 to 35 Hz using the BIOPAC system. The fiAP waveform is recorded using Finapres NOVA (FN) of [33]. The brachial blood pressure waveform (reBP) is reconstructed by FN from fiAP and its extreme values correspond to SBP and DBP. The signals are sampled at 200 Hz.

Once the signals have started to be recorded, the handgrip maneuver is performed after a resting time of 10 minutes. During this period, the FN is calibrated (with the two oscillometric BP measurements shown in Table 1) and the subject can relax and receive instructions about the

handgrip maneuver. Then, the subject must press a device in a sustained manner during a standardised time. The maneuver is performed twice, with a resting time of 10 minutes between them.

Table 1: Characteristics of the subjects (S) participating in the study, which shows their ages, sex and their two oscillometric BP measurements (M1 and M2) performed to obtain DBP and SBP mmHg.

Subjects Characteristics							
S	Code Name	AGE	SEX	DBP		SBP	
				M1	M2	M1	M2
1	S03	18	F	69	78	107	120
2	S04	49	M	81	100	129	161
3	S05	29	F	78	84	117	129
4	S06	28	M	63	92	111	149
5	S07	40	F	73	93	106	141
6	S08	33	F	81	94	130	139
7	S09	50	M	61	109	115	207
8	S10	45	F	63	69	90	100
9	S11	26	F	59	71	102	113
10	S12	26	M	64	102	120	155
11	S13	38	F	75	81	122	134
12	S14	20	F	62	88	117	154
13	S15	29	M	76	108	122	170
14	S16	19	F	60	79	108	138
15	S17	20	F	72	85	115	121

During each handgrip, the subject steadily grips a cuff with his or her deft hand for 3 minutes. The pressure over the cuff is at one third of the subject's maximal strength. After the 3 minutes, the subject releases the cuff and rests for three additional minutes. Afterwards the recording is stopped. These essays were conducted at the School of Biomedical Engineering (EICB), Faculty of Engineering, Universidad de Valparaiso (Chile).

3.3. Photoplethysmography signal processing

Photoplethysmography (PPG) is sensitive to thermal changes, movements and respiration [16]. Consequently, the raw PPG is processed with two FIR filters (detailed description in [22]). Later, PPG first derivative, or velocity of PPG, VPG, is evaluated using a five point stencil algorithm. PPG is segmented beat to beat using ECG and it is then processed to extract the sections that have suffered interference from spiky blocking noise.

3.3.1. Pre-processing of the PPG

The PPG is preprocessed with two symmetric Finite Impulse Response (FIR) filters of order 17 and 799. The low order FIR low passes the signal at 6.5 Hz, smoothing the PPG and decreasing energy in quantisation error frequency band. The high order FIR high passes the signal at 0.2 Hz, stabilising PPG's DC component. VPG is calculated after the two FIR filters have been applied. It is performed with five point stencils (7) instead of the more conventional L'Hopital rule, which is known to produce noisy derivatives.

$$yn \quad \frac{-xn\ \ 2\ \ 8xn\ \ 1 - 8xn - 1\ \ xn - 2}{0.06} \tag{7}$$

3.3.2. PPG Signal Segmentation

Segmentation of PPG, VPG, fiAP and reBP during each heartbeat is needed to estimate fiAP and reBP waveform, and their BP values beat to beat.

A modified Pan-Tompkins Algorithm (PTA) [34], is used to detect R waves from ECG and to segment each cardiac cycle, which is the unit of study in this work. To accomplish this, the PTA's band-pass filter in cascade with a Continuous Wavelet Transform (CWT) with a Mexican-Hat wavelet was applied. From CWT's results, a threshold is established at 30% of the maximum amplitude in a R wave of the signal, which is chosen arbitrarily. Furthermore, a refractory time of 0.3 seconds is established [35], which represents the minimal period before the next QRS complex appears.

3.3.3. Noisy PPG Extraction

While PPG is transmitted from the sensor module to the Biopac system, an algorithm is implemented to detect and remove the PPG segments that have suffered interference from blocking noise [22] if a spiky communication interruption occurs and the signal is blocked. The unaffected segments are isolated and saved.

3.4. Signal Normalisation

Signals are normalised in amplitude and in time duration, or period. Period normalisation is necessary because a fixed number of inputs neurons are needed to train the ELM algorithms. Due to heart rate variability, each heartbeat has a different period and this results in a different numbers of samples in each. Consequently, 180 samples (0.9 seconds) are considered for each heartbeat.

Amplitude is normalised to estimate BP only using PPG and VPG waveforms and not their extreme values. Normalisation is applied on each signal by:

$$\underline{\mathbf{x}}_i \quad \frac{\mathbf{x}_i - \min \boldsymbol{x}_i}{\max \mathbf{x}_i - \min \mathbf{x}_i} \tag{8}$$

where $\underline{\mathbf{x}}_i$ is the normalised signal.

3.5. Derivative Approaches

The standard terminology for photoplethysmogram signals presented in [36] is used in this paper. VPG and the second derivative of PPG (APG) have been studied in relation with Blood Pressure in [37].

Figure 2 shows an example of PPG (blue), its first derivative (red) and an example of the corresponding fiAP and reBP waveform for each heartbeat in black. In previous work [22], the relationship between PPG and fiAP has been studied in four subjects with two different approaches. The first approach is a Linear Combination of Derivatives (LCD):

$$LCD^i \quad \alpha PPG^i \ \ 1 - \alpha PPG^{i1} \tag{9}$$

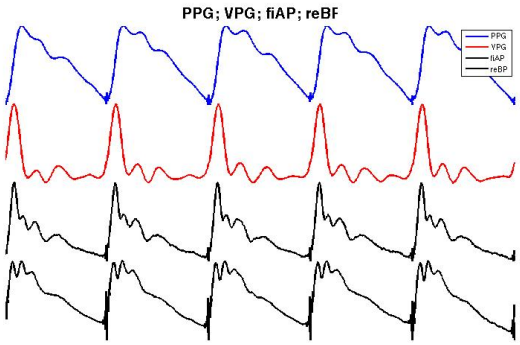

Figure 2: Examples of signals used in this paper, from top to bottom: PPG in blue, VPG in red and fiAP waveform with reBP waveform in black.

where PPG^k is the k^{th} order temporal derivative of the PPG, and α is a single parameter to fit PPG to fiAP and if $LCD \;\; LCD^0$ then:

$$LCD \;\; \alpha PPG \;\; 1 - \alpha VPG. \tag{10}$$

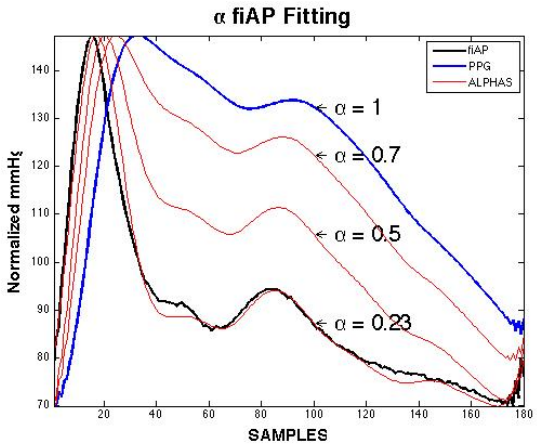

Figure 3: Linear combination of derivatives [22]. Combination of the PPG and VPG to adjust the fiAP waveform by modifying a parameter α.

As shown in Figure 3, by modifying α, the PPG signal (blue) can be fitted in the fiAP signal (black), normalising the LCD result and "de-normalising" it within the BP extreme values of fiAP. Nevertheless, even though the fitting shows a strong relationship between these two signals, it does not have an estimate value because α for the best fit must be evaluated from each PPG waveform using its respective fiAP waveform. In [38], we have introduced a fractional derivative method applied to the PPG to obtain the fiAP signal. In this study, machine learning is used to estimate the fiAP and reBP waveform from different combinations of PPG and VPG waveforms.

3.6. ELM Training and Testing Sets to estimate BP

Each subject performs the handgrip maneuver twice. The signals from the first recording are used as the training set and the signals from the second recording are used as the testing set.

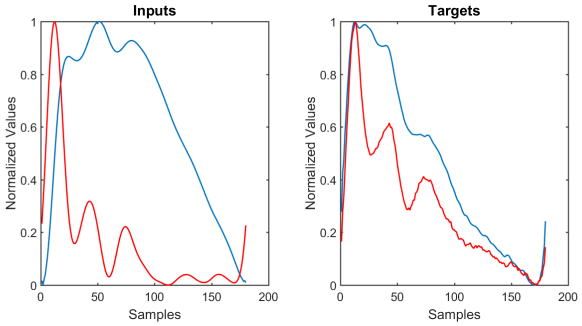

Figure 4: At the left: PPG (blue) and VPG (red) are the two types of input used in this study. Each sample of the signal correspond to a input neuron. At the right: reBP (blue) and fiAP (red) are the two types of targets for the ELM training.

Different ELMs are trained in each subject to estimate different targets: fiAP, reBP and the pair SBP/DBP. Furthermore, three ELMs are trained per target, with different inputs vectors: PPG, VPG and a modular combination of them. In summary, nine ELM algorithms are trained per subject.

To compensate the loss of physiological information produced by signals segmentation and normalisation, the estimation of SBP/DBP includes a second input vector module for each ELM network. This module has two input neurons, one with Pulse Transit Time (PTT) and the other with the Heart Rate (HR) of the corresponding signal's heartbeat.

Figure 4 shows an example of the input and target waveforms. On the left-hand, the PPG signal (blue) and VPG signal (red) are illustrated. On the right-hand, the fiAP signal (blue) and reBP signal (black) are illustrated.

It is important to mention that, only normalised waveforms are considered to estimate fiAP and reBP. Thereafter, ELM outputs are denormalised into SBP and DBP values of the corresponding fiAP or reBP waveform and the results are then evaluated.

3.7. ELM Architectures

Two main approaches are used, depending on whether BP waveforms or systolic and diastolic values are to be estimated.

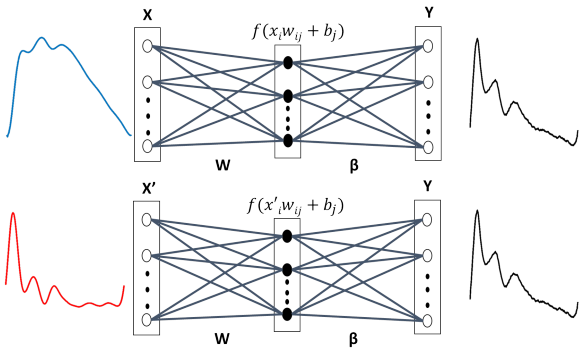

Figure 5: ELM1 and ELM2: General architecture used separately with the PPG (ELM1) and VPG (ELM2) as inputs to train ELMs for fiAP and reBP waveform estimation. In both cases, as an example, only fiAP waveform at the output is shown.

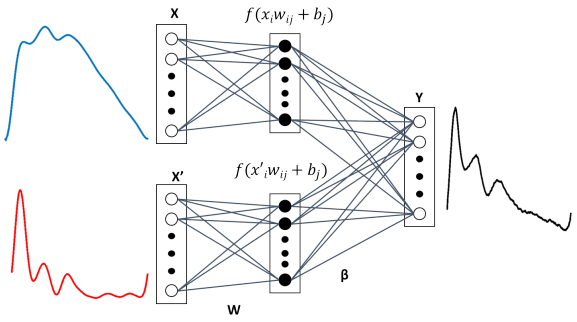

Figure 6: ELM3: Architecture with two modules at the input, inspired on LCD from a previous work [22]. The two types of inputs are not fully connected to the hidden layer, which is fully connected to the output neurons. The same type of architecture is used to estimate fiAP and reBP waveform.

3.7.1. Approach 1: Finger and Brachial BP Waveform Estimates

Both fiAP and reBP waveform estimation use similar ELM architectures, only the target vector is changed. Consequently, the following explanation applies to estimate fiAP or reBP. Architectures illustrated in Figures 5 and 6 are used to estimate either fiAP or reBP.

As mentioned, three types of input vectors—PPG, VPG and combination of them—are used to train ELM algorithms to estimate fiAP or reBP waveform. ELM with either PPG or VPG as input vector use the architecture illustrated in Figure 5, which will referred as ELM1 and ELM2, respectively. ELM1 or ELM2's output vector is obtained in (11):

$$y_k \quad g\left(\sum_{j1}^{M} f\left(\sum_{i1}^{N} w_{ji} x_i \quad b_j\right)\beta_{kj}\right) \tag{11}$$

where $k \quad 1, 2, ..., N$, y_k is the k^{th} value of the output vector, g is a linear activation function, f correspond a *hardlim* activation function, and $X \quad x_1, x_2, ..., x_N$ is the PPG or the VPG input vector.

A third architecture ELM3, is used, which has a modular combination of PPG and VPG as input vector. As shown in Figure 6, ELM3 has two types of input vectors in separate modules and, because the hidden layer is not fully connected to all input neurons, they allow a different influence of PPG and VPG in fiAP or reBP estimation. In both cases, all of the neurons of the hidden layer are fully connected with all of the output neurons. ELM3's output is represented in (12):

$$y_k \quad g\left(\left[\sum_{j1}^{M} f\left(\sum_{i1}^{N} w_{ji} x_i \quad b_j\right)\beta_{kj} \right.\right.$$
$$\left.\left.\sum_{lM1}^{2M} f\left(\sum_{i1}^{N} w_{li} x'_i \quad b_l\right)\right]\beta_{kl}\right) \tag{12}$$

where g and f are the same activation functions of the previous case and $X \quad x_1, x_2, ..., x_N$ is the sampled PPG and $X' \quad x'_1, x'_2, ..., x'_N$ is the sampled VPG.

3.7.2. Approach 2: SBP and DBP Estimates

SBP and DBP values are used as targets to train ELM4, ELM5 and ELM6. They correspond to reBP signal extreme values. To build the ELM models, we have used an ensemble approach to combine the inputs of different signals [39, 40]. The input vectors are those used in BP waveform estimation; except for PTT and HR, which are added as a second input vector module in ELM4 and ELM5, and as a third input vector module in ELM6. The output vectors are represented in two neurons, which codify SBP and DBP values.

Figure 7 illustrates ELM4, which a modified architecture from ELM1. In addition to the sampled PPG waveform, a second module with the PTT and HR values is added. The same architecture is used with ELM5, which uses sampled VPG signals instead of those of the PPG. The ELM4 and ELM5 output vectors are obtained with (13):

$$y_k \quad g\left(\sum_{j1}^{M} f\left(\sum_{i1}^{N} w_{ji} x_i \quad b_j\right)\beta_{kj}\right.$$
$$\left.\sum_{lM1}^{L} h\left(\sum_{i1}^{Q} w_{li} z_i \quad b_l\right)\beta_{kl}\right) \tag{13}$$

where the input signal X is the sampled PPG for the ELM4, and the sampled VPG for the ELM5. The input Z consists of two neurons for the PTT and HR values as input. Finally, f and h are linear activation functions.

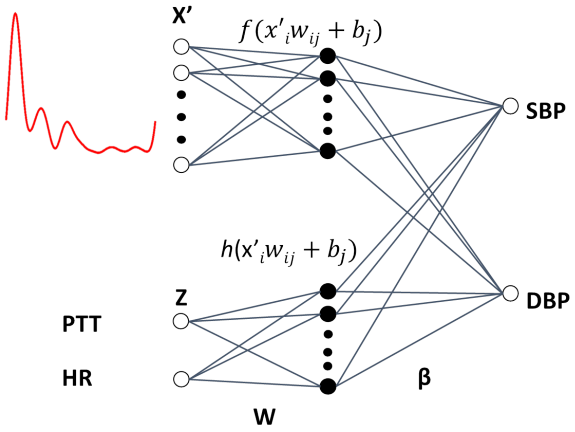

Figure 7: Architecture of ELM4 and ELM5, which are trained to estimate SBP and DBP, which has two modules as inputs—one is the module with PPG waveform ELM4 or VPG waveform (ELM5), and the other module has two neurons: Heart Rate (HR) and Pulse Transit Time (PTT) corresponding to the waveform of the first module. In this figure, ELM5 is shown as an example.

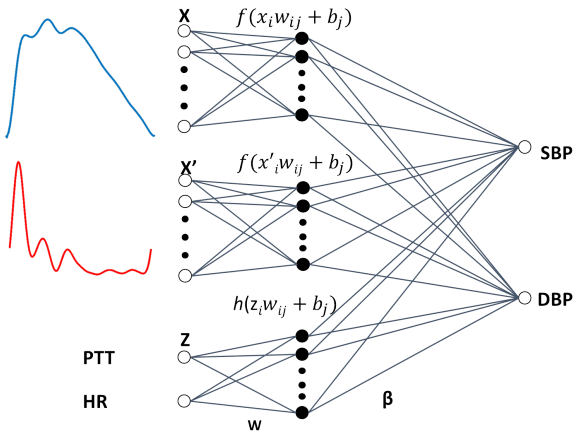

Figure 8: ELM6: A second type of architecture to estimate SBP and DBP from three modules, one module for PPG waveform, the second module to VPG waveform and the third module to PTT with the HR.

Finally, ELM6, which is the last architecture used, is illustrated in Figure 8. In this case, a modular combination of PPG with VPG, together with a third module for PTT and HR, are input vectors. The output vector is obtained in (14):

$$y_k \quad g\left(\sum_{j1}^{M} f\left(\sum_{i1}^{N} w_{ji}x_i \;\; b_j\right)\beta_{kj}\right) \sum_{pM1}^{P} f\left(\sum_{i1}^{N} w_{pi}x'_i \;\; b_p\right)\beta_{kp} \sum_{l2M1}^{L} h\left(\sum_{i1}^{Q} w_{li}z_i \;\; b_l\right)\beta_{kl}\Big) \tag{14}$$

where $P \;\; 2M$, X represents the PPG, X', is the VPG and Z correspond to input neurons for PTT and HR.

3.8. Hidden Layer Dimensionality

We use six different architectures of ELM to estimate BP in each subject. Our aim is to compare the capacity of ELM to estimate fiAP and reBP waveforms either from the PPG and VPG signals, and their combination, or to estimate SBP and DBP from the same signals. Nevertheless, a common problem in the design of the architecture of the multilayer perceptron is how to determine the number of neuron in the hidden layer [41]. This issue is considered in this paper by varying the number of neurons in the hidden layer for each of the ELM architectures and the performance for each architecture was tested. The dimension of the layer producing the smaller error for the test set is selected.

This procedure is especially powerful because one of the main advantages of ELM is its short training times. This characteristic allows us to perform exploratory studies to determine the suitable number of neurons to be used in the hidden layer. Tests in the range of 1–200 neurons in the hidden layer were performed. These tests showed that the best performance is achieved in the range of 14–23 neurons. This range of neurons is used in this work to search for the best architecture for each subject.

4. Results

4.1. Training and Testing Sets

Table 2 shows the number of heartbeats that are used to train and test ELM algorithms per subject. Each number is the result of signal processing and artifacts extraction from ECG, reBP, fiAP and PPG.

Table 2: Number of signals per subject that were used to train and test the ELM models

Subject	Training Set	Testing Set
S03	518	470
S04	430	415
S05	367	282
S06	395	476
S07	439	334
S08	325	107
S09	281	333
S10	493	465
S11	469	474
S12	404	389
S13	501	454
S14	334	179
S15	377	195
S16	380	205
S17	401	219
Average	408	333
Minimum	281	107
Maximum	518	476

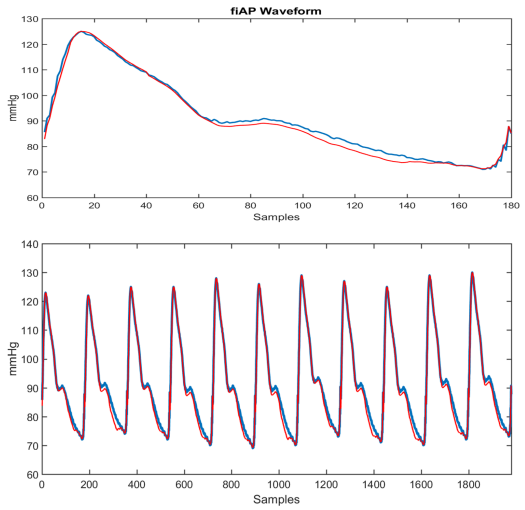

Figure 9: At the top: one fiAP waveform measured by FINAPRES (blue) and an estimated waveform with ELM3 (red), which corresponds to one heartbeat. At the bottom: a train of 13 pressure pulses and their respective estimated waveform by ELM.

4.2. Fitting the fiAP Waveform

The LCD performance is shown in the last column of Table 3. These results are an extension of those in [22]. The main difference with the previous work is that only 160 heartbeats of 4 subjects are considered to fit PPG to the corresponding fiAP in that case, whereas in the current work PPG is fitted to fiAP during 4997 heartbeats of 15 subjects, which are taken from signals in the testing set. A mean relative error of 5.7 ± 1.6 with a mean $r \;\; 0.95$ are achieved for the 15 subjects.

4.3. Estimating the fiAP Waveform

The fiAP waveform (in blue) and the ELM3 estimated waveform (in red) is shown in the upper part of Figure 9. A strong similarity between them can be observed, with $error < 5\%$. At the bottom of the figure, a train of fiAP waveforms (in blue) is shown with the ELM estimation (in red) above it. The estimation of the waveforms within the observed

Table 3: Relative Error, its standard deviation (σ) and the correlation (r) from fiAP waveform estimation by ELMs with three types of training set: PPG waveform (ELM1); VPG waveform (ELM2) and a combination of PPG and VPG (ELM3). Finally a comparison with LCD fitting methodology

fiAP Waveform Estimate

	ELM1			ELM2			ELM3			LCD		
Subject	**Relative Error (%)**	σ	**r**	**Relative Error (%)**	σ	**r**	**Relative Error (%)**	σ	**r**	**Relative Error (%)**	σ	**r**
S03	3.9	0.7	0.97	4.2	0.7	0.96	3.2	0.5	0.98	7.2	0.7	0.90
S04	6.0	1.1	0.94	7.1	1.3	0.93	6.0	1.4	0.96	4.3	0.6	0.96
S05	4.1	1.8	0.97	4.9	2.4	0.97	4.6	2.0	0.98	3.8	1.1	0.96
S06	3.6	1.0	0.98	4.0	1.2	0.98	5.2	1.2	0.98	4.6	0.7	0.96
S07	3.3	1.4	0.98	3.9	1.2	0.98	3.7	1.8	0.98	3.5	1.4	0.97
S08	3.5	1.9	0.98	3.9	1.9	0.98	4.0	1.7	0.97	4.0	1.4	0.96
S09	5.9	2.1	0.98	4.2	1.5	0.98	5.6	1.6	0.98	7.6	1.5	0.94
S10	3.9	1.2	0.97	4.1	1.3	0.97	3.8	1.3	0.98	5.4	1.1	0.95
S11	3.7	0.5	0.98	4.1	0.6	0.97	3.2	0.8	0.98	5.1	1.7	0.94
S12	4.1	1.9	0.98	5.8	2.3	0.97	4.0	2.1	0.97	7.1	3.8	0.91
S13	5.0	2.3	0.98	4.7	2.3	0.98	4.8	1.8	0.97	4.7	1.5	0.97
S14	6.0	2.4	0.96	5.4	1.9	0.96	5.3	1.6	0.97	10.4	1.5	0.92
S15	5.3	2.1	0.96	5.3	2.2	0.96	5.0	2.0	0.96	4.8	2.6	0.96
S16	4.9	2.2	0.97	4.9	2.2	0.98	4.8	2.1	0.97	5.4	1.9	0.95
S17	6.4	2.7	0.97	5.4	2.4	0.97	5.7	2.1	0.97	7.0	2.3	0.96
MEAN	4.6	1.7	0.97	4.8	1.7	0.97	4.6	1.6	0.97	5.7	1.6	0.95

period is performed independently, beat to beat, and is then concatenated to form the train of BP pulses.

Table 3 shows the relative error, with its standard deviation, and the correlation between measured fiAP waveform and ELM estimates for the 15 subjects. After applying the statistical t-test with a resulting p-value bigger than 0.05, we cannot conclude that a significant difference of the relative error exists between the ELM1, ELM2, ELM3 and LCD models. However, with our data, the ELM models obtained the lowest mean relative error compared to the LCD. Moreover, there is no statistical significant difference in the correlations between the waveforms achieved by the models. The ELM models reach a correlation higher than 0.93 with an average of 0.97 ± 0.01.

4.4. Estimating the reBP Waveform

Figure 10 shows at the top a reBP waveform (in blue) and the estimated waveform (in red) from the ELM with architecture of Figure 6. A strong similarity can be seen. A train of reBP waveforms is shown at the bottom of Figure 10, with the ELM estimation above it. The estimation of each waveform is performed independently, beat to beat, and then concatenated to form the train of BP pulses.

Table 4 shows the relative error, with its standard deviation, and correlation between measured reBP waveform and ELMs estimates for the 15 subjects. The best result is slightly achieved by ELM3 (combination of PPG and VPG). After applying the statistical t-test with a resulting p-value bigger than 0.05, we cannot conclude that a significant difference of the relative error exists between the ELM1, ELM2, and ELM3 models. However, with our data, the ELM3, that combines PPG and VPG, obtained the lowest mean relative error of 3.33%. The ELM models reach a correlation higher than 0.96 with an average of 0.98 ± 0.01.

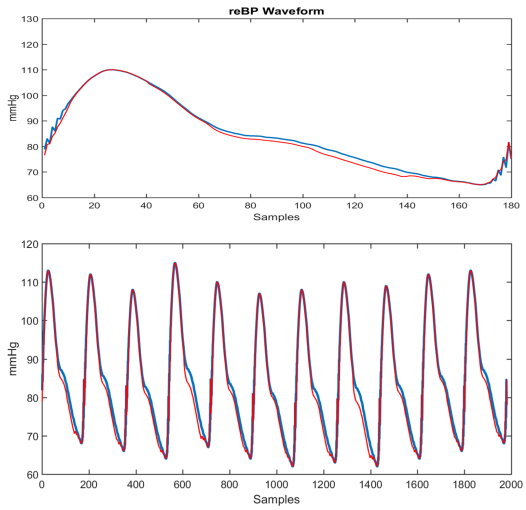

Figure 10: At the top: one reBP waveform reconstructed by FINAPRES from fiAP waveform (blue) and an estimated waveform with ELM6 (red), which corresponds to one heartbeat. At the bottom: a train of 13 pressure pulses and their respective estimated waveform by ELM.

4.5. Estimating SBP

Table 5 shows the results of estimating SBP. After applying the statistical t-test with a resulting p-value bigger than 0.05, we cannot conclude that a significant difference of the relative error exists between the ELM4, ELM5, and ELM6 models. However, with our data, the ELM6 achieves the lowest mean relative error of 5.01% and the lowest average of the Root Mean Square Error of 5.86 mmHg. The minimum error is achieved for subject $S\,04$ in all ELMs, having in ELM6 a RMSE: 2.6 mmHg and a relative error: 2.0%. The worse result is obtained in subject $S\,16$ in all ELMs, having in ELM6 a RMSE: 12.6 mmHg and relative error: 13.5%.

Table 4: Relative Error, its standard deviation (σ) and the correlation (r) from reBP waveform estimation by ELMs with three types of training set: PPG waveform (ELM1); VPG waveform (ELM2) and a combination of PPG and VPG (ELM3)

reBP Waveform Estimate

	ELM1			ELM2			ELM3		
Subject	**Relative** Error (%)	σ	**r**	**Relative** Error (%)	σ	**r**	**Relative** Error (%)	σ	**r**
S03	2.1	0.8	0.99	2.9	0.8	0.97	1.9	0.4	0.99
S04	3.7	1.0	0.96	3.7	0.7	0.96	3.3	0.7	0.97
S05	2.4	1.4	0.98	2.6	1.1	0.98	2.1	1.0	0.98
S06	4.1	1.5	0.98	4.0	1.5	0.98	3.8	1.0	0.97
S07	2.8	1.7	0.99	2.9	1.8	0.98	3.1	1.4	0.99
S08	3.0	1.7	0.99	3.0	2.1	0.98	3.6	1.5	0.98
S09	3.8	1.3	0.98	3.3	1.6	0.98	3.8	1.2	0.98
S10	2.3	1.1	0.98	2.1	1.2	0.98	1.8	1.3	0.99
S11	2.6	0.6	0.99	3.1	0.8	0.98	2.0	0.6	0.99
S12	3.9	1.4	0.98	4.3	1.7	0.97	3.4	1.5	0.98
S13	4.0	2.4	0.98	3.6	2.4	0.99	3.9	2.1	0.99
S14	5.0	2.6	0.97	5.0	3.0	0.97	4.2	1.8	0.98
S15	4.1	2.3	0.97	3.4	2.2	0.98	3.7	2.1	0.98
S16	4.8	2.4	0.98	4.6	2.9	0.98	5.2	2.5	0.98
S17	4.0	2.5	0.98	3.6	2.4	0.98	4.1	2.5	0.98
MEAN	3.51	1.65	0.98	3.47	1.75	0.98	3.33	1.44	0.98

Table 5: Root Mean Square Error (RMSE) and relative error from systolic BP estimation by ELMs with three types of training set: PPG waveform (ELM4); VPG waveform (ELM5) and a combination of PPG and VPG (ELM6). All of them plus PTT and HR correspond to each waveform

Systolic Blood Pressure Estimate

	ELM4		ELM5		ELM6	
Subject	**RMSE** (mmHg)	**Relative** Error (%)	**RMSE** (mmHg)	**Relative** Error (%)	**RMSE** (mmHg)	**Relative** Error (%)
S03	6.3	5.1	5.5	4.5	3.6	2.9
S04	3.3	2.5	2.8	2.2	2.6	2.0
S05	5.5	4.7	5.5	4.7	5.3	4.6
S06	11.3	8.5	11.5	7.9	8.5	6.2
S07	5.9	5.5	5.9	5.4	5.7	5.3
S08	6.6	4.9	9.2	6.4	6.1	4.5
S09	12.7	9.8	13.3	10.3	9.8	7.4
S10	4.0	4.1	3.9	4.0	3.4	3.5
S11	4.4	4.5	4.4	4.4	4.1	4.2
S12	10.0	7.0	10.4	7.3	7.8	6.3
S13	7.6	5.5	7.4	5.5	5.7	4.3
S14	6.1	4.9	5.2	4.3	5.1	4.1
S15	8.0	6.5	4.8	3.9	4.3	3.4
S16	13.6	15.2	13.0	14.1	12.6	13.5
S17	3.5	3.1	4.2	3.7	3.4	2.9
MEAN	7.25	6.12	7.13	5.91	5.86	5.01

4.6. Estimating DBP

Table 6 shows the results of estimating DBP. After applying the statistical t-test with a resulting p-value bigger than 0.05, we cannot conclude that a significant difference of the relative error exists between the ELM4, ELM5, and ELM6 models. However, with our data, the ELM6 achieves the lowest mean relative error of 7.04% and the lowest average of the Root Mean Square Error of 4.78 mmHg.

The minimum error is achieved for subject $S04$ in all ELMs, having in ELM6 a RMSE: 2.3 mmHg and relative error: 2.7%. The worse result is achieved in subject $S016$ in all ELMs, having in ELM6 a RMSE: 9.3 mmHg and relative error: 19.1%.

Table 6: RMSE and relative error from diastolic BP estimation by ELMs with three types of training set: PPG waveform (ELM4); VPG waveform (ELM5) and a combination of PPG and VPG (ELM6). All of them plus PTT and HR correspond to each waveform

Diastolic Blood Pressure Estimate

	ELM4		ELM5		ELM6	
Subject	**RMSE** (mmHg)	**Relative** Error (%)	**RMSE** (mmHg)	**Relative** Error (%)	**RMSE** (mmHg)	**Relative** Error (%)
S03	3.7	4.3	3.9	4.5	2.6	3.1
S04	2.3	2.7	2.2	2.6	2.3	2.7
S05	3.9	5.3	3.9	5.4	4.3	5.8
S06	7.3	9.7	5.9	7.5	5.5	7.6
S07	4.3	6.8	4.2	6.7	4.5	7.2
S08	6.0	6.1	9.3	9.3	5.9	6.4
S09	8.7	11.8	9.9	14.3	7.5	12.0
S10	3.2	4.9	3.4	5.1	3.1	4.7
S11	3.1	5.6	3.4	5.9	3.2	5.8
S12	6.6	9.1	7.7	10.9	7.5	9.4
S13	5.5	6.9	4.6	6.1	4.0	5.3
S14	3.2	4.3	2.5	3.6	2.9	4.2
S15	4.5	6.1	4.4	5.6	4.6	5.8
S16	9.0	19.7	9.0	20.1	9.3	19.1
S17	4.4	6.2	4.5	6.3	4.5	6.5
MEAN	5.05	7.30	5.25	7.59	4.78	7.04

5. Discussion

This work was inspired by a previous work [22], where in the LCD fitting process, 4997 signals are evaluated instead of the 160 signals per subject and the results are still surprising. They show a mean relative error RE 5.7 ± 1.6% and mean correlation r 0.95. These results allow us to assume that LCD really works and that derivative approaches are a suitable tool to fit the PPG waveform into the fiAP waveform.

However the ELM methods outperforms the performance of the LCD fitting process, where the ELM models reach a correlation higher than 0.96 with an average of 0.98 ± 0.01. Moreover, the ELM3 that consists in a modular combination of the PPG and VPG input signals, obtained the lowest mean relative error of 3.33%. Nevertheless, PPG and VPG were tested as inputs without being separated in two modules and the results were no better than PPG or VPG as independent inputs (ELM1 and ELM2).

Considering that PPG is measured with the index finger tip, it is surprising that ELM has better results estimating the reconstructed brachial BP waveform than fiAP waveform. The fiAp is measured in the digital artery of the middle finger, next to the finger where PPG is measured. Consequently, it is expected that fiAP waveform estimates should be better than reBP waveform estimates because digital artery is a distal branch of the brachial artery and, therefore, it could be assumed that it is more complex to estimate reBP waveform than fiAP waveform.

In [23] – [25], the authors have evaluated the performance of the Deep Boltzmann machine and Support Vector Regressions as machine learning models used to estimate the Blood Pressure. These models were tested with BP and PPG waveforms of subjects whose datasets were randomly combined and separated in training and test sets afterwards (Similar signals appears in training and test sets). Moreover, they have not induced a blood pressure rise. Under this scenario, the models show a good performance. On the other hand, our proposed model is able to estimate high pressure data obtained by induced handgrip maneuver, this data is a realistic simulation of high pressure events. Our results shows an acceptable mean relative error.

Improving the results in SBP, DBP and waveform estimations may help to start the development of a new technique in BP estimation, which combines two very important aspects in BP studies: its extreme values and its waveform (See [42] for naming standards of these features).

In addition, in a preliminary way, several tests were carried out with inter-subject data and ELM obtained poor results when the subjects have very different biometric characteristics. However, with two similar subjects, good estimates were obtained, which are: healthy male subjects, aging 26 and 27 years old, and Body Mass Index close to 22.5 [Kg / m2]. In this case, ELM achieved SBP and DBP values estimates with errors less than 10%. This suggests that, as expected, more data needs to be collected to achieve the different existing clusters, each of which with sufficient data size. This may allow the demands for completeness and consistency of the training and testing data to be satisfied. Therefore, following the theorem applicable to single intermediate layer artificial neural networks that can perform as universal Approximators [43], the achievement of nImI methods to estimate BP from PPG is granted for all subjects belonging to any cluster.

This research provides the following contributions and improvements:

- The main goal was to develop a machine learning method to estimate the arterial blood pressure from PPG and VPG signals measured from healthy subjects.
- We have validated the Extreme Learning Machine (ELM) as a model that relates the PPG to fiAP and

brachial reconstructed Blood Pressure (reBP) waveforms.

- We have validated the Extreme Learning Machine as a model used to estimate the Systolic and Diastolic BP values.
- We have evaluated how a combination of PPG and its derivatives can improve the performance compared to using only the signal by itself.
- We have evaluated how the incorporation of significant parameters extracted from the original signal such as PTT and HR can enhance the performance of the ELM.
- We have conducted a clinical essay approved by the Bioethics Institutional Committee for Human Beings Research of the Universidad de Valparaiso. In the procedure, the volunteers performed two handgrips, which is isometric maneuver to induce controlled Blood Pressure rises.

6. Conclusions

In this work, ELM is conclusively shown to be a suitable tool to estimate BP from PPG when input vectors are PPG related data, and target vectors, either, fiAP and reBP waveforms, or, SBP and DBP values that belong to the same subject.

These are promising results and they suggest that we should continue our research into machine learning and its potential in health applications. ELM has good results estimating the brachial BP waveform and other main arteries can perhaps be studied with this type of architecture and method, such as the aorta, which a very important artery in cardiovascular studies.

Although both SBP and DBP estimations show promising results, they still need to be more precise because a maximum error of ±3 mmHg is accepted for BP medical devices. Nevertheless, different architectures and inputs from PPG, and its derivative approaches, can be evaluated to help the ELM learning process.

We have also tested the inter-subject Blood pressure estimation, however more work and research are required to enhance the performance. We think that if the number of subjects recruited is increased considerable, then there will be a chance to have a global model instead of a individual ad-hoc subject model.

Future work is required in order to increase the number of subjects and thus increase the variability of the signals. Furthermore, it would be interesting to explore other methods such as neuro-fuzzy models [40, 44], machine learning models [45], and deep learning techniques [46]. Moreover, analysing the wavelet domain of the signals could be relevant for healthcare applications [47, 48]. On the other hand, information from experts could be included in the models [49] and potential biomarkers could be found using machine learning techniques [50].

Conflict of Interest The authors declare no conflict of interest.

Acknowledgments

The authors acknowledge the support given by Chilean ANID Grants FONDEF IT13I20060, Fondo Nacional de Desarrollo Científico y Tecnológico Fondecyt Nº 1221938, PAI Folio 79140057, CIDIS-UV 14 and ANID - Millennium Science Initiative Program ICN2021-004.

The authors also acknowledge to anonymous healthy volunteers who participate in the clinical essays that were approved by the Interdisciplinary Bioethics Research Committee in Human Beings (CIBI- SH), of Valparaíso University (Chile)

References

[1] R. Victor, *Hipertensión arterial sistémica: mecanismos y diagnóstico*, vol. 1, chap. 45, pp. 944–963, Elsevier, Barcelona, 9th ed., 2013.

[2] S. A. Esper, M. R. Pinsky, "Arterial waveform analysis", *Best Practice & Research Clinical Anaesthesiology*, vol. 28, no. 4, pp. 363–380, 2014, doi:10.1016/j.bpa.2014.08.002.

[3] N. Kaplan, *Hipertensión arterial sistémica: mecanismos y diagnóstico, in Braunwald (Ed) Tratado de cardiología*, Madrid: Marbán Libros.Edition 6., 2004.

[4] I. Moxham, "Understanding arterial pressure waveforms", *Southern African Journal of Anaesthesia and Analgesia*, vol. 9, no. 1, pp. 40–42, 2003.

[5] F. Mahomed, "The physiology and clinical use of the sphygmograph", *Med Times Gazette*, vol. 1, p. 507, 1872.

[6] S. W. Moss, *Edgar Holden, MD of Newark, New Jersey: Provincial Physician on a National Stage*, Xlibris Corporation, 2014.

[7] M. F. O'Rourke, A. Pauca, X.-J. Jiang, "Pulse wave analysis", *British journal of clinical pharmacology*, vol. 51, no. 6, pp. 507–522, 2001, doi: 10.1046/j.0306-5251.2001.01400.x.

[8] I. B. Wilkinson, H. MacCallum, L. Flint, J. R. Cockcroft, D. E. Newby, D. J. Webb, "The influence of heart rate on augmentation index and central arterial pressure in humans", *The Journal of physiology*, vol. 525, no. 1, pp. 263–270, 2000.

[9] M. F. O'Rourke, D. E. Gallagher, "Pulse wave analysis", *Journal of Hypertension-Supplement-*, vol. 14, pp. S147–S158, 1996.

[10] R. A. Payne, I. B. Wilkinson, D. J. Webb, "Arterial stiffness and hypertension emerging concepts", *Hypertension*, vol. 55, no. 1, pp. 9–14, 2010, doi:10.1161/HYPERTENSIONAHA.107.090464.

[11] R. R. Townsend, H. R. Black, J. A. Chirinos, P. U. Feig, K. C. Ferdinand, M. Germain, C. Rosendorff, S. P. Steigerwalt, J. A. Stepanek, "Clinical use of pulse wave analysis: Proceedings from a symposium sponsored by north american artery", *The Journal of Clinical Hypertension*, vol. 17, no. 7, pp. 503–513, 2015, doi:10.1111/jch.12574.

[12] J. Peñaz, "Photoelectric measurement of blood pressure, volume and flow in the finger", "Digest of 10th International Conference on Medical Biological Engineering, Dresden, East Germany", p. 104, 1973.

[13] N. Westerhof, M. F. O'Rourke, "Haemodynamic basis for the development of left ventricular failure in systolic hypertension and for its logical therapy.", *Journal of hypertension*, vol. 13, no. 9, pp. 943–952, 1995.

[14] K. S. Matthys, A. F. Kalmar, M. M. Struys, E. P. Mortier, A. P. Avolio, P. Segers, P. R. Verdonck, "Long-term pressure monitoring with arterial applanation tonometry: a non-invasive alternative during clinical intervention?", *Technology and Health Care*, vol. 16, no. 3, pp. 183–193, 2008.

[15] R. Payne, C. Symeonides, D. Webb, S. Maxwell, "Pulse transit time measured from the ecg: an unreliable marker of beat-to-beat blood pressure", *Journal of Applied Physiology*, vol. 100, no. 1, pp. 136–141, 2006.

[16] J. Allen, "Photoplethysmography and its application in clinical physiological measurement", *Physiological measurement*, vol. 28, no. 3, pp. R1–R39, 2007, doi:10.1088/0967-3334/28/3/R01.

[17] D. Zheng, J. Allen, A. Murray, "Determination of aortic valve opening time and left ventricular peak filling rate from the peripheral pulse amplitude in patients with ectopic beats", *Physiological measurement*, vol. 29, no. 12, p. 1411, 2008.

[18] R. Lazazzera, Y. Belhaj, G. Carrault, "A new wearable device for blood pressure estimation using pthotoplethysmogram", *Sensors*, vol. 19, no. 2557, p. s19112557, 2019, doi:10.3390/s19112557.

[19] Y. Chen, L. Li, C. Hershler, R. P. Dill, "Continuous non-invasive blood pressure monitoring method and apparatus", 2003, uS Patent 6,599,251.

[20] M. Y.-M. Wong, C. C.-Y. Poon, Y.-T. Zhang, "An evaluation of the cuffless blood pressure estimation based on pulse transit time technique: a half year study on normotensive subjects", *Cardiovascular Engineering*, vol. 9, no. 1, pp. 32–38, 2009.

[21] G. Tapia, A. Glaría, "Artificial neural network detects physical stress from arterial pulse wave", *Revista Ingeniería Biomédica*, vol. 9, no. 17, pp. 21–34, 2015.

[22] G. Tapia, M. Salinas, J. Plaza, D. Mellado, C. Saavedra, Veloz, A. Arriola, R. Salas, A. Glaría, "Photoplethysmogram fits finger blood pressure waveform for non-invasive and minimally-intrusive technologies", "Biosignal: 10th International Joint Conference on Biomedical Engineering Systems and Technologies. Biostec 2017", vol. 4, pp. 155–162, Porto, 2017.

[23] M. W. K. Fong, E. Ng, K. E. Z. Jian, T. J. Hong, "SVR ensemble-based continuous blood pressure prediction using multi-channel photoplethysmogram", *Computers in Biology and Medicine*, vol. 113, p. 103392, 2019, doi:10.1016/j.compbiomed.2019.103392.

[24] S. Chen, Z. Ji, H. Wu, Y. A. Xu, "A non-invasive continuous blood pressure estimation approach based on machine learning", *Sensors*, vol. 2585, p. 19, 2019, doi:10.3390/s19112585.

[25] S. Lee, J.-H. Chang, "Dempster–shafer fusion based on a deep boltzmann machine for blood pressure estimation", *Applied Science*, vol. 96, p. 9, 2019, doi:10.3390/app9010096.

[26] G. Huang, G.-B. Huang, S. Song, K. You, "Trends in extreme learning machines: a review", *Neural Networks*, vol. 61, pp. 32–48, 2015, doi:10.1016/j.neunet.2014.10.001.

[27] H. Allende, C. Moraga, R. Salas, "Artificial neural networks in time series forecasting: A comparative analysis", *Kybernetika*, vol. 38, no. 6, pp. 685–707, 2002.

[28] D. E. Rumelhart, G. E. Hinton, R. J. Williams, "Learning representations by back-propagating errors", *Cognitive modeling*, vol. 5, no. 3, p. 1, 1988.

[29] G.-B. Huang, Q.-Y. Zhu, C.-K. Siew, "Extreme learning machine: theory and applications", *Neurocomputing*, vol. 70, no. 1, pp. 489–501, 2006, doi:10.1016/j.neucom.2005.12.126.

[30] E. Cambria, G.-B. Huang, L. L. C. Kasun, H. Zhou, C. M. Vong, J. Lin, J. Yin, Z. Cai, Q. Liu, K. Li, *et al.*, "Extreme learning machines [trends & controversies]", *IEEE Intelligent Systems*, vol. 28, no. 6, pp. 30–59, 2013, doi:10.1109/MIS.2013.140.

[31] G.-B. Huang, Q.-Y. Zhu, C.-K. Siew, "Extreme learning machine: a new learning scheme of feedforward neural networks", "Neural Networks, 2004. Proceedings. 2004 IEEE International Joint Conference on", vol. 2, pp. 985–990, IEEE, 2004, doi:10.1109/IJCNN.2004.1380068.

[32] G. Tapia, J. Plaza, M. Salinas, A. Glaria, "Training set for nimi blood pressure estimates v 1.0 minimally documented training set nimi data 1.0 documentation", http://nimi.uv.cl, 2017.

[33] Finapres, "Finapres medical systems (2015)", http://www.finapres.com/products/finapres-nova, 2015, accessed: 2015-04-18.

[34] J. Pan, W. J. Tompkins, "A real-time QRS detection algorithm", *IEEE transactions on biomedical engineering*, vol. 32, no. 3, pp. 230–236, 1985.

[35] A. C. Guyton, J. E. Hall, *Tratado de fisiología médica*, Elsevier,, Barcelona, 12 ed., 2011.

[36] M. Elgendi, "Standard terminologies for photoplethysmogram signals", *Current cardiology reviews*, vol. 8, no. 3, pp. 215–219, 2012, doi:10.2174/157340312803217184.

[37] E. Zahedi, K. Chellappan, M. A. M. Ali, H. Singh, "Analysis of the effect of ageing on rising edge characteristics of the photoplethysmogram using a modified windkessel model", *Cardiovascular Engineering*, vol. 7, no. 4, pp. 172–181, 2007.

[38] M. Salinas, R. Salas, D. Mellado, A. Glaría, C. Saavedra, "A computational fractional signal derivative method", *Modelling and Simulation in Engineering*, vol. 2018, p. 7280306, 2018, doi:10.1155/2018/7280306.

[39] H. Allende, C. Moraga, R. Ñanculef, R. Salas, "Ensembles methods for machine learning pattern recognition and machine vision", *Series Information Sciences & Tecnology. In honor and memory of Prof. KS. Fu*, pp. 247–261, 2010.

[40] M. Querales, R. Salas, Y. Morales, H. Allende-Cid, H. Rosas, "A stacking neuro-fuzzy framework to forecast runoff from distributed meteorological stations", *Applied Soft Computing*, vol. 118, p. 108535, 2022, doi:10.1016/j.asoc.2022.108535.

[41] G. Feng, G.-B. Huang, Q. Lin, R. Gay, "Error minimized extreme learning machine with growth of hidden nodes and incremental learning", *IEEE Transactions on Neural Networks*, vol. 20, no. 8, pp. 1352–1357, 2009, doi:10.1109/TNN.2009.2024147.

[42] M. Elgendi, Y. Liang, R. Ward, "Toward generating more diagnostic features from photoplethysmogram waveforms", *Diseases*, vol. 20, p. 6, 2018, doi:10.3390/diseases6010020.

[43] K. Hornik, M. Stinchcombe, H. White, "Multilayer feedforward networks are universal approximators", *Neural networks*, vol. 2, no. 5, pp. 359–366, 1989.

[44] Y. Morales, M. Querales, H. Rosas, H. Allende-Cid, R. Salas, "A self-identification neuro-fuzzy inference framework for modeling rainfall-runoff in a chilean watershed", *Journal of Hydrology*, vol. 594, p. 125910, 2021, doi:10.1016/j.jhydrol.2020.125910.

[45] A. Bertini, R. Salas, S. Chabert, L. Sobrevia, F. Pardo, "Using machine learning to predict complications in pregnancy: A systematic review", *Frontiers in bioengineering and biotechnology*, vol. 9, 2021, doi:10.3389/fbioe.2021.780389.

[46] D. Mellado, C. Saavedra, S. Chabert, R. Torres, R. Salas, "Self-improving generative artificial neural network for pseudorehearsal incremental class learning", *Algorithms*, vol. 12, no. 10, p. 206, 2019, doi:10.3390/a12100206.

[47] C. Saavedra, R. Salas, L. Bougrain, "Wavelet-based semblance methods to enhance the single-trial detection of event-related potentials for a bci spelling system", *Computational Intelligence and Neuroscience*, vol. 2019, 2019, doi:10.1155/2019/8432953.

[48] E. Vivas, H. Allende-Cid, R. Salas, L. Bravo, "Polynomial and wavelet-type transfer function models to improve fisheries' landing forecasting with exogenous variables", *Entropy*, vol. 21, no. 11, p. 1082, 2019, doi:10.3390/e21111082.

[49] E. Cantor, R. Salas, H. Rosas, S. Guauque-Olarte, "Biological knowledge-slanted random forest approach for the classification of calcified aortic valve stenosis", *BioData Mining*, vol. 14, no. 1, pp. 1–11, 2021, doi:10.1186/s13040-021-00269-4.

[50] P. Franco, J. Sotelo, A. Guala, L. Dux-Santoy, A. Evangelista, J. Rodríguez-Palomares, D. Mery, R. Salas, S. Uribe, "Identification of hemodynamic biomarkers for bicuspid aortic valve induced aortic dilation using machine learning", *Computers in biology and medicine*, vol. 141, p. 105147, 2022, doi:10.1016/j.compbiomed.2021.105147.

GONZALO TAPIA CABRERA has done his bachelor's degree in Biomedical Engineering from Universidad de Valparaíso (UV) in 2013. He has done his master's degrees from UV and Pontificia Universidad Católica de Valparaíso (PUCV) in 2017 and 2021, respectively. He is currently pursuing his PhD degree in PUCV.

His main research area is biomedical signal processing and image analysis.

RODRIGO SALAS FUENTES received the B.S. and MSc. degrees in Informatics Engineering and the Dr. Eng. degree in informatics from the Federico Santa María Technical University (UTFSM) in Chile, in 2001, 2002 and 2010, respectively. He is currently a Full Professor of the Biomedical Engineering School.

Dr. Salas is main researcher at *Millennium Institute for Intelligent Healthcare Engineering*, and main researcher at the *Center of Research and Development in Health Engineering (CINGS-UV)*. His research interests include Artificial Intelligence, Data Science, and their applications to finance, air pollution, healthcare and medicine.

MATIAS SALINAS SALAZAR received the B.S. and MSc. degrees in Biomedical Engineering from the Universidad de Valparaíso (Chile), in 2016 and 2018 respectively. He is currently a PhD student at the Universidad de Valparaíso.

His main research area is biomedical signal processing and image analysis.

CAROLINA SAAVEDRA RUIZ received the B.S. and MSc. degrees in Informatics Engineering from the Federico Santa María Technical University (UTFSM) in Chile, in 2005 and 2008 respectively. In 2013, she has completed her PhD degree in the area of Biomedical Engineering at INRIA Nancy Grand-Est/Université de Lorraine in France. Currently, she is an associate professor at the Biomedical Engineering School and director of the Master of Science program in Biomedical Engineering at the University of Valparaíso.

Her main research areas are Machine Learning for Signal Processing, Brain Computer Interfaces and Biomedical Data Analysis.

ALEJANDRO VELOZ BAEZA received the B.S. in Biomedical Engineering from the Universidad de Valparaíso (Chile) in 2007. He completed the Master of Science and Dr. Eng. degrees in informatics from the Federico Santa María Technical University (Chile) in 2011 and 2018, respectively. He is currently an Associate Professor of the Biomedical Engineering School at the Universidad de Valparaíso.

Dr. Veloz is main researcher at the *Center of Research and Development in Health Engineering (CINGS-UV)*. His main research areas are functional magnetic resonance imaging, machine learning and fuzzy systems.

ALEXIS ARRIOLA VERA received the degree of Engineer in Business Management from the Valparaíso Catholic University (Chile) in 1982. He obtained the Master in Business Administration from the University of Chile in 1999. He is currently pursuing his PhD degree at the University of Santiago (Chile). He is currently director of the Biomedical Engineering School.

His main research areas are Management of Healthcare Organizations and Technologies, Clinical Engineering, Process Management and Quality Assurance.

STEREN CHABERT received the B.S. in Biomedical Engineering from the University of Technology of Compiègne (France) in 2000. She obtained the Master of Science in Biomedical Engineering from the Washington University in St Louis (USA)in 2000. She completed the PhD. in Biomedical Engineering from the University of Technology of Compiègne, (France) in 2004. She is currently Full Professor of the Biomedical Engineering School at the Universidad de Valparaíso.

Ph.D. Chabert is main researcher at *Millennium Institute for Intelligent Healthcare Engineering*, main researcher at the *Center of Research and Development in Health Engineering (CINGS-UV)* and director of CERTEMED. Her research interests include the development of novel acquisition methods for diffusion and functional MRI, and medical image processing.

ANTONIO GLARIA received the B.S. in Electronics Engineering from the Federico Santa María Technical University (UTFSM) in Chile, in 1975. He has done his master's degree in Biomedical Engineering from the University Newcastle-upon-Tyne in UK, in 1983. He has completed the D.E.A. in Sciences Cognitives from the University of Paris 6 in France, in 1990. Currently, he is an Emeritus Professor at the Biomedical Engineering School from the Universidad de Valparaíso.

He is the main founder of the Biomedical Engineering program at the University of Valparaíso, in 2000. He was dean of the Faculty of Sciences (1994-2002) and director of the Biomedical Engineering program (2003-2005). He participated in at least 10 research grants and has more than 30 publications in journals and conference proceedings.